

Faculty of Science and Engineering  
Department of Exploration Geophysics

**Multidimensional Computation and  
Visualisation for Marine Controlled Source  
Electromagnetic Methods**

**Andrew M. Pethick**

This thesis is presented for the Degree of  
Doctor of Philosophy  
of  
Curtin University

**July 2013**





## **Declaration of Academic Integrity**

I have read the university regulations on cheating and plagiarism, and I state that this piece of work is my own, and this dissertation contains no material previously published by any other person except where due acknowledgment has been indicated in the text.

Signature:

Date: 27<sup>th</sup> March 2013



*Where is the way where light dwelleth?  
and as for darkness, where is the place thereof?*

GOD SPEAKING TO JOB



## Acknowledgements

I extend my heartfelt thanks to my primary supervisor Dr. Brett Harris for his tireless support throughout my honours and PhD years at Curtin University. His enthusiasm for geophysics has been an inspiration to me. I am also thankful for Dr Anton Kepic and Peter Wolfram for their invaluable input.

I would like to acknowledge the Australian Government and Fugro Electro Magnetic for the research scholarship they have provided. I thank the researchers at Fugro. Through them the knowledge base was invaluable to the success of my thesis.

I appreciate the continued support of my parents, brothers and all my family and friends. This work was only achievable with the encouragement and patient endurance of everyone involved.

Finally I would like to thank my loving wife for all the sacrifices she has made for me throughout the duration of my PhD. Thank you for enduring *PhD widowship* for me. I love you and I could not have done this without you.



## List of Publications

### Software

[CSEMoMatic v1.5](#) publically available under GNU v3

[CSEMoMatic Omnium](#) publically available under GNU v3

### Website and Learning Portal

[MCSEM.com](http://MCSEM.com)

### Journals

Harris, B., and A. Pethick, 2008, Marine controlled source electromagnetic methods for hydrocarbon exploration, *Preview*, **137**, 30-34.

Pethick, A., and B. Harris, Interactive Marine Controlled Source Electromagnetic Synthetic Streamline Modelling, 2012, *Computers in Geoscience* (Under Review)

Pethick, A., and B. Harris, Macro Parallelisation for Controlled Source Electromagnetic Applications, *Geophysics*, 2012, (Under Review)

Pethick, A., and B. Harris, Understanding the effect of Bathymetry on the Marine Controlled Source Electromagnetic Method using Electromagnetic Streamlines, *Exploration Geophysics*, 2012 (Under Review)

### Expanded Abstracts

Pethick, A., 2009, Practical Marine CSEM 3D Inversion (Presentation), CRGC, El Caballo.

Pethick, A., 2010, Interactive MCSEM Software to Assist Field Data Modelling and Inversion, CRGC, Rottneest.





Pethick, A., and B. Harris, 2011, Conditioning of the 3D Marine Controlled Source Inversion, ASEG-PESA 21st International Geophysical Conference and Exhibition, Aug 22 2010, pp 91, Darling Harbour, Sydney, NSW, doi:10.1071/ASEG2010ab198.

Pethick, A., 2011, Implications of Bathymetry on MCSEM (Poster), CRGC, Rottneest

Harris, B., and A. Pethick, 2011, Comparison of a vertical electric and a vertical magnetic source for cross well CSEM monitoring of CO<sub>2</sub> injection, Society of Exploration Geophysics (ed), SEG/San Antonio 2011, Sep 18 2011, pp. 1892-1896. San Antonio, Texas, doi:10.1190/1.3627576.

Pethick, A., and B. Harris, 2012, Open Source Marine Controlled Source Electromagnetic Interactive Modelling, ASEG-PESA 22nd International Geophysical Conference and Exhibition, Feb 26 2012, Brisbane, QLD. doi:10.1071/ASEG2012ab241.

Pethick, A., and B. Harris, 2012, Understanding the effect of Bathymetry on the Marine Controlled Source Electromagnetic Method using Electromagnetic Streamlines, ASEG 22nd International Geophysical Conference and Exhibition, Feb 26 2012, Brisbane, QLD, doi:10.1071/ASEG2012ab242.

Swanepoel, R., B. Harris, A., Pethick, 2012, 3D modelling for time-lapse cross-well CSEM monitoring of CO<sub>2</sub> injection into brine filled reservoirs, ASEG-PESA 22nd International Geophysical Conference and Exhibition, Feb 26 2012, Brisbane, QLD, doi:10.1071/ASEG2012ab314.

Pethick, A., B. Harris and K. Lam, 2013, Proof of Concept BCI Electromagnetic Computing Case Study, ASEG-PESA 23rd International Geophysical Conference and Exhibition, Aug 11 2013, Melbourne, VIC.

Pethick, A., and B. Harris, 2013, Poynting Vector Streamlines and the Marine Controlled Source Electromagnetic Airwave, EAGE 75th EAGE Conference and Exhibition, London.



## Abstract

The controlled source electromagnetic method is improving the search for oil and gas in marine settings and is becoming an integral component of many exploration toolkits. While the level of detail and benefit obtained from recorded electromagnetic data sets is limited to the tools available, interpretation is fundamentally restricted by non-unique and equivalent solutions. I create the tools necessary to rapidly compute and visualise multi-dimensional electromagnetic fields generated for a variety of controlled source electromagnetic surveys. This thesis is divided into two parts: the creation of an electromagnetic software framework and the electromagnetic research applications.

The creation of a new electromagnetic software framework is covered in Part I. Steps to create and test a modern electromagnetic data structure, three-dimensional visualisation and interactive graphical user interface from the ground up are presented. Bringing together several computer science disciplines ranging from parallel computing, networking and computer human interaction to three-dimensional visualisation, a package specifically tailored to marine controlled source electromagnetic computation is formed. The electromagnetic framework is comprised of approximately 100,000 lines of new Java code and several third party libraries, which provides low-level graphical, network and execution cross-platform functionality. The software provides a generic framework to integrate most computational engines and algorithms into the coherent global electromagnetic package enabling the interactive forward modelling, inversion and visualisation of electromagnetic data.

Part II is comprised of several research applications utilising the developed electromagnetic software framework. Cloud computing and streamline visualisation are covered. These topics are covered to solve several problems in modern controlled source electromagnetic methods. Large 3D electromagnetic modelling and inversion may require days or even weeks to be performed on a single-threaded personal computers. A massively parallelised electromagnetic forward modelling and inversion methods can dramatically was created to improve computational time. The developed 'macro' parallelisation method facilitated the reduction in computational time by several orders of magnitude with relatively little additional effort and without modification of the internal electromagnetic algorithm. The air wave is a significant component of marine controlled source electromagnetic surveys however there is controversy and confusion over its definition. The airwave has been described as a reflected, refracted, direct or diffusing wave, which has lead to confusion over its physical reality.



Real-time interactive streamlines were built into the electromagnetic framework to represent the electric, magnetic and Poynting vector fields with greater realism. The first images of the evolving air wave are provided. The images show the propagation of energy (i.e., the Poynting vector) exhibits refractive qualities at high resistivity contrast boundaries, while the electric and magnetic air wave show the airwave as a downwardly diffusing rotating vortex. This shape, onset and path of the evolving vortices are highly influenced by the ocean floor shape. Brain computer interface systems are emerging as a breakthrough technology of the 21st century.

This research has culminated in the creation of a new controlled source electromagnetic software framework, enriching understanding in complex coupled vector field behaviour and hopefully inspiring research worldwide.



# Contents

<b>Chapter 1</b>	<b>Introduction</b>	<b>1</b>
1.1	Objectives . . . . .	2
1.2	Thesis Structure . . . . .	3
1.3	Overview of Marine Controlled Source Electromagnetic Methods . . . . .	4
1.4	Software Overview . . . . .	6
1.5	The MCSEM Method . . . . .	8
1.6	EM Field Propagation . . . . .	9
1.7	MCSEM Survey Parameters and Equipment . . . . .	10
1.7.1	Transmitted waveform . . . . .	10
1.7.2	Multi Component Receivers . . . . .	13
1.7.3	Transmitter . . . . .	17
1.8	Survey Design . . . . .	23
1.8.1	CSEM noise sources . . . . .	23
1.8.2	Target Style Considerations . . . . .	26
1.8.3	The Airwave Problem . . . . .	26
1.8.4	Seawater Conductivity . . . . .	29
1.9	MCSEM Visualisation . . . . .	31
1.9.1	1D Profiles . . . . .	32
1.9.2	2D Grids and Contours . . . . .	32
1.9.3	Isosurfaces . . . . .	32
1.9.4	Vector Glyphs . . . . .	32

<b>Part I</b>	<b>Development of an Electromagnetic Framework</b>	<b>37</b>
<b>Chapter 2</b>	<b>Designing the Electromagnetic Data Model</b>	<b>39</b>
2.1	Data Model Overview . . . . .	40
2.2	Requirements . . . . .	40
2.3	Floating Point versus Double Precision . . . . .	41
2.4	Object-Orientated Programming . . . . .	41
2.4.1	Unified Modelling Language and Class Diagrams . . . . .	42
2.4.2	Generalisation and Inheritance . . . . .	46
2.4.3	Implementation and Interfaces . . . . .	46
2.5	Electromagnetic Project Structure . . . . .	47
2.5.1	Transmitters and Receivers . . . . .	50
2.5.2	System Configuration . . . . .	54
2.5.3	Waveforms and Windows . . . . .	61
2.5.4	EM Data Representation . . . . .	65
2.5.5	Geo-Electrical Earth . . . . .	70
2.6	Data Structure Development . . . . .	78
2.7	Conclusion . . . . .	82
<b>Chapter 3</b>	<b>Software Development</b>	<b>83</b>
3.1	Overview . . . . .	84
3.1.1	Licencing . . . . .	84
3.1.2	Java and the Development Environment . . . . .	85
3.1.3	Design Heuristics . . . . .	86
3.2	The Software Structure . . . . .	86
3.2.1	The Graphical User Interface . . . . .	90



3.2.2	Visualisation and Interactive Viewer Development . . . . .	96
3.2.3	2D Visualisation . . . . .	98
3.2.4	3D Visualisation . . . . .	109
3.2.5	Visualization with Fractals . . . . .	112
3.2.6	Interactivity . . . . .	118
3.2.7	Integration of Third Party Algorithms . . . . .	121
3.2.8	Multi-Threaded Execution . . . . .	125
3.3	Improvements . . . . .	127
3.4	Overview of Developed Software Versions . . . . .	128
3.5	Impact of the Software and Online Resources . . . . .	130
3.6	Conclusion . . . . .	130
<b>Part II</b>	<b>Electromagnetic Applications</b>	<b>135</b>
<b>Chapter 4</b>	<b>Macro Parallelisation for CSEM Applications</b>	<b>137</b>
4.1	Overview . . . . .	138
4.2	Introduction . . . . .	138
4.3	Background . . . . .	140
4.3.1	The Basics of MCSEM IE forward modelling . . . . .	140
4.3.2	The MCSEM method . . . . .	142
4.3.3	Grid Computing . . . . .	143
4.4	Developing a Macro Electromagnetic Modelling Framework . . . . .	144
4.4.1	Programming Heuristics . . . . .	144
4.4.2	Electromagnetic data structure . . . . .	144
4.4.3	Macro Parallelisation . . . . .	147

4.5	IE Forward Modelling Parallelisation . . . . .	151
4.5.1	Frequency and Source Dependence . . . . .	155
4.5.2	Implications for Macro Integral Equation Parallelisation . . . . .	157
4.6	Grid Computing Airborne EM Inversion . . . . .	158
4.6.1	Execution . . . . .	158
4.6.2	Results and Discussion . . . . .	161
4.7	Conclusion . . . . .	161
4.8	Macro Parallelisation Pseudo-Code . . . . .	165
<b>Chapter 5</b>	<b>EM Streamlines</b>	<b>169</b>
5.1	Interactive MCSEM Streamlines . . . . .	171
5.1.1	Summary . . . . .	171
5.1.2	Introduction . . . . .	171
5.1.3	Streamline Generation . . . . .	172
5.1.4	Software Development . . . . .	173
5.1.5	Streamline Interpretation . . . . .	176
5.2	The Scale of the Electromagnetic Fields Generated by an MCSEM Survey . . .	187
5.2.1	Three-Dimensional Streamlines . . . . .	189
5.2.2	Conclusion . . . . .	194
5.3	Poynting vector streamlines and the Airwave . . . . .	195
5.3.1	Summary . . . . .	195
5.3.2	Introduction . . . . .	195
5.3.3	Theory and Method . . . . .	195
5.3.4	Results . . . . .	196
5.3.5	Conclusions . . . . .	199

5.3.6 Acknowledgements . . . . .	199
5.4 Streamlines and Bathymetry . . . . .	200
5.4.1 Summary . . . . .	200
5.4.2 Introduction . . . . .	200
5.4.3 Method and Results . . . . .	201
5.4.4 Conclusions . . . . .	206
<b>Chapter 6 Conclusion</b>	<b>211</b>
6.1 Summary . . . . .	211
<b>Appendix A</b>	<b>215</b>
A.1 Overview . . . . .	216
<b>Appendix B</b>	<b>219</b>
B.1 Summary . . . . .	220
B.2 Introduction . . . . .	220
B.3 Method and Results . . . . .	221
B.4 Conclusion . . . . .	225
<b>Appendix C</b>	<b>227</b>
C.1 Summary . . . . .	228
C.2 Introduction . . . . .	228
C.3 Method . . . . .	229
C.4 Example . . . . .	230
C.5 Conclusion . . . . .	234
<b>Appendix D</b>	<b>235</b>

D.1 Summary . . . . .	236
D.2 Introduction . . . . .	236
D.3 Method and Results . . . . .	236
D.4 Interactive Data Investigation . . . . .	238
D.5 Conclusions . . . . .	240
<b>Appendix E Computing, Brains and Geophysics?</b>	<b>243</b>
E.1 Overview . . . . .	244
E.2 Introduction . . . . .	244
E.3 Methodology . . . . .	246
E.4 Results . . . . .	247
E.5 Discussion . . . . .	250
E.6 Conclusion . . . . .	250
<b>Appendix F</b>	<b>253</b>
<b>References</b>	<b>259</b>

# Introduction

---

## Contents

<b>1.1 Objectives . . . . .</b>	<b>2</b>
<b>1.2 Thesis Structure . . . . .</b>	<b>3</b>
<b>1.3 Overview of Marine Controlled Source Electromagnetic Methods .</b>	<b>4</b>
<b>1.4 Software Overview . . . . .</b>	<b>6</b>
<b>1.5 The MCSEM Method . . . . .</b>	<b>8</b>
<b>1.6 EM Field Propagation . . . . .</b>	<b>9</b>
<b>1.7 MCSEM Survey Parameters and Equipment . . . . .</b>	<b>10</b>
1.7.1 Transmitted waveform . . . . .	10
1.7.2 Multi Component Receivers . . . . .	13
1.7.3 Transmitter . . . . .	17
<b>1.8 Survey Design . . . . .</b>	<b>23</b>
1.8.1 CSEM noise sources . . . . .	23
1.8.2 Target Style Considerations . . . . .	26
1.8.3 The Airwave Problem . . . . .	26
1.8.4 Seawater Conductivity . . . . .	29
<b>1.9 MCSEM Visualisation . . . . .</b>	<b>31</b>
1.9.1 1D Profiles . . . . .	32
1.9.2 2D Grids and Contours . . . . .	32
1.9.3 Isosurfaces . . . . .	32
1.9.4 Vector Glyphs . . . . .	32

---

The term “petroleum” originates from the combination of two medieval Latin words *petra* meaning “rock” and *oleum* meaning “oil”. The search for petroleum or hydrocarbon pre-dates modern civilisation predicated by ancient Sumeria. The Sumerians would use a sticky black liquid called bitumen or asphalt to attach flint arrowheads to shafts for hunting. This liquid would become the first petroleum product ever used by the human race (Bilkadi, 1984). Uses of hydrocarbon were limited up until the 1850’s when the distillation of kerosene from artificially produced petroleum resulted in cheaper and superior method to illuminate candles and lamps and eventually replaced whale and rosin oil (Fleming, 1967). The birth of the gasoline powered combustion engines in the 1880’s heralded the start of the petroleum revolution, a world economy based on a cheap high density energy source which brought with it prosperity and an insatiable desire for petroleum products.

With the controversial peak oil crisis looming and the number of world class discoveries decreasing, the demand for oil and gas never been so great (Hall and Day, 2009). With large, easy to produce fields diminishing, exploration companies have to remain on the technological cutting edge to discover new oil and gas fields both in on-land and deeper marine environments. The increased drilling costs and exploration risk has brought new challenges for detecting hydrocarbon in deep water settings. Transition into deep water settings has forced geoscientists to be more certain of the presence and position of hydrocarbon especially in deep water settings where the costs to drill exploratory wells can reach in excess of 100 million dollars (Kulkarni, 2005). Since the 1920’s seismic methods have traditionally detected acoustic properties to reduce exploration risk, however with increasing costs, new geophysical methods must be employed to detect density, magnetic and electrical rock properties to be certain of future discoveries (Coraggio et al., 2012; Yang et al., 2011 and Jain et al., 2008). The 21<sup>st</sup> century obviously brings with it unique challenges, but with new energy technologies, improved hydrocarbon remote sensing techniques and unconventional hydrocarbon sources the threat of peak oil can be overcome.

## 1.1 Objectives

The objective of this thesis is to design, develop, test and utilise a modern computational and interpretational platform for the marine controlled source electromagnetic method (MCSEM). This is split into the following sub-categories:

- i design and develop a generic electromagnetic software framework that encapsulates key parts of all active source electromagnetic methods.

- ii integrate the developed electromagnetic data structure into a multi-touch interactive controlled source electromagnetic modelling graphical package which enables:
  - a real-time synthetic modelling and electromagnetic field data visualisation.
  - b develop real-time methods for representing 2D and 3D MCSEM data.
  - c develop methods that enable survey design, intuitive interpretation and improved understanding of active source EM methods.
- iii integrate high performance cloud computing and develop schemas and libraries suitable for massively parallel electromagnetic forward modelling and inversion applications.
- iv investigate the electromagnetic “air wave” concept within MCSEM.
- v investigate the influence of bathymetry on the marine CSEM method.
- vi investigate the possibility and utility of brain computing interfaces (BCI) for controlling MCSEM software and assisting in geophysical training.

## 1.2 Thesis Structure

The introductory chapter overviews the marine controlled source electromagnetic method, public and privately available software, basic physics of the method and the factors influencing survey design and visualisation of marine controlled source electromagnetic data. The thesis is divided into two parts:

Part I is composed of chapters 2 and 3. These chapters document the development of a generic electromagnetic modelling, inversion and visualisation framework. The software data-structure and software development is covered. For the benefit of readers I overview basics computer science concepts including object oriented design. Chapter 3 This chapter documents the development of the graphical user interface, 2D and 3D visualisation and multi-threaded execution.

Part II is composed of chapters 4 to E. This part presents research into various electromagnetic problems using the developed electromagnetic framework. One application is the creation of an applied cloud/grid computing method for electromagnetic modelling and inversion (See chapter 4). In this chapter I devise and test a simple method to massively parallelise both forward and inverse electromagnetic algorithms at a macro level to produce improvements to computation

time. In chapter 5 streamline visualisation is integrated into the electromagnetic framework. This chapter contains the application of streamlines for marine CSEM method. Key features such as the airwave, phase fronts and scattered hydrocarbon responses are investigated using streamlines. I also provide a new description of an electromagnetic air wave. In chapter E the first brain controlled geophysics software package is presented. This chapter combines computing, neuroscience and geophysics to identify potential benefits and limitations of brain computing in geophysics.

### 1.3 Overview of Marine Controlled Source Electromagnetic Methods

Electromagnetic (EM) methods can be divided into active and passive categories. There has been a transition from passive source EM such as the magneto-telluric (MT) method towards active source EM such as the controlled source electromagnetic (CSEM) method.

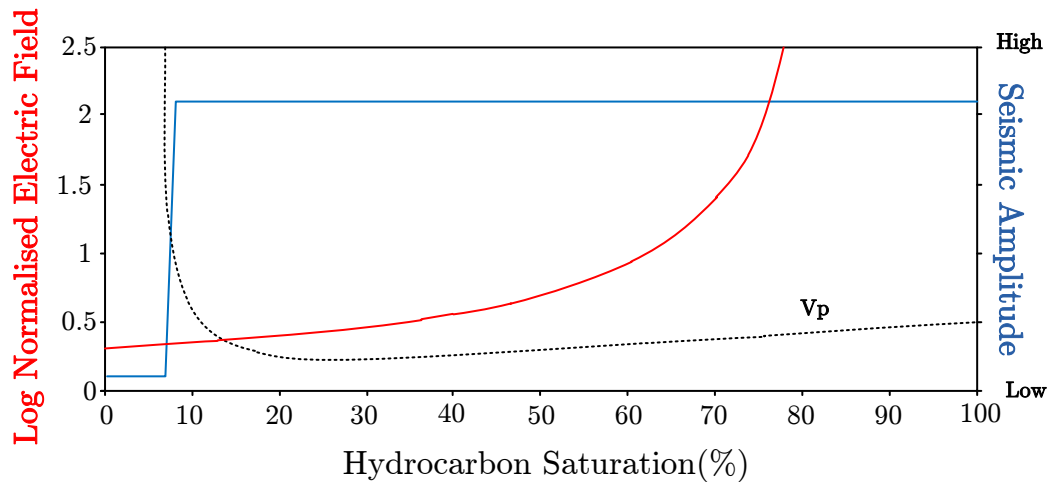
The MCSEM method goes by many other names. Some of these are CSEM imaging (CSEMi) and sea bed logging (SBL). MCSEM detects electrical resistivity contrasts (Kong, 2002). Marine CSEM (i.e., MCSEM or mCSEM) often targets thin electrically resistive hydrocarbon reservoirs in conductive surroundings (e.g., ocean and sub-ocean sediments).

MCSEM was originally developed for deep water studies of oceanic lithosphere in the 20<sup>th</sup> century (Cox, 1981). The method expanded into hydrocarbon exploration, beginning with the first survey carried out on an oilfield in offshore Angola (Ellingsrud et al., 2002). The MCSEM method has been advanced by the efforts of university and industry researchers such as Scripps Institution of Oceanography, The University of Toronto, Cambridge and Southampton University over the past two decades. MCSEM and MT have been linked in their development (Constable, 2010). Early MCSEM research combined both natural and active EM sources to image resistivity variations beneath the sea floor (Constable, 2010), while MT identifies resistivity variations on large scale structures at basin level. Most modern MCSEM are performed to ascertain nearsurface shape resistivity variation, in particular the detection of electrically thin resistive bodies, although they are still useful for deeper oceanographic studies (Peace, 2005).



Seismic methods are an industry standard hydrocarbon exploration technique. Combinations of seismic and non-seismic methods have been utilized to reduce exploration risk in recent times. Methods such as gravity, magnetism, well logging and more recently MCSEM have been incorporated into hydrocarbon exploration (i.e., Coraggio et al., 2012; Yang et al., 2011 and Jain et al., 2008).

MCSEM is useful as a supplementary non-seismic method as it detects resistivity rather than acoustic properties. MacGregor (2006) demonstrates that a strong relationship between the MCSEM electromagnetic response and fluid saturation percentage exists. Phillips (2007) states hydrocarbon reservoir saturation can be characterised ahead of drilling. Hydrocarbon saturation can be characterised because the electromagnetic field amplitude increases proportionally with hydrocarbon saturation. MacGregor (2006) highlights that amplitude and velocity analysis can only accurately detect hydrocarbon saturation between 0 and 10% (see Figure 1-1). MCSEM otherwise has the ability to detect hydrocarbon saturation due its resistivity variation. Typical MCSEM targets include petroleum, natural gas and gas hydrates.



**Figure 1-1:** The relationship between hydrocarbon saturation on seismic and MCSEM electric field observations. The MCSEM electric field response is characterised by increasing normalised electric field response with increasing hydrocarbon saturation. The seismic method fails to distinguish between a hydrocarbon saturation of 10 and 100 percent %. The ability to detect hydrocarbon saturation is the main benefit of the MCSEM method (Figure modified from Phillips, 2007).

Targets which are thin, or underneath thick tabular salt/basalt targets, or deep and with low resistivity comparable to the surrounding geology (see Table 1.1) will limit MCSEM's

effectiveness. MCSEM is useful in deep water turbidites and deltas, over stacked reservoir sequences or where there are large resistivity contrasts such as in shallow gas hydrates (MacGregor, 2006). Geological environments such as reservoirs at the edges of salt diapirs and in carbonates can be explored by the MCSEM method.

MCSEM surveys have become an integral part of deep ocean petroleum exploration and appraisal (Gribenko and Zhdanov, 2007) and future use for monitoring purposes may be possible as investigated by Noel et al. (2010), Noel et al. (2011) and Liang et al. (2012).

Practicality	Geology
Works Well	Deep water turbidites Deep water deltas Stacked reservoir sequences Under shallow gas or gas hydrates
Feasible	Flanks of salt diapirs Carbonate sequences Shallow water areas
Needs Research	Beneath thick tabular salt/basalt Thin deep, low resistivity targets

**Table 1.1:** The practicality of the MCSEM method in different geological environments. MCSEM works in a variety of geological environments however it may not work in some geological settings.

## 1.4 Overview of the MCSEM Software

CSEM software is immature compared to packages found for seismic or potential field techniques. MCSEM data is difficult to understand without adequate software. My research requires a flexible CSEM software package that permits:

- i low level access to the underlying electromagnetic and survey data structure
- ii low level access for the integration of third party algorithms
- iii modification and integration of existing and new execution procedures

- iv 3D visualisation of 3D vector fields
- v low level access to the 2D and 3D rendering core libraries
- vi publishing of modified code

Software, algorithmic code or libraries are proprietary and/or inaccessible by the public due to the highly competitive industry surrounding MCSEM. The market consists of several paid packages, a single free plug-in and several open source and freeware algorithms.

Processing software and algorithms are mainly developed and operated in-house by CSEM contractors and may remain uncommercialised for competitive advantage by choice. Two examples of commercial processing software include Sharkware by Interaction (Interaction, 2012) and Enthought's plugin for Shell (Enthought, 2010). Interaction has produced commercial processing and quality control tools such as a dataset editor, receiver rotation and time adjustments. The Interaction A/S group was acquired by Fugro in 2009 and since been dissolved. Enthought have also created processing software and have developed a proprietary plugin for Shell (Enthought, 2010). This software is written in python and performs CSEM frequency domain data calibration and visualisation of field and synthetic data. Western Geco have developed a Petrel plugin for data processing which facilitates the viewing and QC of processed MCSEM data but does not perform receiver rotations or time adjustments.

Complete CSEM forward modelling and inversion packages have also been developed by Encom and Bridge Electromagnetics (Bridge, 2012). EMGui was developed by Encom, incorporating CSIRO code library from the AMIRA p223 project (AMIRA, 2012). EMGui, the defunct successor to EMVision (Encom, 2012), is a general electromagnetic modelling and visualisation package utilised in-house at CSIRO, which is not available for public use or purchase. Blueback reservoir has developed the Bridge electromagnetics plugin for Petrel. The module is freely available to the public, but licensing is required for Petrel and the forward modelling code (Bridge, 2012). The 2.5D forward modelling code was not designed by bridge EM but was developed externally by EMGS and Technoimaging. The algorithm developed by EMGS and Technomaging is not distributed with the plugin. Key plugin features include visualisation, data quality control, EM attribute analysis, forward modelling and inversion analysis.

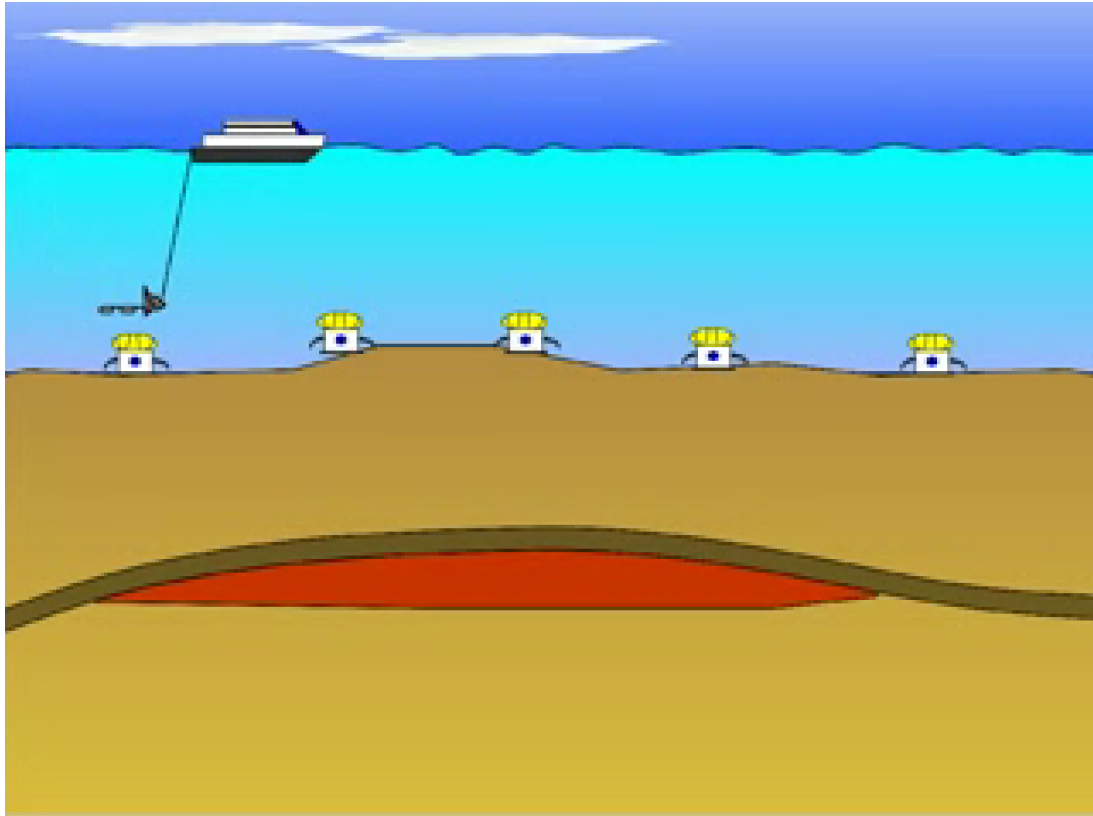
Other than the outcomes from research I know of, no marine CSEM forward modelling and visualisation software suits my research objectives. The competitive nature and fast emergence of the CSEM method has meant there are inadequate resources available for designing, developing and testing controlled source electromagnetic geophysical software packages. I have decided to develop a marine CSEM software package in its entirety. The first part of my research is focused on understanding, creating and implementing and testing a software solution. My intent is also to create a new open source tool that can support ongoing education, development and research.

## 1.5 The Marine Controlled Source Electromagnetic Method

Typical marine CSEM surveys work by using a horizontal electric bipole to transmit a low frequency 0.1 to 5 Hz square wave under high power up to 1000 A (Pethick, 2008). A horizontal electric bipole is a 100 to 1000 m long electric field transmitter towed 50 m above of the ocean bottom (MacGregor, 2006). Receivers can be placed to record the perturbations in the electric and magnetic fields for all Cartesian directions. There is typically a resistivity contrast between the conductive host rock and the resistive hydrocarbon. Saturated mudstone rocks, sandstones and shales with low resistivity dominate deep water environments.

Video 1-2 shows that traditional MCSEM surveys consist of a large moving high power transmitter and stationary magnetic and electric field receivers. Seafloor electromagnetic receivers are deployed to the ocean floor through the use of heavy concrete pads. Three component electrical bipole ( $E_x$ ,  $E_y$  and  $E_z$ ) and two component magnetic ( $H_x$  and  $H_y$ ) fields are typically recorded in modern surveys. These ocean bottom receivers start recording the small changes in the electromagnetic field once deployed. The MCSEM transmitter is dragged as close to the ocean floor as is practical (e.g., approximately 30 to 50 m from the ocean floor). The transmitter is typically towed inline with the receiver line. The transmitter sends a large amplitude transient current into a long electrical bipole source (e.g., 1000 A at 1 Hz into a 300 m long wire cable) (Harris and Pethick, 2008; MacGregor, 2006). The changing current generates 4D coupled electric and magnetic fields. The magnetic and electric fields circulate around each other with a strict geometry. The mathematical expression of the interactions between electric and magnetic fields is captured in Maxwell's equations. A hydrocarbon reservoir can be 10 to 100 times greater in resistivity (Eidesmo and Ellingsrud, 2002). Sediments containing oil

or gas have typically higher electrical resistivity compared to the ocean and brine-saturated host sediments. The electric and magnetic field patterns and amplitudes become altered or distorted if an electrically resistive hydrocarbon reservoir is present.



**Figure 1-2:** A video showing the schematic of a typical MCSEM survey. The video shows the electric dipole transmitter; transmits electric and magnetic fields while the seafloor receivers record subtle variations in the electric and magnetic fields. The end of the video shows the two modes of propagation which are commonly used to describe EM field behaviour. The black line represents the “direct wave”, the green arrow represents the “guided” wave and the blue lines represent the electric field.

See [Videos/method.avi](#) for video source

## 1.6 Mode of Electromagnetic Field Propagation

The electromagnetic fields generated during a MCSEM survey are described by differing and possibly contradictory methods. These include mathematical, electromagnetic wave propagation and seismic analogies. A number of mathematical approaches to define the

electromagnetic field propagation exists (i.e., Zhdanov, 2009), but these approaches cannot easily describe electromagnetic field propagation although they are good for computational applications. A popular method to describe the electromagnetic field behavior is to compare the MCSEM method with seismic refraction (e.g., Thirud, 2002; Fischer, 2005; Pound, 2007 and Carstens, 2009). These articles equate electromagnetic field diffusion as ray-paths. It also has been thought of as a diffusing wave (e.g., Constable, 2010). Figure 1-3 represents a common practice of comparing EM field propagation as raypaths rather than diffusion. This comparison makes it easier to describe MCSEM methods to seismic practitioners but this may ultimately lead to confusion amongst MCSEM practitioners as these two representations appear fundamentally in opposition.

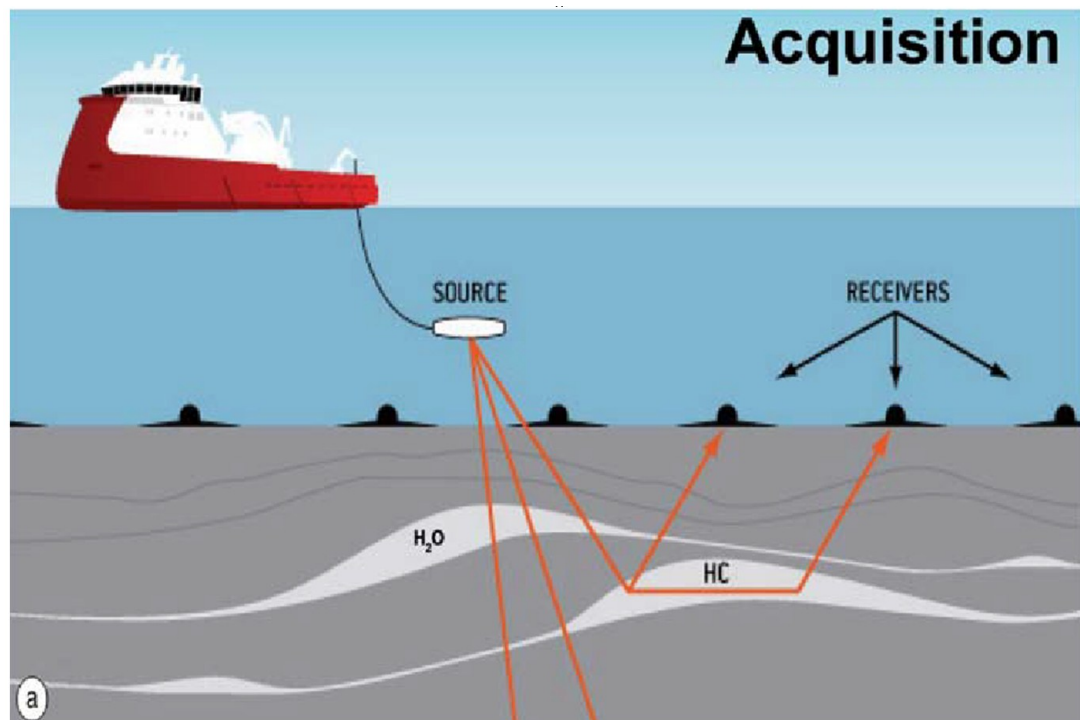
For simplicity the MCSEM method transmits an electromagnetic field from an electrical bipole source. The transmitted wave diffuses through the water column and into seabed. The electric fields attenuate less in resistive mediums. The presence of the reservoir increases the electrical field amplitude which can be measured at the seafloor at offsets roughly double the depth of the reservoir below the seabed (Pethick 2008). As the electromagnetic field encounters a conductive region of earth, the field changes in phase. The level of phase change is on the conductivity (i.e., the greater the conductivity, the greater the phase variation).

## 1.7 MCSEM Survey Parameters and Equipment

### 1.7.1 Transmitted waveform

The choice of transmission waveform controls the frequency content of the transmitted signal. The depth of penetration and resolution is determined by the frequency content. The relationship between depth of penetration of a low frequency electromagnetic signal and frequency and conductivity is described by the skin depth equation. The skin depth (See equation 1.1) is the effective depth of penetration of electromagnetic energy in a conducting medium when the amplitude of a plane wave in a whole space has been attenuated to  $\frac{1}{e}$  (or 37 percent) (Sheriff, 2002).

$$\delta = \sqrt{\frac{2}{\mu_0 \omega \sigma}} \approx 503 \sqrt{\frac{1}{f \sigma}} m \quad (1.1)$$



**Figure 1-3:** An example of representing the MCSEM with seismic refraction, taken from Hesthammer et al. (2010). This diagram represents the electromagnetic field as a number of rays, similar to the seismic refraction method. This comparison is made to demonstrate the path of energy. The authors do state that “the energy propagation is shown as raypaths in the figure, although the energy at the low frequencies used mainly propagates through diffusion”.

where,

$\delta$ – Skin depth ( $m$ )

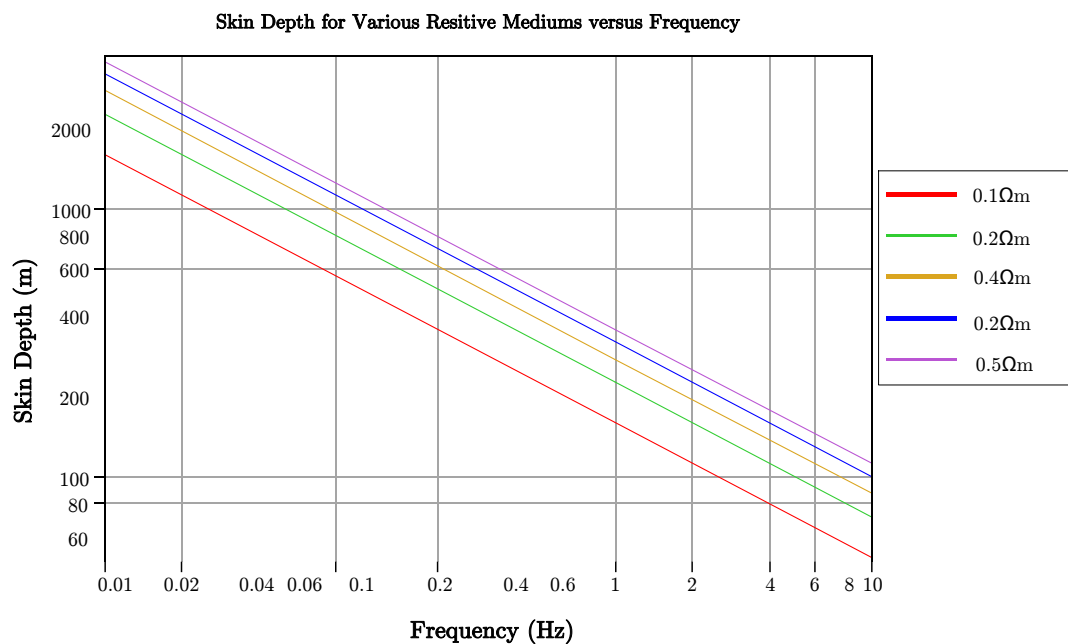
$\mu_0$ – Magnetic permeability in a vacuum  $Hm^{-1}$

$\omega$ – Angular frequency ( $2\pi f$ )

$\sigma$ – Conductivity ( $Sm^{-1}$ )

$f$ – Frequency ( $Hz$ )

The skin depth equation provides the depth of penetration in isotropic conductive whole-space. The skin depth provides a rough estimate of electromagnetic field penetration in complex geo-electrical environments due to the presence of several high contrast boundaries (i.e., air-water, water-sediment and sediment-hydrocarbon boundaries). Sea water is generally considered highly conductive and acts as a low pass filter to incident MT source fields (Constable et al., 1998). Frequency also affects the depth of penetration because energy is lost for every cycle of the wave, causing higher frequencies to be attenuated more, as seen in Figure 1-4. The electromagnetic skin depth is shortest at high frequencies.



**Figure 1-4:** The relationship of skin depth for frequency and conductivity. The skin depth decreases as the conductivity or frequency increases.

MCSEM waveforms are usually variants of the 100 % duty cycle waveform. The square wave contains fundamental frequencies (and odd harmonics) typically within the range of 0.01-10

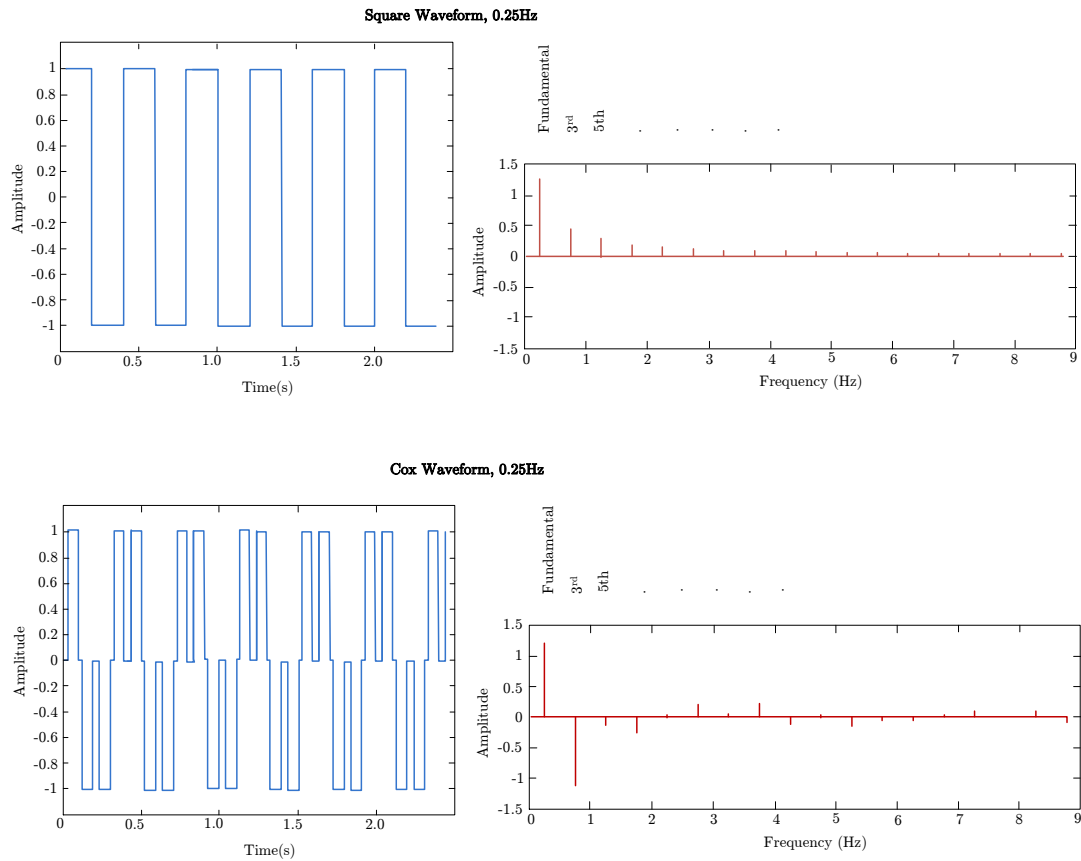


Hz (Pound, 2007).

Myer et al. (2011) have overviewed a number of binary waveform classes (alternating polarity between positive and negative output current). Myer et al. (2011) overview the types of waveform classes including asymmetric, doubly symmetric, singly symmetric (rotationally), doubly symmetric and singly symmetric. The depth of investigation is limited to waveform frequency content. Higher waveform frequencies attenuate more rapidly and are limited to sensing shallower structures. A good transmission waveform choice resolves both shallow, target and deep subsurface geo-electrical properties, whilst being compact, reduces polarizing effects and has a stable controlled phase. As a result, there has been a transition from simple singly symmetric square waves to binary and ternary waveforms such as the doubly symmetric “Cox” (Constable and Cox, 1996) waveform because of the controlled phase reducing polarizing properties (see Figure 1-5). The waveforms remain low frequency variants of the square waveform despite the transition to more complex waveforms. Waveform monitoring is routinely used for stable and consistent signal phase measurements to ensure waveform stability (MacGregor, 2006). The depth of investigation, resolution and sensitivity to the hydrocarbon body is influenced by the frequency content overall.

### 1.7.2 Multi Component Receivers

Technology during the late 1990’s underwent major advancements notably by organisations such as Scripps Institution of Oceanography (Constable et al., 1998). The MCSEM method uses receivers modeled on marine magnetotelluric instrumentation from this period. Receivers have a number of recording devices, including a digital magnetic compass/tilt-meter which records the orientation, a timing system which is synchronised pre and post deployment and magnetic and electric sensors recording multiple axial directions. Receivers record magnetic and electric field time series data. The horizontal electric field receivers are composed of silver-silver chloride electrodes which are between 1 m and 10 m in length (Pethick, 2008). A vertical electric dipole measures the vertical field component and is typically much shorter and light weight (i.e., the Mk II/III Scripps receiver contains a 1.5m long vertical dipole) (Constable, 2013). The magnetic field is typically recorded by light weight induction coil magnetometers (Key, 2003) (See Figures 1-6 and 1-7. The typical components which are detected by commercial designs are x and y magnetic and x, y and vertical electric field directions. The vertical magnetic field is insensitive to thin resistors such as hydrocarbon. The magnetic field sensor is also heavy and its addition to the receiver greatly increases cost. Many commercial operators omit this sensor from their equipment as a consequence of this.



**Figure 1-5:** Typical transmitted MCSEM waveforms and the associated frequency spectra. The frequency spectrums are usually dominated by the fundamental frequency and its harmonics. Waveforms with both low and high frequencies allow both near surface and target geo-electric properties to be resolved. There has been a transition from the singly symmetric waveform (Square wave) to doubly and ternary symmetric waveforms due to phase stability, frequency content and polarizable properties.

There are numerous receiver parameters to be considered when choosing the most suitable receivers for the survey (as seen in Table 1.2). Key attributes to consider when planning a CSEM survey include the noise floor of the instrument, timing calibration, timing stability, battery type and energy use, recording capacity, response calibration, navigation and seafloor orientation. Receiver navigation can be poor (e.g., receivers positioned greater than 5 m accuracy) and can introduce measurable variation (i.e., greater than 1%) at short offsets. The electronic dynamic range of instrumentation is important because of large variations in the signal strength. For instance, electric field voltages can range several orders of magnitude (i.e.,  $1V/Am^2$  to  $10^{-16}V/Am^2$  or lower). 24-bit analogue to digital converters with pre-amplifiers enable high resolution data to be recorded at all source-receiver offsets without signal saturation (Phillips, 2007).

The main source of electric field receiver noise above 1 Hz is caused by amplifier and electrode induced noise rather than ambient noise (Constable and Weiss, 2006 and Hoversten et al., 2006). There is an inverse relationship between the noise level of electric field receivers and the frequency. For example OHM's EFMALS III, has a noise floor of  $1nV/m/\sqrt{Hz}$  (MacGregor et al., 1998). The receiver can detect and resolve smaller amplitudes for higher frequencies. Most MCSEM receivers have a electric field noise floor around  $1 \times 10^{-15}V/Am^2$  and  $4 \times 10^{-12}T$  at 1 Hz for magnetic fields assuming a source dipole length of 300 m and a transmission current of 500 A (i.e.,  $150,000Am^2$ ).

The total noise is given by equation 1.2 and the electric field noise floor (1.3) is the total noise normalized by transmitter moment and receiver electrode dipole arm length:

$$v_n^2 = e_n^2 \Delta f \quad (1.2)$$

$$\eta = \frac{v_n}{Ild} = \frac{\sqrt{e_n^2 \Delta f}}{Ild} \quad (1.3)$$

where,

$v_n$ — Total noise  $3 \times 10^{-10}V$

$e_n$ —Internal amplifier noise (V)

$d$ — Dipole arm length(m)

$v_n/d$ — Electric receiver field noise floor (V/m)

$I$ — Current(A)

$l$ — Transmitter dipole length(m)

Receiver Features	Typical Attribute
Electric Field Noise Floor	$< 10^{-15} V/Am^2$ (at 1Hz)
Magnetic Field Noise Floor	$< 10^{-6} nT^2/Hz$ (at 0.1Hz)
Timing Stability	$< 1$ in $10^6$ intervals result in drift ( $< 1ms/day$ )
Battery Capacity	6-18 days of continuous logging
Storage Capacity	$> 1GB$
Receiver Dipole Arm Length	1 – 10m
Electric Field Receivers	$E_x(inline)$ and $E_y(crossline)$
Magnetic Field Receivers	$H_x(inline)$
Sampling Frequency	128Hz
Dynamic Range	24bit
Sensitivity	2pV/count
Depth Rating	3000 – 6000m
Other Recording Devices	Temperature sensor, magnetic compass Inclinometer, Horizontal magnetic field channels

**Table 1.2:** Typically encountered receiver features and attributes. These values have been taken from two commercial contractors, OHM’s EFMALS III (OHM, 2008) and WesternGeco (WesternGeco, 2008) receivers.

At 0.1 Hz the average recording period is 10 s and the total noise ( $v_n$ ) is  $3 \times 10^{-10} V$  RMS. Commercial EM receivers operate with an electric dipole arm length of 8 to 10 m, however newer lower noise models have been developed to operate with an electrode spacing of 1 m (Quasar, 2012). Their receiver is seen in Figure 1-8.

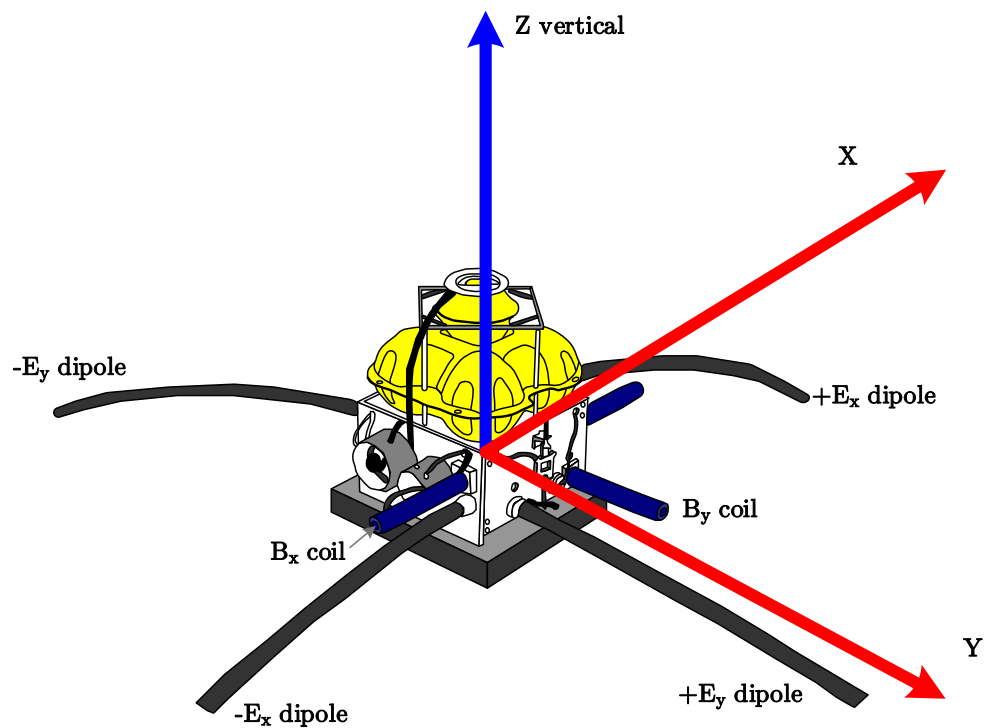
Commercial operators transmit a high amplitude current in excess of 1000 A at peak output. The higher the transmitter moment, ( $I \times l$ , where  $l$  is a transmitter length and  $I$  is current) the better the signal to noise. The noise floor  $\eta$  for a 100 m long transmitter operating at 1000 A is  $4 \times 10^{-16} V/Am^2$  at 0.1 Hz is given by equation (3). This electric field noise floor is close to the values achieved in very deep water marine CSEM surveys.

The antenna length can be extended to improve the signal to noise ratio of the receiver. This voltage is proportional to the receiver dipole length (Flosadattir and Constable, 1996). Synchronous stacking can be also used to recover a repetitive signal from the random ambient or instrument noise. The limits and features of electromagnetic systems over next few decades will improve with technological advancements. Hence the features seen in Table 1.2 should only be taken as a guide. In summary, the main features to consider when planning a survey are the noise threshold of both the E-Field and B-Field sensors and which electric and magnetic axial directions the device will record.

### 1.7.3 Transmitter

The marine controlled source electromagnetic method uses a horizontal electric bipole dipole as a transmitter. The transmitter consists of two electrodes separated between 100-300 m. The transmitter is towed 25-50 m above the seabed at a speed of 1.5 to 2.0 kn (WesternGeco, 2008). The transmitter uses a powerful source and generates around 1000 A. Two examples of transmitters are seen in Figure 1-9 and Figure 1-10. Figure 1-11 is a schematic showing the general components of an electromagnetic transmitter. There are numerous commercially available transmitters that can be selected prior to surveying.

Features to consider when selecting a transmitter include the peak output dipole moment and the stability of the output waveform. Waveform polarity transitions have a temperature-dependent latency ( $1-2 \mu s$ ) that decreases as the transmitter temperature rises and stabilises (WesternGeco, 2008). The output waveform's phase must be stable to around 1 part in 108 (1 ms/day) otherwise the received waveform will be artificially out of phase with

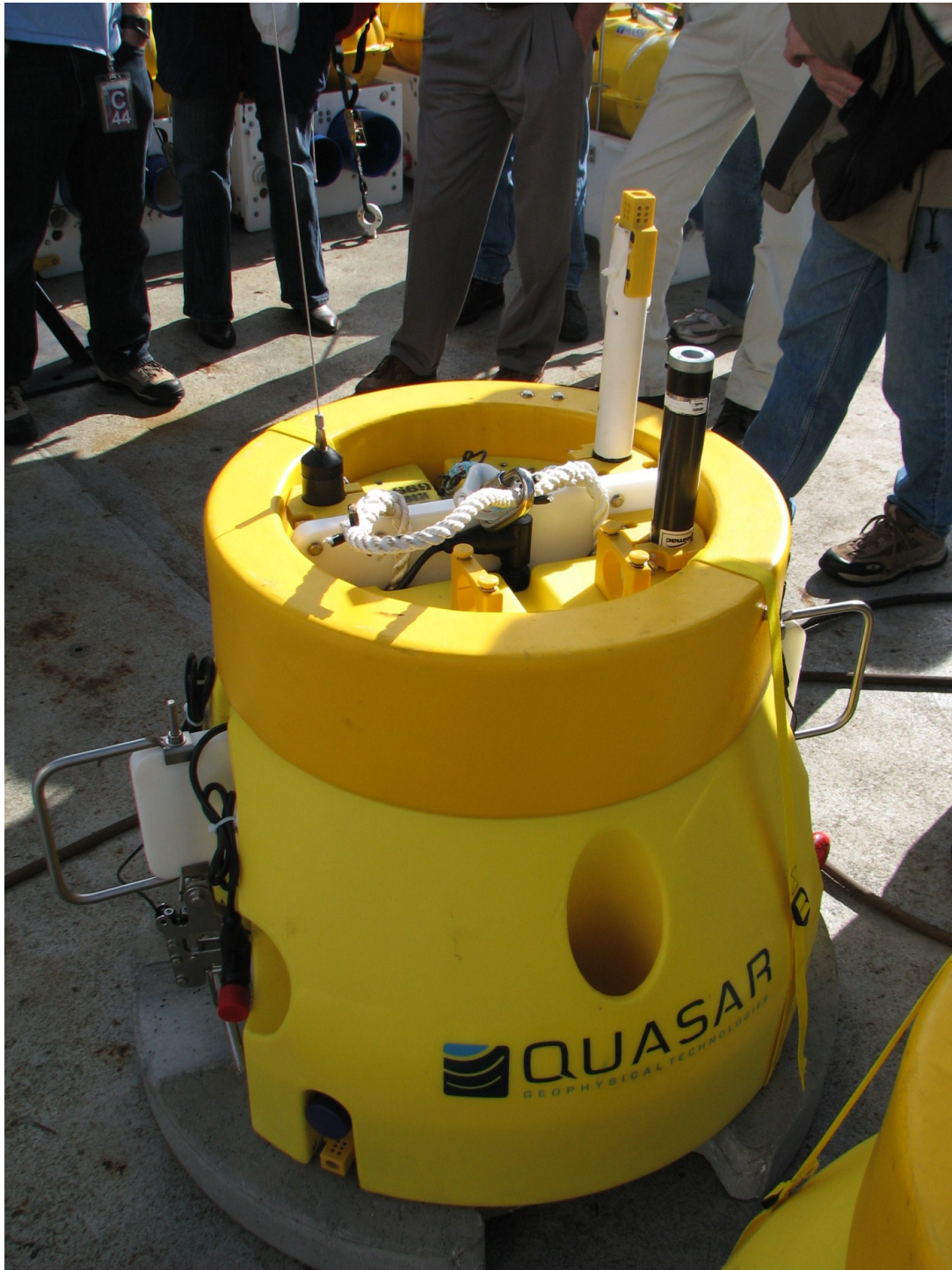


**Figure 1-6:** Diagram of a typical marine CSEM multicomponent receiver. The receiver is the Scripps Institution of Oceanography Mark III design, which only records inline magnetic and electric fields and crossline electric field (reproduced from Constable et al., 1998 and Key, 2003)



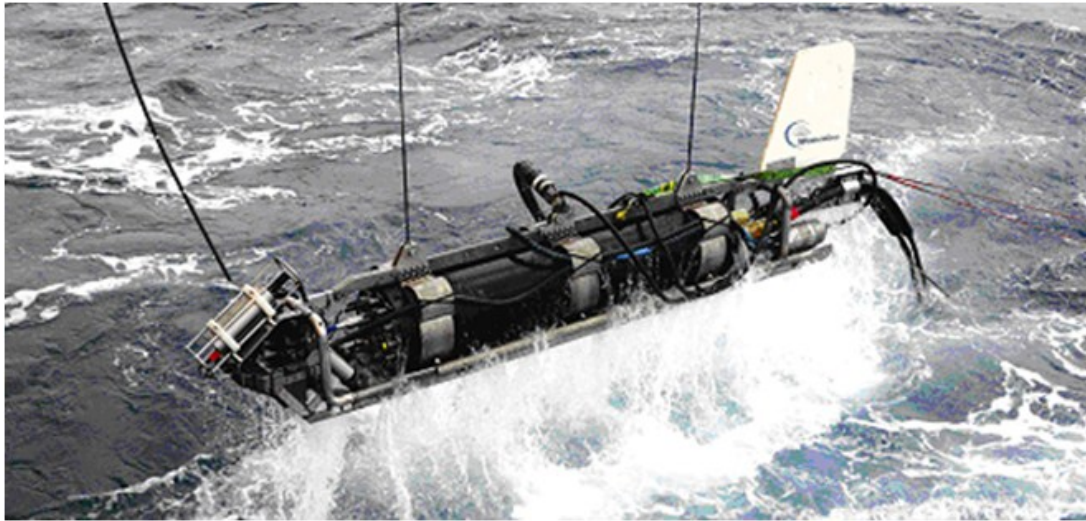
**Figure 1-7:** A receiver from the Scripps Institution of Oceanography. The receiver has all components except the vertical magnetic field. This image was obtained aboard the Scripps Institution of Oceanography's ship, R.V. Roger Revelle, 2008.



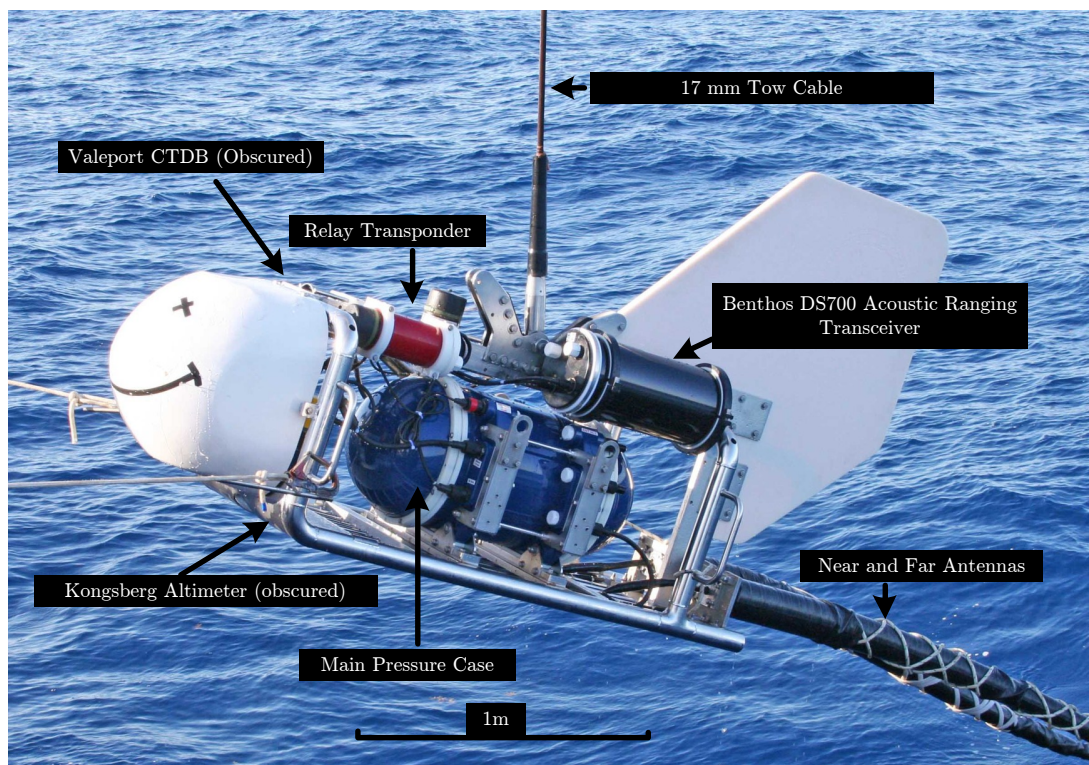


**Figure 1-8:** Quasar’s low noise MCSEM receiver. Quasar Geophysical Technologies took an underwater sensor they developed for the U.S. Navy and redesigned it for ocean bottom surveying with its QMax EM3 underwater electromagnetic receiver (Quasar, 2012). It is the only ocean bottom CSEM receiver to contain all six electric and magnetic components. This image was obtained aboard the Scripps Institution of Oceanography’s ship, R.V. Roger Revelle, 2008.

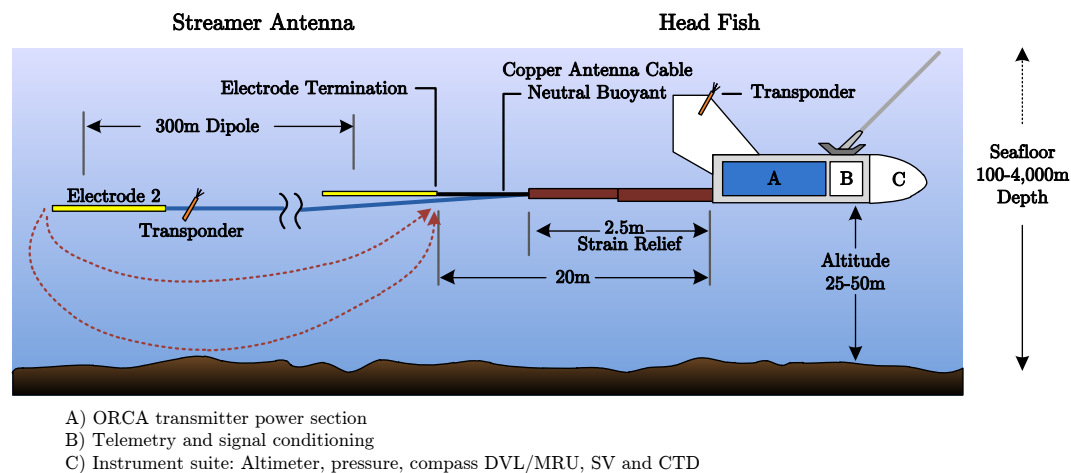




**Figure 1-9:** Picture of a commercial transmitter (Reproduced from WesternGeco, 2008).



**Figure 1-10:** Annotated photograph of the Scripps undersea electromagnetic source instrument (SUESI) horizontal electric dipole source (Modified from Key, 2009b)



**Figure 1-11:** Typical schematic of a marine CSEM transmitter and HED (Reproduced from WesternGeco, 2008).

the transmitted waveform. Phase is controlled by GPS and consistently monitored during the survey.

The dipole moment is the length of the electrodes multiplied by the transmitted current. If the dipole moment is doubled, the amplitude recorded at the receiver is also doubled. The source is deep-towed to optimise signal coupling with the sea floor and to reduce the conductive losses. Heights of around 25-50 m are chosen but can be varied in accordance to bathymetry, ocean conditions and the coupling required. The altitude of the transmitter is constantly monitored by using an altimeter on the source. The tow speed of the transmitter should be considered prior to surveying as it affects the quality of the received data. A receiver records 50 transmitter cycles every 100 m for a given frequency of 0.5 Hz and a towing speed of 1 m/s. Stacking reduces the noise by a  $1/\sqrt{N}$  times and improves with slower towing speeds (Hoversten et al., 2006).

## 1.8 Factors Affecting Survey Design

### 1.8.1 CSEM noise sources

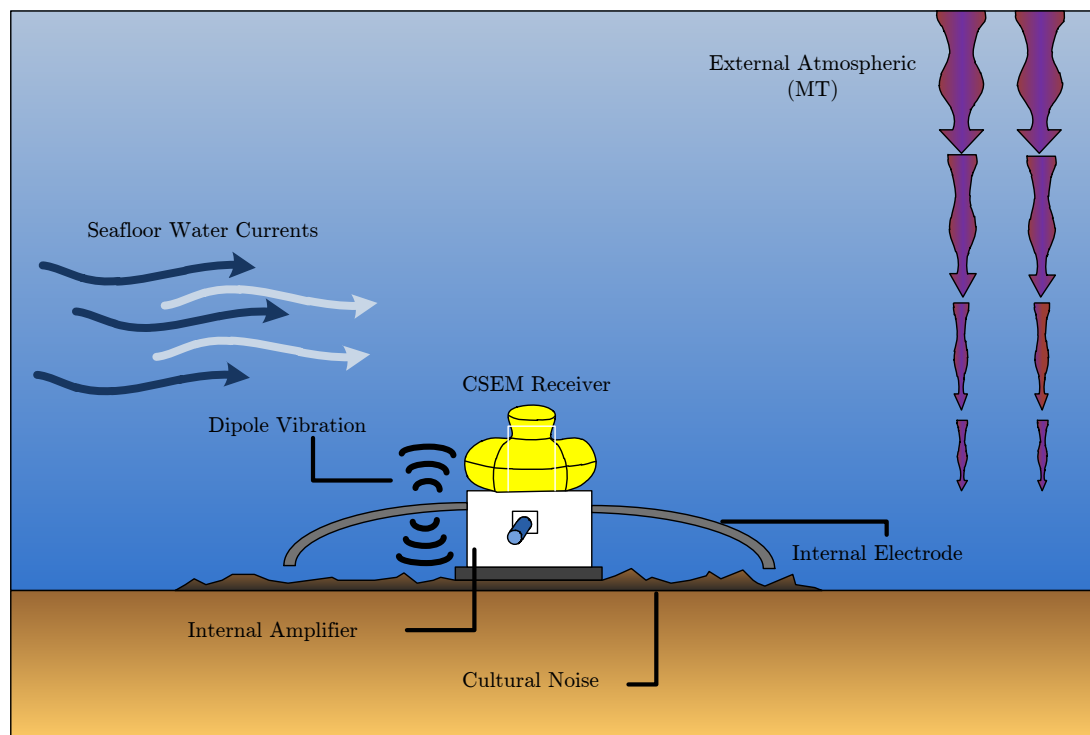
The success of an MCSEM survey depends on many factors including electromagnetic sources of noise. Amundsen et al. (2006), Maaß and Nguyen (2010), Ziolkowski and Wright (2010) cover some aspects of the noise sources found in CSEM. These noise sources include sea water currents, magnetotelluric activity, bipole vibration, internal electrode and amplifier noise and cultural effects, as seen in Table 1-12 and Figure 1-13. It should be noted that there is disagreement as to whether the air wave effect is a noise source or a legitimate signal. Amundsen et al. (2006) have suggested it is a noise to remove from data while others have suggested that this effect could be utilised (e.g., Wirianto et al., 2011).

MacGregor (2006) and Constable (2010) have stated that vibrations of the dipole receiver arms can induce an unwanted signal. A vibration of less than 1 mm for a 10 m dipole can produce an induced voltage comparable to the target signal. These movements can be limited by using bottom weights, weighting each electric receiver dipole arm with glass rods and by using farings on dipole arms.

Spheric noise and ocean induced fields can contaminate the received data at lower frequencies ( $<1$  Hz). The magnitude of spheric noise reaching receivers vary with water depth. Increases in water depth improve noise recording conditions of surveys because seawater acts as a shield from external magnetotelluric signals (Kong, 2002). The motion of a conductor in an electric field will have a voltage induced in accordance with Faraday's law. Seafloor water currents can dominate the intermediate frequencies in a survey. Transmitter feathering caused by seawater currents is also influential. Water cross currents, (i.e., strong water currents resulting from funnelling of water through underwater canyons, river exits etc...) may result in transmitter to become oblique or vary in azimuth. This situation should be avoided or the transmitter orientation must be taken into consideration when processing, performing modelling or inversions. Noise sources including "air-wave", cultural noise, spherics, dipole arm vibrations and water currents must be all considered when dealing with MCSEM data.

Noise Source	Description
Seafloor currents (<1Hz)	The motion of a conductor in an electric field will induce a voltage
Spherics (<1Hz)	Lightning and ionic field disturbances resulting in low frequency noise. Spheric noises reduce with water depth.
Cultural	Highly conductive or resistive materials close to the receiver will skew the signal
Bipole vibration	Vibrations of the electric dipole receiver arms can induce a voltage comparable to the target signal
Internal electrode and amplifier noise(>1Hz)	The instrument's internal noise

**Figure 1-12:** A list of MCSEM noise sources to consider.



**Figure 1-13:** Overview of standard MCSEM noise sources. Noise sources can be split into two areas, external and internal. Internal sources are within the instruments which are internal amplifier and electrode noise, whilst external noises are caused by seafloor water currents, magnetotelluric (MT) signals, dipole vibration and cultural noises. It is best to conduct a survey in deep water to reduce the effect of seafloor water currents and external atmospheric noise.

### 1.8.2 Target Style Considerations

The geo-electrical environment effects target detectability and must be considered. Considerations include water depth, target depth, geological type of target, reservoir style, resistivity contrast, resistive non-hydrocarbon geological targets, reservoir complexity and the purpose of the survey (Peace, 2005).

Peace (2005), Pethick (2008), Orange et al. (2009), Sasaki and Meju (2009) and Weidelt (2007), have covered the factors influencing the detectability of a target. Water depth and bathymetry is one of the biggest factors influencing detectability. The bathymetry influences the onset of the airwave which may mask a hydrocarbon response. Water bottom channels, canyons and sloping or having the target sit above the water bottom when surveying off a shelf edge will influence the survey Pethick (2008). Water channels and canyons can produce lateral water current flow which can cause transmitter feathering and movement of receiver electrodes. Secondly, the target depth from the water bottom and aerial size of the target compared to the depth affects the detectability of the target. Targets smaller in aerial size in comparison to their depth are harder to detect. Thirdly, the geological type and shape of the target influences the receiver response on the ocean floor. Resistivity contrast also influences a survey plan. If the resistivity contrast between the hydrocarbon and the host is insufficient, it will be unlikely that the survey could detect the hydrocarbon. Resistive structures which are not a result of hydrocarbon, such as salt diapirs, could also lead to false positives. Therefore it is necessary to model a range of geological settings. Salinity and water temperature influences the resistivity of the water column (Orange et al., 2009). Lateral variation caused by salinity cells or temperature variation will greatly influence inversions requiring the water column to be structured as 1D layering. Lastly, the purpose of the survey influences the final survey design. For example, reconnaissance surveys utilise widely spaced receivers and transmitter lines to target hydrocarbons. 3D surveys use many closely spaced receivers and densely positioned transmitter line locations at multiple azimuths to characterize or appraise a known field Pethick (2008). All geological and survey considerations are encapsulated in Figure 1-14.

### 1.8.3 The Airwave Problem

The airwave is a complex interference effect between the air, water and seabed layering. The airwave poses problems for MCSEM surveys because it masks the received seabed signals at far offsets (Eidesmo et al., 2002). It can be identified by a gradient break in inline electric

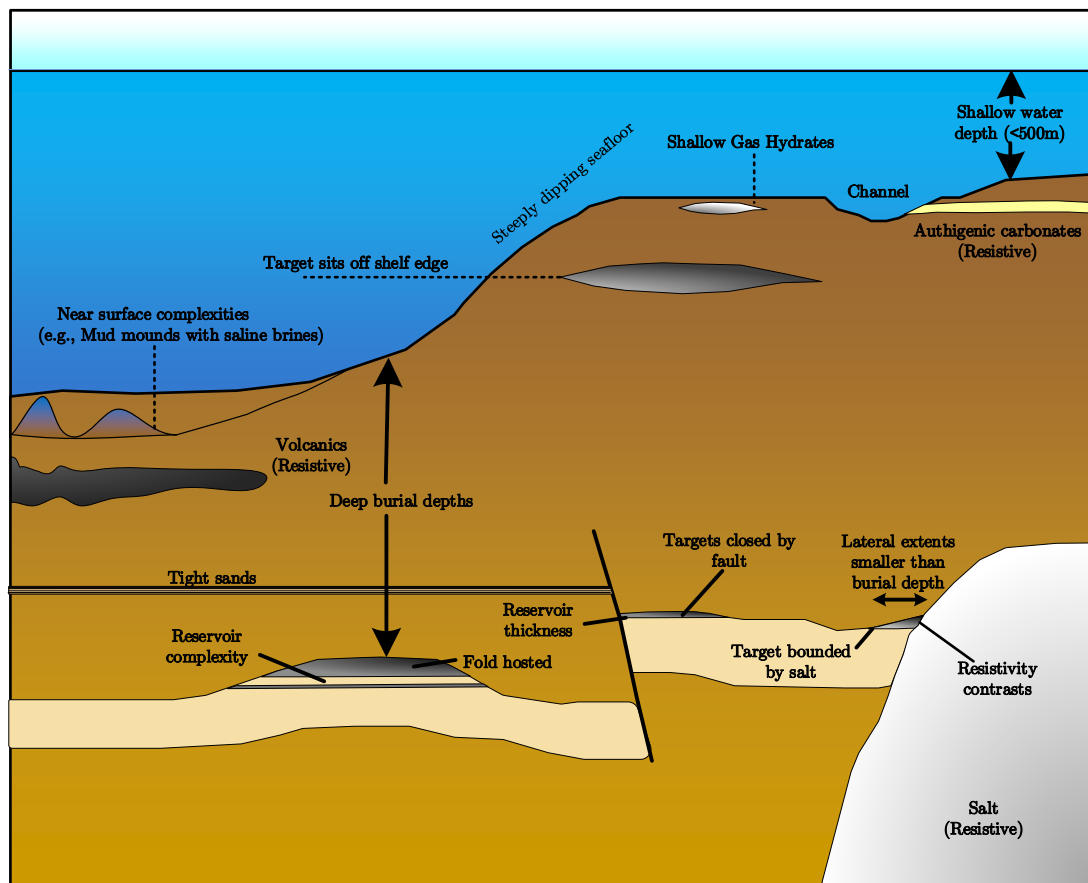


Figure 1-14: Geological considerations for MCSEM survey planning.



field profiles and there is also a total phase lag which is dependent on the offset and water depth (Eidesmo and Ellingsrud, 2002). The airwave is affected by the transmitter-receiver offset, transmitter dipole orientation, transmission frequency, resistivity structure and the water depth. Eidesmo and Ellingsrud (2002); (Eidesmo et al., 2002); Wirianto et al. (2011) have offered solutions to the airwave problem but none offer a 'silver bullet' solution. It is an ongoing problem for industry. The companies EMGS, OHM and Fugro Electro Magnetic are working to resolve it by using various data processing techniques and by limiting its effect by using novel acquisition practices (Ellingsrud et al., 2002). Possible solutions to the airwave problem include selecting acquisition parameters that limit the generation of an airwave, signal processing and even using information in the airwave (Weidelt, 2007). The company, PGS, has claimed to have mitigated the airwave by transmitting and measuring in the time domain. This has reduced the problems associated with the airwave masking deeper responses, but the air wave is still present in the data and can mask subocean responses given the right conditions. Forward modelling should be performed to provide the airwave influence prior to surveying (Mittet, 2004 and Johansen, 2005).

Constable and Weiss (2006) have suggested that the air wave effect can be reduced by utilizing a vertical dipole transmitter. Air-water interface coupling is influenced by transmitter orientation. Horizontal current loops create poloidal magnetic (PM) modes which will enhance the air-water interface coupling (i.e., stronger air wave effect), while vertical current loops create transverse magnetic (TM) modes which reduce the airwave's influence (MacGregor, 2006) (See Figure 1-15).

Transmission frequency also affects air wave onset and amplitude (Eidesmo et al., 2002). Eidesmo et al. (2002) found that higher transmission frequencies have a larger airwave effect. They also found that the higher frequencies result in shorter onset air-waves (as seen in Table 1.3). Therefore the benefits of low frequency must be balanced against reduced resolution. The maximum depth of investigation before contamination of the airwave can be calculated by using localization Eidesmo et al. (2002). The depth at which this occurs can be calculated by multiplying the scale factor from Equation 1.4 ( $\alpha$ ) with the water depth (Tompkins et al., 2004). For example, if  $\alpha = 1.76$  and the water depth is 1000 m, then the maximum depth of investigation would be 1760 m.



$$\frac{Re\{k_{H_2O}\}}{Re\{k_{Earth}\}} = \frac{\sqrt{\frac{\omega\mu_{H_2O}}{2}}}{\sqrt{\frac{\omega\mu_{Earth}}{2}}} = \sqrt{\frac{\sigma_{H_2O}}{\sigma_{Earth}}} = \alpha \quad (1.4)$$

where,

$\sigma_{H_2O}$  – Seawater conductivity ( $Sm^{-1}$ )

$\sigma_{Earth}$  – Sediment conductivity ( $Sm^{-1}$ )

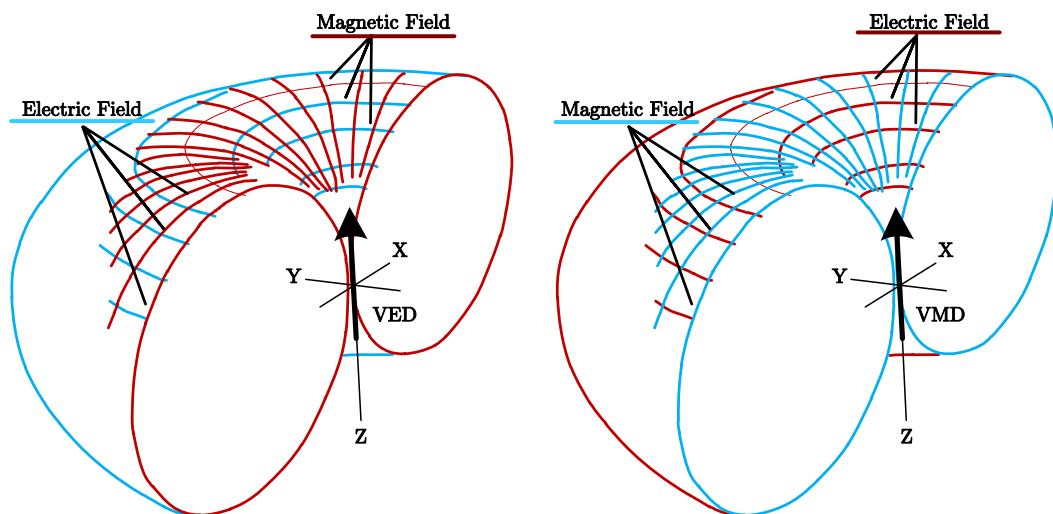
$\alpha$  – Unitless scale factor

Water Depth(m)	0.25Hz	0.5Hz	1.0Hz	2.0Hz
500	4.8	4.0	3.4	3.0
600	5.2	4.3	3.9	3.5
700	5.7	4.7	4.3	3.8
800	6.1	5.0	4.6	4.1
900	6.5	5.4	4.9	4.5
1000	6.9	5.8	5.4	4.9
1200	7.6	6.7	6.1	5.6
1400	8.5	7.5	6.8	6.2
1600	9.3	8.3	7.5	7.1
1800	10.1	9.0	8.3	7.8
2000	11.0	9.8	8.9	8.4

**Table 1.3:** The distance from the source (in km) at which the airwave starts to dominate the overall response. The point at which the response is dominated by the airwave is represented as function of water depth and the signal frequency. Reproduced from Eidesmo et al. (2002).

#### 1.8.4 Seawater Conductivity

Seawater constitutes a large and important element of the geoelectric framework relevant for MCSEM surveying. Determining the correct seawater conductivity is important for both forward modelling and inversion. The conductivity of the sea water varies in the water column and also in the seabed structure itself. Auxiliary instruments record seawater conductivity over the duration of most MCSEM surveys (an example can be seen in 1-16). Sea water varies in resistivity due to temperature, salinity and pressure as described in equation 1.5. The largest variation in sea water conductivity occurs at the near surface (i.e., less than 200 m depth). The sharp gradient in the thermocline is due to temperature variation with depth. Myer



**Figure 1-15:** The magnetic and electric field patterns from vertical electric (VED) and magnetic (VMD) dipoles. Horizontal current loops strongly couple with the air-water interface resulting in a large air wave response. The airwave phenomenon can be minimised by using a vertical electric dipole. Reproduced from MacGregor, 2006.

et al. (2012) have measured this temperature variation and demonstrates the importance of incorporating this effect in any uncertainty analysis.

$$\sigma = 3 + \frac{T}{10} Sm^{-1} \quad (1.5)$$

where,

$\sigma$ — Seawater conductivity ( $Sm^{-1}$  )

$T$ — Seawater temperature (degrees C)

Sea water conductivity is around at  $0.3 \Omega \cdot m$  , typical ocean floor temperatures and reaches a minimum conductivity of  $0.04 \Omega \cdot m$  at  $350^\circ$ . This large variation in conductivity has a significant effect on the bulk resistivity of the formation. Archie's (1942) law can be used to find the saturated formation's true resistivity in  $\Omega \cdot m$  (see equations 1.6 and 1.7).

$$F = \frac{R_0}{R_w} = \frac{a}{\phi^m} \quad (1.6)$$

$$s_w^{-n} = \frac{R_t}{R_0} \quad (1.7)$$

where,

$F$ — Formation Factor

$R_0$ — Formation resistivity when 100 % saturated with brine ( $\Omega \cdot m$ )

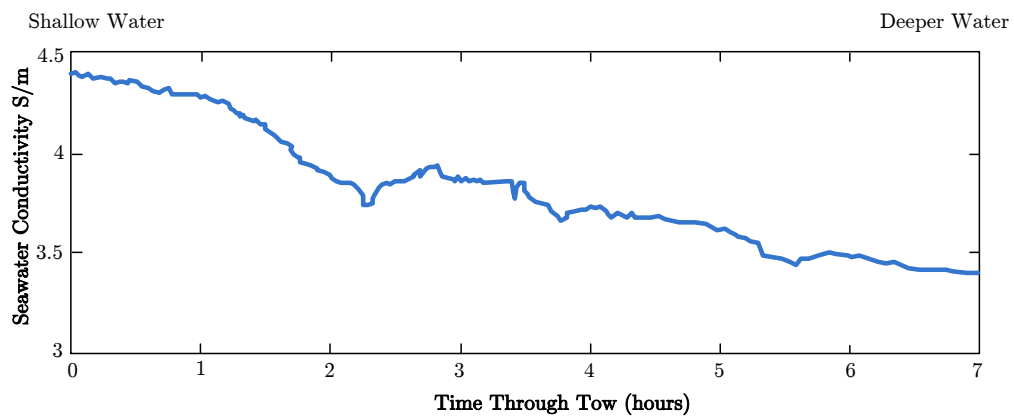
$R_w$ — Fluid resistivity ( $\Omega \cdot m$ )

$R_t$ — Formation resistivity when 100 % saturated with fluid resistivity ( $\Omega \cdot m$ )

$\phi$ — Porosity (%)

$m$ — Cementation factor (between 1.3 and 3)

$a$ — Tortuosity factor



**Figure 1-16:** Typical seawater conductivity measurement over the duration of a typical MCSEM survey. The conductivity varies over time and position. The recorded data should be incorporated into the geoelectric model for forward modeling or inversion. Reproduced from MacGregor (2006).)

## 1.9 An Overview of MCSEM Data Visualization

Visualizing MCSEM data for analysis is complicated because of the limitless possibilities for transmitter-receiver arrangements, transmission frequencies and any geoelectric models. A software platform allowing systematic analysis of possible outcomes from different survey configurations is required. This requires some method for expressing behaviour of the amplitude and phase of the axial (x, y, z), electric and magnetic fields. Traditional visualisation techniques that may assist in displaying the data in an intuitive format for analysis include:

- i 1D profiles
- ii 2D grids

- iii 2D/3D vectors
- iv 3D scalar planes (3D Grids)
- v 3D isosurfaces (i.e., 3D Contours)

### 1.9.1 1D Profiles

Profiles are used extensively in MCSEM interpretation. They are the most popular device used to describe one dimensional datasets where only one independent variable is being tested. Popular examples of using profiles in MCSEM include plotting electric, magnetic field amplitude or phase against offset (for example see Pethick, 2008; Phillips, 2007; Dobrich, 2010; MacGregor et al., 1998 and Paten, 2010).

### 1.9.2 2D Grids and Contours

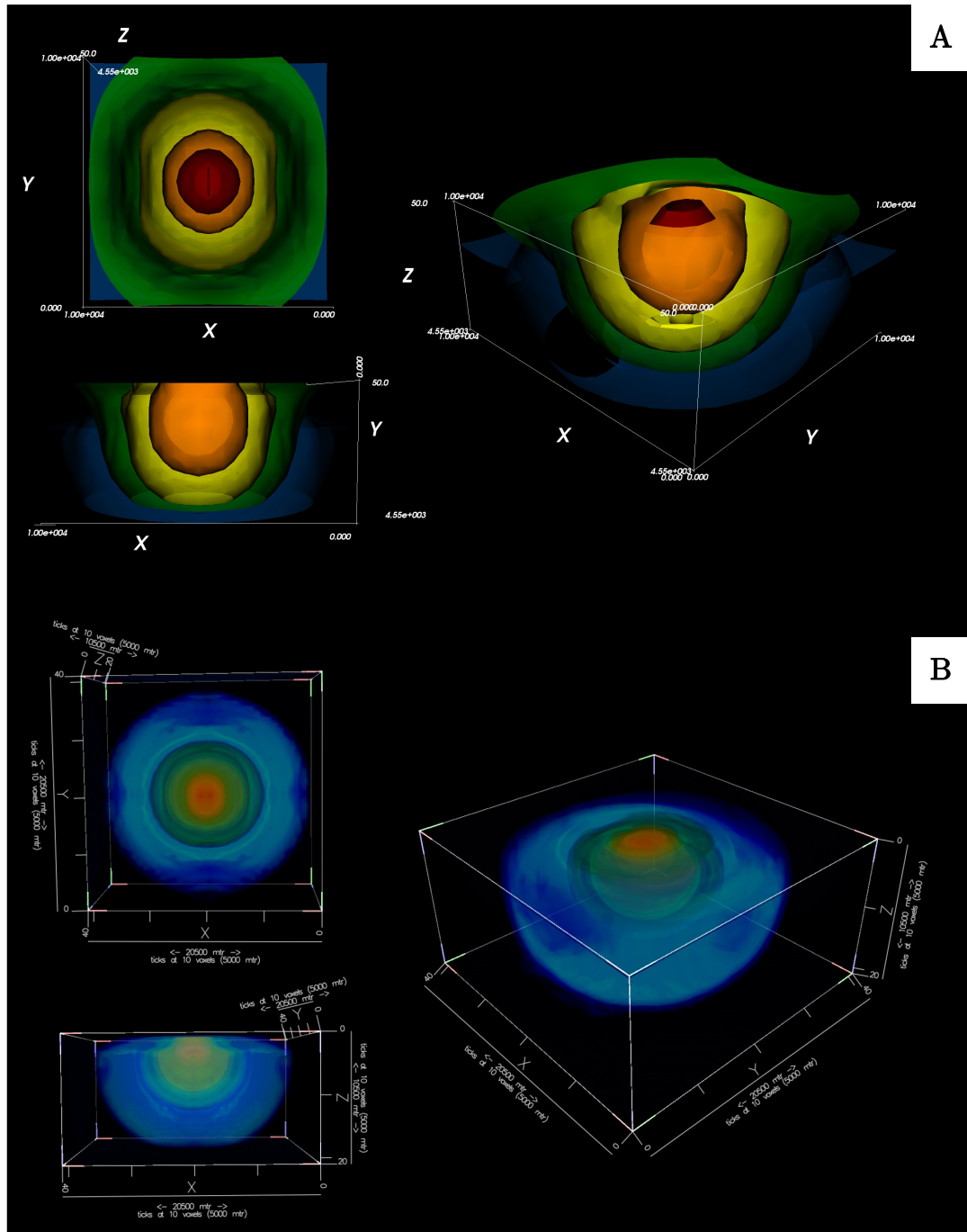
Grids and 2D contours can show scalar data on a 2D plane. Common uses of grids and contours in MCSEM include displaying amplitude, phase or normalized responses versus offsets. Grids with multiple contour overlays are often cluttered and convoluted, making interpretation difficult.

### 1.9.3 Isosurfaces

Isosurfaces represent a surface of scalar equipotential value and is the 3D contour. Much like 2D contours, multiple isosurfaces can clutter a visualisation. 2D contours can represent two variables and a scalar whilst isosurfaces can test three variables and a scalar. Two examples of isosurfaces can be seen in Figure 1-17.

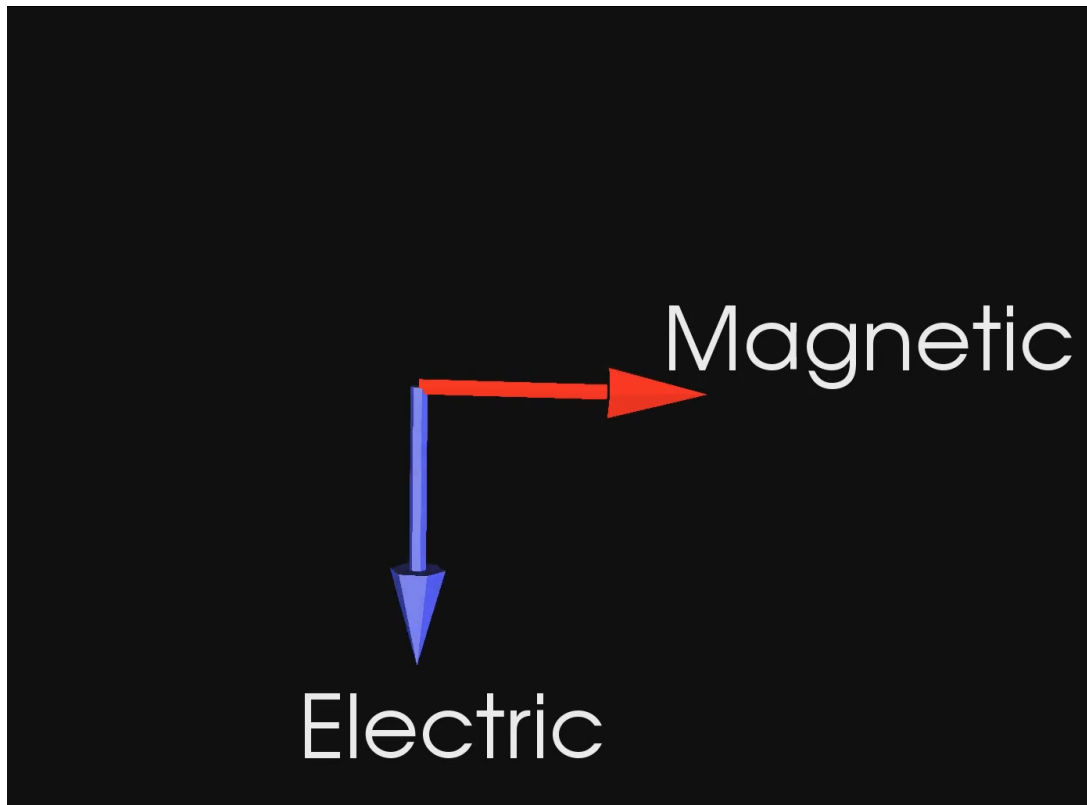
### 1.9.4 Vector Glyphs

A vector glyph is a 3D object containing geometric and magnitude information. In mathematics, they are essentially Euclidean, geometric or spatial vectors. Vectors are not commonly utilised in geophysical visualisation. However Weidelt (2007) and Harris and Pethick (2008) offer some examples of 2D vector representation. 3D vector glyph can be easily applied to represent electromagnetic fields. Vector algebra is used to compute various pieces of information including, Poynting, current density vector and scattered, total and background responses.



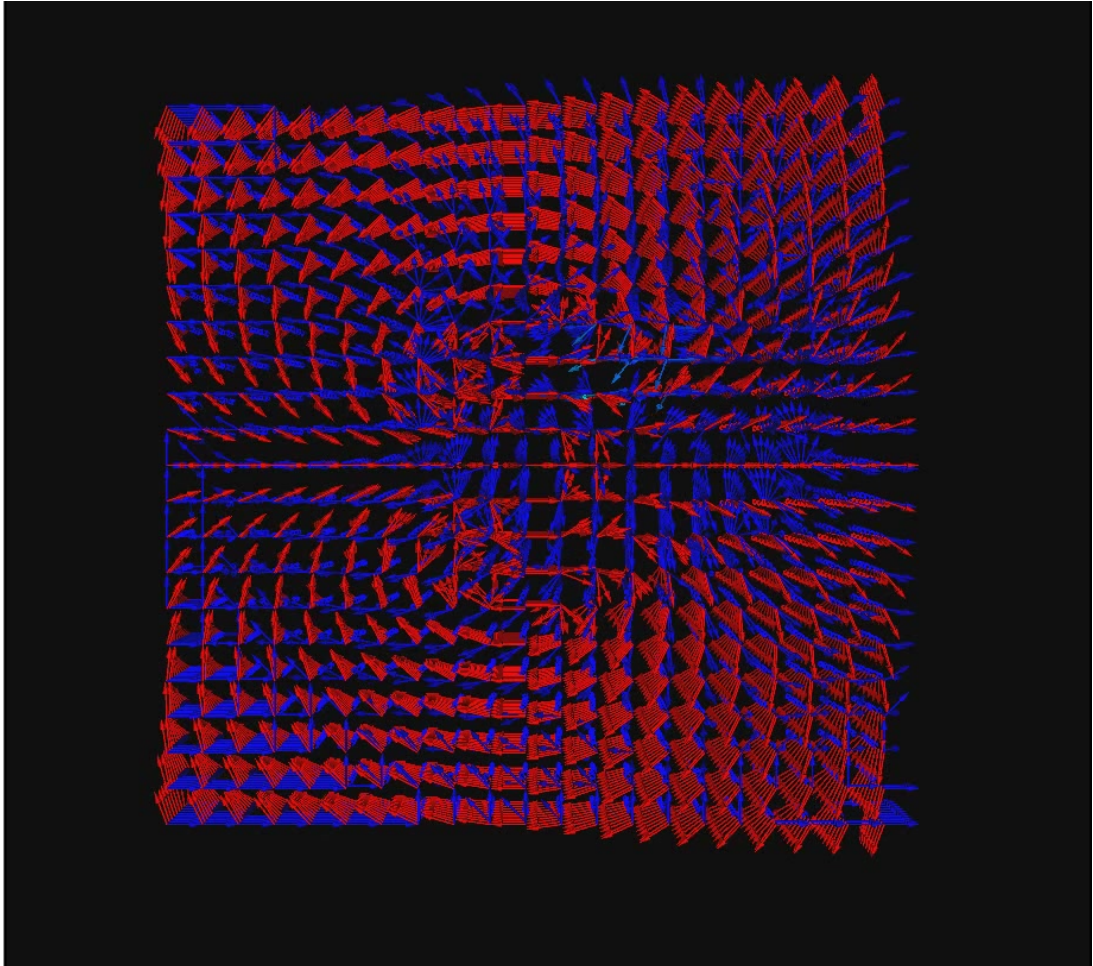
**Figure 1-17:** Example of isosurfaces at  $10^{-15}$  (blue),  $10^{-14}$  (green),  $10^{-13}$  (yellow),  $10^{-12}$  (orange),  $10^{-11} \text{ V/Am}^2$  (red), being used to represent the total electric field behaviour for a single time slice. Generated in MayaVi (top) and Drishti (bottom). (Derived from Pethick (2008))

Multiple attributes can be visualized using vectors as the direction, scale, length and color can all contain attributes. As a result, vectors can represent scalar amplitude, scalar phase, time amplitude vector, real and imaginary vectors (See Videos 1-18 and 1-19). It is difficult to use vector glyphs to display field paths as they only visualize the field direction at a point in time.



**Figure 1-18:** Video visualizing an electric and magnetic field vector.

See [Videos/EHVectors.avi](#) for video source



**Figure 1-19:** A video showing the volume electric (blue) and magnetic (red) vectors. The video is comprised of  $21 \times 21 \times 10$  electric and magnetic field receivers. Electric fields and magnetic fields are complex and the right representation is required to investigate the data.

See [Videos/EHVectorsComplex.avi](#) for video source





## Part I

# Development of an Electromagnetic Framework



# Designing the Electromagnetic Data Model

Chapter 2 covers my flexible electromagnetic data model. The data model has been designed for use in most controlled source electromagnetic problems. I have written this for the benefit of geophysicists rather than computer scientists. The chapter overviews object oriented programming (OOP) and the unified modelling language (UML). I show how real world electromagnetic structures are translated into a data model using OOP principles and the UML representation. This chapter to my knowledge represents the first example of designing an electromagnetic data model for geophysical applications.

## Contents

<b>2.1</b>	<b>Data Model Overview</b>	<b>40</b>
<b>2.2</b>	<b>Requirements</b>	<b>40</b>
<b>2.3</b>	<b>Floating Point versus Double Precision</b>	<b>41</b>
<b>2.4</b>	<b>Object-Orientated Programming</b>	<b>41</b>
2.4.1	Unified Modelling Language and Class Diagrams	42
2.4.2	Generalisation and Inheritance	46
2.4.3	Implementation and Interfaces	46
<b>2.5</b>	<b>Electromagnetic Project Structure</b>	<b>47</b>
2.5.1	Transmitters and Receivers	50
2.5.2	System Configuration	54
2.5.3	Waveforms and Windows	61
2.5.4	EM Data Representation	65
2.5.5	Geo-Electrical Earth	70
<b>2.6</b>	<b>Data Structure Development</b>	<b>78</b>
<b>2.7</b>	<b>Conclusion</b>	<b>82</b>

## 2.1 Data Model Overview

There is a need for a generic electromagnetic data model. Many proprietary data structures are used for MCSEM. There is no universal or standard data structure or file format for the MCSEM method. In this chapter I propose and test my data structure. The developed software is built upon the previously described data model. Geophysical electromagnetic methods generate diverse ranges of complex datasets. These datasets are manipulated and analysed by an exhaustive number of methods. I am focusing my data model on processed MCSEM datasets, which are relatively small (i.e., hundreds of megabytes, when processed) in comparison to marine 3D seismic data (i.e., gigabytes). This chapter translates the major real world controlled source electromagnetic components into an object-oriented form for use in a larger software package.

## 2.2 Requirements

The data model is required to represent all aspects of any controlled source electromagnetic survey. The MCSEM method is constantly changing. This evolving method prevents the development of a single “static” MCSEM data structure. Traditional MCSEM surveys consist of a towed electric bipole source that may transmit a range of waveforms. The generated EM field is recovered by ocean bottom receivers. This method may not always be the standard. MCSEM time-domain oriented setups (Ziolkowski, 2008), towed transmitter-receiver arrays (Mattsson et al., 2010), down-hole marine CSEM systems (Scholl and Edwards, 2007) and mixed systems have been used and will continue to be developed. The data model structure must be able to handle a range of survey designs (i.e., borehole, towed and traditional CSEM) and geo-electrical earth model type (i.e., 1D layered, 1D layered anisotropic, 2D/3D finite difference, 2D/3D finite element and 3D integral equation models). The software design must also have the flexibility to incorporate changes and updates whilst maintaining the general electromagnetic data structure. The data model must:

- i match real world objects
- ii incorporate any transmitter type
- iii incorporate any receiver type
- iv be flexible to incorporate most survey designs
- v incorporate both time domain and frequency domain waveforms

- vi incorporate both time domain and frequency domain data types
- vii incorporate any geo-electrical model type
- viii easily incorporate most electromagnetic algorithms
- ix enable the easy import and export of datasets
- x be efficient data manipulation to enable real-time interactive modelling
- xi be easily modifiable and maintainable

These requirements provide a flexible base to handle any controlled source electromagnetic survey and dataset. This flexibility avoids potential issues when trialing novel or experimental survey designs, not only for marine CSEM but for most controlled source electromagnetic surveys.

## 2.3 Floating Point versus Double Precision

Double precision was chosen over floating point precision. Double precision can be used to improve numerical stability because of increased precision. Single floating precision is 32bit. This equates to a minimum value of approximately  $1.4 \times 10^{-45}$ . Double precision is 64bit with a minimum value of  $5 \times 10^{-324}$ . Deep ocean marine CSEM can encounter incredibly small noise floors ( $10^{-16}V/Am^2$  for electric fields and  $10^{-19}T$  for magnetic fields). The floating precision limit becomes significant when sequential computations introduce precision errors. Cross products (i.e., in the case of the Poynting vector) can reach the limits of floating point precision. For example, the cross product of the electric field and magnetic fields can produce values on the edge of the minimum 32 bit floating value (i.e.,  $10^{-45}W \cdot Am^{-2}$ ).

Double precision takes longer to compute (10 to 15% slower) on modern CPU's and uses up twice as much memory. Despite memory and performance shortfalls, all numbers are defined by double precision to ensure numerical stability.

## 2.4 Object-Orientated Programming

Most developers hope to achieve stable and easily maintainable software. Object-oriented programming is one approach that can be used to achieve this goal. The object oriented

programming (OOP) paradigm translates real world objects into a data structure. OOP paradigms produce easily maintainable software architectures, enabling flexibility through modular designs (Smith, 2011). A number of OOP languages exist including Java, C++, Visual Basic.NET, C# and Smalltalk. There has been an increased use of OOP languages such as C++ and Java over the last decade due to ease of creation, maintenance and intuitive design associated with their use (Al Dallal and Briand, 2010). Objects form the basic units of OOP software design. In Java these objects are called classes (Wu, 2003). These classes contain the attributes and functions which are related to the purpose of the objects. OOP translates real world objects and ideas into their digital equivalent.

I have chosen Java as the primary programming language because of its object-oriented design, stability, platform independence and the availability of public software libraries. Java is an extremely structured programming language, unlike Fortran90 and C programming. Java and OOP allow a smooth transition from real world MCSEM surveys to a software structure.

I will overview and describe several concepts related to object orient programming and basic software engineering for the benefit of readers unfamiliar with this content. These concepts include class diagrams, inheritance, interfaces, methods and attributes.

### 2.4.1 Unified Modelling Language and Class Diagrams

In Java, objects are defined by classes. Class diagrams describe the structure and relationships between other classes. The unified modelling language (UML) visualizes the class structure (Cali et al., 2002). A class diagram maps real world objects into programming classes. A Java method performs an action with the object and its attributes (i.e., a function). Class diagrams are strictly defined and are divided into sections including,

- i name (top of UML class)
- ii attributes (middle of UML class)
- iii methods (bottom of UML class)

The relationships between other classes are shown using lines, symbols and numbers. Types of relationships are shown by a symbol. The numbers define the multiplicity, which defines the number of instances of a class for each class relationship. A list of relationships, symbols and


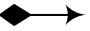
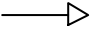

meanings are shown in Table 2.1. Relationships describe how the class fits into the larger data model. These relationships include,

- i aggregation
- ii composition
- iii generalization

Aggregation represents a strong relationship between classes and is symbolized as a hollow diamond (Cali et al., 2002). Both classes can exist without the presence of each other but are strongly linked. Consider the relationship between a airplane and a passenger as an example. A passenger can exist without a plane and vice versa. Composition represents ownership and is symbolized as a solid diamond. Composition implies that one class cannot exist without the other. Now consider the relationship between an airplane and its wings (i.e., an aircraft is composed of two wings). An aircraft cannot exist without wings. Generalization indicates a specialized relationship and is symbolized as empty triangle. It is also known as inheritance, a concept that will be covered in depth later in this chapter. A relationship's multiplicity describes the number of instances per object. Consider the previous example of an aircraft with wings. The multiplicity of an aircraft with wings is two to one. Every aircraft is composed of two wings and each wing belongs to a single aircraft. UML, through the use of symbols, arrows, classes and numbers, represents the internal data structure in an intuitive way.

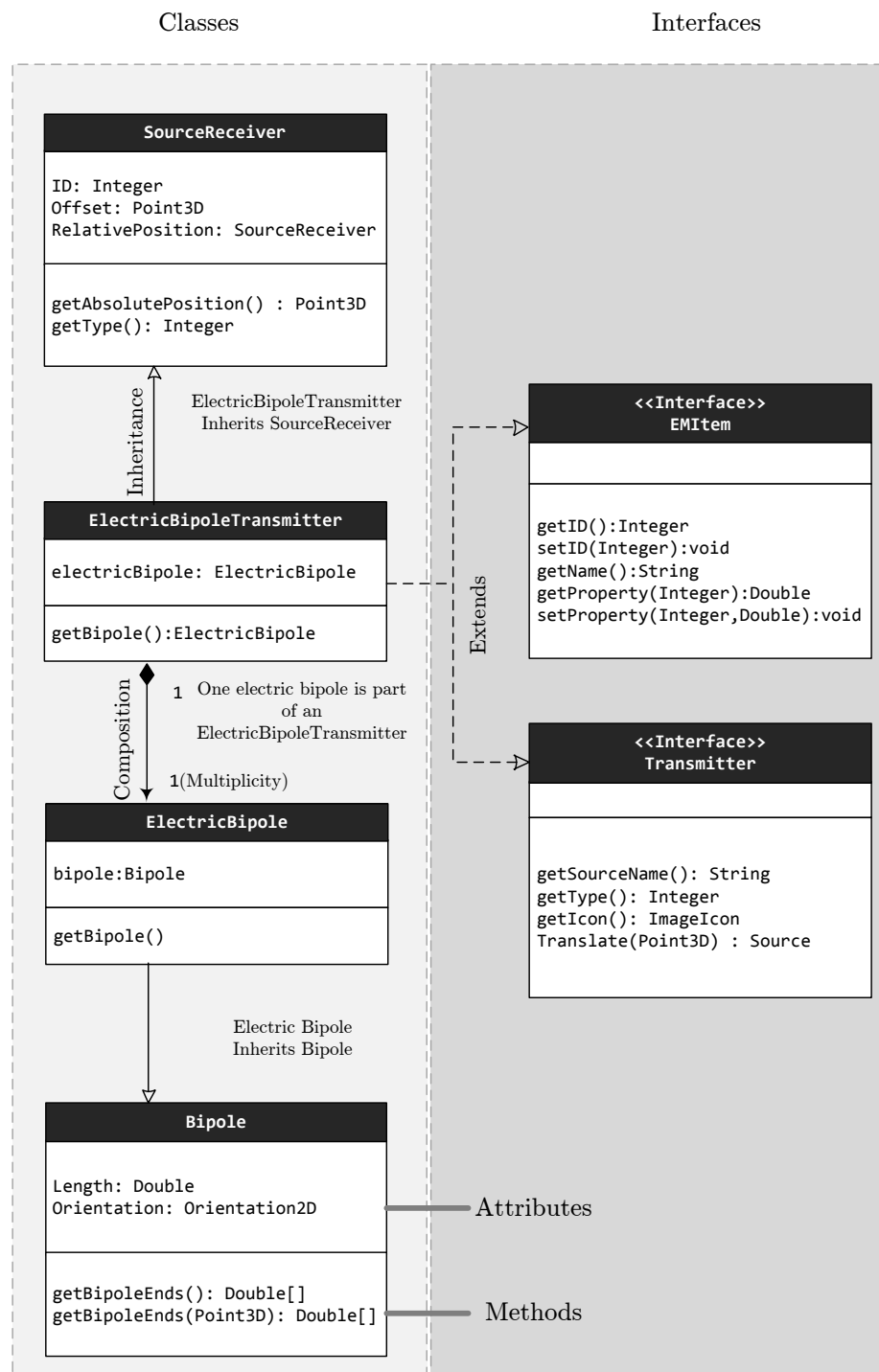
These relationships can be used to describe all electromagnetic relationships. For example, a physical real world electric bipole transmitter can be represented by an object/class called an 'ElectricBipoleTransmitter' object. The object electric bipole transmitter contains the same attributes of a real life transmitter such as bipole length, orientation and position and virtual functionality. Every electric bipole transmitter must contain a bipole. An electric bipole transmitter owns an electric bipole (i.e., composition). The multiplicity of the composition of an electric bipole transmitter to an electric bipole is one to one (i.e., one electric bipole transmitter per electric bipole and one electric bipole per electric bipole transmitter). All electric bipoles are bipoles (i.e., generalization). The UML representation of an electromagnetic bipole source can be seen in Table 2.1.

UML enables real world objects to be represented in a structured form ready to be implemented by an object oriented language. Any electromagnetic object with attributes can easily be represented using this language. The following sections will demonstrate how real world objects are converted into a working data model suitable for any controlled source electromagnetic method using UML.

Relationship	Symbol	Description
Aggregation		Aggregation represents a very strong relationship between classes and is usually read as "...is part of ..."
Composition		A composition relationship implies ownership of a class and is usually read as "...owns a ...". This is subtly different from a basic association and is used in cases where there is a stronger relationship.
Generalization		Generalization is a relationship that is a general or less specific version of the source class or interface. It is usually read as "...is a ...". The arrow points to the more general class.
Multiplicity		<p>Multiplicity represents the number of instances of a particular class for each relationship. The multiplicity can be:</p> <p>0..1 : No Instances, or one instance</p> <p>1 : One instance exactly</p> <p>0..* : Zero or more instances</p> <p>1..* : One or more instances</p>

**Table 2.1:** An overview of several different class relationships described using UML. The relationship, associated symbol and description are included for reference. (Cali et al., 2002)





**Figure 2-1:** An example of the UML class diagram structure for the Electric Bipole Transmitter Class demonstrating inheritance, interfaces, classes, attributes and methods. This ability to inherit properties and methods enables code reuse, reducing the amount of code which requires to be written and maintained.

### 2.4.2 Generalisation and Inheritance

The parent and child paradigm is a commonly used software engineering concept. Inheritance is one way of describing this relationship. The parent class, also considered as the base class, contains generalized methods and attributes (Ewan and Biddle, 2000). The child class has properties and methods specific to itself but also contains the properties and methods of the parent class. Generalization involves the properties of the child class to be inherited from the parent class (Ewan and Biddle, 2000). Inheriting code and methods enables the reuse of code from the parent class. Inheritance reduces code maintenance through code reuse. Inheritance is a method for creating subtypes of existing objects.

Inheritance can be used to structure areas of the controlled source electromagnetic method. Electromagnetic methods contain a number of transmitting and receiving antennae. Electric bipoles, electric dipoles, magnetic dipoles and magnetic loops are all forms of transmitting or receiving antenna. These transmitters and receivers have common attributes and functions. A dipole has a strict definition. A dipole contains a moment or amplitude and three dimensional orientation. This definition is independent of its function (i.e., transmitting dipole or receiving dipole). Defining two dipole classes for both transmitting and receiving magnetic dipoles offers no benefit. Employing inheritance, the magnetic dipole receiver inherits properties from a magnetic dipole, which in turn inherits its properties from a dipole definition. All electric and magnetic transmitter and receiver dipoles all contain the same ‘dipole’ properties. A dipole is written only once by using inheritance.

Electromagnetic data structures can benefit from inheritance. Inheritance improves structure and reduces the time spent maintaining code through code reuse.

### 2.4.3 Implementation and Interfaces

An interface is a collection of functions and attributes that ideally define an object. Ewan and Biddle (2000) states that interfaces force associated classes to implement, or ‘take on’, the required attributes and functions. Interfaces are used when a strict representation is required.

Imagine a person, let’s call him ‘Andrew’. ‘Andrew’ has similar properties to all people. Like are people you expect ‘Andrew’ to abide by a set of rules. When you give him coffee

you expect him to go to work and not go to sleep. However, like all people ‘Andrew’ is unique and he performs his work in accordance with his unique personality. In this example ‘Andrew’ implements the interface ‘CoffeeWorker’. ‘CoffeeWorker’ contains an instruction ‘work’. ‘CoffeeWorker’ contains no strict rules on how the person should ‘work’ but only that they should work or at least react when given coffee. The individual person defines how the work is performed. As a person, ‘Andrew’ can have multiple skills (i.e., implement a number of interfaces), in addition to implementing the ‘CoffeeWorker’ interface, he can also implement ‘GeophysicalProgrammer’, ‘FrogOwner’ and ‘ReviewerNo2Lamenter’ interfaces.

Geo-electrical earth models can benefit from interfaces. A number of geo-electrical earth model representations exist. Various electromagnetic modelling methods utilize these forms. Geo-electrical models include the forms 1D layered earth, 1D layered earth with 3D scatterers and 2D/3D finite difference earth models. Earth models should have some uniformity and should contain a generic method to obtain the lithology at a single point (x, y and z). Writing a single method to complete this task is highly complex and would be difficult to maintain. Writing each implementation separately without an interface may lead to inconsistency between the various earth models. Each earth model type implements the ‘EarthModel’ interface to ensure uniformity of methods and attributes. Implementing an interface forces all earth models to implement the same basic functions; get depth to boundary and get lithologic at a specific position (x, y, z).

Interfaces specify which rules must be followed to be defined as a particular object type. Electromagnetic methods can easily benefit from the use of interfaces. Interfaces allow new electromagnetic types to be created and integrated quickly into the data model. Earth model types, waveforms and survey configurations may need to be integrated into the data model. Having a standard ‘template’ speeds up the creation of new classes.

## 2.5 Electromagnetic Modeling Project Structure

The primary goal of this chapter is to represent electromagnetic methods as a single coherent data structure. All controlled source electromagnetic surveys have the same common features including,

- i system or survey configuration

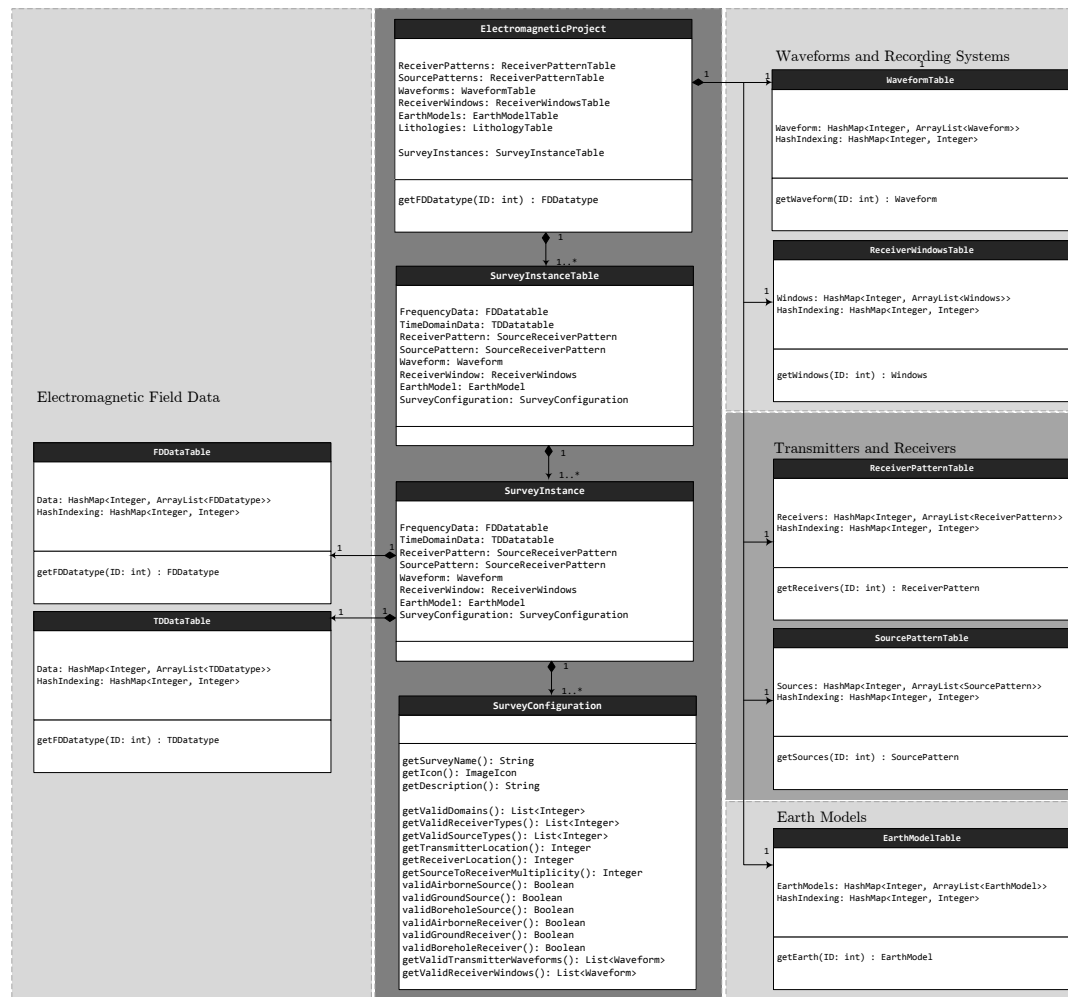
- ii transmitter arrays
- iii receiver arrays
- iv transmission waveforms
- v receiver windows (for time domain systems)
- vi geo-electrical earth models
- vii output electromagnetic data

The system, or survey configuration, defines the transmitter and receiver relationship. The transmitter array describes transmitter properties and geometry. The receiver array describes receiver properties and geometry. The geo-electrical model defines the conductivity distribution. The transmission waveform describes the electromagnetic field generated from the transmitter. The output electromagnetic data is the recorded at each receiver transmitter location for each transmission frequency or time window. These elements form a controlled source electromagnetic survey. Each object type will be covered later in this chapter.

I have created an electromagnetic project (i.e., the ‘ElectromagneticProject’ class) to map real world electromagnetic structures into a coherent data model. The electromagnetic project stores all waveforms, transmitters, receivers and earth models (see Figure 2-2).

The electromagnetic project can contain multiple survey instances. Each survey instance (i.e., ‘surveyInstance’ class) contains a single instance of a survey. Everything an electromagnetic survey needs is defined by the survey instance class. Only one system configuration, earth model, transmitter and receiver pattern, waveform and receiver window setting is allowed per survey instance. Frequency and time domain data are stored in the survey instance rather than the electromagnetic project because the data is specific to the survey instance. This survey instance is then used as the main file to create input files for electromagnetic forward and inverse algorithms. Multiple survey geometries and earth model parameters can be compared because multiple survey instances can be created. This discrete survey instance structure allows survey instances to “mix and match” survey elements.

The electromagnetic project is the overarching class which stores all receivers, waveforms, geo-electrical models, survey configurations and survey instances. The electromagnetic project



**Figure 2-2:** The overall EM project structure. This structure allows all the main components of an electromagnetic survey (i.e. waveform, earth model, transmitter and receiver set, system configuration and dataset) to be stored and to then be used individually for electromagnetic modeling via a survey instance. This structure enables multiple survey instances to be created and modeled for comparison of varying survey structures and earth model responses.

is the essential node which is traversed to obtain all survey and electromagnetic data information.

### 2.5.1 Transmitter and Receiver Data Model

All controlled source electromagnetic surveys contain sources and receivers. I have summarized receivers and transmitters together because both have almost identical properties. Loops, dipoles and bipoles are different forms of sources and receivers.

Physically, loops are a wire circuit with known geometry. Loops transmit and receiver magnetic fields (Nabighian, 1988). Bipoles consist of two electrodes separating positive and negative charges over distance. Bipoles are used to receive and transmit electrical current (Nabighian, 1988). Dipoles are can be thought of as negligibly small magnetic field loops, or negligibly small electric field bipoles. Electric dipoles have no significant separation of charges and magnetic dipoles have no area over which current travels. Both are defined by a moment, with the electric dipole moment defined by ampere meters (Am) and magnetic dipoles by Ampere meters squared ( $Am^2$ ).

Loops, bipoles and dipoles are essentially transceivers. They can either transmit or receive magnetic fields. Transmitters and receivers are fundamentally different in reality, but contain the exact same attributes. Figure 2-3 overviews each of the existing transmitter/receiver types.

A source receiver class (i.e., ‘SourceReceiver’ class) was created to capitalize on the similarities between all source and receivers. The source receiver class forms the base of all transmitters and receivers. The source receiver class contains the property ‘position’ to define the source or receiver in relative co-ordinates. An overview of the physical real world types and forms of transmitters and receivers are shown in Figure 2-3 whilst the UML representation is shown in Figure 2-4. The UML diagram contains all eight forms of transmitters and receivers,

- 1 electric bipole transmitter (i.e., ‘ElectricBipoleTransmitter’ class)
- 2 electric dipole transmitter (i.e., ‘ElectricDipoleTransmitter’ class)
- 3 electric bipole receiver (i.e., ‘ElectricBipoleReceiver’ class)
- 4 electric dipole receiver (i.e., ‘ElectricBipoleReceiver’ class)

- 5 magnetic loop transmitter (i.e., 'MagneticLoopTransmitter' class)
- 6 magnetic dipole transmitter (i.e., 'MagneticDipoleTransmitter' class)
- 7 magnetic loop receiver (i.e., 'MagneticLoopReceiver' class)
- 8 magnetic dipole receiver (i.e., 'MagneticDipoleReceiver' class)

While all eight have different electromagnetic functions, they all contain the same geometrical properties. All eight inherit properties from the 'SourceReceiver' class. The eight source and receiver types are composed of four modes,

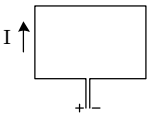
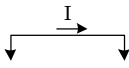
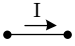
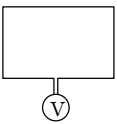
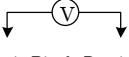
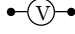
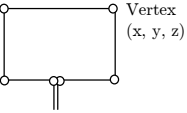
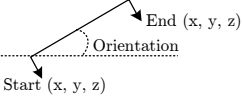
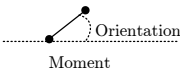
- 1 electric dipole (i.e., 'ElectricDipole' class)
- 2 magnetic dipole (i.e., 'MagneticDipole' class)
- 3 electric bipole (i.e., 'ElectricBipole' class)
- 4 magnetic loop (i.e., 'MagneticLoop' class)

These four modes represent the physical structure of the electromagnetic transceivers. These four modes can be simplified into the three most basic forms,

- 1 dipole (i.e., 'Dipole' class)
- 2 bipole (i.e., 'Bipole' class)
- 3 loop (i.e., 'Loop' class)

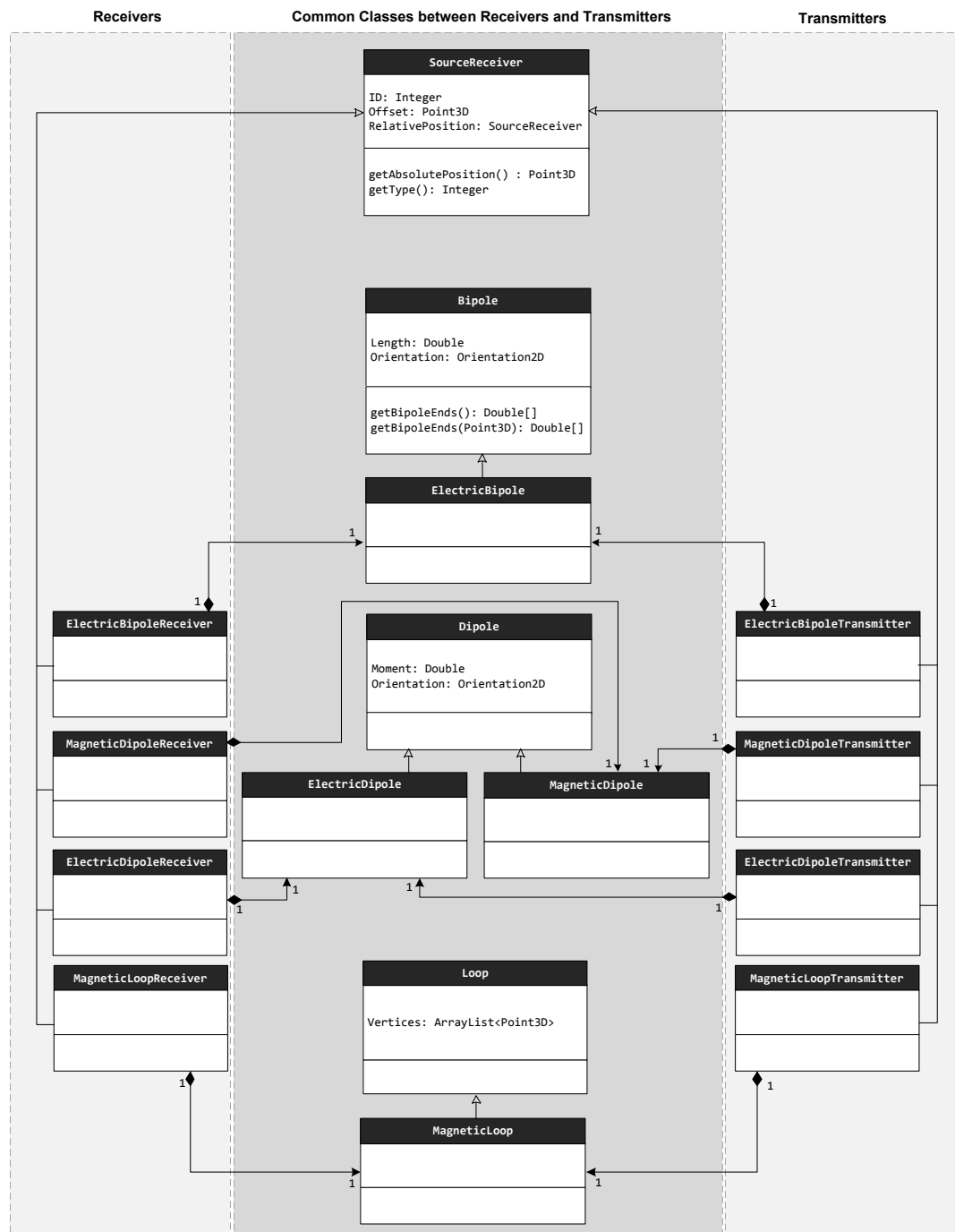
This hierarchical structure allows the eight different source and receiver types to be maintained by only three classes. This structure is clean and reduces maintenance and complexity.

These individual sources and receivers are typically structured in a group of receivers and sources. I define a source/receiver set called a pattern table (i.e., 'PatternTable' class). The pattern table associates a number of sources and receivers into a geometrical pattern. Lines, grids, volumes or custom patterns are the typical forms encountered and are included in my data structure. There are two pattern tables including receiver (i.e., 'receiverPatternTable' class) and transmitter (i.e., 'sourcePatternTable' class) patterns. The receiver pattern table contains all the defined receiver patterns, while the source pattern table contains all the defined source patterns. Patterns contain geometrical information on all sources and receiver attributes. Geometry can be structured or unstructured. I have implemented an unstructured geometry,

Type	Loop	Bipole	Dipole
Form	Loop - Magnetic Loop	Bipole - Electric Bipole	Dipole - Electric Dipole - Magnetic Dipole
Transmitter	 Magnetic Loop Transmitter	 Electric Bipole Transmitter	 Electric Dipole Transmitter Magnetic Dipole Transmitter
Receiver	 Magnetic Loop Receiver	 Electric Bipole Receiver	 Electric Dipole Receiver Magnetic Dipole Receiver
Definition	 <b>Loop</b> A 'Loop' class defines a wire configuration. The vertices represent the positions of a wire. Typically the loop is in the form of a rectangle or square. Extensions of this class could easily be created off this design, such as rectangular loop, circular loop or triangular loop, in fact any geometry.  <b>MagneticLoop</b> An extension of the loop class. A magnetic loop is an insulated wire with geometry. This geometry defines the transmitter or receiver moment.	 <b>Bipole</b> The 'Bipole' class defines the length and orientation of a bipole electrodes. Bipoles can be constructed by one of two methods. Firstly it can be created by defining the electrode start and end positions and secondly by defining the bipole length and orientation. Each produce the same result.  <b>ElectricBipole</b> An extension of the Bipole class. The electrical bipole class only defines that the structure is electrical and a bipole. Physically the electrical bipole is a wire terminated with two electrodes.	 <b>Dipole:</b> A 'Dipole' is more similar to a bipole than a loop. A dipole defines moment and orientation is defined rather than orientation and length. No geometry is defined in the dipole class.  <b>ElectricDipole</b> A 'ElectricDipole' is an extension of the 'Dipole' class. The electrical dipole defines that it is electrical and a dipole. Physically a dipole essentially a bipole with no physical length, instead the dipole is defined by a moment (Am).  <b>MagneticDipole</b> A 'MagneticDipole' is an extension of the 'Dipole' class. A magnetic field sensor has a moment and an orientation. The step type (B-field and/or dB/dt-field) sensor is defined by the survey instance.

**Figure 2-3:** Examples of sources and receiver types. Both sources and receivers have the same attributes. A magnetic loop geometry is defined the same regardless of whether it is a transmitter or receiver. A dipole is defined by a moment and orientation and does not need to know whether it is either a electric or magnetic receiver or source.





**Figure 2-4:** Source and Receiver UML Data Model showing the inheritance between each of the transmitter and receiver components. This is the UML representation of the electric and magnetic field receivers and sources shown in Figure 2-3. Each of the specified receivers and transmitters (i.e. 'ElectricBipoleReceiver') are composed of specific transmitter/receiver modes (i.e. electric bipole). These forms inherit their properties from the corresponding form (i.e. bipole). This is a heirarchical approach to define all survey transmitter and receiver elements. This approach maps to the real world and is easy to maintain as all eight transmitter and receiver types. Only three classes (i.e. the three forms) need to be maintained (i.e. the bipole, dipole and loop classes) .

1 custom i.e., ‘CustomGeometry’ class

and three different structured geometries,

1 profile (i.e., ‘StructuredProfile’ class)

2 grid (i.e., ‘StructuredGrid’ class)

3 volume (i.e., ‘StructuredVolume’ class)

Figure 2-5 overviews the strict geometries. The UML representation is shown in Figure 2-6. Structured datasets enable faster interpolation and computation of data. Faster computations improve user feedback, resulting in efficient and smoother 2D and 3D visualization. Unstructured datasets can be interpolated into a stricter geometries if computational and visualization speed is an issue.

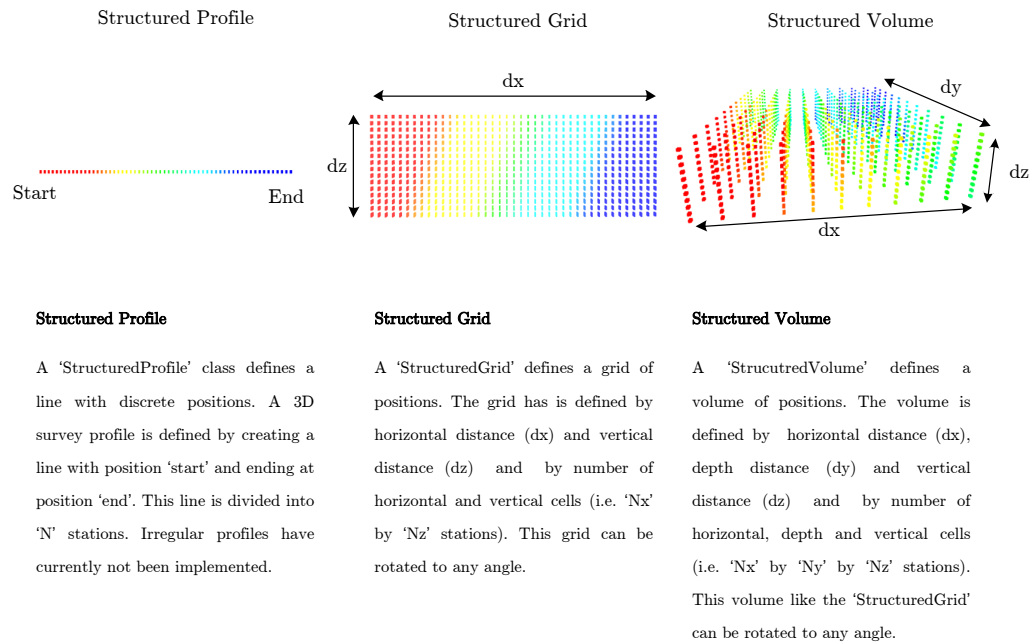
Each pattern defines a bulk datum offset. This enables a group of sources and receivers to be located in local or relative coordinates. For example, a towed EM system is composed of a towed receiver and source array. The receivers are located at some offset from the transmitter. The bulk datum offset allows the positioning of an array of receivers relative to an array of transmitters (i.e., in the case of the towed system). The ‘SourceReceiverPattern’ contains three constructors,

- 1 importing receivers/sources from a survey (each source receiver has its own geometry and attributes).
- 2 creating a receiver table from a single ‘SourceReceiver’ and a geometry specifying the positions (each source receiver has the same attributes, but with a unique position).
- 3 creating a receiver table from a geometry with an array of ‘SourceReceiver’s’ with different attributes (each source receiver has different attributes and a unique position)

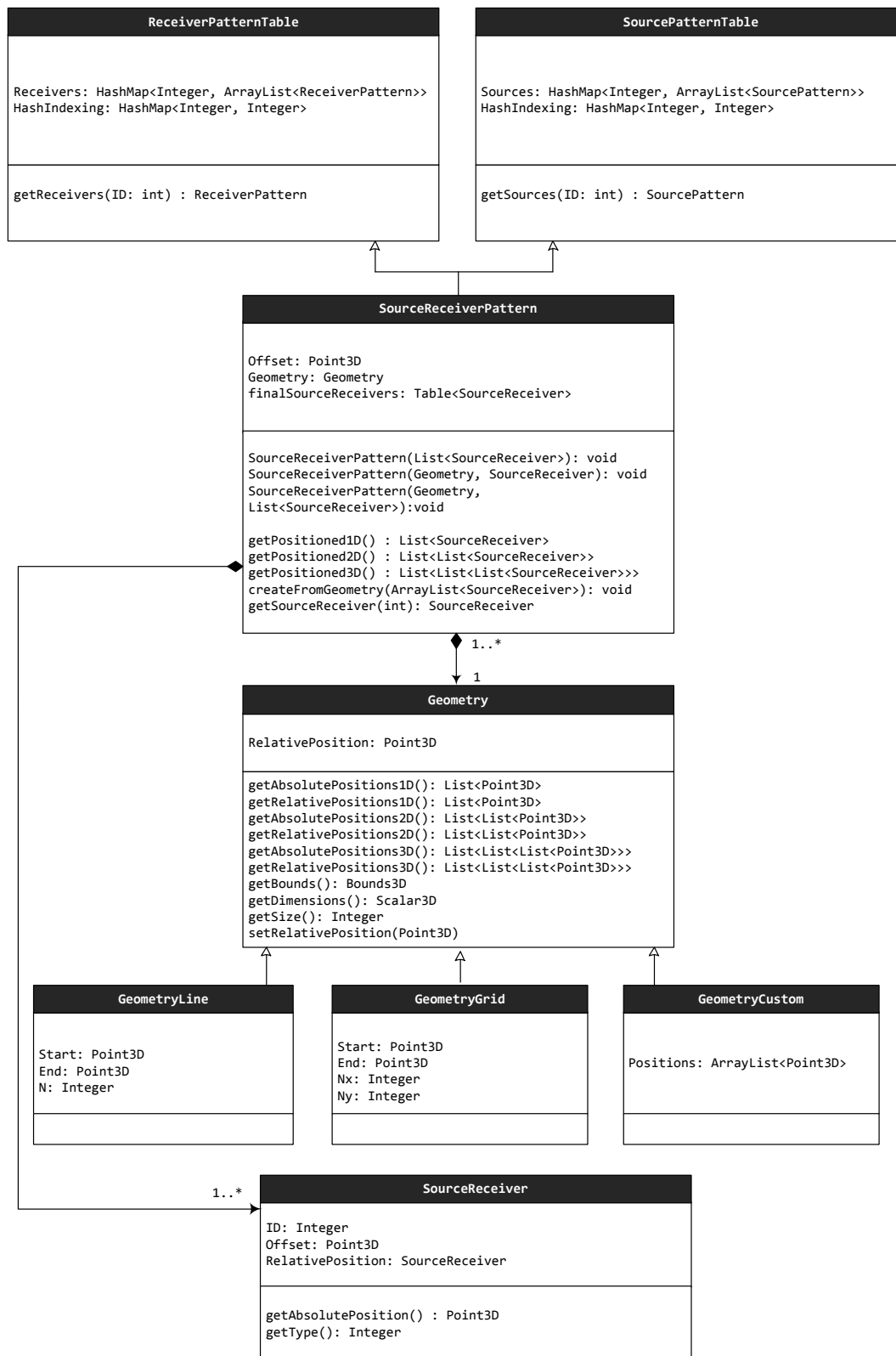
### 2.5.2 System Configuration Data Model

The system configuration or survey configuration data model defines how the receivers and grid geometries are positioned. The survey configuration can be thought of as the survey type. It has two main purposes,

- 1 to convert all receiver and source positions into absolute coordinates



**Figure 2-5:** Three different structured geometries implemented by the software data model. All receivers/sources must be defined in some form of geometry. The 'Geometry' class enables sorting and bounds and dimension determination. It also transforms the geometry from local to absolute co-ordinates. All 'SourceReceivers' are in relative positions and are converted into absolute coordinates by the survey configuration. The default relative position is defaulted at origin. By using structured datasets visualization time and computation time is improved. Unstructured datasets often require interpolation to be visualized (i.e. gridding) to be useful.



**Figure 2-6:** UML Diagram displaying the relationship between sources, receivers and the various geometries. Structured geometries such as lines, grids and volumes, enable faster computation and visualisation of datasets.

2 validate the survey setup

The survey configuration table (i.e., the ‘SurveyConfigurations’ class) contains all the survey configurations which are implemented by the data model. The survey configuration is an interface (i.e., the ‘SurveyConfiguration’ interface) and enforces that all necessary methods to define a survey configuration. Multiple survey configurations are produced by implementing the methods found in the survey configuration interface.

The source-receiver relationship must be defined to create a survey configuration. The source to receiver multiplicity defines the type of relationship and in turn the coordinates of the sources and receivers. The source to receiver multiplicity can either be,

- i many to many (i.e., many sources to many receivers)
- ii many to one (i.e., many sources to one receiver)
- iii one to many (i.e., one source to many receivers)
- iv one to one (i.e., one source to one receiver)

If the relationship is many to many, no relationship exists between transmitters and receivers and both transmitters and receivers are in absolute coordinates. If the relationship is many to one, the transmitter is located at relative coordinates to the receiver. If the relationship is one to many, the receivers are located in relative co-ordinates to the transmitter. The relationship between transmitter and receivers defines how both transmitters and receivers are positioned in relation to each other. This array is then finally positioned in absolute coordinates using the geo-electrical model.

The absolute position is finally obtained through the survey configuration class. The methods ‘getTransmitterLocation()’ and ‘getReceiverLocation’ in the ‘SurveyConfiguration’ interface returns the method to convert relative into absolute coordinates. Transmitters and receivers are in relative co-ordinates and are positioned relatively against a component of the geo-electrical model (i.e., ocean surface, ocean floor and a particular layers surface). For example, a towed array system (i.e., a receiver array is towed behind a moving transmitter) is geometrically defined as a moving source system with ocean bottom receivers. That is, the towed array system has receivers positioned in relative co-ordinates to the transmitter and the transmitter is in position relatively against the ocean-air surface (i.e.,  $z = 0\text{m}$ ).

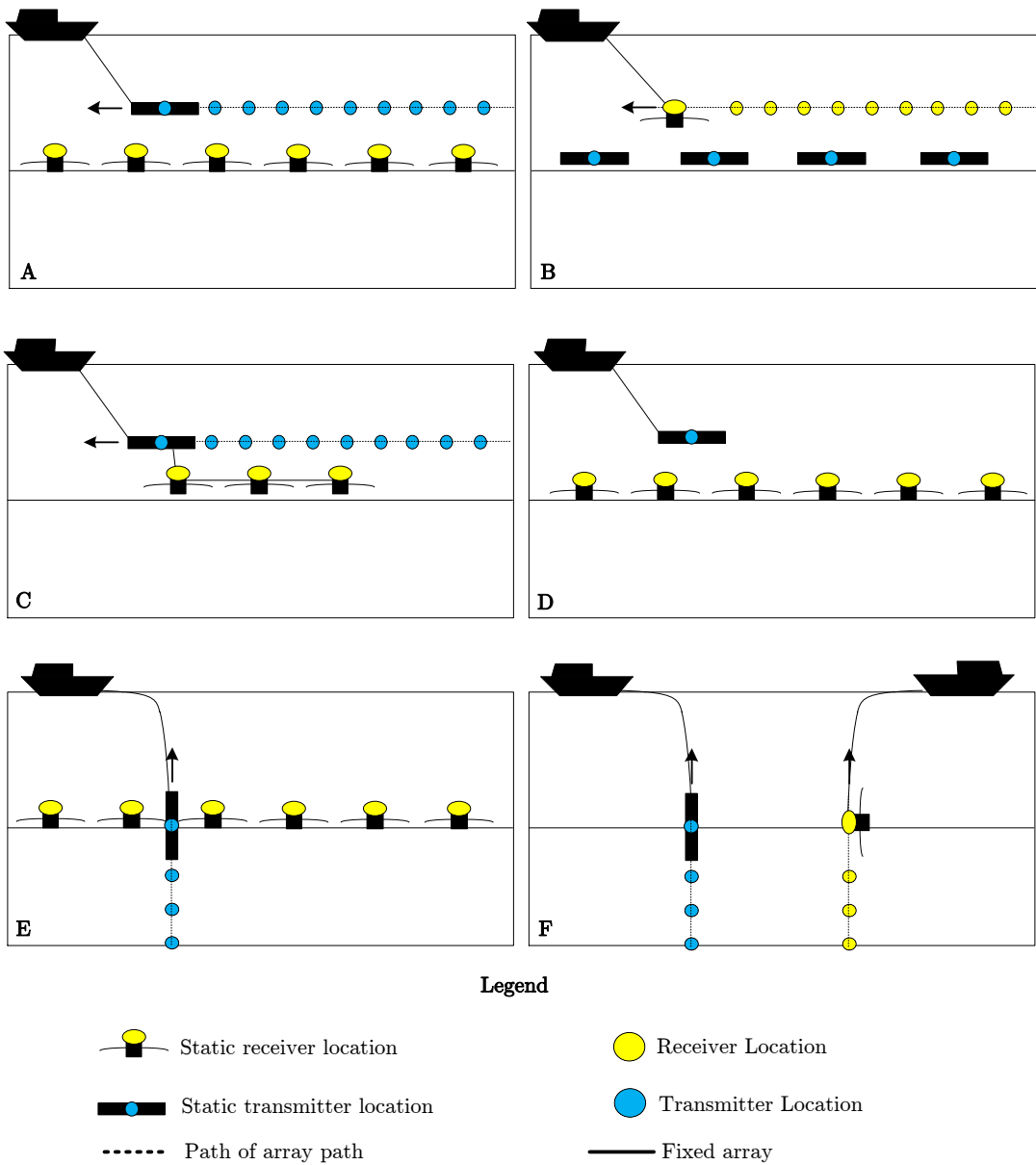
A traditional MCSEM survey with a towed source has receivers and transmitter locations in absolute x, y positions but its vertical position is relative to the ocean bottom. In essence, receiver/source arrays can be in absolute or relative positions. This opens the possibility for many survey configurations,

- i traditional marine CSEM
- ii towed marine CSEM
- iii airborne towed transmitter with ocean bottom towed receivers
- iv receiver borehole with towed transmitter

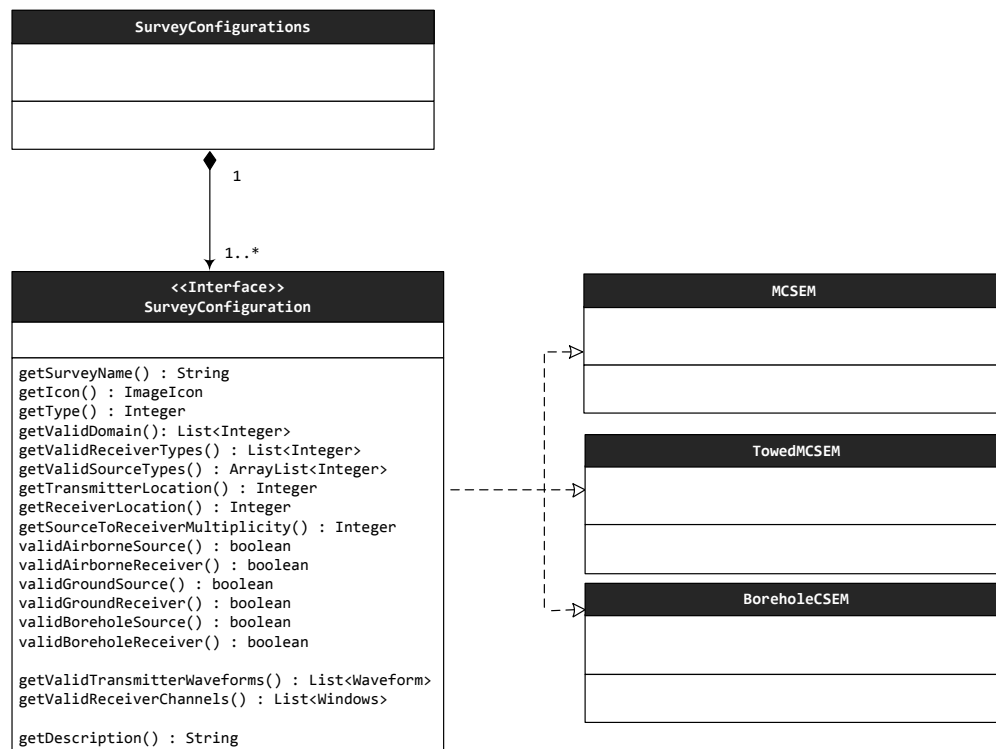
A few examples of different survey geometries encountered in marine electromagnetic methods are shown in Figure 2-7. Figure 2-8 shows the UML representation of a survey configuration data model. The data model demonstrates that the ‘SurveyConfigurations’ table is composed of many ‘SurveyConfiguration’ interfaces. Implemented versions of the survey configuration interface include the traditional MCSEM method (i.e., the ‘MCSEM’ class) and towed MCSEM (i.e., the ‘TowedMCSEM’ class).

The UML model also shows several methods to validate a survey configuration. These contain the valid sources, receivers, waveforms and windows for a particular survey instance. For example, a MCSEM survey uses a towed electric bipole/dipole transmitter and electric and magnetic dipole receivers. If the user unknowingly uses a towed MCSEM survey with a magnetic dipole transmitter, the survey configuration will invalidate the survey. This form of error checking also allows survey configurations to be cross referenced with the electromagnetic modelling and inversion algorithm at runtime. For example Dipole1D (Key, 2009a) operates with an electric dipole transmitter. If an electric bipole transmitter is used, the survey will be invalidated and will the used will be prevented from executing the survey.

The absolute coordinates are controlled by the survey configuration. The survey configuration positions sources and receivers in relation to each other and the geo-electrical model. The survey configuration is essentially the survey type (i.e., towed MCSEM, borehole CSEM and airborne TEM). This model allows receivers and transmitters to be located in terms of relative and absolute coordinates. Receivers are located at a relative offset to the transmitter in towed MCSEM systems as an example. The position of the receivers is set to this offset. The transmitter may be towed at some altitude relative to the ocean survey. The transmitter position is set to the relative altitude (See Figure 2-9). My survey configuration design enables

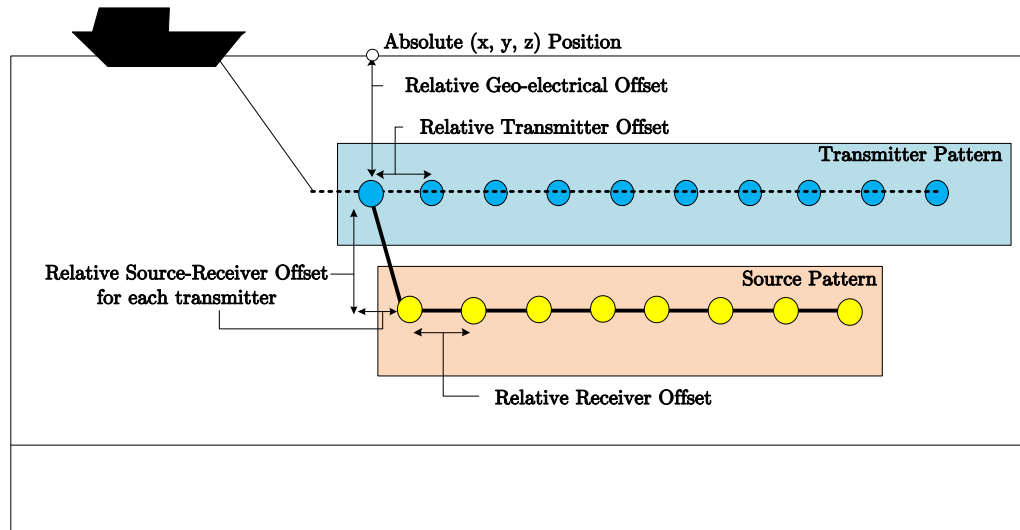


**Figure 2-7:** Various survey geometries. My software should attempt to be able to simulate any type of survey geometry. This Figure does not show an exhaustive list but a subset of what is possible. (A) Absolute receivers with the vertical position related to the geoelectrical ocean bottom with a single towed transmitter (B) Stationary transmitter locations with the vertical position fixed to a height above the seafloor with a single towed receiver. (C) A complete towed system, the receivers are located in relation to the transmitter. (D) Completely fixed array, no movement of transmitters or receivers, both the transmitter and receivers are located at some offset from the ocean floor. (E) Borehole survey with stationary seafloor receivers. (F) Cross well survey with moving transmitter and receiver arrays.



**Figure 2-8:** The System configuration data model. This purpose of the survey configuration is to position sources and receivers in absolute coordinates and to validate survey instances. Multiple survey configurations can be produced by creating a new classes implementing the methods in the `SurveyConfiguration` interface.





**Figure 2-9:** An example of a towed MCSEM survey for a many-to-one relationship. This many sources to one receivers demonstrates how each co-ordinate systems is placed into absolute co-ordinates. Each receiver pattern contains receivers in relative co-ordinates. This is the towed receiver line. Each receiver line is positioned in relation to each of the the towed transmitter locations. The transmitter pattern contains each transmitter location, these are in relative co-ordinates. Finally the survey configuration places the transmitters and in turn the receivers into absolute co-ordinates by positioning the transmitter pattern in relation to the ocean surface.

any electromagnetic survey configuration to be created.

### 2.5.3 Waveform and Receiver Windows Data Model

The waveform and receiver windows structure is significantly more straightforward than the receiver-transmitter relationship. All CSEM surveys require a transmission waveform. These transmission waveforms are all performed in the time domain, but the received signal is typically converted into the frequency domain for the MCSEM method. My waveform structure enables both time domain (TD) and frequency domain (FD) waveforms.

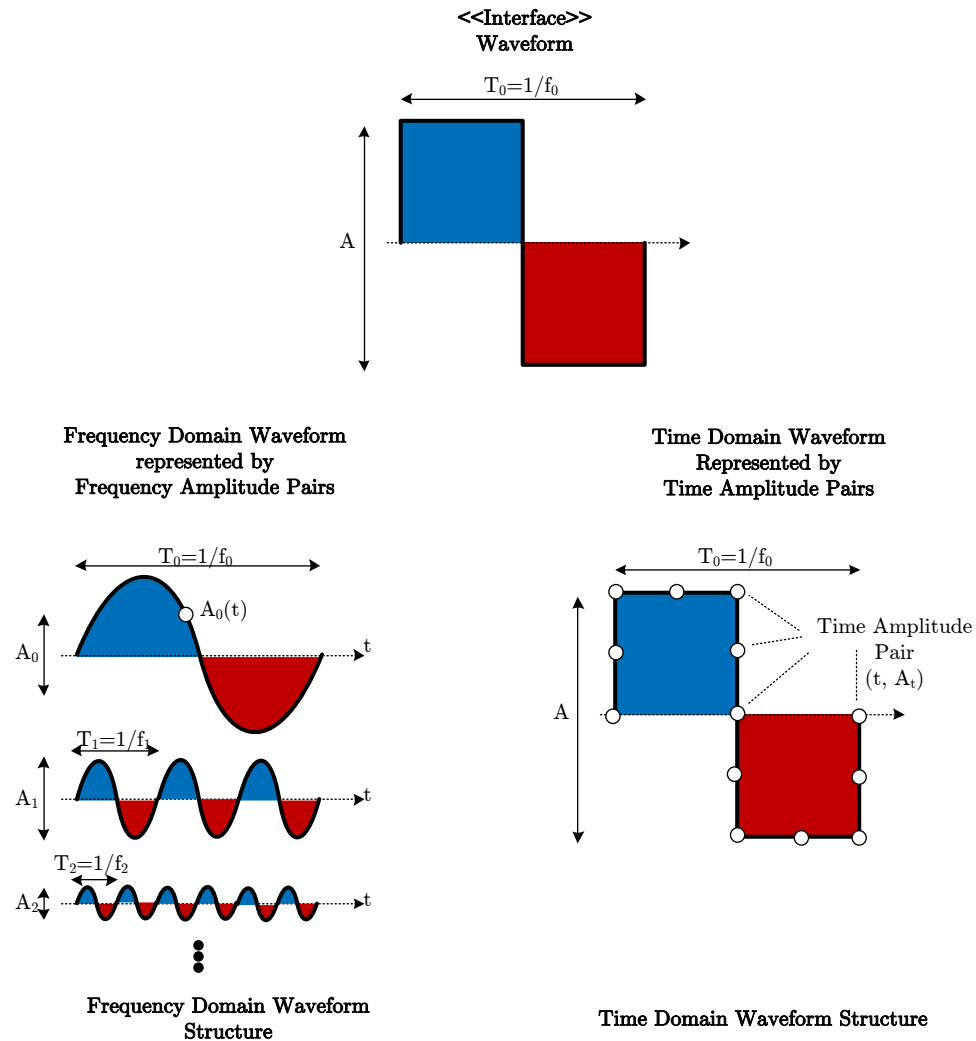
The waveform interface contains a generic instruction set which retrieves the time domain and frequency domain equivalents. Transitions between FD and TD waveforms are not as simple as a fast Fourier transform (FFT) in reality. Computationally defined waveform definitions require more flexibility. For example, a variant of a square wave is transmitted during a MCSEM survey. The interpretation of the recorded data occurs in the frequency

domain. Only several (three to seven) frequencies are interpreted typically despite square waves containing an infinite number of frequency harmonics. If a FFT or inverse FFT (IFFT) were applied to the original waveform it could not be reproduced from the subset of frequencies. The waveform definition requires both frequency and time domains to be implemented independently (See Figure 2-10). The UML representation of frequency domain and time domain waveforms are shown in Figure 2-11

The waveform interface also contains both a waveform name and waveform type. All waveforms implement the ‘getTimeDomainWaveform’ and ‘getFrequencyDomainWaveform’ methods. These methods are used to obtain the generic time domain and frequency domain waveforms. Waveforms generally have a reciprocal, however occasionally users may not require waveforms to have a reciprocal waveform type (i.e., to have a time domain waveform with no frequency domain equivalent). The method will return a null value in cases where there is no reciprocal. An instance of a reciprocal waveform would be a square wave. The base frequency, peak amplitude and number of terms for frequency domain conversion is defined at this level. Both frequency and time domain waveforms can be derived from these attributes.

The frequency domain waveform contains frequency amplitude pairs. These describe each transmission frequency harmonic. Time domain waveforms contain time amplitude pairs. Each time amplitude pair consists of a time and current amplitude. A number of time amplitude pairs define the shape of the waveform.

Time domain systems record the electromagnetic response over time rather than in the frequency domain. The electromagnetic response is recorded in windows. The receiver window, also known as a recording channel, defines the time interval over which the electromagnetic field is recorded. To represent this a ‘Windows’ class was created. The ‘Windows’ class represents an electromagnetic recording system. Each system records over a number of time bins. Each window consists of a start time, end time and gain. The structure of windows and bins are shown in Figure 2-12. These bins have an associated amplitude gain. Clipping of extreme voltages caused by analogue to digital converters can occur in reality. Multiple gains may be required for the same bin to record the voltage accurately. Each window allows multiple gains for the same bin. Figure 2-13 graphically represents the UML data model for the receiver window object. The bin can be constructed by start and end times or midpoint and width. Each bin specifies its gain independently. Bins are structured in this



Frequency domain systems transmit in-phase repetitive signals. Each waveform can be broken down into individual frequency-amplitude pairs with each frequency-amplitude pair representing a continuously transmitted sine wave.

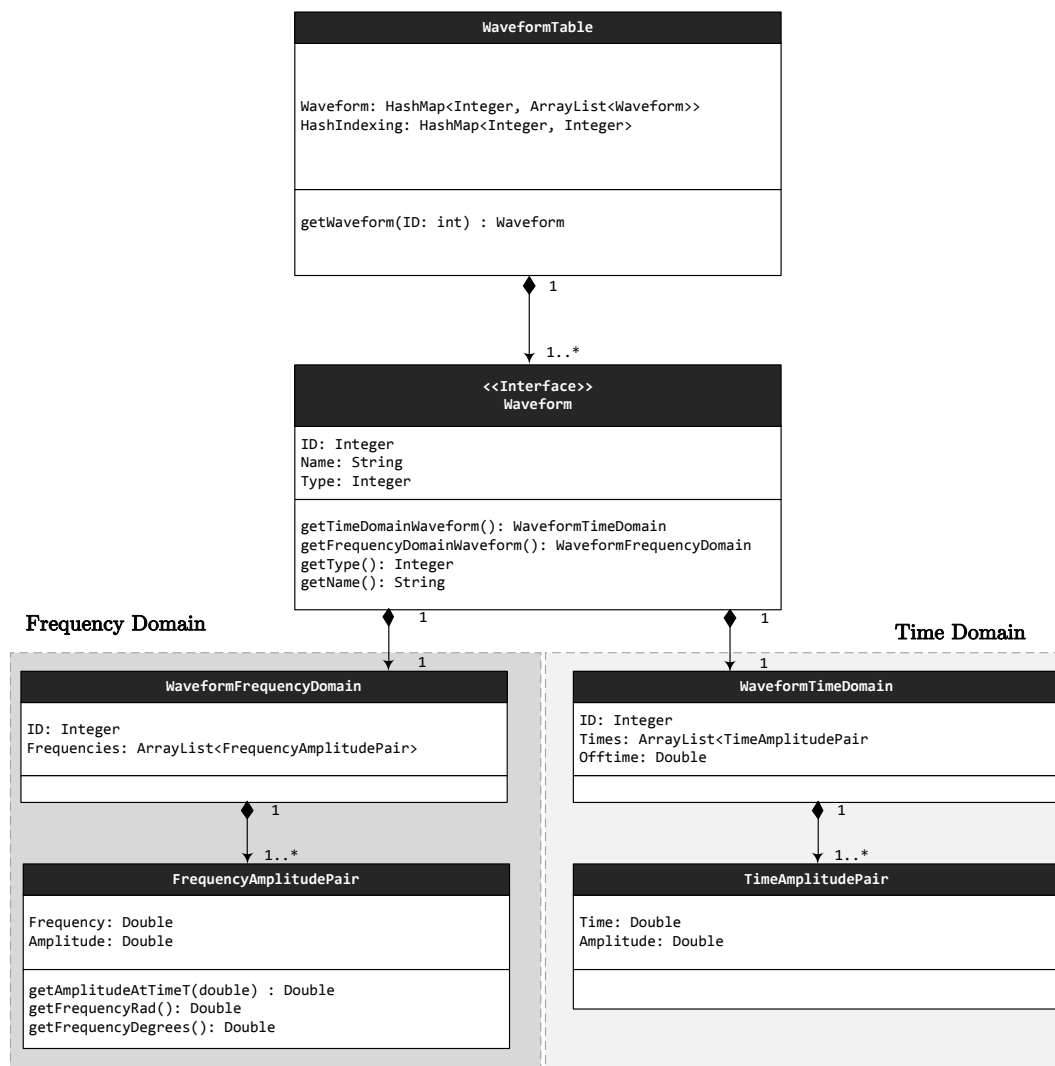
A frequency domain waveform must have anywhere from 1 to N frequencies. The upper bounds has no restraints on the number of terms because it determines the accuracy of the frequency domain waveform (i.e. a square wave will be the resultant of the sum of the odd harmonics of the base frequency). Highly accurate waveforms may require in excess of 50 frequencies to be computed. This class contains several helper methods including a radian to degree conversion method and the 'GetAmplitudeAtTimeT()' which solves the standard equation.  $A(t) = A_0 \sin(2\pi f t)$

The time domain waveform is similar to the frequency domain waveform. It contains time-amplitude pairs instead of frequency-amplitude pairs.

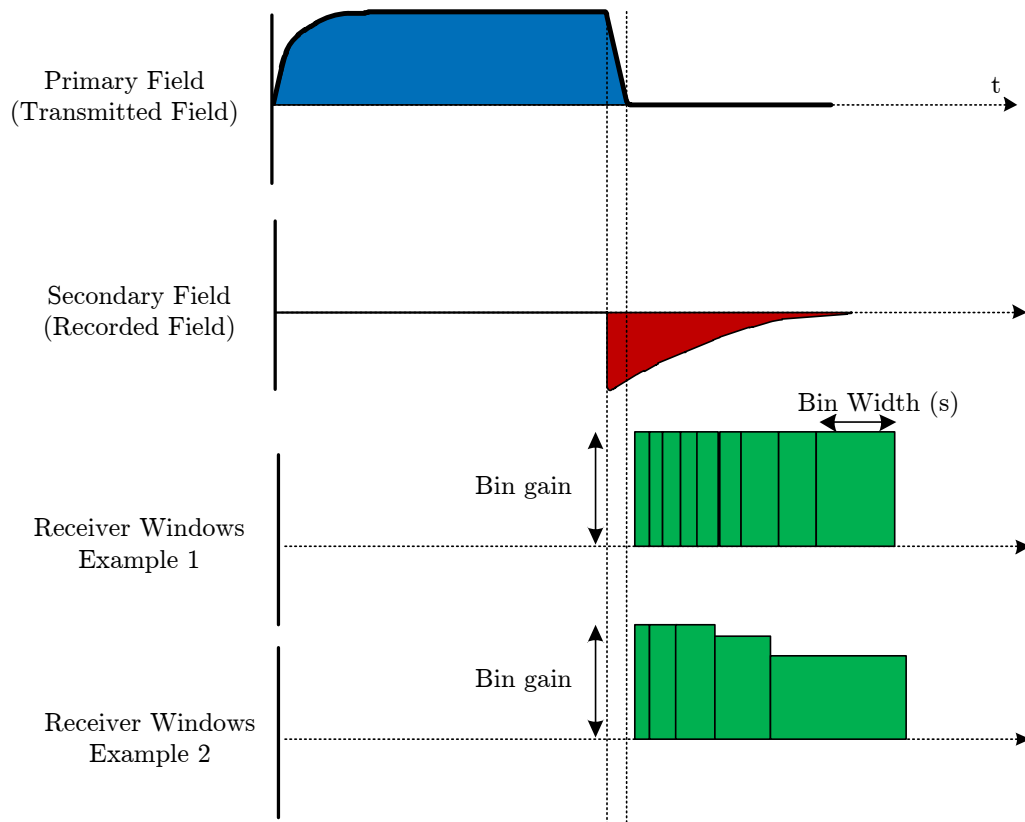
A fast Fourier transform could be performed between these two classes but may result in poor accuracy, in particular if the frequency domain waveform is defined using insufficient terms. Any conversions between the two domains must be performed by the parent waveform class.

Time domain waveforms are defined by the current-amplitude at a particular time. This simple definition could easily be replaced by a 'Scalar2D' class but for the sake of consistency a 'TimeAmplitudePair' class was created.

**Figure 2-10:** An overview of time domain and frequency domain waveforms. There are two main waveforms, frequency domain and time domain. Each are structured differently. The two forms of waveforms are shown above with the corresponding explanations. Each of the two forms can be created from each waveform type. In this case a square wave can be defined in the frequency domain (i.e. base frequency and odd harmonics) and in the time domain (i.e. by time amplitude pairs)



**Figure 2-11:** Waveform data model. The waveform class creates the frequency domain and frequency domain waveforms independently.



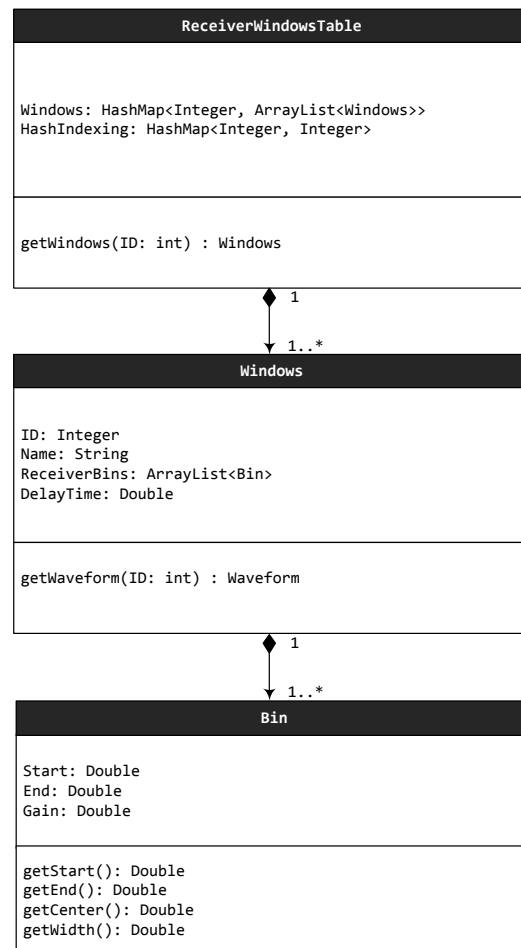
**Figure 2-12:** The receiver window and receiver bin structure. A system represents the system's receiver window setup. The receiver windows setup indicates how the electromagnetic field will be recorded over time.

manner because a system may have the same receiver bins but be recorded at different gains.

Real life waveforms and receiver window structures can be represented by a UML equivalent. My waveform data model allows for any frequency domain or time domain waveform to be constructed.

### 2.5.4 Electromagnetic Vector Data Model

Good data management is at the heart of all data models. The most memory intensive part of the data model is the electromagnetic vector data model. All controlled source electromagnetic



**Figure 2-13:** The UML representation of the receiver window data model. This receiver windows represents a recording system. This system defines how the electromagnetic field is recorded in the time domain. Each window is composed of discrete recording intervals called receiver bins. These bins define by start and end recording times and gain.

surveys produce data. MCSEM surveys records the resulting electromagnetic field produced from high amplitude alternating current flowing through a towed horizontal electrical bipole. MCSEM transmits with an electric field source to drive current through resistive earth. This electric field and induced magnetic fields are altered by the subsurface electrical structure. These perturbations are observed at the sea floor which enables the method to discriminate between subsurface geo-electric structures. This is typically recorded in the time domain and processed and converted into the frequency domain. The resulting electromagnetic field is comprised of the electric field and magnetic fields.

In electro-statics the electric field exists in the region of space around a charged object (i.e., the source). Serway et al. (2010) states the “electric field vector ( $\vec{E}$ ) at a point in space is defined as the electric force ( $F_e$ ) acting on a positive test charge  $q_0$  placed at that point divided by the test charge” (see eq 2.1). Simply, the electric field is the force on a free electron when placed in the region of space around a charged object.

$$\vec{E} = \frac{F_e}{q_0} \quad (2.1)$$

where,

- $\vec{E}$ — electric field ( $NC^{-1}orVm^{-1}$ )
- $F_e$ — force ( $N$ )
- $q_0$ — electric charge ( $C$ )

The electric field has the SI units of newton per coulomb ( $NC^{-1}$ , i.e., force divided by charge) or volts per meter. The MCSEM method records the electric field in terms of volts like other electromagnetic methods. The voltage is normalized against with transmitter moment for consistency.

The magnetic field is induced in accordance with Maxwell’s equations (Maxwell, 1881). Serway et al. (2010) defines the magnetic field ( $B$ ) at some point in space as “the magnetic force ( $F_B$ ) that the field exerts on a charged particle moving with a velocity  $v$ ”. A simplified constant current field relationship is defined by the Lorentz Force equation (see eq 2.2),

$$F_b = qv \times \vec{B} \quad (2.2)$$

where,

- $\vec{B}$ — magnetic field ( $N/Cms^{-1}orT$ )
- $F_b$ — magnetic force ( $N$ )

$q$ – electric charge ( $C$ )

$v$ – charged particle velocity ( $ms^{-1}$ )

The magnetic field is recorded in SI units of newton per coulomb-meter per second ( $N/Cms^{-1}$ ) which is called the tesla ( $T$ ).

The Poynting vector and current density fields are derived from the electric and magnetic fields and geo-electrical earth properties (if known). In free space, the Poynting vector is considered to be the flow of energy flux. The instantaneous Poynting vector for time domain fields is defined by equation 2.3 whereas the time-averaged Poynting vector is defined by equation 2.4 (Nabighian, 1988) and represents the average flow of energy,

$$\vec{S} = \vec{E} \times \vec{H} \quad (2.3)$$

$$\vec{S}_a = \frac{1}{2} Re(\vec{E} \times \vec{H}) \quad (2.4)$$

where,

$\vec{S}$ – Poynting vector ( $W \cdot m^{-2}$ )

$\vec{E}$ – electric field (complex) ( $NC^{-1} or Vm^{-1}$ )

$\vec{B}$ – magnetic field (complex) ( $N/Cms^{-1} or T$ )

Poynting vectors are covered in much more detail by Chave (2009), Nabighian (1988), Weidelt (2007) and is investigated in section 5.3.

Electromagnetic data can be interrogated by an exhaustive number of methods. Analysis of EM data involves the comparison of a large variety of EM field properties. For example six component frequency domain MCSEM data sets can give rise to over 80 different properties. The breakdown includes four field properties,

1 electric ( $\vec{E}$ )

2 magnetic ( $\vec{H}$ )

3 Poynting vector ( $\vec{S}$ )

4 current density vector ( $\vec{S}$ )

These four fields vectors derive four direction attributes,



- 1 inline (x)
- 2 crossline (y)
- 3 vertical (z)
- 4 total field (T)

Each of these attributes contain five properties including,

- 1 amplitude
- 2 phase
- 3 real
- 4 imaginary
- 5 amplitude at time (t)

There are two categories of data, frequency domain and time domain. Each category has its own unique structure. Data was originally stored in tables for maximal speed performance. Table and volume approaches are similar to most seismic processing software packages. Electromagnetic datasets and survey geometries within a table structure can become unmanageable. The sheer number of parameters and electromagnetic properties make any table structure overly complex. Eventually, the code becomes unreadable and inefficient due to the repetition of data.

Inefficiencies in the table design were resolved by storing electromagnetic data in an objected oriented design. EM methods require flexibility rather than the rapid manipulation of highly structured datasets like those found in seismic software packages. The flexibility issue was a major factor contributing to the decision to choose an object oriented approach, as this allowed all objects to be easily traversed and manipulated.

The frequency domain data model is split into four main parts,

- 1 frequency domain data type (i.e., the 'FDDatatype' class)
- 2 field data (i.e., the 'FDField' class)
- 3 electromagnetic vector (i.e., the 'FDVector' class)

4 low level complex number (i.e., the ‘Complex’ class)

This four level system enables the 80 different properties to be represented by only four classes.

The main class ‘FDDatatype’ contains a single data point and related survey information including, receiver, transmitter, earth and waveforms. Data (i.e., ‘FDDatatype’) is located in both time and space and can contain a reference to the waveform, frequency amplitude pair, earth model, transmitter and receiver. The ‘FDField’ class contains the electric and magnetic field vectors. The ‘FDField’ derives the Poynting and current density vectors from the electric and magnetic field vectors. The ‘FDVector’ contains the x, y and z individual complex numbers. The total vector is computed by the ‘FDVectorClass’. The complex number is a simple structure containing real and imaginary components. Amplitude, phase and amplitude at time can be computed from the ‘Complex’ class. An overview of the data model of the EM Field is shown in Figure 2-14 while the UML representation is shown in Figure 2-15.

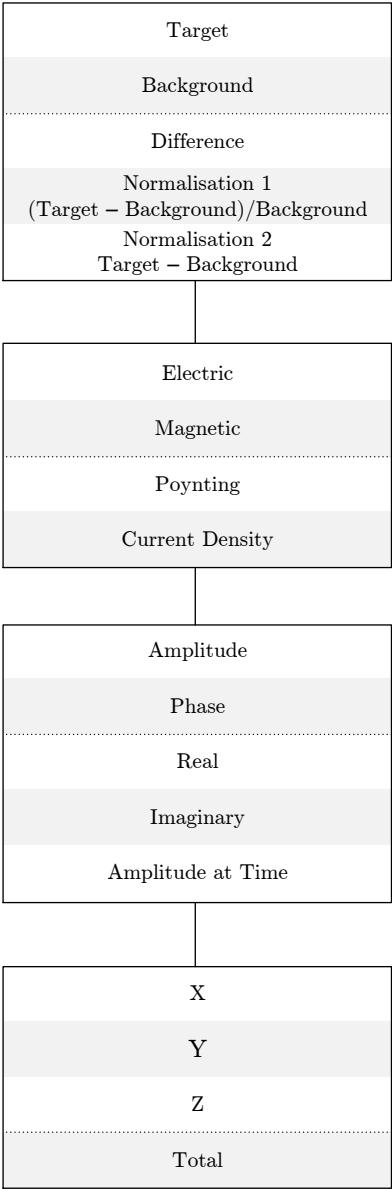
The time domain data model is similar to the frequency domain data model. The complex number is the main structural difference. Frequency domain systems have a complex number as its primitive measurement. Time domain systems record an amplitude for a given receiver bin (See Figure 2-16).

The electromagnetic vector data model has been designed for flexibility. This flexibility enables the easy retrieval of the 80 possible electromagnetic vector field properties. Using a flexible structure over a table structure has resulted in cleaner code that is more maintainable.

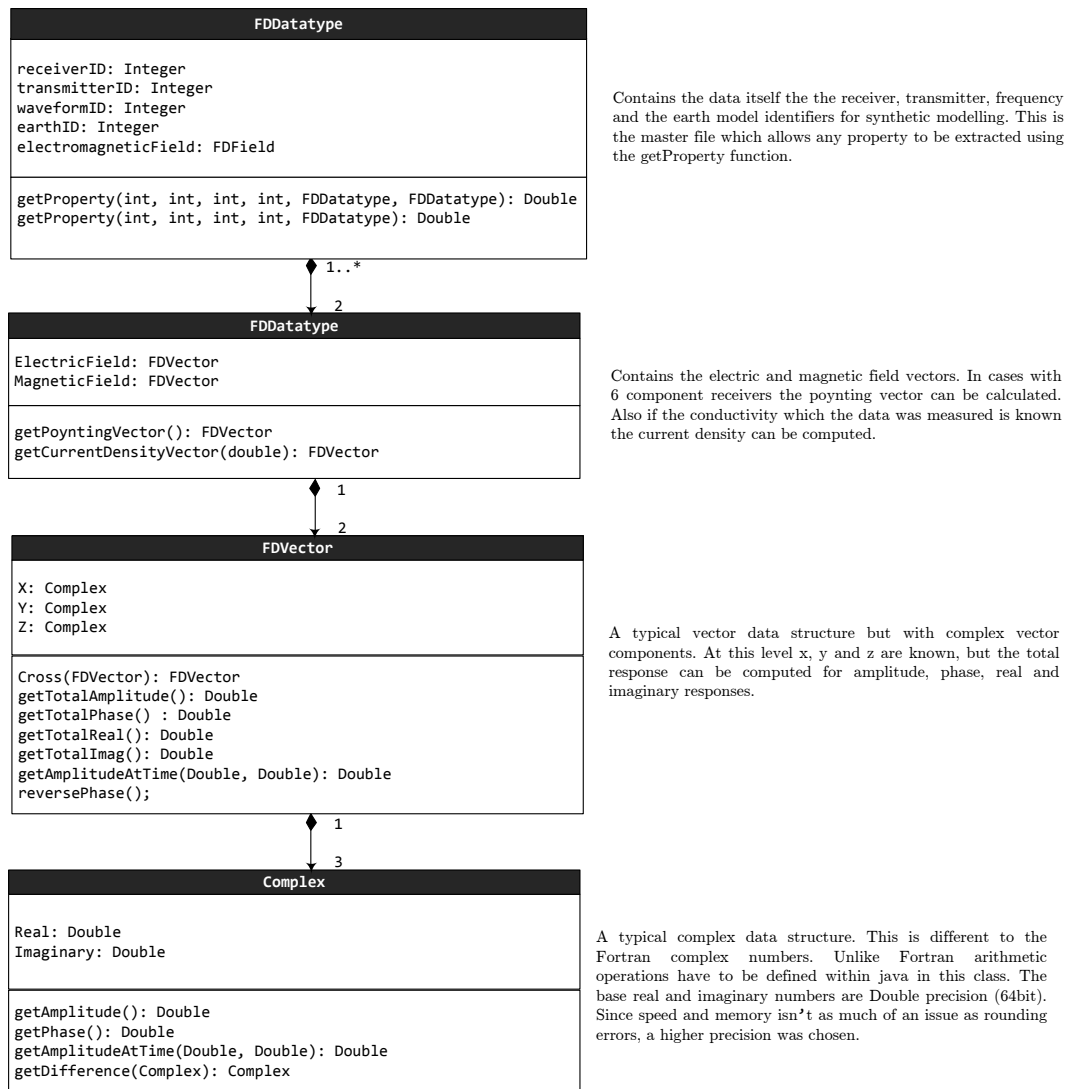
### 2.5.5 Geo-electrical Earth Data Model

The geo-electrical model defines a synthetic earth model in terms of its electrical properties (i.e., resistivity, anisotropy and induced polarization properties). In real life, there is only one earth model, the earth. There are a range of geo-electrical model representations of the real life earth for computational convenience. Each computational earth model types have unique features to suit a diverse range of electromagnetic modelling algorithms. The standard model types include,

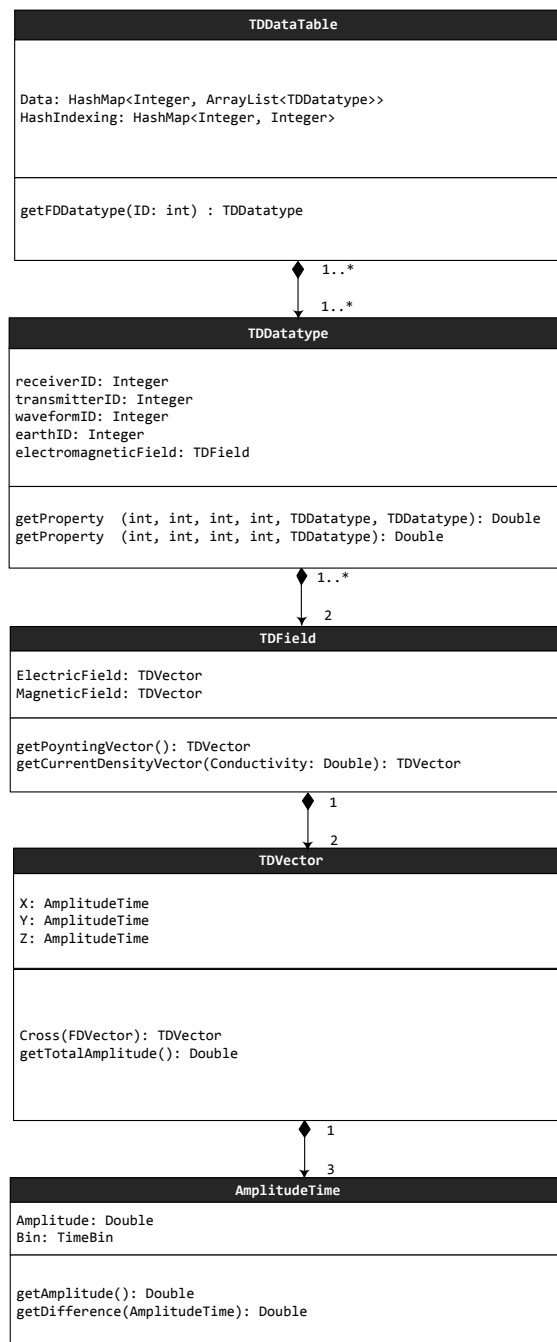
- i 1D layered earth



**Figure 2-14:** Possible electromagnetic field parameters which can be analyzed and compared. The model is broken into component, field, property and direction. The dotted line represents the values which are calculated from the recorded signal. This Figure is not exhaustive and other comparison could be generated such as the average pointing vector, sum of two fields, Mittet normalisation values and frequency difference calculations.



**Figure 2-15:** The frequency domain UML data model. Frequency domain data consists of four main components. The frequency domain datatype contains time and survey geometry related to the measurement. The field datatype contains electric and magnetic field vectors. The vector contains the three component directional complex numbers. Lastly the complex number allows the computation of amplitude and phase properties from real and imaginary measurements. This four layered approach allows the calculation of over 80 different electromagnetic properties.



**Figure 2-16:** The time domain UML data model. This model is similar to the frequency domain system, however the difference is that the complex number has been replaced by an 'AmplitudeTime' class. This amplitude-time relationship places the recorded amplitude at a given time bin.

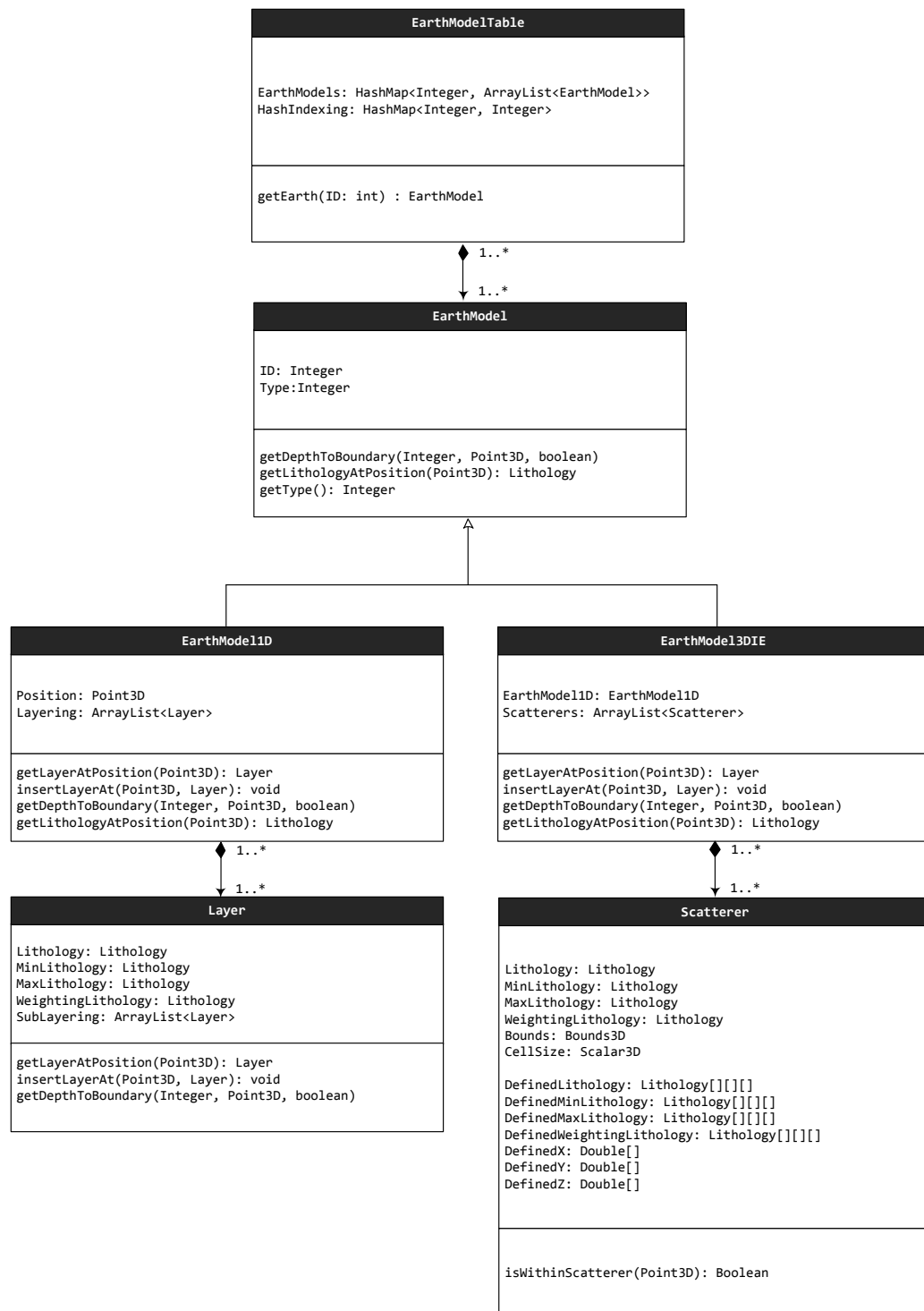
- ii 1D stitched layered earth
- iii 2D finite difference (irregular, regular, quad-tree)
- iv 3D finite difference(irregular, regular, oct-tree)
- v 2D finite element (Mesh)
- vi 3D finite element (Prismatic Mesh)

OOP enables code reuse and class sharing for 1D layered earth and 1D stitched layered earth between 2D and 3D finite difference models and 2D and 3D finite element models. Unfortunately, there are limited structural similarities between the core earth model types (i.e., layered, finite difference and finite element). Independent definitions of each earth model type are required. Lithology is the only shared property between all model types.

The UML representation of the geo-electrical structure is shown in Figure 2-17. The earth model interface (i.e., the ‘EarthModel’ interface) was created for all earth model types. This interface enforces commonality between all earth models. Each earth model implements two methods, ‘getLithologyAt’ and ‘getDepthToBoundary’. These methods provide the rest of the data model access to lithological and structural information independently for each earth model type.

Lithology forms the base unit of all earth models. Lithology contains vertical resistivity, horizontal resistivity, thickness, conductance, relative magnetic permeability, relative dielectric and Cole-Cole parameters. Other properties can be easily added programmatically through a property hash map.

The 1D earth model is the most basic of earth model type apart from an isotropic whole-space. The earth model 1D structure forms the base of stitched earth models and is commonly used as a background model for more complex 2D and 3D geo-electrical earths. 1D earth models contain single one dimensional layers in the vertical (z) direction. There are many situations where inhomogeneity exists within a single 1D layer. Layers need to be composed of other 1D layers in this case. Sea water should be considered a single layer for example. The MCSEM receivers and transmitters are typically placed at the bottom of this layer. Sea water varies vertically in electrical conductivity (Pethick, 2008). Seawater is considered to be a single layer in reality but with a vertical distribution of resistivity. My 1D layer structure consists of either



**Figure 2-17:** A subset of the geo-electrical UML data model. This model shows two examples of earth models; a 1D layered earth and 1D layered earth with integral equation 3D scattering bodies.

a single or multiple 1D sub layers. This sub layering enables groups of layers, like sea water, to be represented by a single layer. 1D layers also may require a vertical electrical anisotropic layer. However, many 1D modelling algorithms do not support 1D vertical anisotropy. By employing cyclic electrical transverse isotropy layering (CETI) (Harris, 2001), vertical electrical anisotropy can be achieved. CETI layering involves decomposing a single layer with anisotropy into a number of interbedding 1D layers of isotropic resistivities. The effective horizontal or vertical resistivity are calculated (i.e., vertical anisotropy) through equations 2.5 and 2.6,

$$\rho_v = \frac{1}{2}\rho_1 + \frac{1}{2}\rho_2 \quad (2.5)$$

$$\rho_h = \frac{2\rho_1 \bullet \rho_2}{\rho_1 + \rho_2} \quad (2.6)$$

where,

$\rho_v$ — effective vertical resistivity ( $\Omega \cdot m$  )

$\rho_h$ — effective horizontal resistivity ( $\Omega \cdot m$  )

$\rho_1$ — resistivity of layer 1 ( $\Omega \cdot m$  )

$\rho_2$ — resistivity of layer 2 ( $\Omega \cdot m$  )

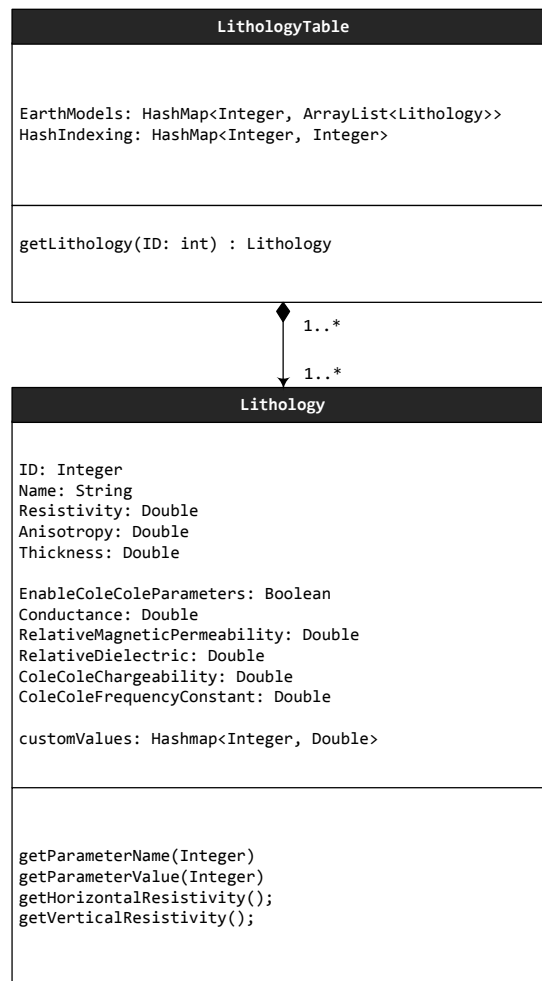
The maximum and minimum resistivities of the cyclic beddings are obtained using these two equations. I have the number of layers in cyclic bedding defaulted at 40 currently.

Single layers contain sub-layering or even more layers as in the case for sea water in cases requiring single layers to contain vertical inhomogeneities in electrical resistivity. The structure seen in Figure 2-18 enables multiple subsets of layering. Each layer contains a lithology which contains the electrical properties and the layer thickness.

Each geo-electrical element contains four lithologies. These four lithologies define the current lithological values, minimum, maximum and weightings. Minimum, maximum and weighted lithologies are included for inversion applications but are not utilized during forward modelling applications.

The real life earth model can be described by many different forms for computational purposes. Since earth model structure widely varies between the main earth model types, each model was created independently. The only common structure is the lithology structure, which contains all electrical properties for a particular geological feature. The earth model interface enables





**Figure 2-18:** The lithology UML data model. Lithology is defined for all geo-electrical units and can be extended to include not only resistivity, anisotropy and thickness but any parameter.

the addition of future earth model types. Overall the earth model can be described in UML format for computational applications.

## 2.6 Development and Implementation of the Data Structure

The data model was developed in Java. Java was chosen for its object oriented design. The data structure was compiled into its own library called ‘open.em’. This library contains approximately 10,000 lines in 100 classes.

System responsiveness is highly important for interactivity (see 14 rules of polite software in Design Heuristics Cooper, 1999). An emphasis was placed on import, sorting and exporting efficiency to achieve a highly responsive system. Unfortunately, electromagnetic data structures require a flexible design. Increased flexibility typically requires a trade-off for speed. A generic table data structure was created for frequency domain surveys whilst maintaining a constant import and export speed for any dataset size. The aim was to create logical objects which fully represent a MCSEM survey whilst minimizing expensive sort and retrieval functions.

All survey information and data is stored in memory to improve computational speed. A database, such as Oracle’s Java DB (JavaDB, 2012) or MySQL (MySQL, 2012), could just as easily be integrated into the software. This design was created to minimise future efforts to convert to a database connection instead of an internal memory structure. Appropriate “SELECT” statements would also need to be written. A generic table class was developed to store the electromagnetic object including transmitters, receivers, waveforms and earth models. An excerpt of the main table code is shown in Figure 2-19. The table class utilizes multiple hashmaps to optimize retrieval and additions of new items. The object table contains all objects indexed by an integer identifier. The indexing Hashmap links the electromagnetic object hashcode with its identifier. This allows objects to be retrieved by index or hashcode. A nested hashmap is used to store property information, with each property containing its own hashmap. All electromagnetic objects including survey, waveform, electromagnetic fields and geoelectrical objects are of a type ‘EMItem’. The ‘EMItem’ interface requires the indexing and property to be defined. For example, an electric bipole transmitter has bipole length, azimuth, dip and bipole start and end for x, y, and z. Each property is stored in the hashmap.

All transmitters can be sorted and retrieved for any property.

Speed influences the interactivity of software. The table structure is the most crucial controllable factor influencing computational time. An experiment was performed to examine the degree of degradation in read/write performance with increasing table size (See Figure 2-20). I compared the average read and write operation times for various table sizes. This test was performed by sequentially adding random generic receivers to the table. This test was carried out six times and then averaged. No decrease in performance with increasing table size was found. Read operations were faster than write operations. Write operations require the indexing of properties and is up to 100 times slower per operation as a result. Read operations can be typically performed in  $1\mu s$  (i.e., 1,000,000 read operations per second) while write operations are performed in  $100\mu s$  (i.e., 10,000 write operations per second). The table structure is adequate for real time interactivity with smaller surveys (i.e., surveys with less than a thousand transmitter-receiver pairs).

The data structure was tested by,

- 1 populating a survey instance with a random survey over a preset 1D earth model
- 2 writing the input file
- 3 executing a single forward model
- 4 importing the created survey

The test was performed using the Dipole1D algorithm (Key, 2009a). A small rapidly changing survey was used for testing. The survey consisted of 100 receivers, one transmitter and one transmission frequency over a 3 layer 1D earth. The below table 2-21 demonstrates the performance between,

- 1 executing the code directly without any data model (i.e., input file already written)
- 2 execution within the data model context (no interface/visualization)
- 3 the final data model within a software package

There is a 20% increase in the total time to execute the survey instance through the created software package and data model. It was found that 10% of the total time was spent in disk access (writing and reading the input and output files without accessing the data model). This

```

package open.em.main.tables;

public class Table <E> {
    public HashMap<Integer, ArrayList<E>> objectTable = new HashMap<Integer, ArrayList<E>>();
    public HashMap<Integer, Integer> indexing = new HashMap<Integer, Integer>();
    public HashMap<Integer, HashMap<Double, SortedIntegerLinkedList>> properties
        = new HashMap<Integer, HashMap<Double, SortedIntegerLinkedList>>(); //Prop ID to property value

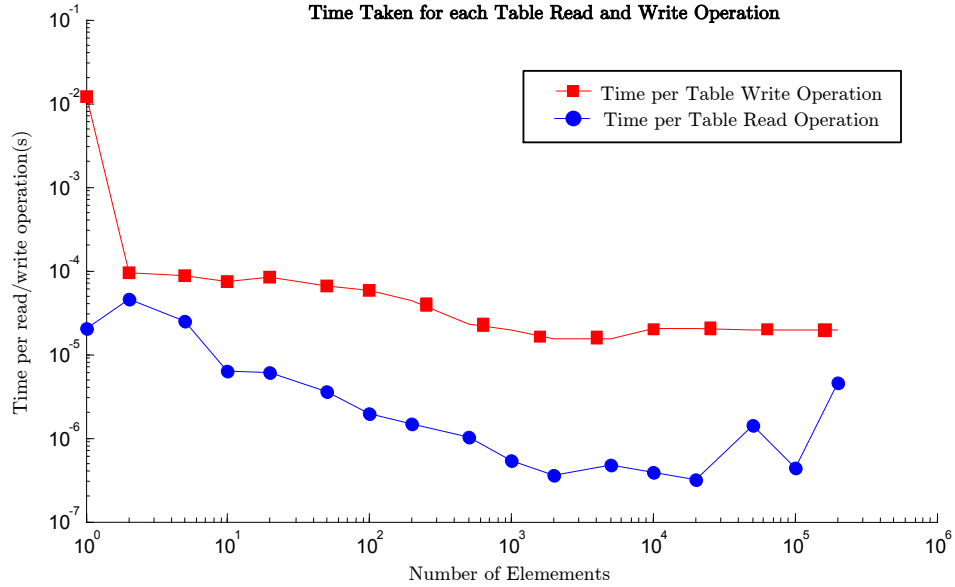
    private int currentID = 0;

    public int add(EMItem i) {
        int hashCode = i.hashCode();
        ArrayList<EMItem> list = (ArrayList<EMItem>) objectTable.get(hashCode);
        if(list == null){
            //No Collision
            list = new ArrayList<EMItem>();
            if(i.getID() == Index.UNKNOWN) i.setID(nextID());
            list.add(i);
            objectTable.put(hashCode, (ArrayList<E>) list);
            indexing.put(i.getID(), hashCode);
            for(int pID : i.getEMpropertyList()) {
                double d = i.getPropertyValue(pID);
                addProperty(pID, d, i.getID());
            }
            return i.getID();
        } else {
            if(list.size() > INNEFFICIENT_LIST_SIZE) {
                System.err.println("Modify Hashcode !" + list.size() + " " + i.getClass());
            }
            if(i.getID() == Index.UNKNOWN) i.setID(nextID());
            list.add(i);
            indexing.put(i.getID(), i.hashCode());
            for(int pID : i.getEMpropertyList()) {
                double d = i.getPropertyValue(pID);
                addProperty(pID, d, i.getID());
            }
            return i.getID();
        }
    }

    public void addProperty(Integer property, Double value, Integer ID) {
        HashMap<Double, SortedIntegerLinkedList> propertyMap = properties.get(property);
        if(propertyMap != null) {
            SortedIntegerLinkedList indexing = propertyMap.get(value);
            if(indexing != null) {
                int identifier = indexing.findIndex(ID);
                if(identifier >= 0) {
                    if(!indexing.containsInteger(ID)) {
                        indexing.add(ID);
                    }
                } else {
                    indexing.add(ID, 0);
                }
            } else {
                indexing = new SortedIntegerLinkedList();
                indexing.add(ID);
                propertyMap.put(value, indexing);
            }
        } else {
            propertyMap = new HashMap<Double, SortedIntegerLinkedList>();
            SortedIntegerLinkedList list = new SortedIntegerLinkedList();
            list.add(ID);
            propertyMap.put(value, list);
            properties.put(property, propertyMap);
        }
    }
}

```

**Figure 2-19:** An excerpt of the significant methods from the Table class. The table structure stores data and properties in multiple hashmaps. Hashmaps enable the fast retrieval and storage of data.



**Figure 2-20:** Time taken for read and write operations to the Table data structure. The example performed is done by adding and retrieving randomly positioned receivers. There is no degradation in table performance with increasing table size.

suggested that the data model resulted in an extra 10% overhead in the worst case scenario (rapidly varying surveys). A 10% overhead in performance was considered acceptable.

Time(s)	Dipole1D	Data Model	Within Package
Average	0.138	0.169	0.168
Median	0.136	0.167	0.169
Minimum	0.120	0.159	0.135
Maximum	0.150	0.198	0.210

**Figure 2-21:** The time taken to compute a survey of 100 receivers for 1 transmitter position and a single transmission frequency over a four layer 1D earth integrated at different stages (i) At the algorithmic level (i.e. the time taken to finish execution and output) (ii) At the data model level (i.e. the time taken to execute and import the data into a data model) and (iii) Within the package (i.e. the time taken to execute, import the data into the data model and finally visualise the response). The table shows that there is not a significant difference between the three different levels.

## 2.7 Conclusion

The data model has been designed on the basis of real world requirements of any controlled source electromagnetic survey. UML has been used to structure the relationship between all components of a CSEM survey. The data model considers any realistic variations and evolution of the MCSEM method. All major transmitter and receiver types and the addition of more transmitter and receiver forms are supported. The survey configuration design supports any survey type ranging from towed streamer systems to fixed receiver systems. Any survey can be represented within the data model. A flexible data model was used to represent frequency-domain and time-domain data. This structure enabled fast access to any electromagnetic property. Incorporation of any geo-electrical model type is also possible. The object-oriented design has been crucial in the development of this model. OOP paradigms have led to an easily modifiable, extendable and maintainable code base which can be utilised for any electromagnetic modelling problem. It was developed to be embedded into any EM software package. The data model was found to be efficient to store, retrieve and represent real world and synthetic electromagnetic surveys and data.

# Development of Interactive Open Source Electromagnetic Software

Chapter 3 covers the development of the new interactive open source electromagnetic software as discussed in Chapter 2. This chapter covers the need for publicly available controlled source electromagnetic software. Design heuristics, the development process, software progression and the worldwide usage is covered by this chapter. The following chapters are based on this software package. A summarised overview can be found in [Appendix D](#)

## Contents

<b>3.1 Overview</b>	<b>84</b>
3.1.1 Licencing	84
3.1.2 Java and the Development Environment	85
3.1.3 Design Heuristics	86
<b>3.2 The Software Structure</b>	<b>86</b>
3.2.1 The Graphical User Interface	90
3.2.2 Visualisation and Interactive Viewer Development	96
3.2.3 2D Visualisation	98
3.2.4 3D Visualisation	109
3.2.5 Visualization with Fractals	112
3.2.6 Interactivity	118
3.2.7 Integration of Third Party Algorithms	121
3.2.8 Multi-Threaded Execution	125
<b>3.3 Improvements</b>	<b>127</b>
<b>3.4 Overview of Developed Software Versions</b>	<b>128</b>
<b>3.5 Impact of the Software and Online Resources</b>	<b>130</b>
<b>3.6 Conclusion</b>	<b>130</b>

## 3.1 Overview

There has been a notable lack of publicly available marine CSEM software despite technical advancements over the last decade. I contend that MCSEM software is still in its infancy, with only a small number of open source algorithms and packages available to the public. My objective is to create an open source, user-friendly CSEM forward modelling package providing users with a way to research the intricacies of MCSEM and general electromagnetism. This package is to be built upon the data model design discussed in Chapter 2.

The main requirement of the software is to be able to model marine controlled source electromagnetic method. The created software is required to:

- i be free and open source to encourage the development of the MCSEM in industry and research institutions
- ii be fully written in Java 1.6 or higher software development language to improve portability and to interface with the data structure
- iii be executed on major operating platforms including Debian Linux, Mac OSX and Windows
- iv be easy and intuitive to use
- v contain an integrated 2D viewer to render 1D and 2D structures such as profiles, earth models, borehole logs, grids and vectors
- vi contain an integrated, 3D viewer for rendering 3D objects
- vii encourage interactivity between the user and survey, earth model and data elements
- viii easily incorporate any third party geophysical electromagnetic modelling algorithms.

### 3.1.1 Licencing

An open source paradigm was used to encourage further development of MCSEM in both industry and educational institutions. My CSEM software is licenced under the GNU v3.0 agreement (GNU, 2007). The GNU GPL licence allows the free modification and distribution of source code. GNU GPL requires the provision of source code for the base program, however plug-ins can be developed allowing the integration of third-party algorithms without compromising the privacy of the proprietary code. The open source code is available on a



public SVN server (Pethick, 2012b).

The grid and cloud computing and networking code has licensed under the “do What The F- you want to Public License” version 2.0 (Hocavar, 2004). This provocative public licence agreement is usually referred to as WTFPL. The licence (originally written by the Linux Debian project leader Sam Hocavar (Garbee et al., 2010) is an extremely permissive licence which has absolutely no restrictions. The clear licencing removes possible fears geophysical users and developers may have without users/developers worrying about breaking licence agreements.

### 3.1.2 Java and the Development Environment

Java was chosen as the primary programming language because of its flexibility in object orientation. It is also a multi-platform language enabling software to run any operating systems that supports the Java runtime environment. Testing and maintaining my software on all operating systems is unreasonable, however I have chosen produce software which runs on the three major operating system systems, Linux, Macintosh and Windows, all of which are supported by Java. It is tempting to use a mix of external non-Java libraries for the ease of development, but using non-Java libraries may remove the software’s portability between the major operating systems. The only exception is using Java OpenGL (JOGL, 2012a) used for 2D and 3D rendering.

The Eclipse integrated development environment (IDE) was chosen as the development environment. Eclipse is an integrated development package combining rapid development, debugging and compilation tools in a single environment, making it highly superior to console Java compilers and the IDE of choice for many Java developers (Murphy et al., 2006). The combination of the Java programming language and eclipse IDE allows for rapid development of structured, portable and visually rich software packages.

### 3.1.3 Design Heuristics

I have employed every effort to make this software interactive, efficient and intuitive. The “14 Principles of Polite Applications” (Cooper, 1999), “8 Golden Rules of Human Computer Interaction” (Shneiderman and Ben, 1998), and “10 Usability Heuristics” (Nielsen, 1994) were applied to make the software as interactive and user friendly as possible. Figure 3-1 overviews the rules of the design heuristics which my software attempts to employ. It is evident in past geophysical software practices that functionality is valued over user friendliness, increasing the time spent in training users. Adhering to these heuristics and rules would improve human computer interaction (HCI).

CSEMoMatic must be user friendly reducing the need for complex human computer interactions (HCI). My software is operable without a keyboard and can be easily transferred onto a modern touch screen tablet, running on Windows or Linux operating systems (Pethick and Harris, 2012). The learning curve is significantly reduced when these principles are applied, allowing geophysicists to concentrate on data analysis rather than software complexity. Since software interactivity is a major requirement, certain rules become more important. Rules including, “Polite software gives instant gratification” (Cooper, 1999), “polite software is taciturn about its personal problems” (Cooper, 1999), “visibility of system status” (Nielsen, 1994) and “aesthetic minimalist design” (Nielsen, 1994) are exercised to promote the interactivity of the software. The process of forward modelling and investigating CSEM data should be a “enjoyable” learning experience rather than “just being tolerated” for utility, when these principles are employed.

## 3.2 The Software Structure

My software builds upon the data model created in chapter 2. CSEMoMatic consists of several development layers (see Figure 3-2). These layers are hierarchical and modular allowing lower levels to be integrated into other applications. The layers include,

- i java compiler
- ii persistence layer
- iii data model
- iv execution

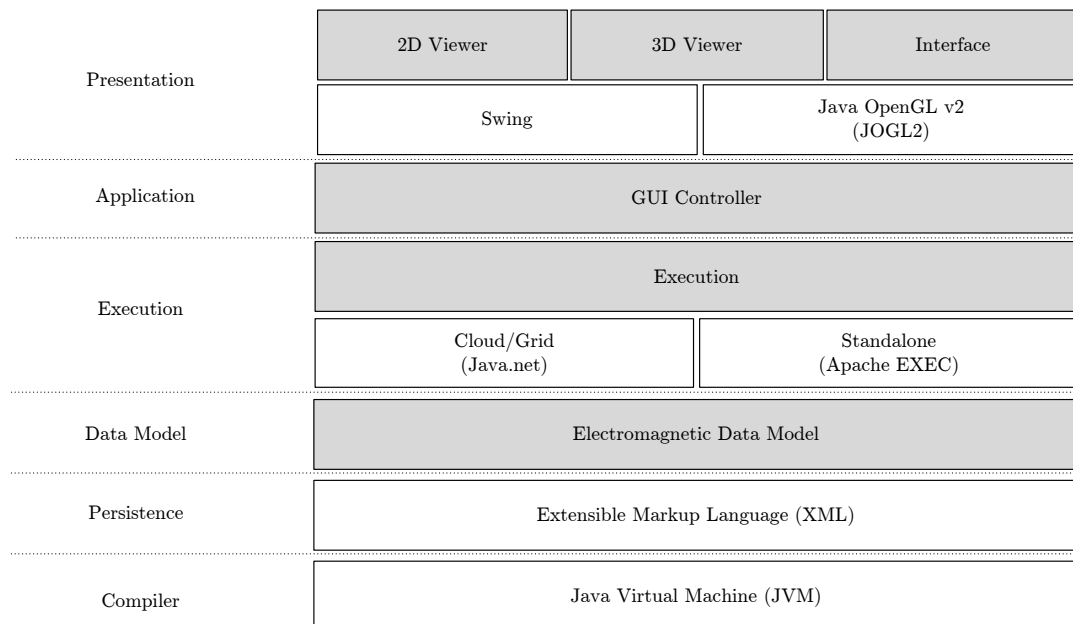
14 Rules of Polite Software	
1.	Polite Software Is Interested in Me
2.	Polite Software Is Deferential to Me
3.	Polite Software Is Forthcoming
4.	Polite Software Has Common Sense
5.	Polite Software Anticipates My Needs
6.	Polite Software Is Responsive
7.	Polite Software Is Taciturn About Its Personal Problems
8.	Polite Software Is Well-Informed
9.	Polite Software Is Perceptive
10.	Polite Software Is Self-Confident
11.	Polite Software Stays Focused
12.	Polite Software Is Fudgable
13.	Polite Software Gives Instant Gratification
14.	Polite Software Is Trustworthy
10 Usability Heuristics	
1.	Visibility of system status
2.	Match between system and the real world
3.	User control and freedom
4.	Consistency and standards
5.	Error prevention
6.	Recognition rather than recall
7.	Flexibility and efficiency of use
8.	Aesthetic and minimalist design
9.	Help users recognize, diagnose, and recover from errors
10.	Help and documentation
8 Golden Rules of HCI	
1.	Strive for consistency
2.	Enable frequent users to use shortcuts
3.	Offer informative feedback
4.	Design dialogs to yield closure
5.	Offer error prevention and simple error handling
6.	Permit easy reversal of actions
7.	Support internal locus of control
8.	Reduce short-term memory load

**Figure 3-1:** The design heuristics which are employed in CSEMoMatic. These design heuristics, when followed, produce quality software which users appreciate rather than tolerate. These three design heuristics, the 14 rules of polite software (Cooper 1999), 10 usability heuristics (Nielsen 1994) and the 8 golden rules of HCI (Shneiderman and Ben 1998) cover different philosophies for creating user friendly software.

v application

vi presentation

The Java compiler forms the base of my software. Java was chosen as the primary programming language for development. The base layer of Java is the Java Virtual Machine (JVM). The JVM forms the cornerstone of the Java Platform. It is responsible for running the binary class files (Lindholm et al., 2012). It forms the base for all programming. Java was also chosen because it is capable of object orientation (See Chapter 2) to represent real life objects and their properties in a structured programmatic form.



**Figure 3-2:** Current software structure. The software structure contains several layers. The grey components have been designed and written by myself while the white components are third party software libraries and compilers

The persistence layer stores program settings on secondary memory (i.e. the hard disk drive). This persistence layer is created by using XML libraries to store and retrieve programming settings in the XML file format. The XML file format is well established, highly structured and flexible (Quin, 2012) making it well suited for electromagnetic applications.

This data model layer was described at length in chapter 2. The data model stores electromagnetic survey structures, ranging from receivers, transmitters, earth models, survey configurations, waveform and TD and FD data. My developed software package is based on this layer.

The execution layer primary purpose is to execute external algorithms through system calls. The execution layer converts survey instances into algorithm specific input files by communicating between the electromagnetic data model and the algorithm instance. Algorithm executables are run and is monitored for errors or completion through the execution layer. Finally the execution layer reads the computed data either through piped streams or data files and re-organises the data into the data model of the corresponding survey instance. The execution layer controls multi-threading for single PC, cloud and grid based computing applications. A number of third party libraries were integrated into the execution layer including; the Java.net package (Java, 2012) for network protocols and the Apache EXEC (Apache, 2012a) for execution and monitoring.

The application layer controls the behaviour between the data model, execution and presentation layers. It is essentially the program without the interface.

The presentation layer the graphical representation and user interface (GUI). This presentation layer contains GUI components for data visualisation, input and manipulation of survey properties, data, geo-electrical models and algorithmic execution properties. This presentation layer utilizes Swing (Swing, 2012) and JOGAMP's version of Java OpenGL (JOGL2) version 2 (JOGL, 2012a).

Overall this layered heirachical structure produces modular software which can be invoked as a background service, graphically for user interactivity and within other packages as a library.

My final electromagnetic software version is called CSEMoMatic - Omnium. The Latin word '*Omnium*' was chosen because it roughly translates in English to "for all". As of now (January, 2013), the CSEMoMatic software has publically integrated Dipole1D (Key, 2009a) and AMIRA's 3D Integral Equation Marco (Xiong, 1992) algorithms. A number of proprietary algorithms have been developed and integrated into a proprietary versions including Hursan and Zhdanov (2002) 3D integral equation algorithm INTEM3D, a quasi-analytical inversion

algorithm QAINV (Zhdanov et al., 2000) and a 2.5D irregular finite difference modelling Otze (Scholl and Sinkevich, 2012). Considerable work has been placed into CSEMoMatic. Overall approximately 100,000 lines of Java code have been written by myself for all the versions of CSEMoMatic.

### 3.2.1 The Graphical User Interface

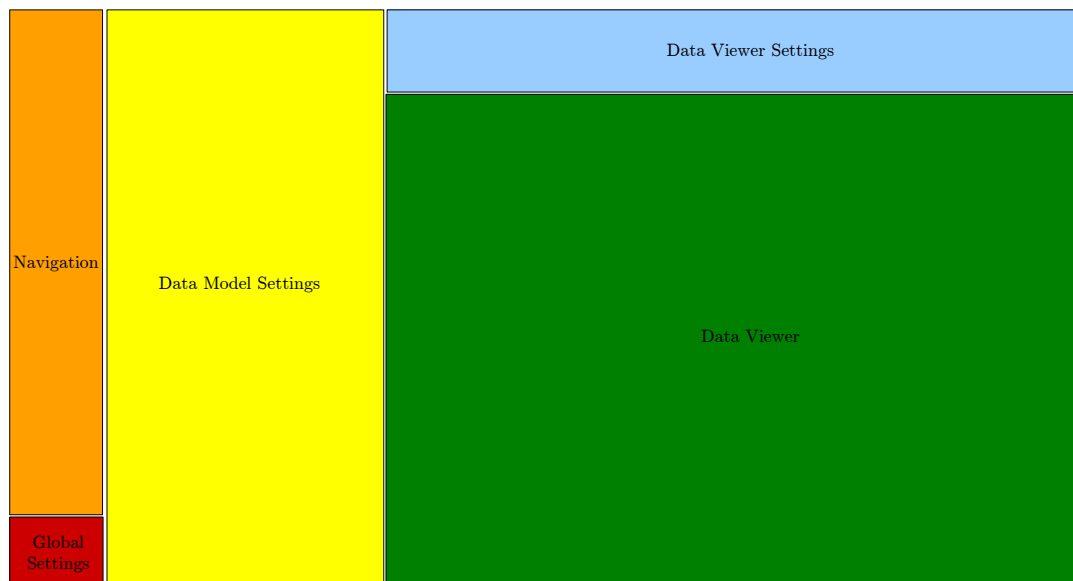
An emphasis on user friendliness was placed on the development of the software. It is challenging to produce clean user friendly geophysics software. The large range of geophysical parameters coupled together with geophysical specific visualisation places limits on a programmer's ability to develop clean user friendly interfaces. I aim to create software which can be used by students and professional researchers alike with minimal training. This was achieved by following the paradigms found in Figure 3-1.

The structure of the graphical user interface program is shown in Figure 3-3. The components which make up the interface include,

- i navigation
- ii data model settings
- iii global settings
- iv data viewer
- v data viewer settings

#### 3.2.1.1 Look and Feel Consistency

Standardized naming for all labeled GUI elements allows users to recognize real world structures in software (Nielsen, 1994). All terms used in CSEMoMatic to describe or label any object was made familiar to geophysicists. Computer science jargon was avoided when possible. Using common geophysical terms reduces learning time. All graphical user elements (i.e. buttons, forms and sliders) are consistent with one another. Using standard icons, button styles, menus and right-click context menus and maintaining the same GUI slider structure delivered consistent interactive parameter modification. For example, each numerical parameter (i.e. frequency) was represented with a slider panel. Each slider panel contained a label and a parameter input slider, text input and preset menu input. The slider input



**Figure 3-3:** The overall GUI design. To create a user friendly software I opted for a simple user interface which is responsive, aesthetically pleasing with a minimalist design and consistent. The rules and paradigms found in Figure 3-1 were employed to achieve this.

enabled users to continuously vary parameters whilst text input enables users to include a specific user input value. All methods of input were standardised.

Maintaining a consistent look and feel via standardized naming conventions adheres to the rules found in (Nielsen, 1994). Making software which is coherent between real world terms and software labels and maintaining consistent input methods reduces the time for end users to learn the nuances of the software.

### 3.2.1.2 Navigation

The graphical user interface is structured to be as simple and as intuitive to navigate as possible, reducing the time needed for training. Navigation between electromagnetic function is done through the color coded navigation pane. Each navigation options is labeled, color coded with a simple icon. Two graphical user interfaces have been produced (i.e. CSEMoMatic 1.4 and CSEMoMatic Omnium). Both interfaces have been similarly constructed (See Figure 3-4). Users navigate to settings via the navigation options (left). Select data model components (i.e. waveform, receivers, transmitters, geo-electrical model and survey setup) have a corresponding user options panel. When selected the settings panel becomes visible, replacing the previous

settings panel (see Figure 3-3). The options panel enables interactivity between the visualized component and the data model.

Limitations on human memory requires programs to be structured to reduce the “short term memory load” on users (Shneiderman and Ben, 1998). That is, information needs to be consolidated so users do not have to remember large volumes of information. Electromagnetic components are split into its individual settings panel. Each of the real world options (i.e. transmitter, receiver or waveforms) are consolidated into an individual settings panel to the right of the navigation menu (see Figure 3-5). Navigation options of similar function are grouped using a “common sense” approach (Cooper, 1999). Each function is colour coded, labelled and contains a simplistic memorisable icons. This creates multiple distinction between each function, minimizing the need to remember the location of each option or function. The tabbed navigation menu button is also highlighted using a color coded spacer. This highlighting reduces the need for the users to remember the active menu option (i.e., following the rules “reduce short term memory load” and “recognition rather than recall”; Nielsen, 1994 and Shneiderman and Ben, 1998).

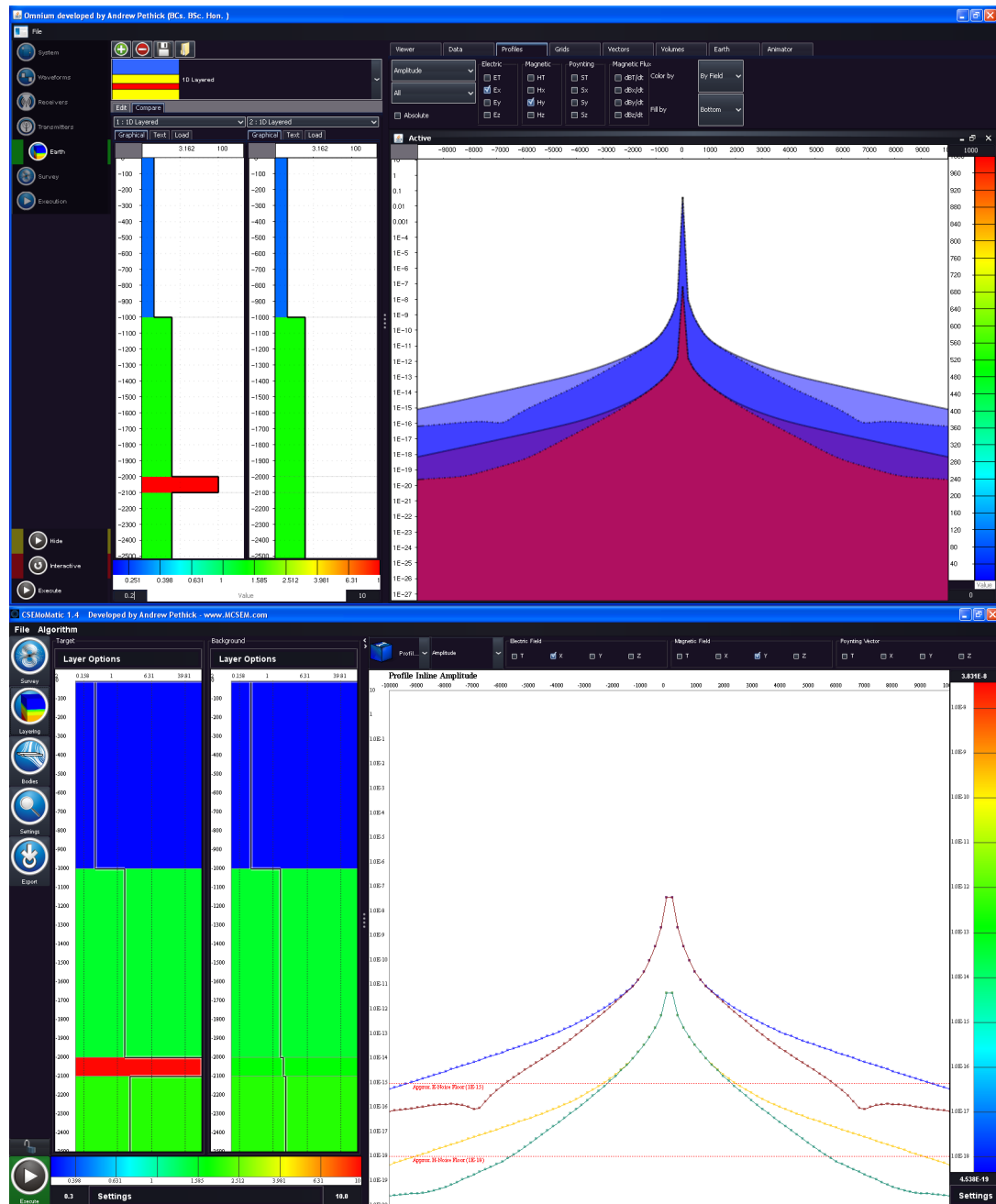
### 3.2.1.3 Data Model Settings

The data model settings panel accesses the underlying data model. The data model settings panel is located to the right of the navigation panel. The settings panel contains the settings corresponding to the selected electromagnetic component (i.e. receivers, transmitters, earth models etc.). Each settings panel is labeled with the corresponding geophysical term. Figure 3-6 shows several types of settings panels. The development of each panel is highly dependent on its function. The data model settings and visualisation settings are separated. There is a marked difference in function. Separating data model and visualisation settings is more consistent in design and I believe is more intuitive for usability.

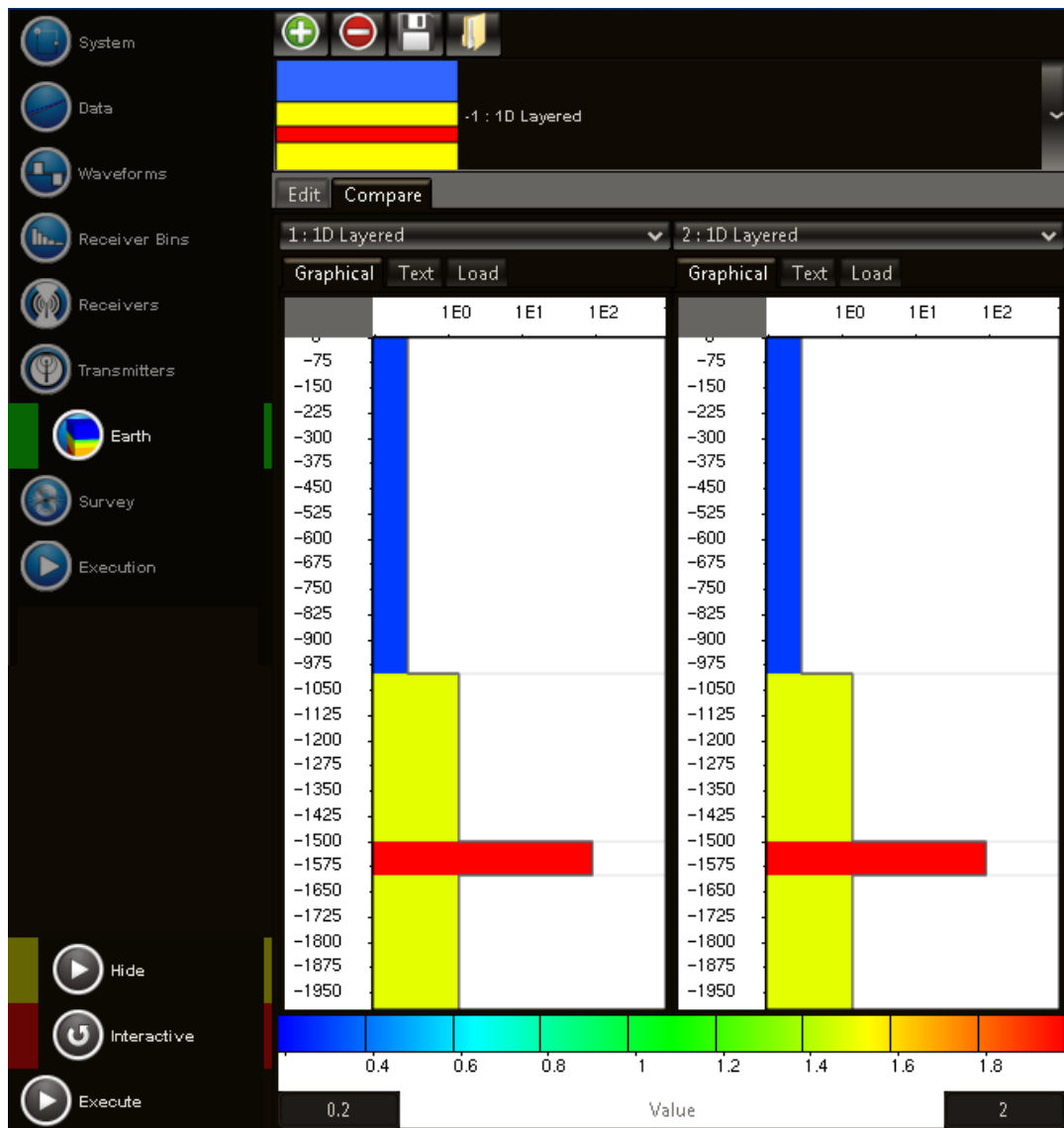
### 3.2.1.4 Global Settings

The global settings panel contains functions related to the immediate execution of algorithms. This includes an execution monitor and manual execution button. The visibility of the system status is shown in the execution monitor. The monitor, shows the status of the currently executed task. The monitor also consists of a controls which selects the type of execution

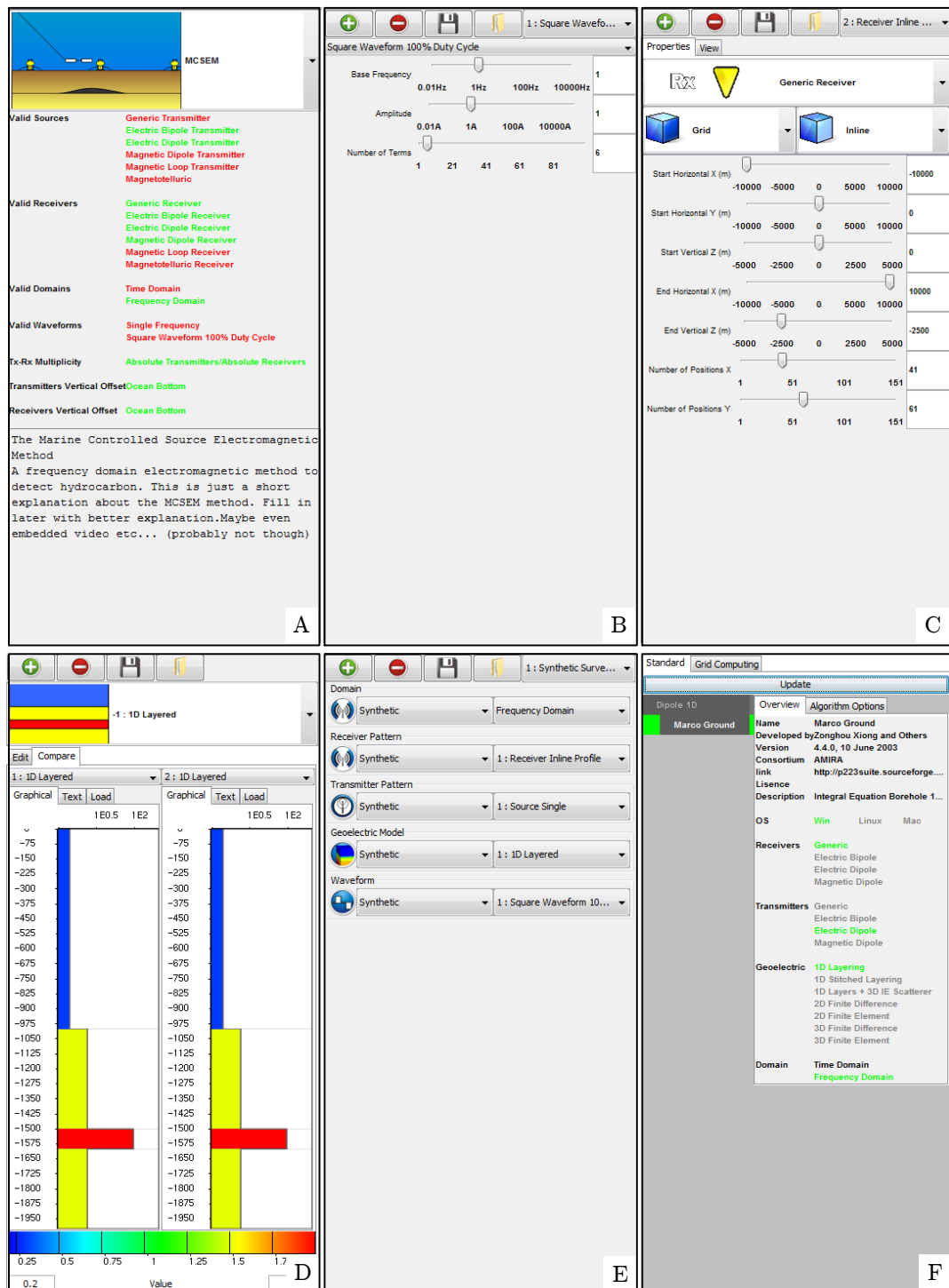




**Figure 3-4:** Comparison of CSEMoMatic 1.4 (top) and CSEMoMatic Omnium (bottom) graphical user interfaces. The two versions of CSEMoMatic have the same main structure. Global settings (bottom left), navigation (left), data model settings (centre) and viewer and viewer settings (right) are all included in both designs. This Figure also shows the differences between Swing and JOGL implementations. JOGL enables 2D graphics to be rendered with greater efficiency resulting in a faster and smoother display of results.



**Figure 3-5:** A screenshot from CSEMoMatic Omnium showing the navigation (left) and settings panel (right). Each of the navigation options is linked to a specific electromagnetic component. This electromagnetic component settings connects the GUI with the data model. Each labeled navigation option is color coded and contains an icon improving usability. As each option is selected the corresponding electromagnetic settings are shown in the right panel.



**Figure 3-6:** Examples of different electromagnetic component setting panels. Each panel represents a GUI feature which enables the data model to be modified by the user. These six panels show generally the steps taken to model a CSEM survey. (A) shows the survey type, this is where the main survey configuration is selected (B) waveform selection and options (C) receiver type, pattern options (D) geo-electrical earth model type selection and settings (E) Survey instance creation (F) Execution options.

(i.e. interactive or manual execution). This execution monitor can be paused, which stops any interactive forward modelling.

### 3.2.1.5 Data Viewer and settings

The data viewer panel is comprised of multiple internal viewer panes. The viewer settings panel contains the visualisation options for the selected internal viewer pane. The data viewer pane and data viewer settings pane is linked. Each viewer has its own viewer settings stored in an XML format. The settings pane is updated with these XML settings when the viewer is selected. The settings include data visualisation options and data selection. For example electromagnetic component profile selection is included (i.e. Ex, Ey and Ez). The option to compare between datasets (i.e. normalised and differences options) is also included in the settings. The XML settings are updated with each user interaction with the viewer settings GUI.

## 3.2.2 Visualisation and Interactive Viewer Development

Electromagnetic fields can be visualized by several unique representations not typically encountered in potential field and seismic methods. The level of understanding complex electromagnetic field behaviour is influenced by visualising method. Seismic and potential field software packages focus visualisation on volume rendering and interpolation methods. These methods are similar to the volume extraction and investigations methods developed for the medical industry (Marsh et al., 2000) rather than vector or tensor visualisation techniques. I was unable to integrate an existing seismic, potential field or medical visualisation library because the methods insufficiently visualise the complex tensor nature of electromagnetic field behaviour.

### 3.2.2.1 Swing vs JOGL

Two-dimensional visualisation performed by Java Swing (Swing, 2012) in earlier CSEMoMatic versions (i.e. versions prior to v1.4). Although successful for simple two-dimensional datasets, Swing was unable to visualize large 3D datasets with sufficient speed. Swing is much slower rendering complex datasets than JOGL2 and was limited to rendering profiles, small 2D grids with 2D vectors and 2D streamlines. 2D and 3D rendering with JOGL enables large

electromagnetic datasets to be visualised quickly and accurately. JOGL renders data smoothly and is responsive to user feedback (Cooper, 1999).

The rendering capabilities were then upgraded in CSEMoMatic Omnium. A flexible 2D and 3D visualisation library integrating the Java open graphics library (JOGL2) library was developed. JOGL, a wrapper library to the C-programming library OpenGL, bridges the programming gap by calling C-library functions via the Java native interface (JNI) (JNI, 2012). JOGL has successfully been integrated into other scientific and geophysical applications such as NasaWorldWind (Hogan, 2011), SciLab (SciLab, 2012) and Dave Hales Java tool kit (Hale, 2006). The 2D and 3D visualisation library enabled vector fields to be rendered.

#### 3.2.2.2 Visualised Entities

I call each visualisation entity a structure. A structure contains rendering instructions specific to the datatype. For example ‘Structure3DVector’ contains rendering instructions for a vector defined by a three-dimensional scalar and co-ordinate. A structure may also implement instructions involved in responding to user input (i.e. keyboard and on-screen mouse interactions). Both 2D and 3D viewers have a unique set of structures. Any structure can be created which utilises any low level JOGL rendering commands (i.e. draw buffer, line, polygon etc. . . )

#### 3.2.2.3 Core Viewer

2D and 3D data viewers are based on the same core viewer. The viewer core is built upon the JOGL ‘GLJPanel’ class. ‘GLJPanel’ is a “lightweight swing component which provides OpenGL rendering support (JOGL, 2012a). The GLJPanel acts like any other swing ‘JPanel’ and is compatible with the integration of heavy weight Swing GUI components (JOGL, 2012a). The core viewer contains common functions to both 2D and 3D viewers. This viewer is a low level structure manager and low level user input parser. The core viewer does not render the final image or dictate what is done with user inputs. All visualisation is performed in a base viewer built upon JOGL. Each viewer contains basic methods to add, remove and render structures. The interactive viewer also receives user input. Keyboard, mouse motion and mouse button and mouse wheel input listeners have been integrated into the base viewer class.

These inputs are handled independently by the 2D and 3D viewers. Overall the purpose of a viewer is to,

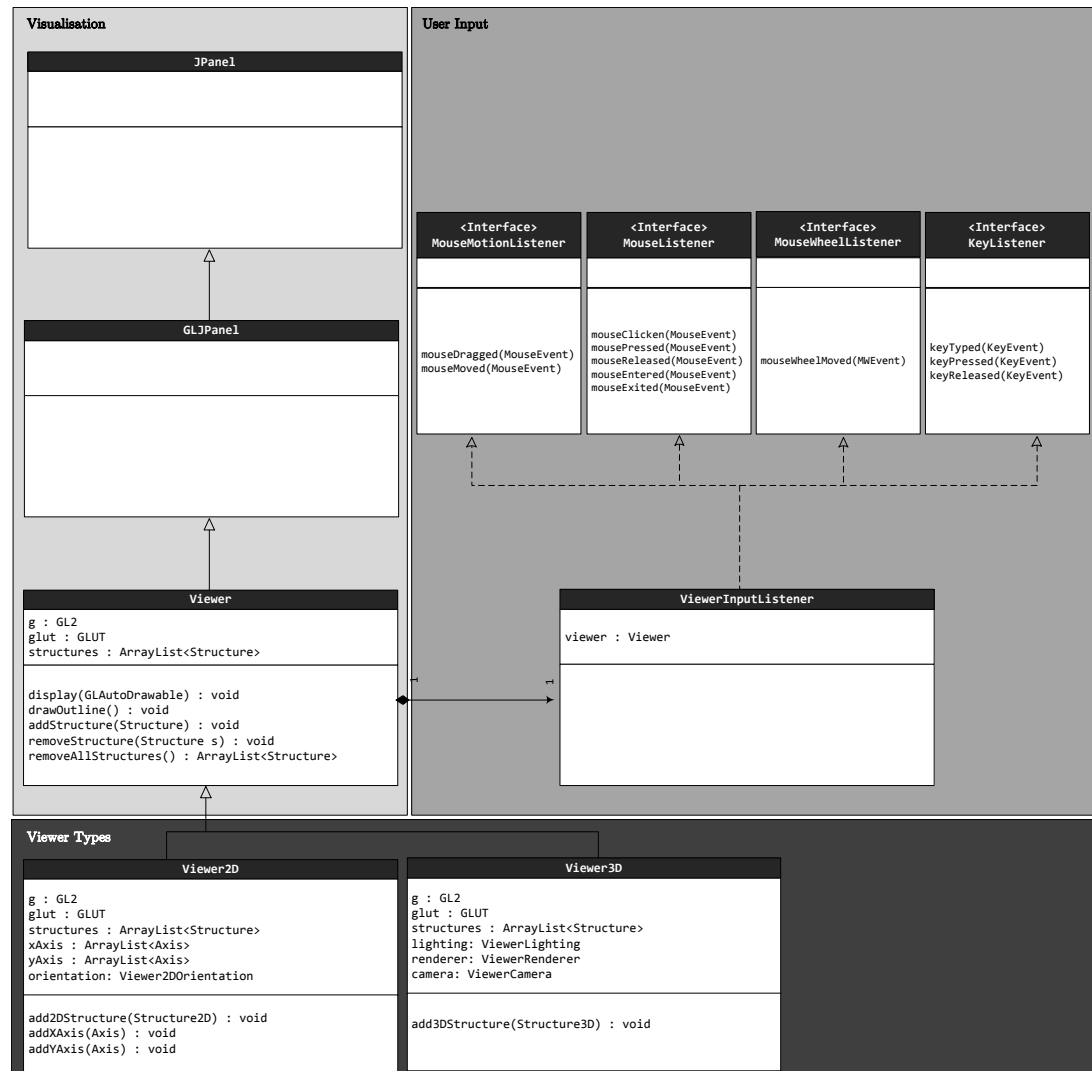
- i manage the rendering order of electromagnetic structures
- ii control structures (i.e. add, remove and update structures)
- iii receive user interactions by mouse and keyboard and pass user input to the selected visualised structure

The 2D and 3D viewers extend the viewer base (See Figure 3-7). Figure 3-7 shows the UML representation of 2D, 3D and base viewers. The 2D and 3D viewers contain higher level functionality. For example 3D viewers have user camera controls and rendering options including lighting and shading. The 2D viewer has no adjustable camera or lighting, but have x and y axis controls. These development of these two viewers are covered in the next two sections. Java OpenGL enables both 2D and 3D visualisation of electromagnetic data. My implementation of a viewer uses low level JOGL controls to facilitate visualisation of any complex 3D or 2D electromagnetic field structure. Overall the viewer structure enables the access to low level rendering capabilities through JOGL and manages the visualised structures and user input.

### 3.2.3 2D Visualisation

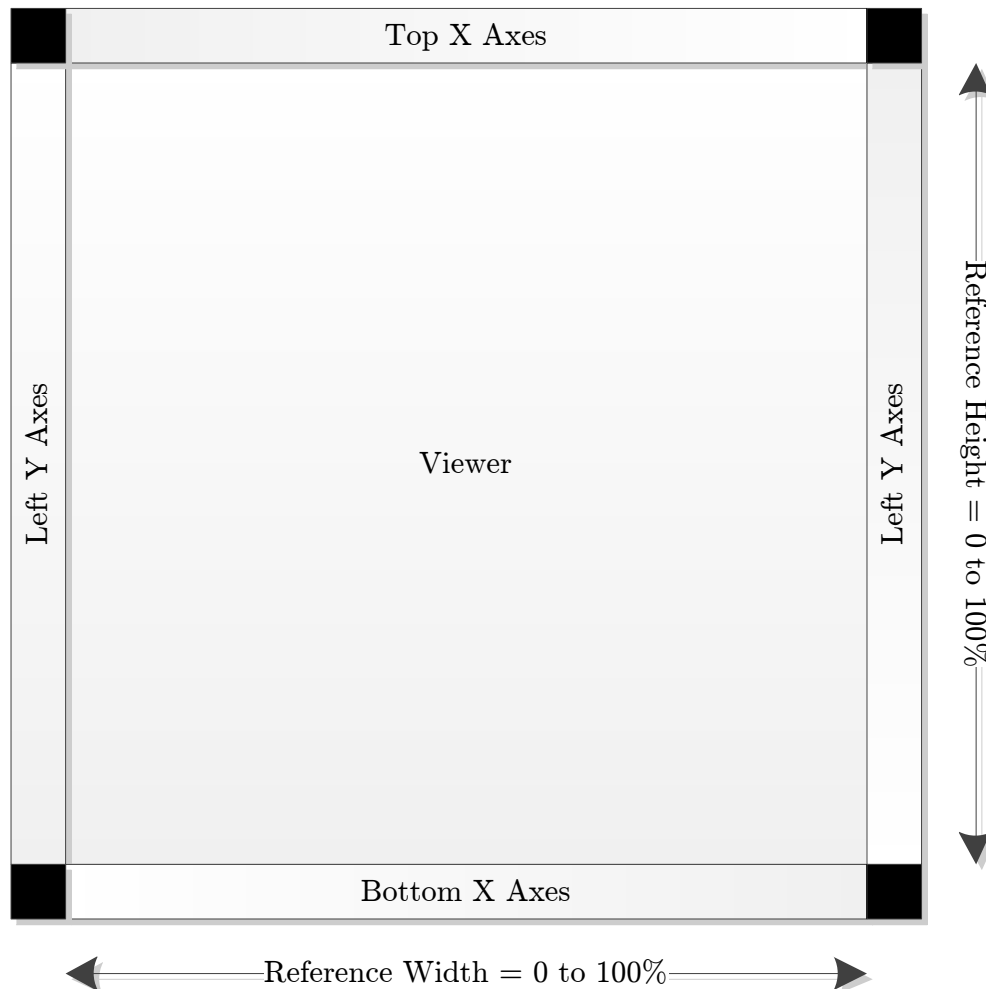
The 2D viewer visualises point data and two-dimensional datasets. The 2D viewer is an extension of the viewer class. The 2D viewer requires the flexibility to paint 2D complex shapes specific to electromagnetism (i.e. polarisation ellipses and vectors). A number of Java visualisation packages exist (i.e. Hale, 2006; SciLab, 2012 and Hogan, 2011). However these packages do provide the structures necessary to represent unique MCSEM or electromagnetic datatypes. A 2D plotting package was developed ontop of the base viewer.

The standard layout of the 2D viewer can be seen in Figure 3-8 while a screenshot of a blank viewer is seen in Figure 3-9. Each viewer is composed of a viewing area surrounded by a number of independent axes. Each axis has two responsibilities, firstly to map a co-ordinate system into viewer area co-ordinates. The second responsibility is to automatically compute axis ticks and visualise the resulting axis. The viewing area has a static co-ordinate system; it is represented by a floating point value from 0 to 1 in both horizontal and vertical co-ordinates. This percentage represents the position seen by the user on the viewer. The axis maps the



**Figure 3-7:** The UML Structure of both 2D and 3D viewers. JOGL forms the foundation of the GLJPanel which contains the low level 2D and 3D rendering functions. My base viewer is based on this class. The base viewer receives user instructions to be passed to the higher level 2D and 3D viewers. The user input includes mouse motion, click and wheel listener and keyboard input. The 2D and 3D viewers contain the main functions for 2D and 3D rendering respectively. The 2D viewer contains interactive x and y axis while the 3D viewer contains camera, lighting and rendering options. Each 2D and 3D viewer contains its own visualized structure class contain the final rendering and user control actions.

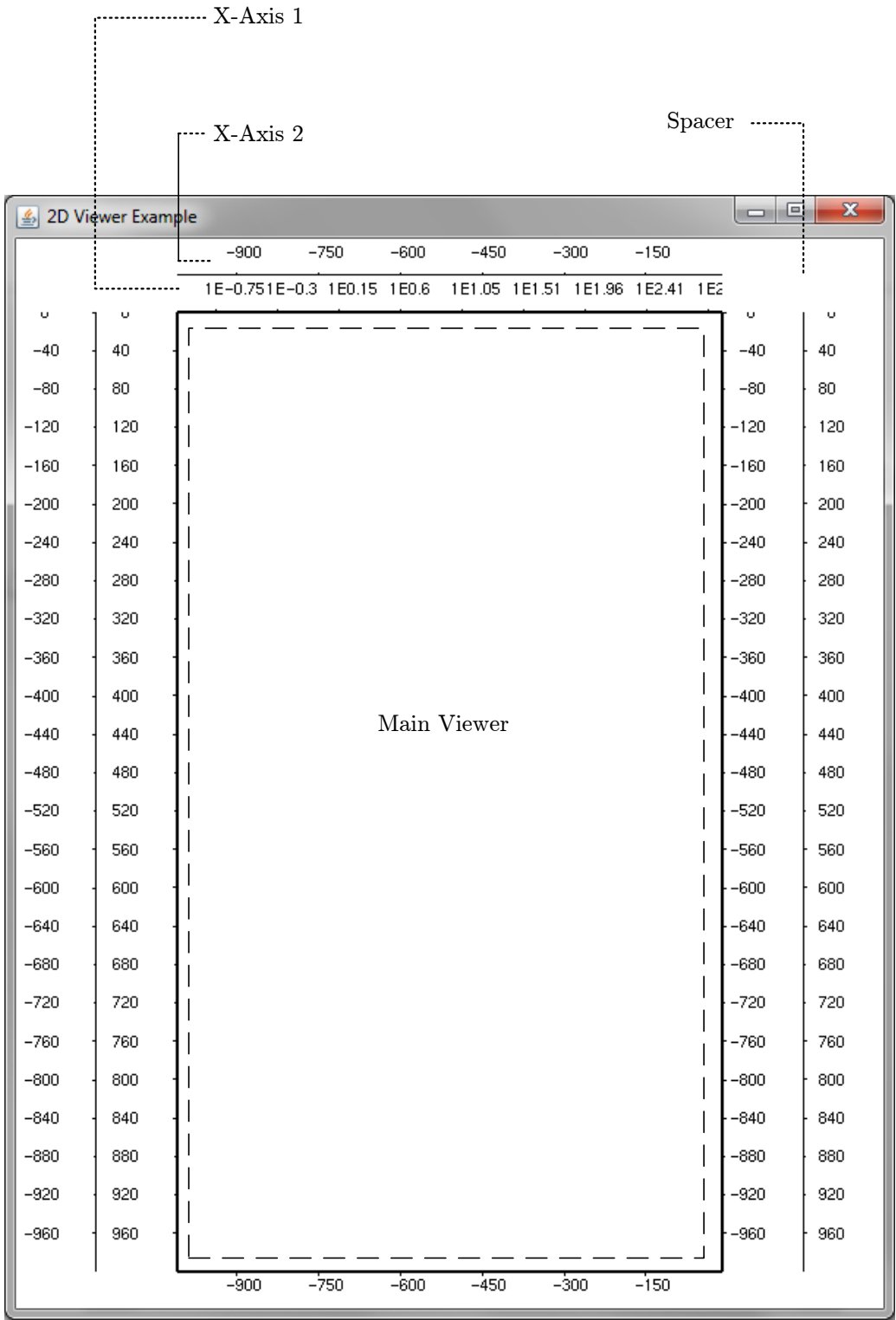
data coordinates into this XY percentage coordinate.



**Figure 3-8:** The layout of the 2D viewer. The whole 2D viewer extends the JPanel class and contains the axes and GLJPanel viewer. The 2D viewer is the data visualisation area and is based on the 'Viewer' class. The 2D viewer allows multiple independent axes to map various co-ordinate systems onto the reference grid via a floating point percentage (i.e. 0 to 100%)

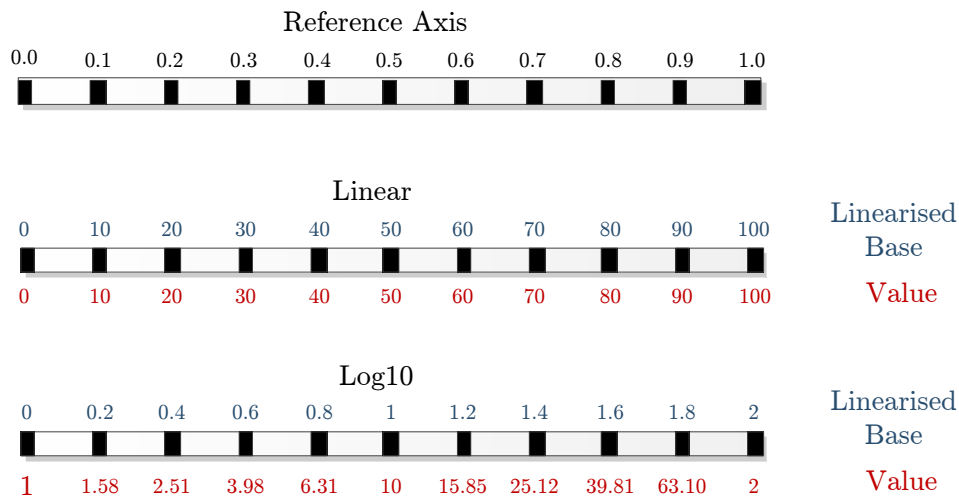
To simplify the mapping of axis to viewer co-ordinates, all axis transforms are linearised. This linear mapping allows the automatic computation of the axis ticks (i.e. the axis numbers). For example  $\text{Log}_{10}$  transforms are linearised prior to axis tick computation. If an axis is ranged from 0.01 to 1000, the resulting ticks may be 0.01, 0.1, 1, 10, 100 and 1000. If the axis has a linear transform, the axis ticks may be 250, 500, 750 and 1000. The  $\text{Log}_{10}$  transform has a linear form (i.e.  $10^n$  where  $n$  is the linearised term) (See Figure3-10). Several axis transforms





**Figure 3-9:** An example of a blank 2D Viewer. The 2D viewer can utilize multiple independent horizontal and vertical axis.

were created including,  $\text{Log}_{10}$ ,  $\text{Log}_2$ ,  $\text{Log}_e$ , Linear and a rudimentary Psuedo-Log scale using this linearized approach. The 2D viewer enables several co-ordinate systems to be plotted on the same viewer by using multiple axes.



**Figure 3-10:** Transforming between axis-coordinate system and the linearised base. This demonstrates how the viewer axis maps a value to the viewer area. The example shows a range of values from 1 to 100 in both linear and  $\text{Log}_{10}$  systems transformed into the linearised base and finally the reference axis coordinate system. This reference coordinate represents the onscreen position. In this same fashion a pseudo log axis was included into the software.

A structure is a single visualised element in a viewer. The ‘Structure’ class was extended to create a 2D specific structure. This 2D structure (i.e. the ‘Structure2D’ class) is linked to an x and y axis through an initial binding. Any change to the bound axis co-ordinates will refresh all the structures linked to that axis.

Each structure is static by default. Users cannot interact with any structure unless the interface ‘GLInteractive’ is implemented. The ‘GLInteractive’ class contains input functions which are to be implemented. The ‘2DStructure’ UML representation shows the relationship between the 1D earth model and the structure 2D class (Figure 3-11). The earth model 1D (i.e. the ‘StructureEarth1D’ class) is an extension of ‘Structure2D’ which is an extension of the more low level ‘Structure’ class. The ‘Structure’ class contains the low level access to the OpenGL scene. The ‘Structure2D’ class contains access to 2D specific components (i.e. axis and 2D viewer) and ‘StructureEarth1D’ contains the specific rendering and user interactivity instructions. Using the ‘Structure’ several 2D visualised structures were created (see Figure 3-12) including,

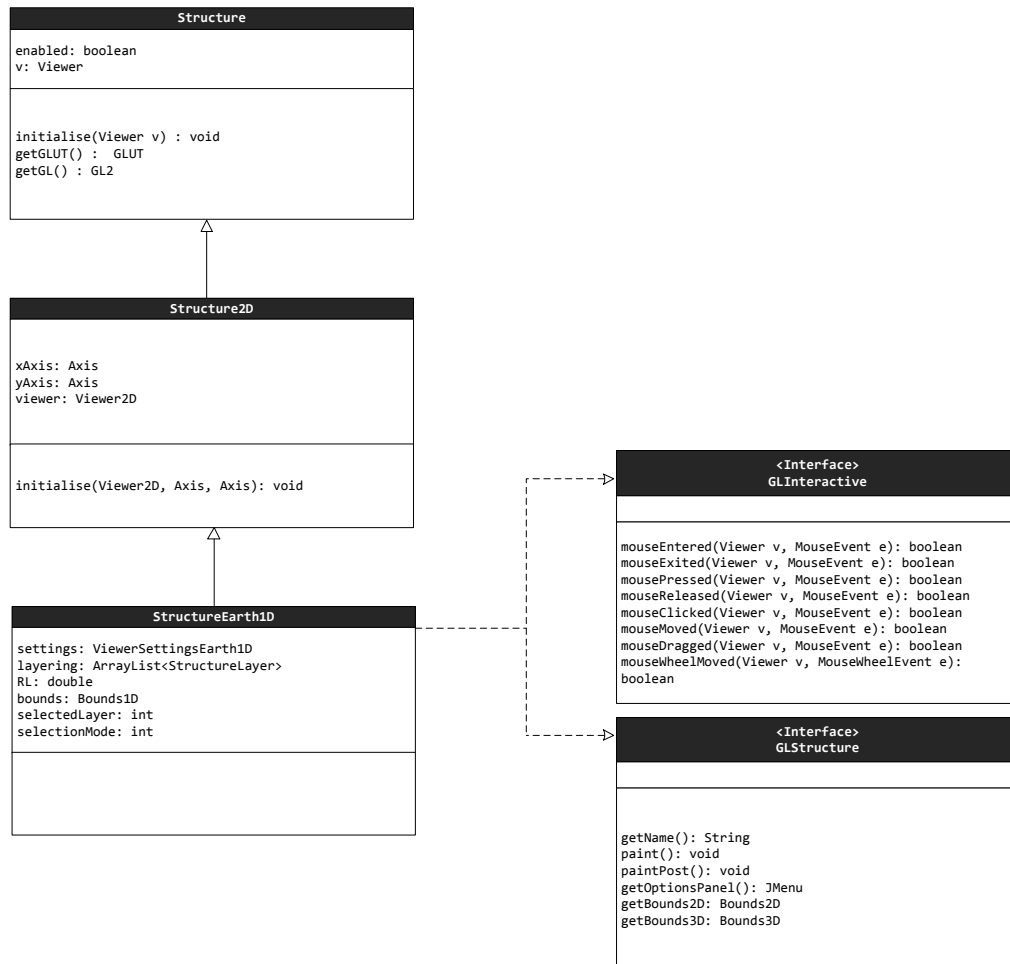
- i profiles
- ii grids
- iii vectors
- iv ellipses
- v contours
- vi colour scales
- vii geo-electric models including 1D layered earth with vertical resistivity, horizontal resistivity and anisotropy profiles
- viii 3D bodies models
- ix receiver and transmitter locations
- x waveform shapes

The 2D viewer does not show only a single structure. Multiple structures can be overlaid to increase the amount of information visualised on a single screen. For example a number of 1D transmitter-receiver profiles can be rendered on the same screen, the order of which is controlled by ‘Viewer’ class (See Figure 3-13). In the same way structures of differing type (i.e. contours and 2D grids) can be visualised on top of each other (See Figure 3-14).

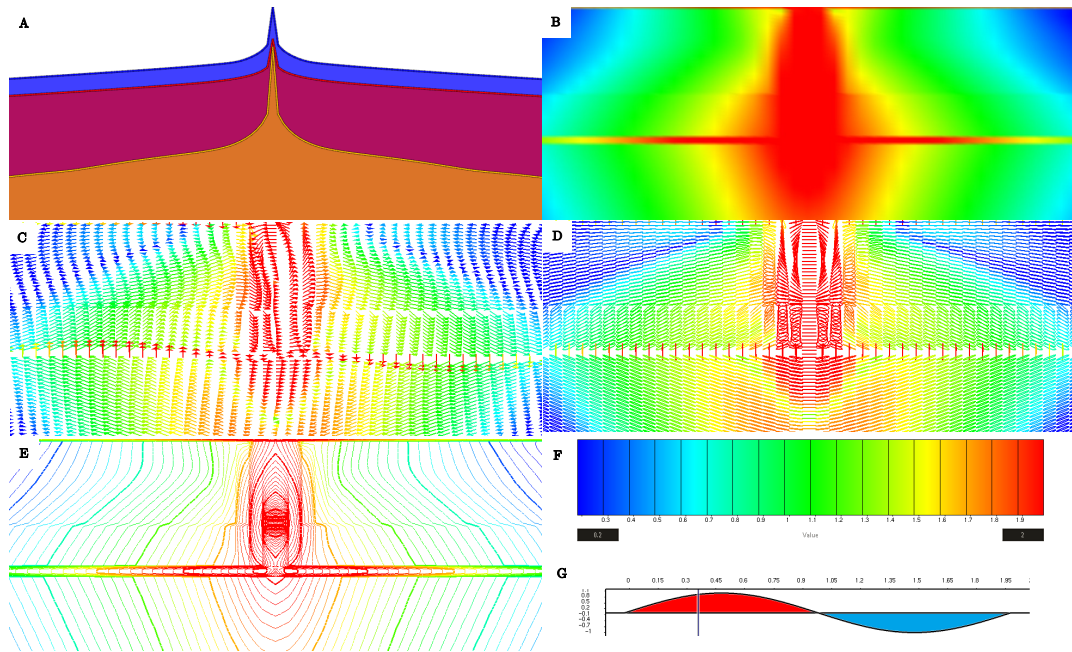
The 2D viewer enables any geometrically defined structure to be visualised as a 2D structure. The 2D viewer can visualised multiple structures at once with multiple co-ordinate systems and using different co-ordinate transforms. Any structure can be rendered withing the 2D viewer, making it well suited for representing the unique vector field data found in electromagnetism.

### 3.2.3.1 Polarisation Ellipses

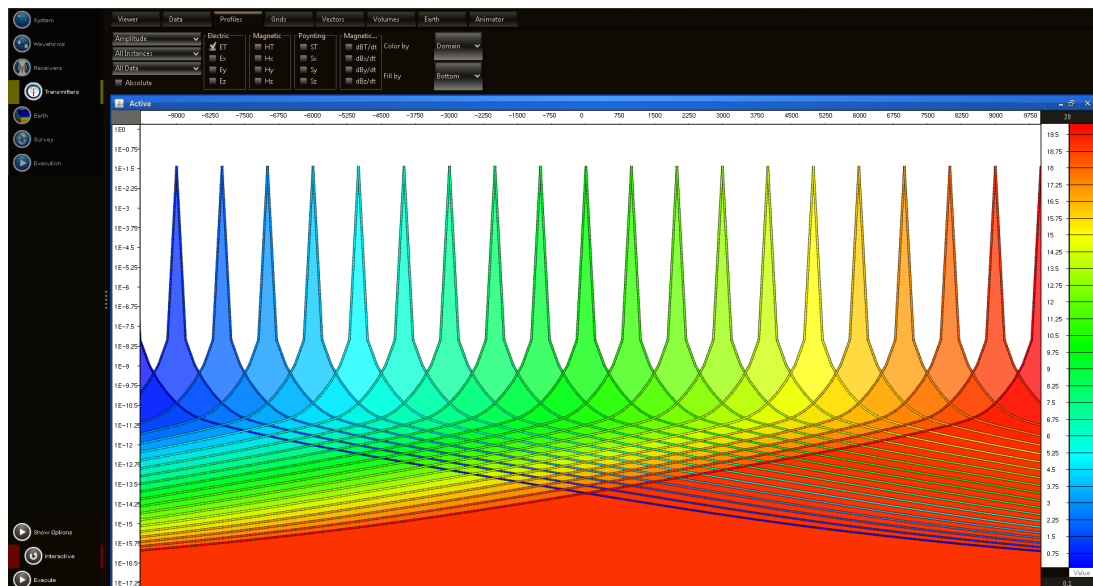
Polarisation ellipses represent the complete range of amplitudes and phase for magnetic, electric and Poynting vector fields. Polarisation ellipses are not a common method for visualising electromagnetic fields, however several key examples demonstrating the application of electromagnetic polarisation ellipses include Pethick (2008) and Li and Key (2007). In essence polarisation ellipses encapsulate the complete range in vector directions of a particular field (i.e., electric, magnetic, Poynting vector) at a fixed location for a complete transmitted wavecycle. Polarisation ellipses can be generated by computing the multiple time domain computations of the resulting field at a fixed receiver position. The amplitude of each vector



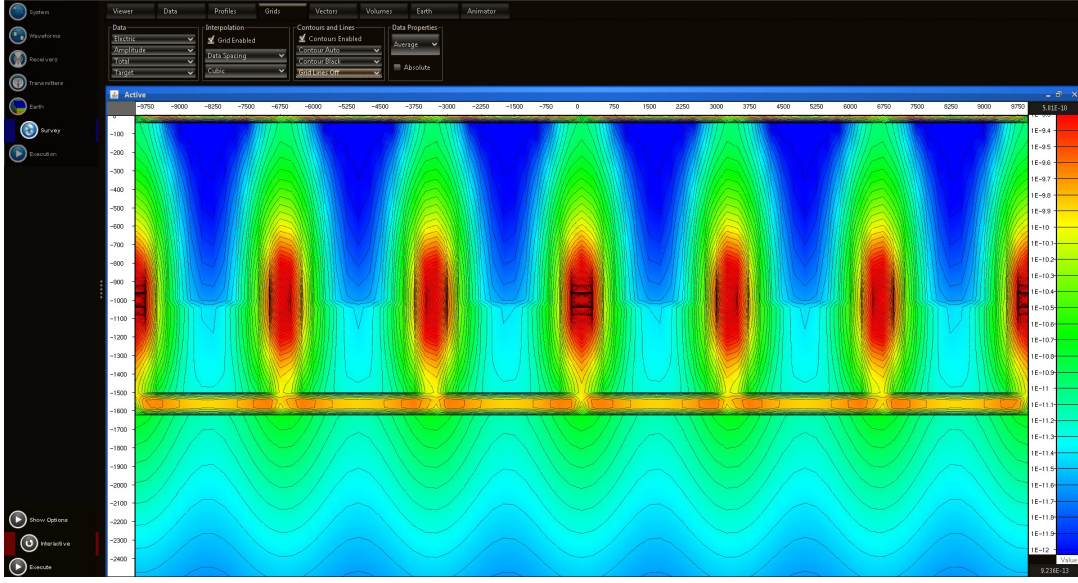
**Figure 3-11:** An example of a visualized Structure shown as a UML diagram. This example demonstrates how the 1D earth is visualized. The class Structure is the generic class which contains the viewer and access to the low level Java openGL scene. The structure 2D is an extension of the 'Structure' class and contains 2D specific viewers and axis. The 'StructureEarth1D' extends the 'Structure2D' class. The earth model 1D is interactive and requires to be rendered onto the 2D scene. The GLInteractive class contains all interactions which the 1D earth model must be able to perform, while the GLStructure contains specific commands to render the earth, get earth model specific options and get the bounds of the earth for rendering purposes.



**Figure 3-12:** Several implementations of the 2D structure class. The 2D structure class enables accelerated two and three dimensional OpenGL visualisation. The structures include (A) profiles, (B) grids, (C) vectors, (D) polarisation ellipses, (E) contours, (F) color scales and (G) Waveforms.



**Figure 3-13:** A demonstration of the profile visualization capabilities of the 2D Viewer. This Figure is displaying the electric field response from a CSEM survey with 25 transmitter locations.



**Figure 3-14:** A demonstration of the grid and contouring visualization capabilities of the 2D Viewer. This Figure is displaying the maximum electric field response from a CSEM survey with 7 transmitter locations. Multiple structures can be overlaid upon each increasing the amount of information visualized.

( $A_x$ ,  $A_y$  and  $A_z$ ) at a several times are computed and stored in an array. A complete time series must be computed from the amplitude and phase by using the transmitter waveform, in the case of the frequency domain MCSEM method it is the vector addition of multiple sinusoidal functions, for all Cartesian directions. The amplitude for a given time can be computed by Equation 3.1:

$$A(t) = A_0 \sin(2\pi ft + \phi) \quad (3.1)$$

where,

$A(t)$ – Amplitude at time t

$A_0$ – Total amplitude =  $\sqrt{Re^2 + Im^2}$

$\phi$ –Phase (rad) =  $\text{atan2}(Im/Re)$

$f$ –Frequency (Hz)

$t$ –time (s)

As seen in Figure 3-15 the completed array of amplitude over the whole cycle forms the points of an ellipse. This ellipse is best represented by a polygon. This polygon is created from the

array of stored time amplitude vectors. These amplitudes are then normalised by the maximum amplitude to transform the ellipse into a unit ellipse centred at point P(0,0,0),

$$\vec{N}(t) = \frac{\vec{A}(t)}{\vec{A}_{Max}} \quad (3.2)$$

or more precisely,

$$\vec{N}(t) = \frac{\vec{A}(t)}{A_0} \quad (3.3)$$

where,

$\vec{N}(t)$ – Normalised amplitude vector at time t

$A_{Max}$ – Maximum total amplitude over whole period

To visualise the ellipse, the ellipse needs to be scaled to reasonable proportions and positioned. The ellipse is scaled by multiplying the normalised values by the ellipse size. This ellipse size can be either a constant (i.e., single ellipse size) or variable (i.e., scaled by amplitude). The scaled vector can be simplified as,

$$\vec{S}(t) = \vec{\varepsilon} \frac{\vec{A}(t)}{\vec{A}_{Max}} \quad (3.4)$$

where,

$\vec{S}$ – Scaled normalised amplitude vector at time t

$\vec{\varepsilon}$ – Scaling factor

The ellipse is then positioned into the final cartesian co-ordinates. It's final position depends on the user-selected geometry (i.e., receiver location, transmitter location, transmitter-reciver midpoint etc...),

$$\vec{E}(t) = \vec{S} + P_o \quad (3.5)$$

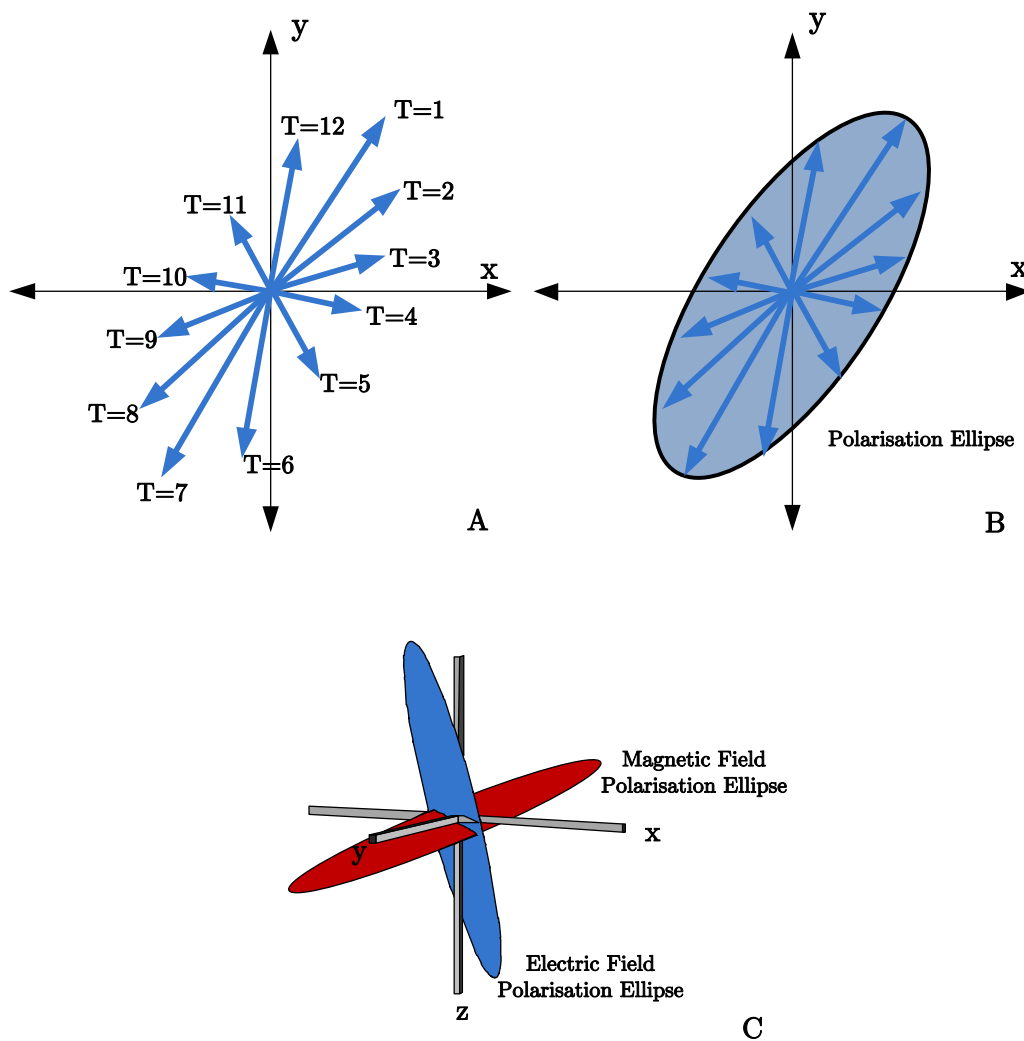
where,

$\vec{E}(t)$ – Final ellipse vertex co-ordinate at time t

$P_o$ – Centre of ellipse (determined by user-selected geometry)

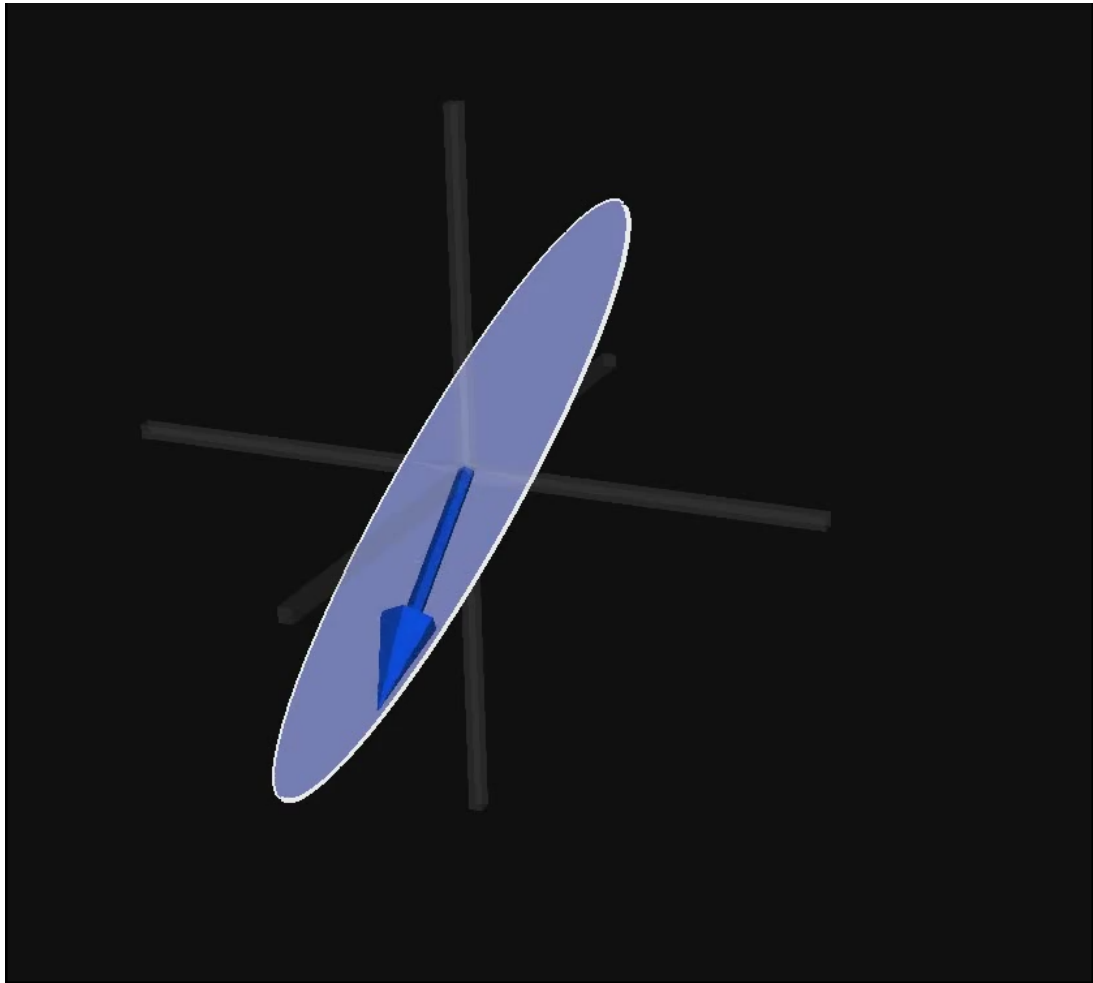
To clarify the formulation of polarisation ellipses Video 3-16 shows the formulation of a three-dimensional electric field ellipse. This representation can be used to establish the direction of maximum amplitude and can be used to infer the generalised path of electric and magnetic fields. Polarisation ellipses also contain phase information phase for each of

the components. These polarisation ellipse polygons are stored as vertex buffers to improved visualisation speed. Vertex buffering is covered later in this chapter.



**Figure 3-15:** The schematic demonstrating the formulation of a polarisation ellipse. Electromagnetic field vectors vary in amplitude over time. Figure A highlights twelve 2D electric field vector orientations. The complete elliptical rotation of the field can be encapsulated by a polygon (see Figure B). The polarisation ellipse representation contains amplitude, and phase and polarisation directions. Polarisation ellipses can also be used to visualise the 3D magnetic, electric and Poynting vector fields to contrast the electric and magnetic fields or show the differences in attributes of the scattered, total and layered responses (see Figure C).





**Figure 3-16:** The formation of an electric field ellipse

See [Videos/ElectricFieldPolarisation.avi](#) for video source

Also See [Videos/ElectricAndMagneticPolarisation.avi](#) for examples of electric and magnetic field polarisation ellipses.

### 3.2.4 3D Visualisation

3D visualisation is achieved through the JOGL2 package. The 3D viewer is similar to the 2D viewer and is also based on the ‘Viewer’ class seen in Figure 3-7. Unique challenges must be overcome to create a 3D viewer. 3D viewers require low level control over the camera and lighting. Performing 3D data manipulation and selection on a 2D screen also complicates the task of building a 3D viewer. Key differences between my 2D and 3D viewers are highlighted in Table 3.1.

	2D Viewer	3D Viewer
Co-ordinate Transforms	Variable	Only linear
Co-ordinate system	x, y percentage	Absolute x, y and z
Camera	Single fixed	3D rotation and zoom capable
Lighting	Single fixed	Multiple variable lights
Data Interactivity	Available	Not implemented
Rendering	Using sequential GL commands	Vertex buffering

**Table 3.1:** A table highlighting the key differences between 2D and 3D viewers.

The 2D viewer can have multiple axis transformations (i.e.  $\log_10$ , pseudolog and linear). The 3D viewer has no axis structures. The 3D viewer currently is an open 3D space and is represented in linear co-ordinates and in absolute positions. The 2D viewer has a co-ordinate system in percentage (i.e. viewing the region  $x(0 \text{ to } 1)$  and  $y(0 \text{ to } 1)$ ) while the 3D viewer represents data in absolute co-ordinates.

The 2D viewer is essentially a 3D viewer however it has a single fixed camera facing the scene on a x-z plane with viewing extents 0 to 1 in the x direction and 0 to 1 in the z direction. The 3D scene has a variable camera. I have implemented a spherical camera to pan, rotate and zoom into the scene. This spherical camera implementation is controlled via the ‘SphericalCamera’ class. This class receives mouse and touch input from the 3D viewer passed from the low level viewer input listeners. These movements are recognized by the spherical camera class which updates the position and angle of the camera.

The 2D viewer has a single preset light to ensure the correct colours are maintained. Both lit surfaces and shadows must be visible to perceive 3D structures accurately. The 3D viewer can have up to eight lights, the maximum number of lights available in Java OpenGL. Each light has a position, color and a specular, diffuse and ambient components (JOGAMP, 2012). Definitions of each lighting method is explained in Hansen and Johnson (2004).

Currently there is no capability to manipulate data within the 3D viewer. Data interaction and data picking can be implemented by using a collision system. Several collision detection methods include Oct-trees, BSP-trees and R-trees and are covered by (Barequet et al., 1996). Typically collision detection system computes a vector from the camera to the location of a

user interaction (i.e. mouse click). This vector computation is a form of ray-tracing. If the vector intersects the bounding surface in the object tree, the object is selected. Using this method data can be manipulated in a 3D space but on a 2D screen. The 3D viewer already implements an object structure via the ‘Viewer’ class, however each structure would require to implement a sub-object hierarchy to interact with individual components.

The amount of data visualised in 2D is typically less than in 3D visualisation. This means 2D visualisation can be inefficiently performed without a significant decrease in performance. 2D datasets sizes are typically small and interactivity occurs infrequently. Flexibility was chosen over efficiency as the highest priority of 2D visualisation. Large 3D datasets are common and cameras positions are typically updated frequently. 3D visualisation requires fast camera panning with larger datasets present. Instead of rendering the scene a single primitive at a time (i.e. line by line, dot by dot and polygon by polygon), all 3D datasets are stored on the graphics card buffer and only recreated/modified when necessary (i.e. changing colour, changing data etc.) (Watt and Watt, 1991). All 3D shapes can be created from a series of 3D vertex points and are stored in vertex buffers. (Watt and Watt, 1991 and Gumhold and Straber, 1998). A vertex buffer is an OpenGL feature that stores an array of numerical values (JOGL, 2012a). In my program these buffers are stored as floats on the GPU on-board memory. These buffers enable the visualisation of datasets quickly. Instead of rendering each object individually by sequential sending CPU commands to the GPU, the vertex buffer is stored on the graphics card memory (Watt and Watt, 1991). The reduction in time spent communicating between the two devices significantly improves rendering speed.

Line segments, triangles and quadrilaterals form the base of all visualised structures. I have created three vertex buffer classes, ‘VertexBufferLine’, ‘VertexBufferTriangle’ and ‘VertexBufferQuad’. Each vertex buffer has its own separate location on the GPU memory. Vertex buffers do not just represent a single triangle, line or quadrilateral but rather a group of shapes. Unlike ray-tracing, and volume rendering (Upson and Keeler, 1988), vertex shading requires individual elements to be ordered according to transparency (Watt and Watt, 1991). For example the final rendered is performed sequentially. Transparent objects must be sorted by transparency to avoid obscuring objects (Watt and Watt, 1991). All vertex buffers are sorted according to the transparency of the individual elements, rendering from most transparent to least transparent.

Consider how a group of vectors are rendered. Electromagnetic vectors can be represented by

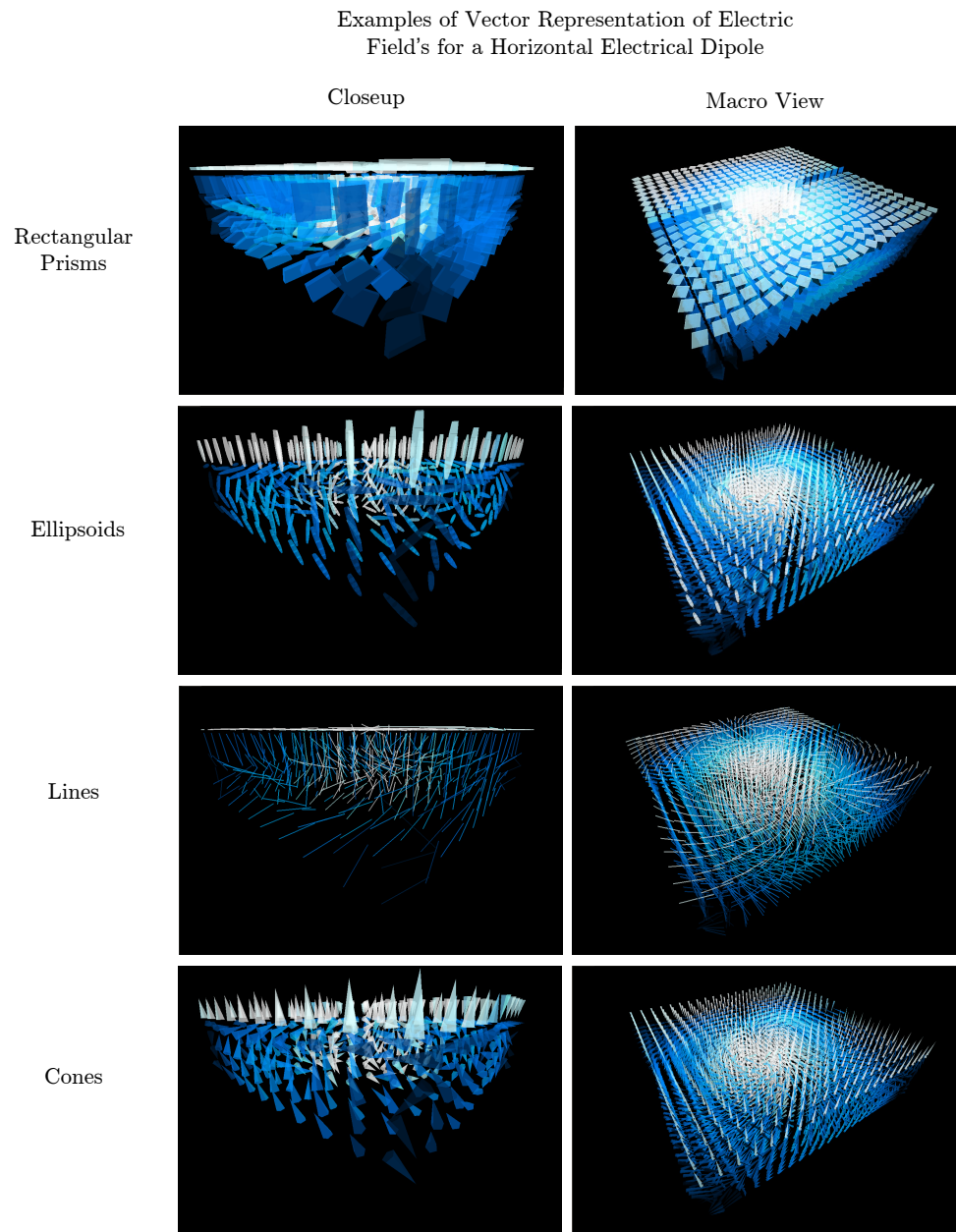
rectangular prisms, ellipsoids, cones and lines. A superclass ‘Vector3D’ was created to generate the required vertex buffers. Rectangular prisms, ellipsoids, cones and lines are made up of different shapes. For example rectangular prisms can be broken down into six quadrilaterals, ellipsoids into multiple triangles, cones into triangles and lines into two-dimensional line segments. Examples of the various vector representations are shown in Figure 3-17. These structures all require different buffers despite representing the same data. This is because the data is represented by different primitives (i.e. triangles, quadrilaterals and lines). Figure 3-18 shows how a cone vector is represented and stored in a vertex buffer. The vector is first converted into a series of triangles. Each triangle has a number of vertex points. Each vertex point contains a number of properties. This includes a position  $V(x, y, z)$  stored as a three floating points, a RGBA color  $C(R, G, B, A)$  representing the color at that position, and a normal vector  $N(x, y, z)$  representing the vector normal to the surface at point  $V(x, y, z)$ . Each vertex and its properties for each triangle are added to the vertex float buffer. Each vertex consists of 10 floating point values (i.e. 30 floating points per triangle). If a vector consists of 5 triangles, a total of 150 floating points are required to represent the vector.

Benchmarking was performed on the 3D viewer to establish the speed of visualisation. Using vertex buffering on at NVidia 9800 GTX, 750 million quadrilateral polygons or 900 million triangles are visualized per second. In comparison without vertex buffering only 180,000 triangles can be rendered every second. These modest achievements may appear slower than the maximum graphics card output, but a number of factors influence efficiency. These factors include calling c methods via JNI, using GLJPanel instead of GLJCanvas, not using vertex indexing and using colour not striping. There are no significant differences to the look of the same data in 2D and 3D forms, but a visual comparison of the same data type but on two viewers are shown in Figure 3-19 and Figure 3-20.

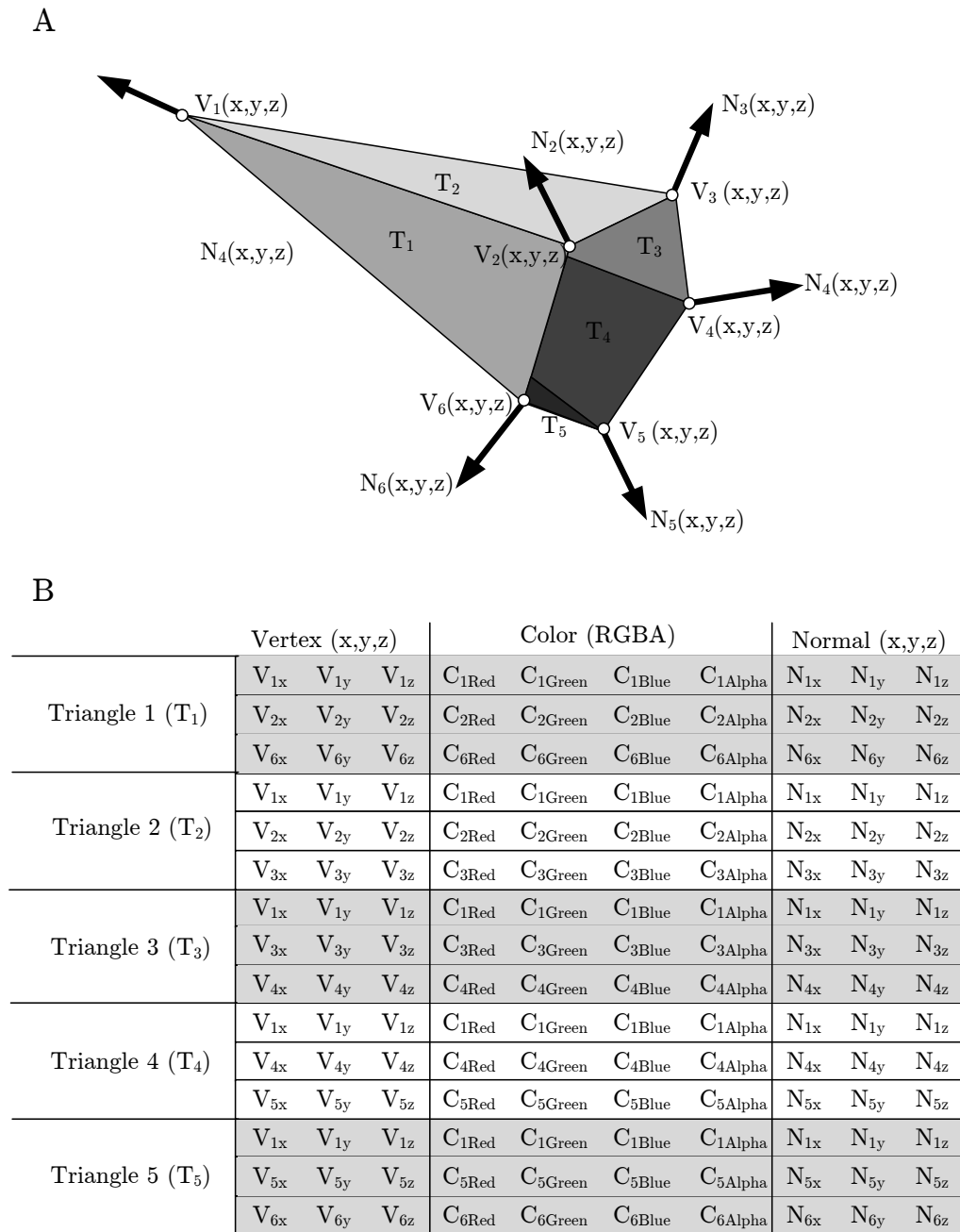
A 3D viewer was created integrating the JOGL2 library. A 3D spherical camera, custom lighting and vertex buffering functions were developed and integrated into the base 3D viewer. Using these concepts a fast rendering, interactive 3D viewer was created for the purpose of visualising electromagnetic datasets.

### 3.2.5 Visualization with Fractals

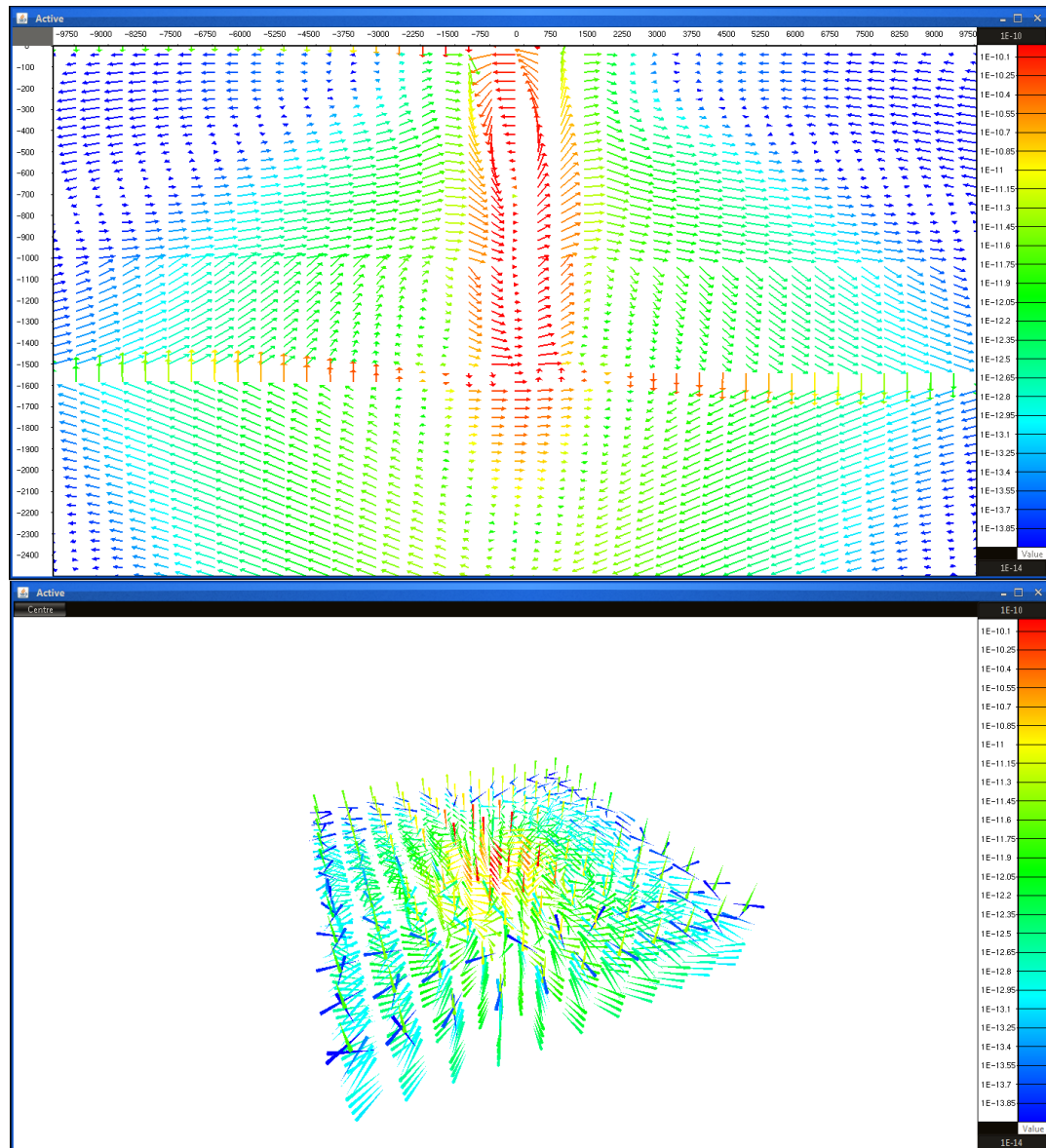
Resistivity borehole logs can contain in excess of 100,000 measurements. Theoretically, a resistivity log can be used as a 1D geo-electric model. The visualisation of the complete borehole dataset can be inefficient due to the dataset size. A fractal is “a geometrically



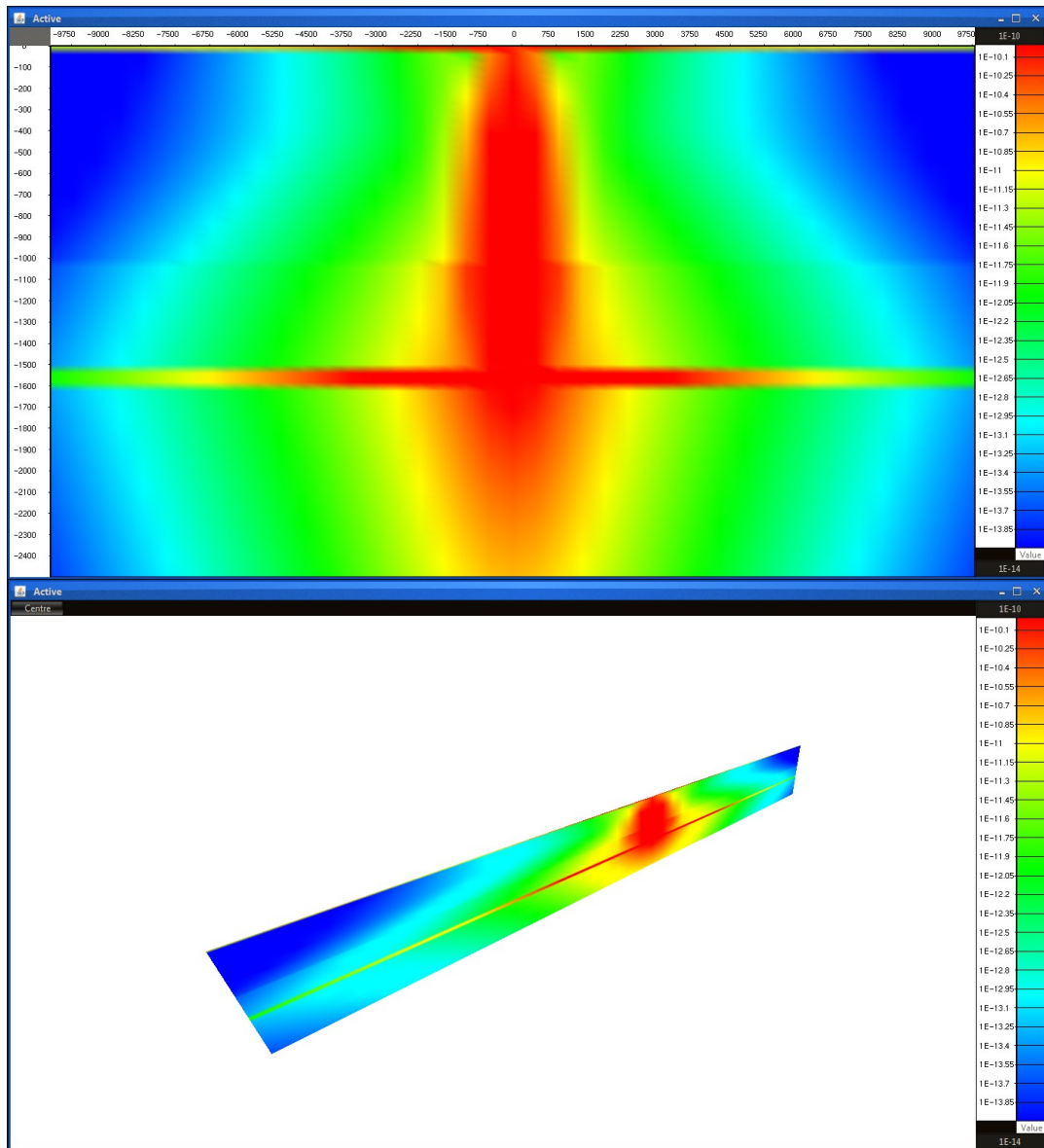
**Figure 3-17:** Different representations of the 3D vector structure. Vector are represented by the rectangular prisms, ellipsoids, 1D lines and cones.



**Figure 3-18:** Visualization of triangles with vertex buffers. (A) The representation of a cone consisting of triangles (T), vertices (V) and normals (N). The above cone consists of five triangles defined by six vertices. Each vertex has a normal, which represents the surface angle at that point. The normal is used in visualisation for lighting and to simulate continuous surfaces. (B) represents the memory allocation of the cone in the vertex buffer. The vertex buffer defines each vertex for each triangle sequentially. Each vertex has a position, color and normal. This means there are 10 floating point values per vertex. Overall 150 floating points are used to define the cone.



**Figure 3-19:** Comparison of 2D and 3D viewers. Each viewer uses the same base functions such as display, add and remove structures. The input streams (i.e. keyboard, mouse motion, mouse button and mouse wheel listeners) are handled differently by the 2D and 3D viewers. The predominant mouse listeners in the 2D viewer only controls the structures however the 3D viewer enables higher level mouse control functions related to the viewer camera.



**Figure 3-20:** Comparison of 2D (top) and 3D (bottom) viewers for visualising 2D grids.

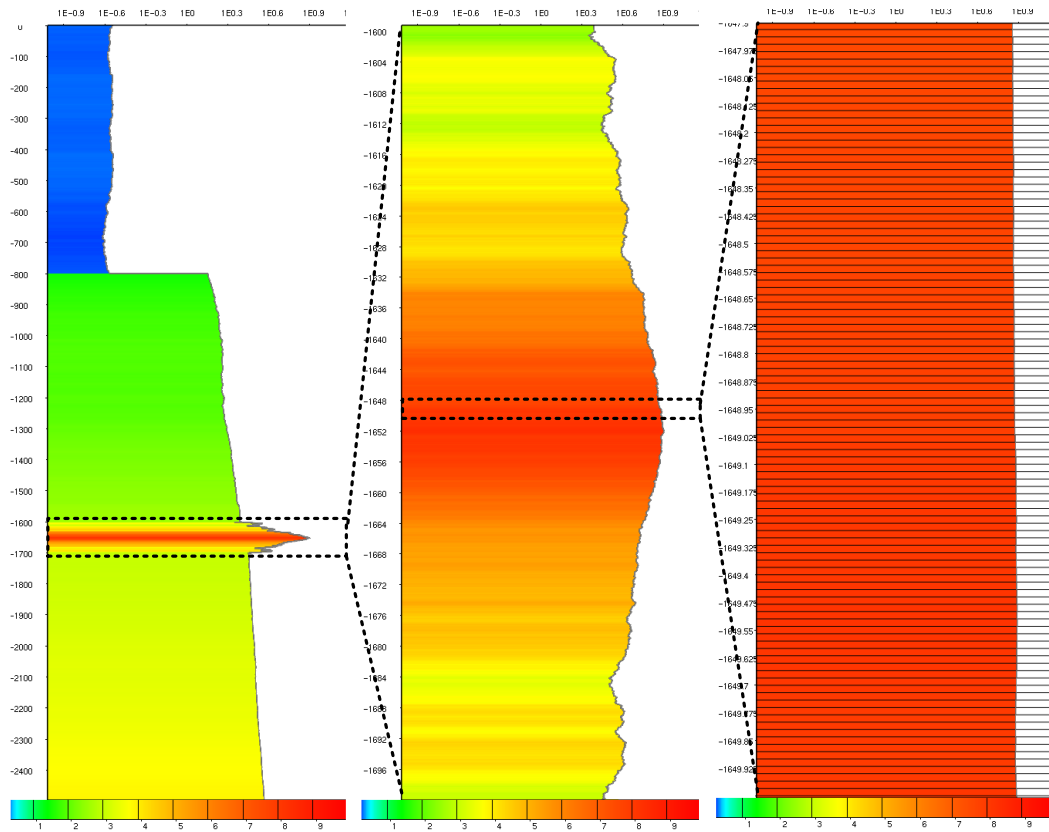


complex object, the complexity of which arises through the repetition of form over some range of scale.” (Tucker, 2004). Tucker (2004) states that “many natural objects exhibit this characteristic, including mountains, coastlines. . .” and the amount of roughness or detail “can be mathematically characterised by its fractal dimension”. Fractal concepts enable visualized to occur faster and more efficiently (Peitgen et al., 2004). More often than not the speed of visualisation is highly important, requiring specialised and high-level graphics API to render masses of data (Hughes, 1998).

A pixel may have a vertical resolution of 100cm while the borehole log can be measured at 5cm increments. Twenty data points exist per pixel. Not all twenty are needed to be visualised. Only the viewable data at that scale should be visualized. My approach detects large variations in the data (i.e. spikes) so only the ‘important’ data is visualised without affecting the quality. The approach is similar to the “Diamond-Square” algorithm (Martz, 1997). Borehole data is generally 1D in nature so a 1D approximation of the “Diamond-Square” algorithm was created. The algorithm generally is used to generate random 3D landscapes, however the idea of increasing the complexity iteratively can be applied to render 1D borehole data. The process begins by creating a rough model of the data. The starting roughness is computed so a vertical pixel equals a single depth datapoint. The algorithm takes the nth datapoint so a single vertical pixel has a single depth. The approach adds “details” to this rough borehole log. This fractal method detects spikes (large variation in log data) add the peak amplitudes to the data log. The size of peak is controlled by a gradient threshold I have defined. Each vertical pixel may represent multiple depths and in that depth a number of different values (y-pixels) may be present. Maximum and minimum values are computed within a single “depth-pixel” and if greater than the designated threshold are added to the log. It is in this way, all major variations in borehole log values are shown without rendering all datapoints. I have written my own code to visualise the ‘important’ data at the pixel scale rather than the sub-pixel scale. To test the efficiency of visualisation using fractals I have performed an experiment on a large synthetic borehole log with 100,000 measurements. The earth model that I have used to test fractal visualisation of earth models is shown in Figure 3-21.

I visualised 100,000 borehole measurements on a NVidia 9800GTX on an Intel Core2 Quad computer at an average frame rate of 0.1 fps without the use of fractals. When fractals were implemented the framrate increased to 26.1 fps. This is an astounding difference in speed. Vertex buffering was not utilised to render the earth model in 2D. The detailed method of fractal visualisation can be found on the MCSEM.com SVN server in the “StructureEarth1D”

java class in the "open.opengl.viewer2d.structures.earth" package.



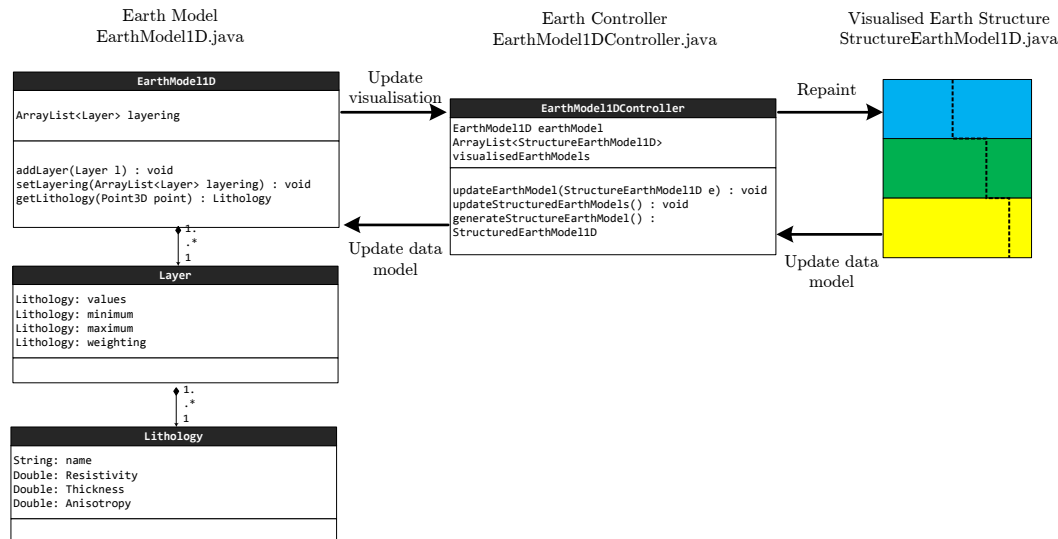
**Figure 3-21:** A large synthetic borehole earth model consisting of 100,000 layers at three different vertical scales. The synthetic borehole log was rendered using my fractal visualization algorithm. Fractal visualization sped up visualization from 0.1fps to 26.1fps. Representing an improvement for visualizing large datasets.

### 3.2.6 Interactivity

Interactivity makes software more intuitive and therefore easy to use. User directed text based input occurs discretely and results in relatively 'slow' updates of survey parameters. For example if a user wants to determine the influence of transmitter frequency on the electromagnetic response, they can sequentially enter one frequency after another on a keyboard. Even if they are a quick typist they can expect two updates a second. This approach does not encourage the rapid analysis of geo-electric parameters on data.

Mouse and touch based input manipulates data continuously rather than discretely like keyboard input. Simons and Levin (1997) state that discrete changes in visual images can result in ‘change blindness’ which is the “the inability to detect changes to an object or scene”. An increase in blindness results from increasing the time between changes in a scene. Imperceptibly continuous changes in data produce less ‘change blindness’ resulting in a faster learning experience.

Interactive features represent the ability for the user to continuously alter the data model and view the effects on electromagnetic data in real time. The properties of a 1D geo-electric model include layer boundary locations, electrical resistivity and anisotropy. Interactivity comes from continuously updating these earth model parameters and updating the electromagnetic response. Each time the data model is updated, a new invocation of the survey is executed and the resulting data visualised. Using a ‘model-view-controller’ paradigm (Veit and Herrmann, 2003) and utilising multi-threading capabilities structures could be made to produce interactivity. This paradigm separates the data model from the visualised data. The model-view-controller paradigm results in cleaner code and to modularise the program so that the model can be used without the GUI (Leff and Rayfield, 2001). This also ensures that the visualised data can be run on a separate execution thread resulting in faster visualisation and in turn a higher level of interactivity (i.e. less change blindness) (Leff and Rayfield, 2001). The 1D earth modelling model-view-controller is shown in Figure 3-22. Each of the model’s, view and controller components are separate classes. In this example the view is the ‘StructureEarthModel1D’ class, the controller is the ‘EarthModel1DController’ class and the model is the ‘EarthModel1D’ class. The ‘StructureEarthModel1D’ is a visualised earth model structure which receives user input via touch gestures or mouse input. It is visualised in the 2D viewer. Every time the StructureEarthModel1D is altered, a command is sent to the earth controller to update the data model. There is a separation in the visualised earth model and the data model. There is no direct access between the model and the view except via the controller. The controller ensures that updates to either the data model or the visualised earth model are reflected in both the view and model (Veit and Herrmann, 2003). The visualisation and user interactions with the earth structure are run on a separate thread. This allows a single CPU core to concentrate on smooth visualisation and another on using the user interactions to update the model. The controller and data model is run on a separate thread. By using multi-threading only the latest structure parameter change is reflected in the data model, resulting in smoother updates.

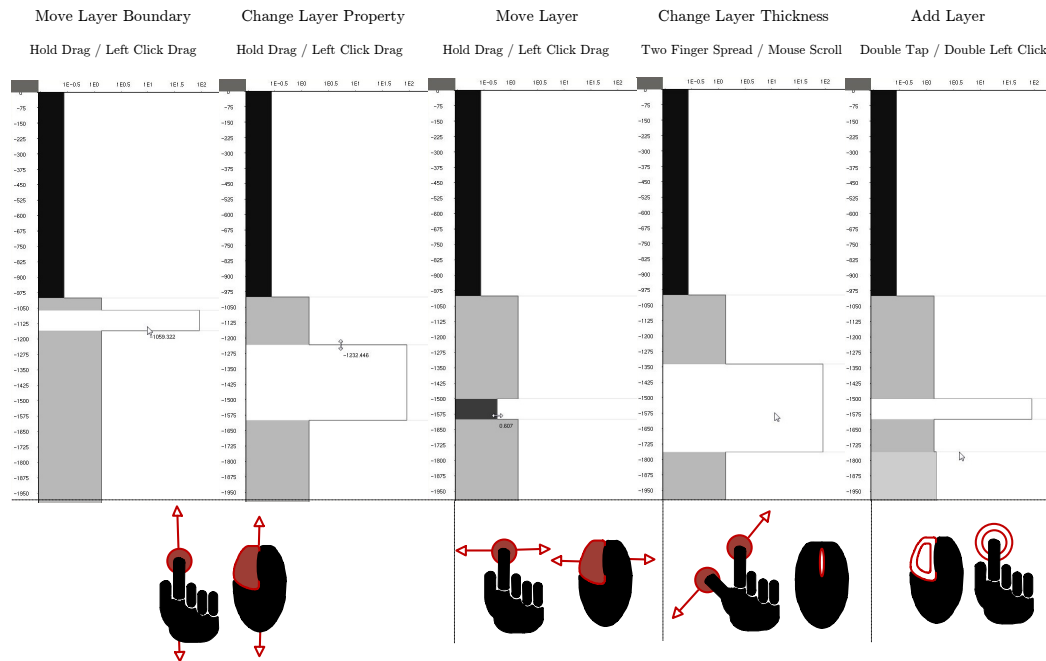


**Figure 3-22:** Interactivity between the model-view-controller UML structure for the 1D layered earth. The earth model contains a number of layers and parameters. These parameters are rapidly changed by the user to allow for an interactive experience. The visualised earth structure must be able to obtain user input and update the earth data model. This is achieved through the earth controller.

My software has been designed to be interactive and easy to use. A model-controller-view paradigm was implemented to separate the visualised model from the data model. The continuous interaction and updates overcomes change blindness quickening the user's understanding of a parameters effect on the data.

User interaction comes from mouse presses and mouse drags, mouse double clicks and mouse wheel movements. These motions can be translated into multi-touch gestures for tablets. Figure 3-23 shows possible earth model interactions and the corresponding data model updates. For example the left click drag has three actions. Firstly, if the mouse/finger is placed inside a layer, the whole layer is selected for vertical layer translation. Secondly, if the mouse/finger is place on a layer boundary, only that layer boundary is selected for layer thickness alteration. Interactivity is achieved by using methods to continuously vary a single data parameter. Thirdly, if the action is performed on the vertical parameter line (i.e. resistivity, anisotropy or horizontal resistivity) the selected parameter varied. Other user interactions include, the two finger spread or mouse scroll which increases the thickness of the layer in both directions. A

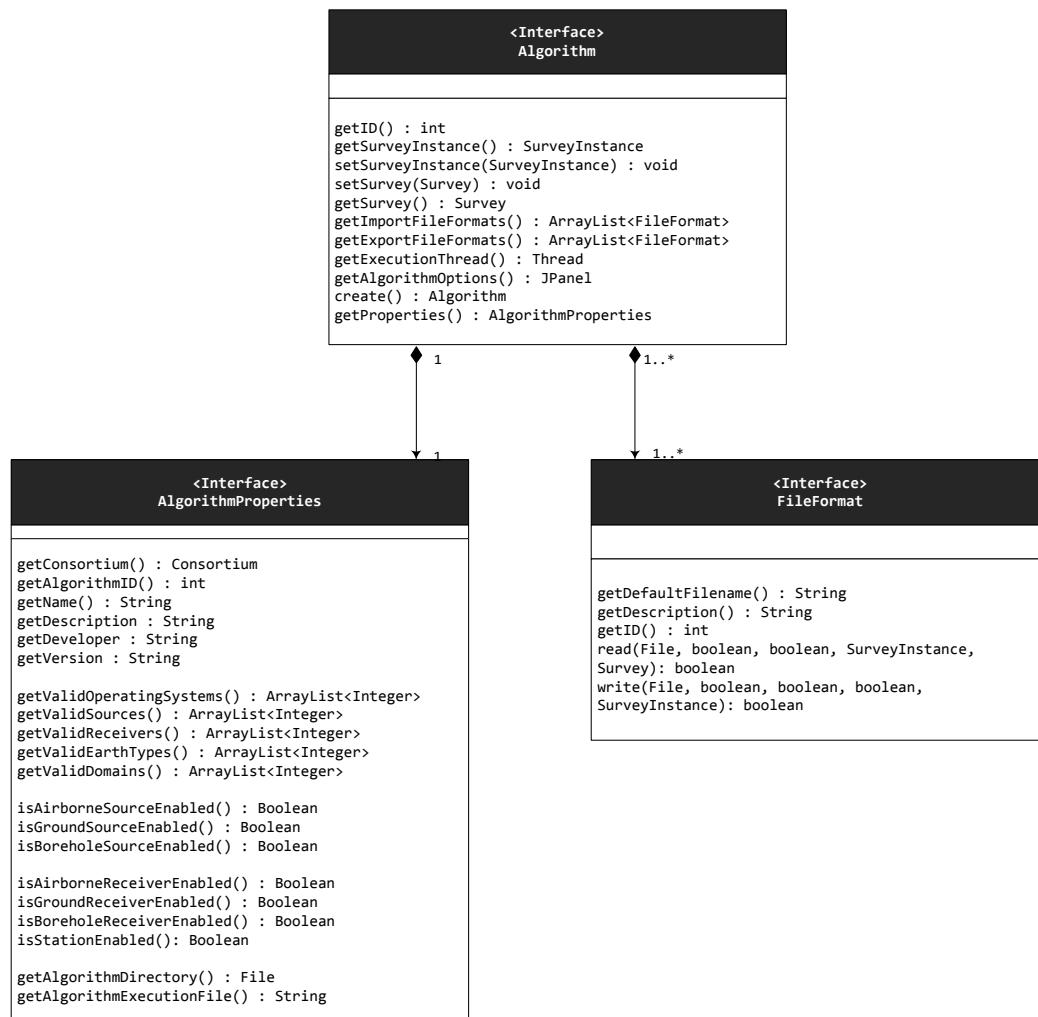
double click or double tap action adds a layer boundary. These translations between mouse and multi-touch gestures are intuitive and are commonly used.



**Figure 3-23:** User interactions with the 1D geo-electrical earth model. This software is compatible with multi-touch devices such as the Asus EP121. Each mouse action has a multi-touch gesture equivalent.

### 3.2.7 Integration of Third Party Algorithms

The primary goal of this chapter is to outline the creation of a MCSEM research package. This includes the ability to execute any external electromagnetic code ranging from compiled C, C++, Fortran executables to Matlab (.m) files. All electromagnetic surveys define transmitter, receiver, waveform properties and occasionally the recorded data and survey configuration. The data model covered in chapter 2 overviews the generic electromagnetic structure. Each algorithm is given access to this data structure through the ‘Algorithm’ interface (See Figure 3-24). The ‘Algorithm’ takes into account specific algorithm file formats, execution sequences and electromagnetic limitations. Every third party typically possesses its own input, output and execution file formats. The ‘FileFormat’ interface covers import, export and execution functionality.



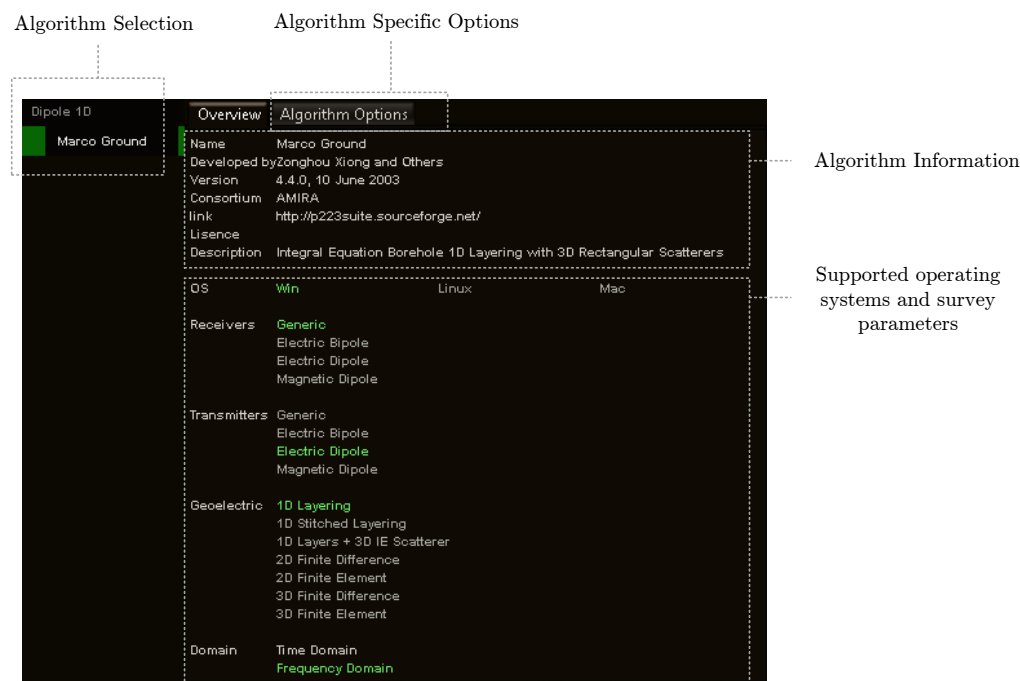
**Figure 3-24:** The generic algorithm structure. Each algorithm has several functions including input and output file handling, execution procedure handling and error and survey validation. Each algorithm implements these simple generic methods in order to be fully integrated into the software.

The 'FileFormat' contains the ability to import and export data from a particular survey configuration or to create a survey configuration from a pre-existing import and export files. Both methods of import and export enables programs to create, import and convert electromagnetic data and surveys between algorithm input, my own electromagnetic data structure or proprietary data formats.

Algorithm's may have different execution sequences. An execution thread is generated to handle the initial arguments, run-time and completion detection inside each execution method. For example, the Marco algorithm from the AMIRA p223 project (Xiong, 1992) has a simple execution sequence. Marco is executed by launching the program using the algorithm name via the execution handler. Marco uses default input and output file names so no other arguments are required. The program will execute on the systems dispatch thread. On completion the execution watchdog detects the completion of the program and import the modelled results. Intem3D developed by Zhdanov and Cox (2008), as part of the CEMI group, has a much more complex execution procedure. Intem3D is composed of both un-compiled and compiled Matlab files. Intem3D is run through the Matlab engine. To execute Intem3D, Matlab must be initialised, the Intem3D script launched using various input arguments and Matlab has to close upon completion to allow the execution watchdog to detect the closure of the execution thread prior to import. Separate execution methods were developed to overcome these large differences in execution procedures.

Error prevention is the last function of the algorithm class to be performed. Error prevention is important. One of my favourite heuristics is from the 14 rules "programs need to be taciturn about their personal problems" (Cooper, 1999). This means that programs should not present users with error messages; rather programs should be quiet about their problems by not allowing the error to occur in the first place. Error messages are one of the leading causes of demoralization, frustration and infuriation for end-users (Ceaparu et al., 2004). Each algorithm validates the input survey prior to execution. For example, if the algorithm is unable to support magnetic dipole transmitters, it will invalidate the survey and prevent the user from executing the code. This validation procedure is performed by the 'AlgorithmProperties' interface. This interface provides the means to validate surveys. It tells the program which receivers, transmitters, earth model types, survey configurations, source-receiver multiplicity and operating systems are supported by the algorithm. This approach prevents error messages from occurring.

The algorithm selection panel overviews each algorithm information, supported electromagnetic elements and operating systems (See Figure 3-25). The algorithm panel enables users to select each algorithm. It also shows the user what in their survey is not supported and algorithm specific options (i.e. algorithm accuracy). The panel presents to the user what is possible by which algorithm. For example Dipole1D can forward model the EM fields with an electric dipole or bipole only. If a magnetic dipole transmitter is present in the survey instance the magnetic dipole transmitter will appear in red. All unsupported transmitters, receivers, earth models, system configurations appear in red and prevent the program from executing the algorithm.



**Figure 3-25:** The algorithm selection panel. The panel enables users to quickly switch between algorithms and to validate their survey with the algorithm. If the algorithm does not support the current survey, the items will be highlighted in red rather than green. If the algorithm does not support the current survey instance, CSEMoMatic will not allow the survey to be executed. This approach is taciturn about its problems (Cooper, 1999), resulting in less error messages being presented to users.

My algorithm structure allows any controlled source electromagnetic algorithm to be integrated into the software with minimal effort. Only a few classes need to be implemented to fully integrate a proprietary algorithm into the generic electromagnetic data structure. This generic approach to algorithm integration enables rapid comparisons of algorithms for the same survey



instance.

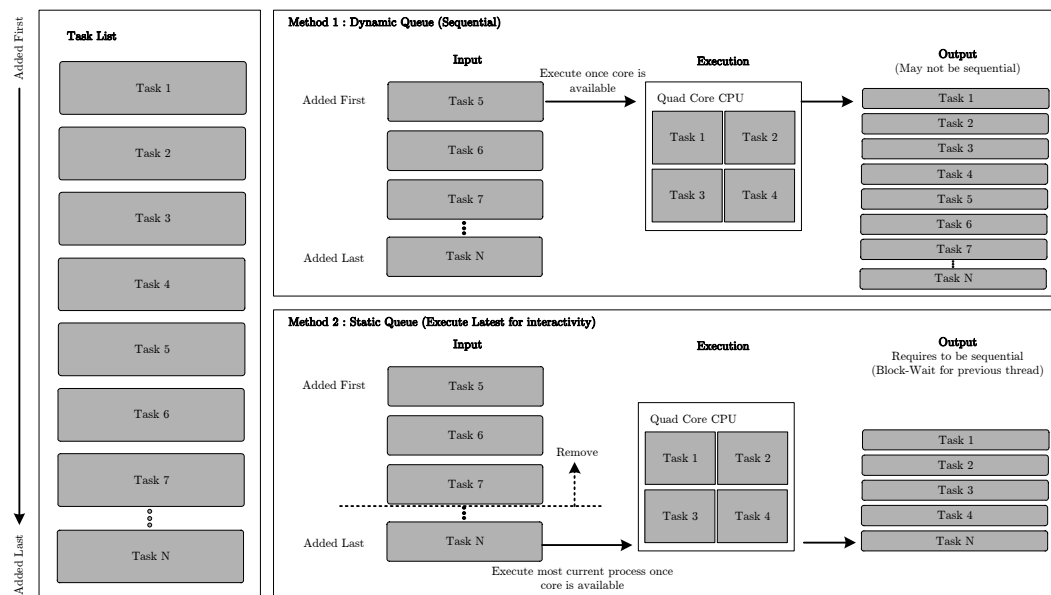
### 3.2.8 Multi-Threaded Execution

Multi-threading enables fast responsive modelling by utilising the full potential of the CPU. Modern CPU's are multi-core. A multi-core CPU can simultaneously perform computations on multiple threads at any single moment. Using traditional execution methods, execution on a single thread only utilises a single core, leaving the rest of the cores under-utilised. Multi-threading is a process to distribute a task over multiple cores, resulting in a faster program.

The execution environment contains two methods of multi-threading. These two methods include a dynamic and static queue method. Figure 3-26 demonstrates how a number of tasks (N) are executed on a quad core PC. Method 1 is based on a dynamic queue. This is a sequential queue which continually grows with each added task. The CPU will retrieve tasks sequentially from the queue until either the CPU is full or there are no more tasks. If all threads are busy the queue continually grows. This method only executes the oldest task once a core becomes available. This is a batch method that executes all tasks that have been added to the queue.

Method 2 is a static queue and only allows a single task in the queue. As tasks are added to the task list, the first four tasks are computed by the CPU. After the CPU has no more cores available, the single task in the queue is continually replaced by the newest task until a core is available. That is, only the newest task is ever in the queue. The output of this method can be variable. In the example shown in Figure 3-26 only the first four tasks (because the Quad core CPU can only handle 4 threads) and the latest task N are computed. This method is good for interactive modelling as only the latest iteration is required to be computed

Overall, these two execution methods provide a basis for any form of forward modelling problem. The execution handling is performed by the 'AlgorithmStandaloneExecutionHandler' class. The number of cores is established upon program initialisation using system calls. This number of utilised cores can be changed by the user from the settings menu. The execution itself is performed through Apache commons Exec library (Apache, 2012a). These two execution approaches allow the execution of any EM modelling algorithm for most purposes.



**Figure 3-26:** The execution environment of the CSEMoMatic software package. Two methods of multi-threaded execution are either dynamic or static methods. If eight tasks are quickly and sequentially added to the execution handler, the dynamic queue will continue to grow and eventually execute all tasks. This is good for processes where all tasks need to be executed, like forward modeling feasibility studies. The Static queue will only model the latest added task. This static method is useful for interactive survey modeling, where not all changes to the data model are required, but the latest change is.

### 3.3 Possible Design Improvements

Hindsight is 20-20. A number of improvements could be made from looking at recent developments in Java programming and provided hindsight in project development. As of October 2011, JavaFX 2 (JavaFX, 2012) succeeded Swing as its user interface of choice (Bien, 2012). JavaFX is an ideal choice for the presentation layer due to its customisation and binding capabilities. JavaFX also is a software platform for cross-platform programming. It is used for creating rich internet across a variety of devices including desktops, browsers, mobile phones, TV set top boxes, gaming consoles and Blu-ray players (Shankland, 2009). It would be a better choice for future proofing the software package. Approximately 50% to 80% of the interface would have to be re-written to incorporate JavaFX as the presentation layer. Less affect components include the 2D and 3D viewers which are built on JOGL, which can also run on mobile devices (JOGL, 2012b). The use of JavaFX and its inbuilt use of bindings would also reduce time required to design the controller classes.

Secondly, the use of a database structures to store and sort electromagnetic data may have been beneficial. The original decision to store data in memory resulted in fast interactive software. Memory issues were occasionally encountered on 32bit computers, as the available memory was not able to support larger datasets. The addition of databases such as JavaDB (JavaDB, 2012) or object storage db4o (Paterson and Edlich, 2006) would improve the persistence of objects and data. The addition of such a system would only require minor alterations to existing code by adding tags and replacing the table structure. It is unknown whether this will influence performance.

Thirdly, the use of pre-existing math libraries would have benefited time spent developing the software. Libraries such as the Apache Math Library (Apache, 2012b) do not include the complex vector math required for electromagnetic fields and would still need to be written.

Lastly I would have changed the name to something more professional. Despite these setbacks, the program was successfully created. This program is not just an isolated project but it will evolve beyond the scope of this thesis.

### 3.4 Overview of Developed Software Versions

Many variations to the main CSEMoMatic base have been developed. An overview of the different features of each version is shown in Figure 3-27. Several versions of the software have been developed for different purposes,

- i CSEMoMatic - The primary version (CSEMoMatic) is available to the public and contains the open source algorithms and the standard modelling tools. This version forms the base for most versions.
- ii Otze CSEMoMatic - A proprietary Fugro EM version which is Linux only and performs 2.5D finite difference modelling and contains a 2.5D finite difference model builder.
- iii Touch CSEMoMatic - A tablet version specifically designed for the ASUS EP121 tablet and is only a minor modification of the primary version.
- iv Neuro CSEMoMatic - This version is a highly experimental, enabling computer brain interfacing (BCI) using the Neurosky Mindwave (Neurosky, 2012) to control variables. NeuroCSEMoMatic is the first brain controlled geophysics software.
- v CSEMoMatic Omnium: Omnium is modified from the original CSEMoMatic versions and is tailored to professional and research use, providing higher levels of control over the survey geometry and visualisation. The key difference between Omnium and other versions is the method of visualisation. The visualisation is performed in Java OpenGL rather than Swing, which does not provide 3D support. The name Omnium self describes its open source, freeware nature. *Omnium* is a Latin word which loosely means "for all". Omnibus would be a more correct use, for the sake of style, the final name, *Omnium*, was chosen for my software.

All versions utilise common electromagnetic libraries written by myself, which include the gridding, plotting and 3D visualisation, written from scratch. In addition to the benefits of visualising electromagnetic specific structures, I prevented some licensing issues by avoiding integrating third party code by writing the plotting routines myself. Most versions are highly experimental and for research purposes only. The primary version CSEMoMatic and CSEMoMatic Omnium beta have been made available on a public SVN server (Pethick, 2012a).

	CSEMoMatic 1.4	Touch CSEMoMatic	NeuroCSEMoMatic	CSEMoMatic Otze	CSEMoMatic Omnium
1D Forward Modelling	Available	Available	Available	Available	Available
3D Integral Equation Modelling	Available	Available	Available	Available	In Development
2.5D Finite Difference	Unavailable	Unavailable	Unavailable	Available	Unavailable
1D Profile Visualisation	Available	Available	Available	Available	Available
2D Grid Visualisation	Available	Available	Available	Available	Available
2D Contour Visualisation	Unavailable	Unavailable	Unavailable	Unavailable	Available
2D Vector Visualisation	Available	Available	Available	Available	Available
2D Ellipse Visualisation	Available	Available	Available	Available	Available
3D Vector Visualisation	Unavailable	Unavailable	Unavailable	Unavailable	Available
3D Grid Visualisation	Unavailable	Unavailable	Unavailable	Unavailable	Available
3D Ellipse Visualisation	Unavailable	Unavailable	Unavailable	Unavailable	In Development
3D Isosurfaces	Unavailable	Unavailable	Unavailable	Unavailable	In Development
Multiple Frequency/Transmitter	Unavailable	Unavailable	Unavailable	Unavailable	Available
Multiple Frequency/Transmitter	Unavailable	Unavailable	Unavailable	Unavailable	Available
Brain Controlled	Unavailable	Unavailable	Available	Unavailable	Unavailable

Available

Unavailable

In Development

Figure 3-27: An overview of the different features included in each of the developed software packages

### 3.5 Impact of the Software and Online Resources

CSEMoMatic has been successfully used across the world for training geophysicists in MCSEM. A number of organisations have been using the software including Curtin University, Scripps Institution of Oceanography, University of Calgary, Imperial College London, Fugro Electro-Magnetic, Woodside Petroleum and the Brazilian National do Petroleo Government. This software has also been used as a core geophysical software training package for the Advanced EM 432 & 632 honors and masters courses conducted at Curtin University. Advanced electromagnetic university course students were asked to forward model the one dimensional and three-dimensional MCSEM response for the Scarborough gas field, North West Shelf in a two hour lab session with this software. They were successful in describing the influence of water column resistivity, equivalence, near-surface resistive layer, hydrocarbon resistivity, burial depth and size. The software has been utilised in several Bachelor of Science geophysics honours theses including Paten (2010), (Dobrich, 2010) and (Swanepoel, 2011).

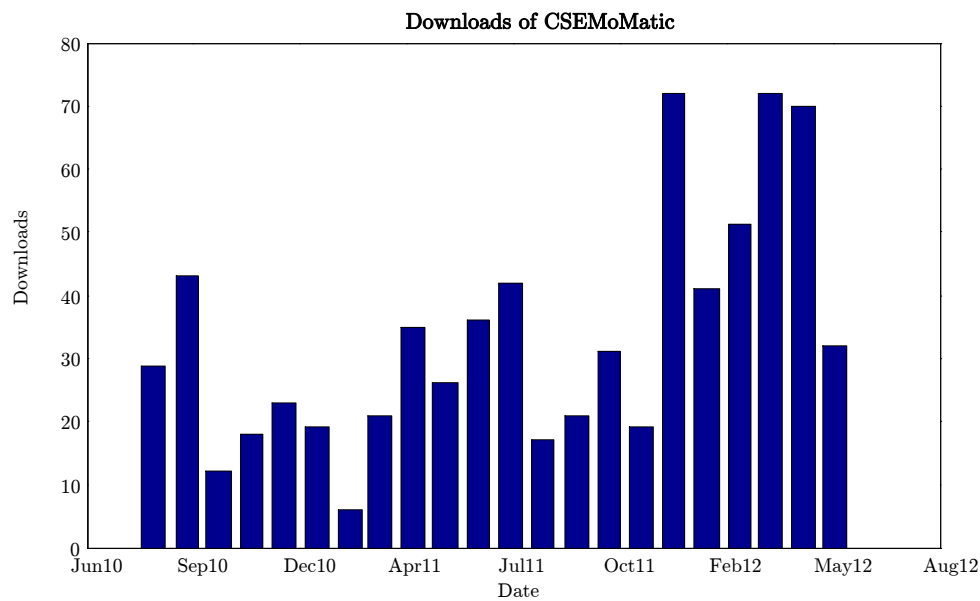
As of November 2011 the CSEMoMatic software and website has impacted over 2500 visitors from 77 countries. There have been 736 downloads of all software versions to date (See Table 3.1). It has been positive to observe a steady increase in popularity over the short period of time since its release (See Figure 3-28). The distribution of users can be seen in Figure 3-29. The heat map visualises the countries accessing and downloading the software. High density, 'hot-spot' areas include Norway, Germany, San Diego, Salt Lake City and Perth and represents practitioners of CSEM. This relates to EMGS, Fugro EM Germany, Scripps, CEMI and Fugro EM/Curtin University, Perth. There is strong following in south-east Asia, including China and Japan. This map could represent the emergence and development of private MCSEM technology in the region. Overall, this heat map is a good way of demonstrating the world-wide impact of the software.

### 3.6 Conclusion

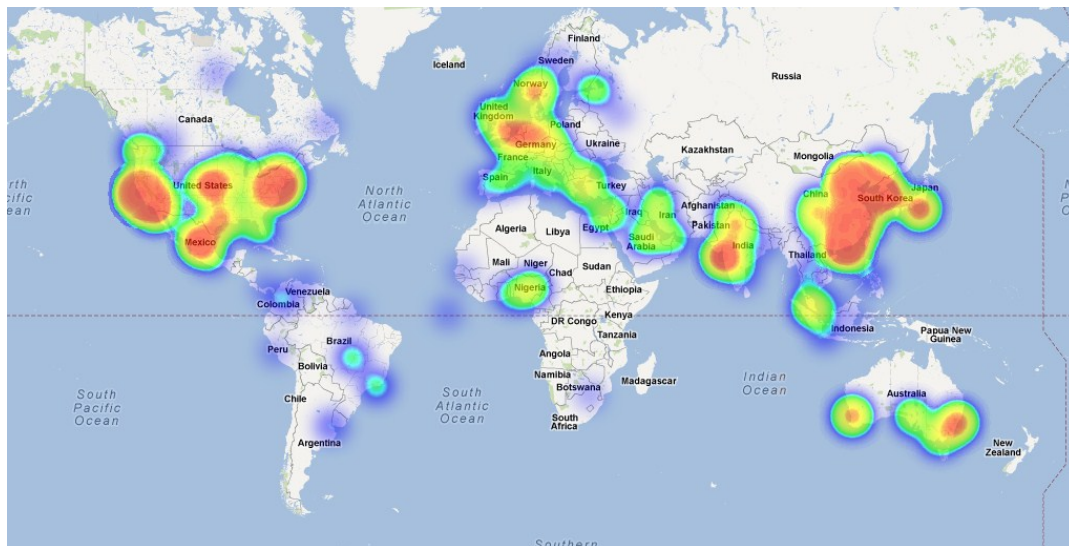
I have developed an open source software package to encourage the development and use of the marine controlled source electromagnetic method in both industry and educational institutions. The software was written in Java and was created to perform interactive real-time synthetic modelling for varying earth models or survey parameters. My open source CSEMoMatic (Pethick and Harris, 2012) software package was developed for the benefit of prospective

Version	Downloads
1.00	125
1.01	19
1.03	27
1.04	35
1.05	104
1.10	2
1.20	82
1.30	72
1.40	299
Total	736

**Table 3.2:** Breakdown of downloads for each version of CSEMoMatic



**Figure 3-28:** Downloads of CSEMoMatic versus time



**Figure 3-29:** Distribution of geo-located downloads of CSEMoMatic. Red represents regions with high visitor traffic and light blue represents regions with less than 10 visitors. The distribution of geographical interest correlates with countries practicing MCSEM.



MCSEM practitioners and to contribute to existing commercial and educational MCSEM communities. CSEMoMatic facilitates rapid forward modelling and visualisation of marine controlled source electromagnetic data through the integration of open source algorithms Dipole1D and Marco.



## Part II

# Electromagnetic Applications



# Macro Parallelisation for Controlled Source Electromagnetic Applications

---

## Contents

---

<b>4.1</b>	<b>Overview</b>	<b>138</b>
<b>4.2</b>	<b>Introduction</b>	<b>138</b>
<b>4.3</b>	<b>Background</b>	<b>140</b>
4.3.1	The Basics of MCSEM IE forward modelling	140
4.3.2	The MCSEM method	142
4.3.3	Grid Computing	143
<b>4.4</b>	<b>Developing a Macro Electromagnetic Modelling Framework</b>	<b>144</b>
4.4.1	Programming Heuristics	144
4.4.2	Electromagnetic data structure	144
4.4.3	Macro Parallelisation	147
<b>4.5</b>	<b>IE Forward Modelling Parallelisation</b>	<b>151</b>
4.5.1	Frequency and Source Dependence	155
4.5.2	Implications for Macro Integral Equation Parallelisation	157
<b>4.6</b>	<b>Grid Computing Airborne EM Inversion</b>	<b>158</b>
4.6.1	Execution	158
4.6.2	Results and Discussion	161
<b>4.7</b>	<b>Conclusion</b>	<b>161</b>
<b>4.8</b>	<b>Macro Parallelisation Pseudo-Code</b>	<b>165</b>

---

## 4.1 Overview

Many geophysical computational problems could be referred to as “embarrassingly parallel”. Grid computing is a parallel computing method that utilises large numbers of linked computers to solve computational problems. Most universities and companies have thousands of cores readily accessible over high speed networks. We create “macro” parallelisation method to rapidly recover solutions for a range of electromagnetic modelling problems. We create software operating above a generic electromagnetic data structure to test our parallelisation method. We demonstrate the implementation and potential benefits of grid computing with the aid of two examples. The first example quantifies the reduction in computational time requirements where macro parallelization is applied to forward modelling of marine controlled source electromagnetic surveys. In the second numerical experiment we apply macro parallelisation to recover the subsurface conductivity distribution from a large airborne transient electromagnetic survey spanning more than 2,000 square kilometres. Our numerical experiments show that when given access to approximately 12,000 CPUs, the entire airborne TEM survey requiring 1D inversions of more than 100,000 soundings should reasonably be completed in less than 10 seconds. Grid computing provides the possibility to invert entire airborne electromagnetic (EM) datasets in near real time.

There is no doubt that parallel computing will be an increasingly significant tool for geophysicists. We provide description, sequence diagrams, pseudo-code and examples to illustrate how parallelisation can be readily built over the top of carefully designed CSEM data structure. The “macro” parallelization methods we present is intended as parallelization for the masses.

## 4.2 Introduction

It is clear that new high performance computing methods should be highly beneficial for geophysical modelling in earth science applications. Parallel electromagnetic computing methods are used to alleviate memory or speed limitations or both. It is not clear whether this technology is being fully exploited by practicing geophysicists. We have set out to develop, test and convey practical methods for taking advantage of grid computing and embarrassingly parallel nature of electromagnetic problems. The phrase “embarrassingly parallel” refers to a computational process which can be easily divided into smaller processes,

computed independently on separate computers and reassembled at the end. We aim to develop and implement a publically available macro parallelisation code and method. Our 'macro' parallelisation approach enables single single-threaded electromagnetic algorithms to be integrated into a grid computing software. It is a 'macro' process because a wrapper is formed around the algorithm so the internal EM modelling code is not altered. With the above in mind, our objective was to develop software incorporating the grid computing methods with the following baseline requirements:

- i it must be simple to understand and implement
- ii it should require no modification of source EM code
- iii several orders of magnitude improvement in computational speed should be achievable
- iv the applications should be scalable from a grid of 10 CPU's, to clusters with hundreds of thousands of CPUs.

Parallelisation of MCSEM modelling algorithms is not new. Key and Oval (2011) utilised MPI routines to reduce 2.5D forward modelling finite element problems to seconds on an 800 node cluster. (Commer et al., 2008) imaged large scale field MCSEM data using a parallel algorithm on the IBM Watson Research Blue Gene/L supercomputer. Commer et al. (2008) reduced computation time from four months of processing time on distributed clusters to 24 hours on a super computer utilising 32,768 tasks/processor. Newman and Alumbaugh (1997) created and tested a parallel conjugate gradient 3D electromagnetic inverse problem to alleviate memory issues and to improve execution time. Key and Oval (2011) present a similar parallelisation technique to the one we present, however our parallelisation is for removes the need to modify existing algorithmic code. Key and Oval (2011) present a 2.5D parallel finite element electromagnetic modelling method while parallelisation method is for 3D MCSEM modelling and 1D airborne inversion codes. This is particularly useful for legacy, compiled, closed source, licence restricted or poorly document electromagnetic modelling code. Computer scientists use many acronyms and a wide range of jargon to refer to concepts that have much in common with "grid computing". Examples are "cloud computing", "cluster computing" and "GPU computing". While the architecture, implementation and branding may vary slightly, in essence all these provide the possibility of simultaneous distribution of computational tasks.

Integral equation (IE) based algorithms are routinely used to simulate ground electromagnetic surveys. Several 3D IE based codes for computing EM fields exist. (e.g., Wannamaker et al.,

1982; Xiong, 1992; Xiong and Tripp, 1995; and Hursan and Zhdanov, 2002) with several being used for MCSEM (e.g., Gribenko and Zhdanov, 2007). Typical MCSEM surveys can require thousands of source positions and multiple frequencies to illuminate a target. The reconstruction of sub-surface conductivity using an IE method requires the solution of large system of equations.

We present a parallelisation technique to improve computational time for forward and inverse controlled source electromagnetic problems. Our approach integrates existing EM codes as subroutines within a high level multi-threaded electromagnetic framework. We illustrate our methods with a 3D forward modelling and 1D inversion example. In the first example we apply grid computing to simulate an entire MCSEM survey using 3D integral equation code. In the second example, grid computing is applied to the 1D inversion of soundings from a large Airborne TEM survey in a sedimentary basin.

## 4.3 Background

### 4.3.1 The Basics of MCSEM IE forward modelling

The electromagnetic response from different survey configurations and geo-electrical models can be computed using a variety of methods. Numerical methods for computing electromagnetic fields in complex earth structures are: finite difference (FD), finite element (FE) and IE. We chose to focus on the IE method. This method is used to calculate the electromagnetic response of 3D heterogeneous scattering bodies in a 1D layered background. Calculations are performed by replacing these heterogeneities with point-dipole scattering currents. Solving the tensor Green's function is a significant part of the IE method for computing EM fields (Raiche, 1974). The IE equation method recovers total, layering and scattering EM fields. The propagation of electromagnetic fields must satisfy Maxwell's equation as shown in equations 4.1 and 4.2 below:

$$\nabla \times E = -i\omega\mu H \quad (4.1)$$

$$\nabla \times H = (\hat{\sigma} + i\omega\varepsilon)E + J_0 = \sigma E + J_0 \quad (4.2)$$

$$\sigma = \sigma_p + \sigma_s \quad (4.3)$$



$$\nabla \times H = \sigma_p E + (\sigma - \sigma_p)E + J_0 = \sigma_p E + J_s + J_0 \quad (4.4)$$

Hohmann (1987) and Raiche (1974) offer solution to the integral equation problem but for convenience we have reproduced part of Raiche (1974) description of the IE method below. EM fields in a 3D conductivity distribution must also clearly comply with Maxwell's equations. This relationship is expressed below. Raiche (1974) expresses each inhomogeneous cell by an equivalent scattered source. That is, each inhomogeneous cell is replaced by an equivalent source.

Inserting 4.1 into 4.4 yields

$$\nabla \times \nabla E + i\omega\mu\sigma_p E = -i\omega\mu(J_s + J_0) \quad (4.5)$$

$$\nabla^2 E - i\omega\mu\sigma_p E = i\omega\mu(J_s + J_0) + \nabla(\nabla \bullet E) \quad (4.6)$$

$$\nabla^2 E + k_p^2 E = i\omega\mu(J_s + J_0) + \nabla(\nabla \bullet E) \quad (4.7)$$

$$k_p^2 = -i\omega\mu\sigma_p = -i\omega\mu\hat{\sigma}_p + \omega^2\mu\varepsilon_p \quad (4.8)$$

Taking the divergence of 4.4 gives

$$\nabla \bullet (\nabla \times H) = 0 = \nabla \bullet (\sigma_p E + J_s + J_0) \quad (4.9)$$

$$\nabla \bullet (\sigma_p E) = -\nabla \bullet (J_s + J_0) \quad (4.10)$$

$$\nabla \sigma_p \bullet E + \sigma_p \nabla \bullet E = -\nabla \bullet (J_s + J_0) \quad (4.11)$$

$$\nabla \bullet E = -\frac{\nabla \sigma_p}{\sigma_p} \bullet E - \frac{\nabla \bullet (J_s + J_0)}{\sigma_p} \quad (4.12)$$

Plugging that back into 4.7 gives

$$\nabla^2 E + k_p^2 E = i\omega\mu(J_s + J_0) - \nabla \left( \frac{\nabla \sigma_p}{\sigma_p} \bullet E + \frac{\nabla \bullet (J_s + J_0)}{\sigma_p} \right) \quad (4.13)$$

$$\nabla^2 E + k_p^2 E + \nabla \left( \frac{\nabla \sigma_p}{\sigma_p} \bullet E \right) = i\omega\mu(J_s + J_0) - \nabla \left( \frac{\nabla \bullet (J_s + J_0)}{\sigma_p} \right) \quad (4.14)$$

The solution to equation 4.14 is expressed as below in equation 4.15. The electric field, tensor Green's function  $G^E(r, r')$ , is a kernel function to solve the inhomogeneous partial differential equation (i.e., equation 4.14). It relates the electric field at a radial position  $r$  in layer 1 to a source element at  $r'$  in layer  $j$ .

$$E(r) = E_p(r) + \int_v G^E(r, r') \bullet \sigma_a(r') E(r') dv' \quad (4.15)$$

The IE solution can fully describe the electric and magnetic fields. The total field is the sum of the primary (layering) and scattered (3D inhomogeneous body) fields. The tensor Green's

function must be solved independently for each conductivity distribution, source position and transmission frequency to compute the scattered response. Note that the tensor Green's function does not need to be recomputed for every receiver position. Computations for large numbers of receiver positions are many orders of magnitude faster than computations for large numbers of transmitter positions. This invites the use of the principle of reciprocity to increase the computational efficiency for MCSEM where there are considerably more transmitter positions than receiver positions. Reciprocity involves the practice of switching the position source and receiver components (Nabighian, 1988). In cases with larger numbers of transmitters than receivers (i.e., MCSEM) the number of computed excitations can be reduced through the application of Reciprocity. Jakobus (1997) demonstrated the IE method can be parallelised by looping over each frequency and has applied this approach to analysing electromagnetic radiation and scattering problems. Complete derivation and description of a range of IE solutions can be seen in Farquharson et al. (2006), Newman and Hohmann (1988), Raiche (1974) and Slob and van den Berg (2005). IE methods require the computation of the tensor Green's function for every source, frequency and conductivity distribution. Harris (2001) shows that for a three layer earth, parts of the layered solution can be solved independently from the source position and this could speed up the solution. The problem still requires a solution to the tensor Green's function for every source, frequency and conductivity distribution. Since various algorithms already exist, our methods seek to provide a generic solution to parallelise any suitable MCSEM IE modelling algorithm. A generic MCSEM data structure was created to allow the integration of any IE algorithms. Our software utilise these IE algorithms at a macro level.

### 4.3.2 The MCSEM method

MCSEM surveys are conducted by towing a horizontal electric bipole transmitter close to the ocean floor. The transmitter typically sends a square bipolar waveform with peak current of up to 1000 amps into a long (e.g. 300 m) horizontal wire. The measured electrical and magnetic fields are decomposed to amplitude and phase for a range of frequencies from 0.05 to 1 Hz. MCSEM surveys with multiple receiver deployments may have thousands of transmitter locations, while the number of multi-component electric and magnetic field receiver positions is usually below 250. The number of deployed receivers is typically limited by the carrying capacity of the MCSEM vessel. For example, a MCSEM survey with multiple receiver deployments, conducted over the offshore Santos Basin in Brazil, recovered 8 frequencies from 180 multi-component receiver positions (Buonora et al., 2009). This survey would likely have

consisted of many thousands of source positions. Most forward modelling algorithms and software packages were created in a time prior to multicore and hyperthreading technologies. Forward computation of a full MCSEM survey for complex geology on a single thread can take months or years, necessitating a new computational paradigm. Some parallel commercial 3D modelling and inversion codes for MCSEM exist (e.g., TechnoImaging, 2012; and EMGS, 2012). However the algorithms are all proprietary. We chose to focus on an algorithm available to all users. Optimisation methods currently exist to decrease the computational time. These include using reciprocity principles and selectively modelling cells sensitive to the footprint, which is both source and receiver dependent, of the survey parameters (Cox and Zhdanov, 2006; Cox and Zhdanov, 2007 and Cox et al., 2011). Zhdanov et al. (2000) has developed fast approximations (i.e., Born approximation and Quasi-analytic) to the full IE algorithm. The IE method as described by Endo and Zhdanov (2009), precomputes the nonvarying inhomogeneous background fields and Green tensors, allowing it to be stored and reused in subsequent iterations/forward models and inversion schemes. This method has been applied by Zhdanov et al. (2010). Some of these optimisations limit the effectiveness of parallelisation, which is discussed further on. There are many variations on the integral equation method. We seek to develop a ‘macro’ parallelisation approach that is able to improve computational speed using base IE code.

### 4.3.3 Grid Computing

Grid computing is a mainstream paradigm for resource intensive applications (Menasce and Casalicchio, 2004). Grid computing involves utilising networks of computers as a single unified computing tool (Tarricone and Esposito, 2004). Examples of modern parallel computing include grid computing, cloud computing and high performance computing on clusters. Networked computing resources are combined to solve large mathematical problems for grid computing. Grid computing has been applied for a variety of purposes including the Search for Extra Terrestrial Intelligence (SETI) project (Werthimer et al., 2001), identifying the cause of protein misfolding (i.e., Folding@Home; Anderson et al., 2002) and the modelling of earthquake generated seismic wavefields (Youn et al., 2008).

## 4.4 Developing a Macro Electromagnetic Modelling Framework

We have developed an electromagnetic modelling framework to provide higher level functionality to most electromagnetic modelling algorithms. This framework provides methods to store, retrieve and sort electromagnetic data and survey information. It also controls network protocols and execution functionality. Both the client and server is built upon this framework.

### 4.4.1 Programming Heuristics

Java is an example of a modern high level programming language. We have used the Java programming language for its versatility and ease of use. Java enables rapid cross platform software development with minimal for memory management requirements and vast system functions. Java has been selected because graphical user interface, network IO, file IO, memory management, execution and threading capabilities are provided without the need for external third party algorithms. The traditional geophysical programming stables, Fortran and C, offers limited graphical user interface (GUI), network or multi-threading capacity without the help of third party libraries, which may be platform dependent. Java overcomes this problem without the need for third party libraries which reduces install time, improves cross platform versatility and development time.

### 4.4.2 Electromagnetic data structure

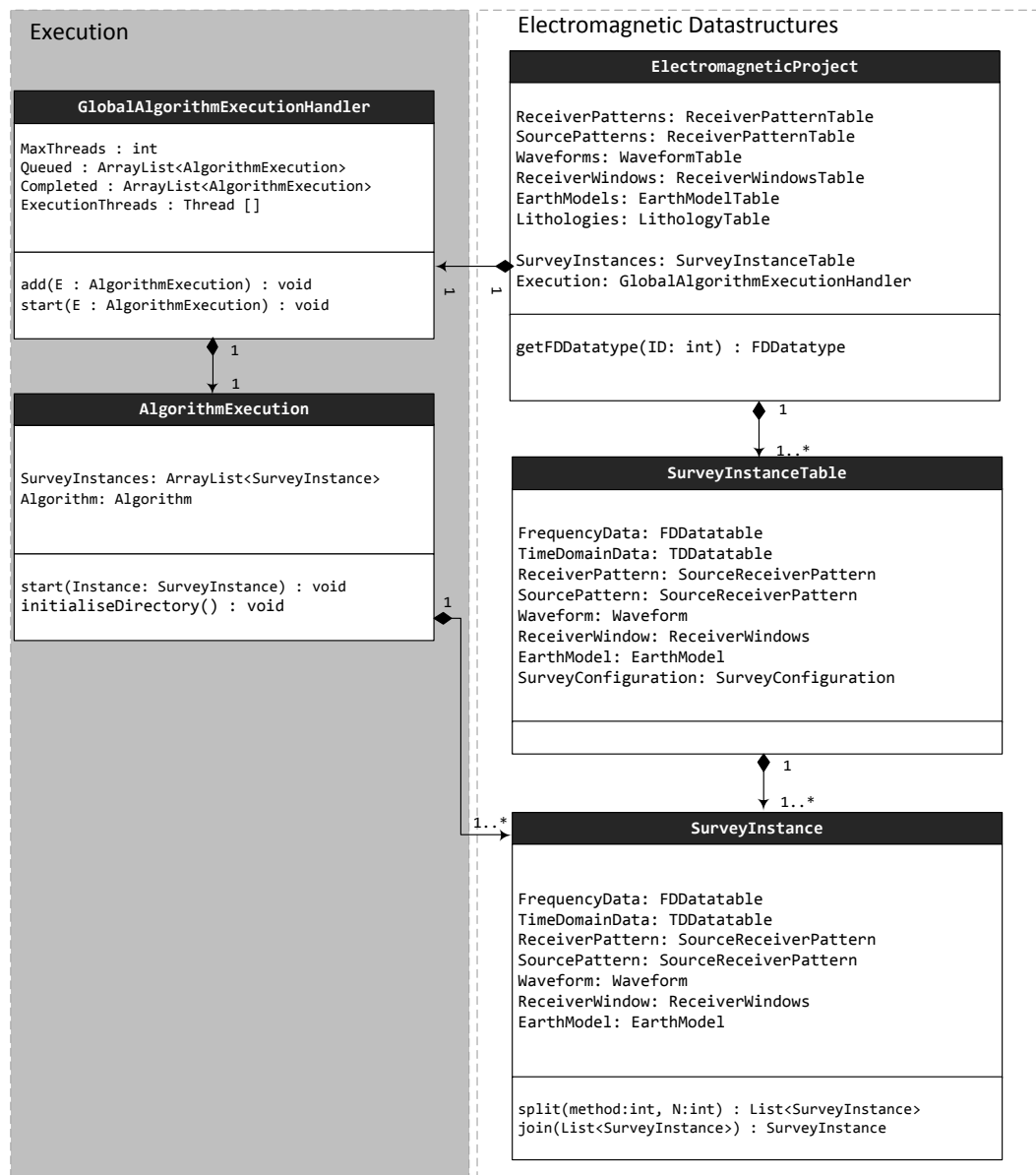
A generic electromagnetic data structure can be used to enable the storage, sorting and retrieval of any electromagnetic survey component (e.g., receivers and data). We have developed a generic EM data structure to enable the integration of most third-party EM compiled codes. The algorithm has access to higher level functions such as survey division and system execution functions through the dat amodel. This data model is used to “wrap” the electromagnetic algorithm in a sophisticated data management package. The data structure is open source license and is freely available Pethick (2012b). We summarise the key elements of our electromagnetic data structure Figure 4-1 using UML class diagrams (Pilone and Pitman, 2005). Controlled source electromagnetic surveys have the same common features including,

- i system or survey configuration
- ii transmitter arrays
- iii receiver arrays
- iv transmission waveforms
- v receiver windows (for time domain systems)
- vi geo-electrical earth models
- vii output electromagnetic data

The system, or survey configuration, defines the transmitter and receiver relationship. The transmitter array describes transmitter properties and geometry. The receiver array describes receiver properties and geometry. The geo-electrical model defines the conductivity distribution. The transmission waveform describes the electromagnetic field generated from the transmitter. The output electromagnetic data is recorded for each transmitter-receiver location for each transmission frequency or time window. These elements form a controlled source electromagnetic survey.

We have created an electromagnetic project (i.e., the 'ElectromagneticProject' class) to map real world electromagnetic structures into a coherent data model. The electromagnetic project stores all waveforms, transmitters, receivers and earth models (see Figure 4-1). The electromagnetic project can contain multiple survey instances. Each survey instance (i.e., 'surveyInstance' class) contains a single instance of a survey. The survey instance class contains all the components required to create a CSEM survey. Only one system configuration, earth model, transmitter and receiver pattern, waveform and receiver window setting is allowed per survey instance. Frequency and time domain data are stored in the survey instance rather than the electromagnetic project because the data is specific to the survey instance. The survey instance enables the conversion between the generic data structure and the external algorithm's specific input and output files.

Each EM modelling and inversion algorithm must implement the 'Algorithm' interface get access to the electromagnetic framework. (See Figure 4-2). The interface is essentially a strict template. Every third party typically possesses its own input, output and execution



**Figure 4-1:** An overview of the EM project structure. This structure allows all the main components of an electromagnetic survey (i.e. waveform, earth model, transmitter and receiver set, system configuration and dataset) to be stored and to then be used individually for electromagnetic modeling via a survey instance. This structure enables multiple survey instances to be created, split and modeled. Any algorithm has access to higher level functionality using this data model (i.e. survey division via the 'SurveyInstance' class and execution via the 'AlgorithmExecution' class).

file formats. The 'Algorithm' interface enables the conversion between the electromagnetic framework and the algorithm's own input and output file formats and enables custom execution sequences to be created for each algorithm executable. The 'FileFormat' interface covers import, export and execution functionality.

#### 4.4.3 Macro Parallelisation

Any modern computer can forward model a controlled source electromagnetic response. The forward and inverse solution needs to be completed in a practical time frame, especially when many forward models are computed, analysed and updated based on previous results. More computing power is required with increasing survey and geo-electrical complexity. Two descriptions have been chosen to represent our macro parallelisation method include Sequence diagrams and Pseudo-code (see Appendix B). Our macro parallelisation method involves several steps,

Step 1 Initialise a grid of computers

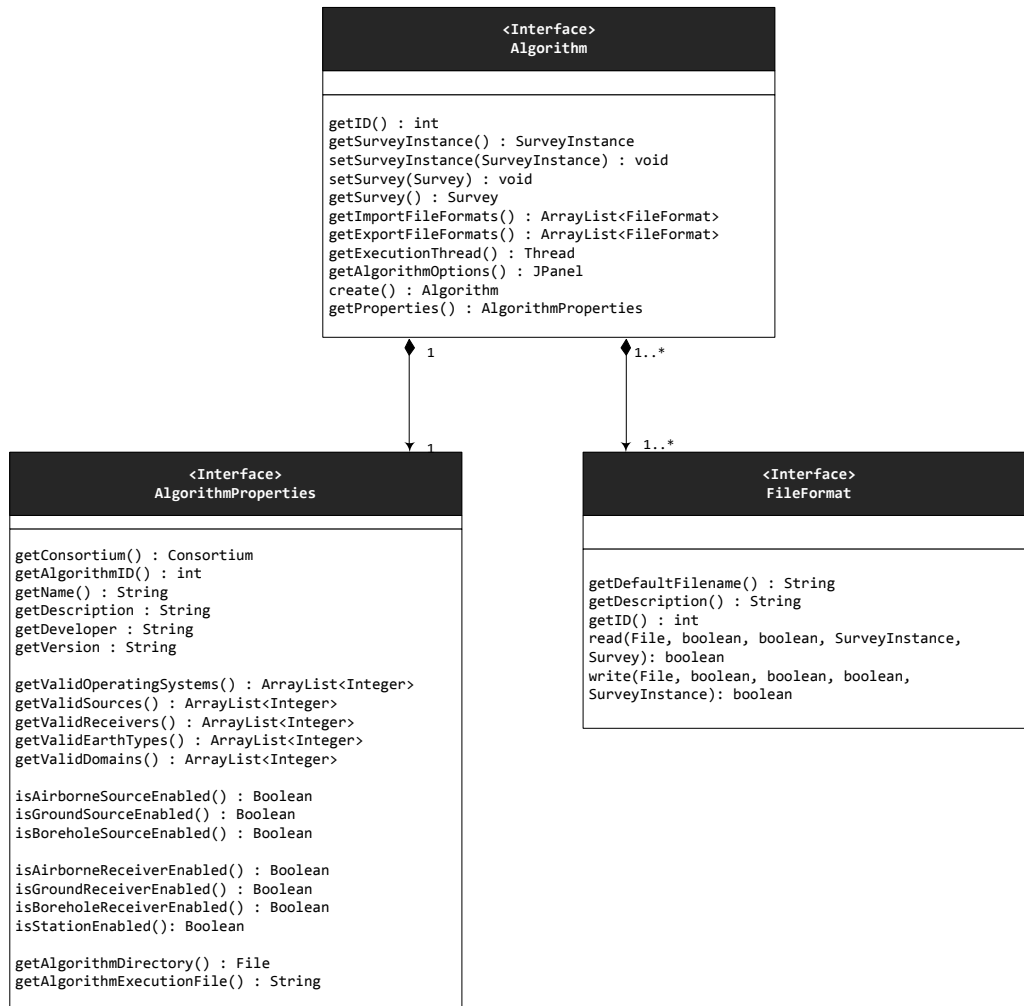
Step 2 Create independent execution environments

Step 3 Divide the survey into an optimal number of input files

Step 4 Compile results

The first step of the macro parallelisation process is to initialise the computer grid. A server application was developed to handle connections and distribute tasks (See Figure 4-3) . The server creates a connection by opening a new server socket on a predetermined port. A server thread is then created to listen for incoming client connections. Upon each client connection an individual thread is added. This thread controls incoming and outgoing requests and file transfers. Upon the successfully connection between client and server sockets, the server's client thread sends a success command to the client. Upon retrieval of the "success" command the client transmits it's known IP-address, number of maximum available threads and latency between the client and server. The client-server connection procedure can also be represented by a sequence diagram (Figure 4-4). This Figure shows the sequence of events between the client and server.

In the second step an independent execution environment is created. We take advantage of typical operating system management to create independent execution environments.



**Figure 4-2:** The generic 'Algorithm' class structure. Each algorithm has several functions including input and output file handling, execution procedure handling and error and survey validation. An implementation of the 'Algorithm' interface allows the algorithm to be integrated into the electromagnetic modelling and inversion framework.



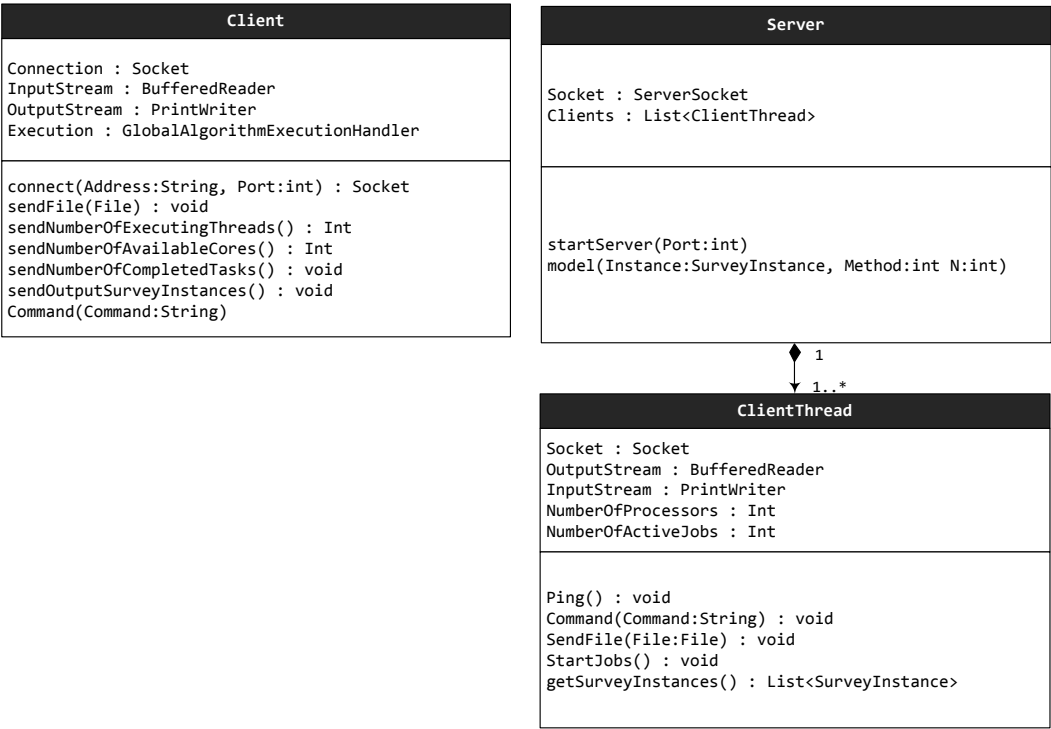


Figure 4-3: An overview of the network class structure.

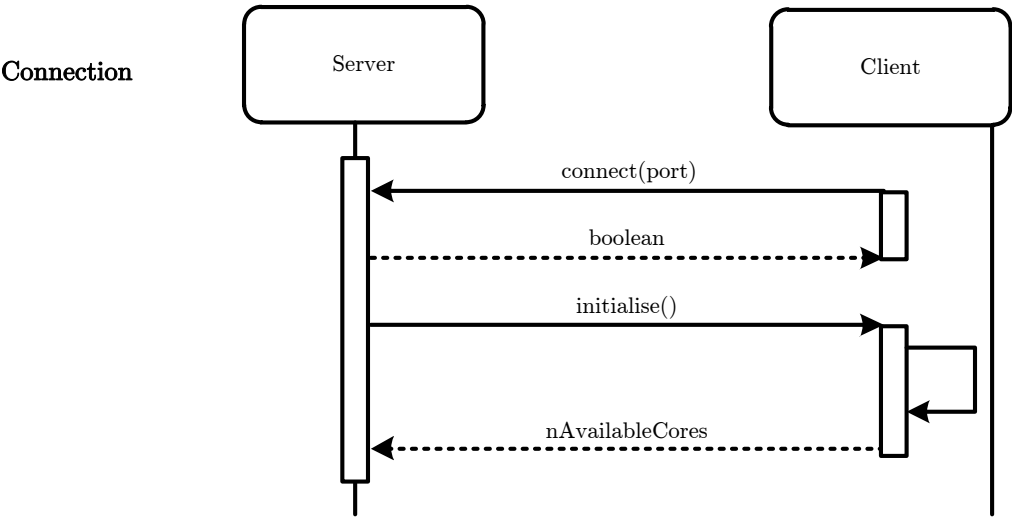


Figure 4-4: Sequence diagram showing the connection procedure between the server and client in the macro parallelisation process.

Contrary to popular beliefs, operating systems are not fancy graphical user interfaces. Primarily operating systems are resource managers that controls behaviour between the hardware and the software. Operating systems manage primary memory, secondary memory and schedule processor time between all executing applications. Operating systems also manage network protocols found in the seven layer OSI model (i.e., the data-link, network and transport layers handle all client-server interactions). Our macro parallelisation takes advantage of OS resources management (i.e., execution and networking). It is not always necessary to utilise low-level memory and application functions to spawn off new processes (i.e., using C to fork new running applications). Separate independent execution environments are created by replicating compiled executable code into individual directories, one for each CPU core (i.e., the maximum running threads). Creation of independent execution environments are performed via the 'initialiseDirection' method in the 'AlgorithmExecution' class (See Figure 4-3). The operating system treats each of these instances as independent process upon execution, removing the need to micro-manage each block of memory, single execution thread or network transmission or connection. Each execution thread must be independent to remove the threat of deadlock or memory sharing violations. Results are sent back to the server upon completion of each thread.

Thirdly, the server analyses the survey instance (i.e., the entire survey description) and divides the survey into a number of smaller partial surveys based on the number of CPUs available. As established in Appendix A, most EM modelling problems can be broken down into source-frequency pairs or individual earth models. Survey splitting is performed by the 'split' function in the 'SurveyInstance' class (see Figure 4-1). If processor speed is ignored, the optimal number of independent source-frequency pairs per CPU can be roughly estimated through equation 4.16.

$$N_{(T,\omega)} = \text{Ceiling}(\text{Complexity}/N_{\text{Cores}}) \quad (4.16)$$

where,

$N_{(T,\omega)}$  – Nuber of Source-Frequency pairs per thread

*Ceiling* is the mathematical function to round a decimal number up to the nearest integer

$T$  – Transmitter source position

$\omega$  – Transmission frequency

The server generates multiple input survey instances, one for each execution thread. Each survey instance is asynchronously sent to the corresponding CPU once generated (See Figure 4-5); as each client receives a new partial survey instance the client begins to model the results.

Lastly the results are compiled by the Server. This is performed by the higher level functions within the electromagnetic modelling framework. The result is a significant increase in global computational speed.

We have developed a graphical user interface to accompany our electromagnetic framework. The application (See Figure 4-6) was developed to create synthetic surveys (i.e. 'SurveyInstance') of varying survey complexity. Options providing finer control of the the framework settings, such as splitting of survey's by a custom number of frequencies or transmitter locations have been integrated into the GUI. The application provides real time monitoring of each of the clients. The status of every client CPU core is visible to the server and is represented by a red (active) or green (inactive) core indicator.

## 4.5 IE Forward Modelling Parallelisation

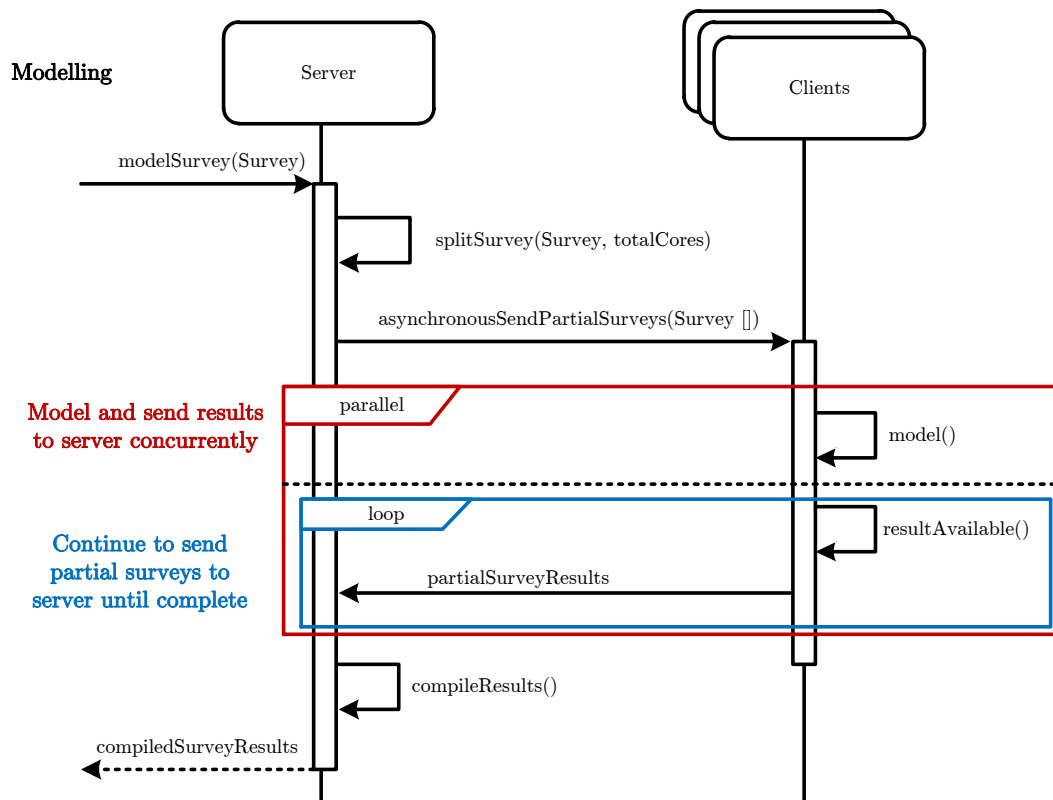
In Appendix A we established that the tensor Green's function used in the IE methods is dependent on source, frequency and subsurface conductivity distributions. Given this result from Appendix A, each thread thread can be allocated a computational task for each frequency, source position and geo-electrical model set or tuple. That is, thousands of tasks can be computed simultaneously with the multithreading approach. Our IE macro parallelisation process is demonstrated with the following scenario: A MCSEM survey consisting of 25 receivers, 128 transmitter positions and 8 transmission frequencies is completed within a 3-layer earth containing an 1125 cell ( $15 \times 15 \times 5$ ) 3D anomalous region, as illustrated in Figure 4-7. The computation of EM fields for 1024 (i.e.,  $128 \times 8$ ) independent combinations of source and frequency is required. We start by considering one conductivity distribution (Figure 4-7). We define the complexity of the surveys as:

$$Complexity = N_s \times N_f \quad (4.17)$$

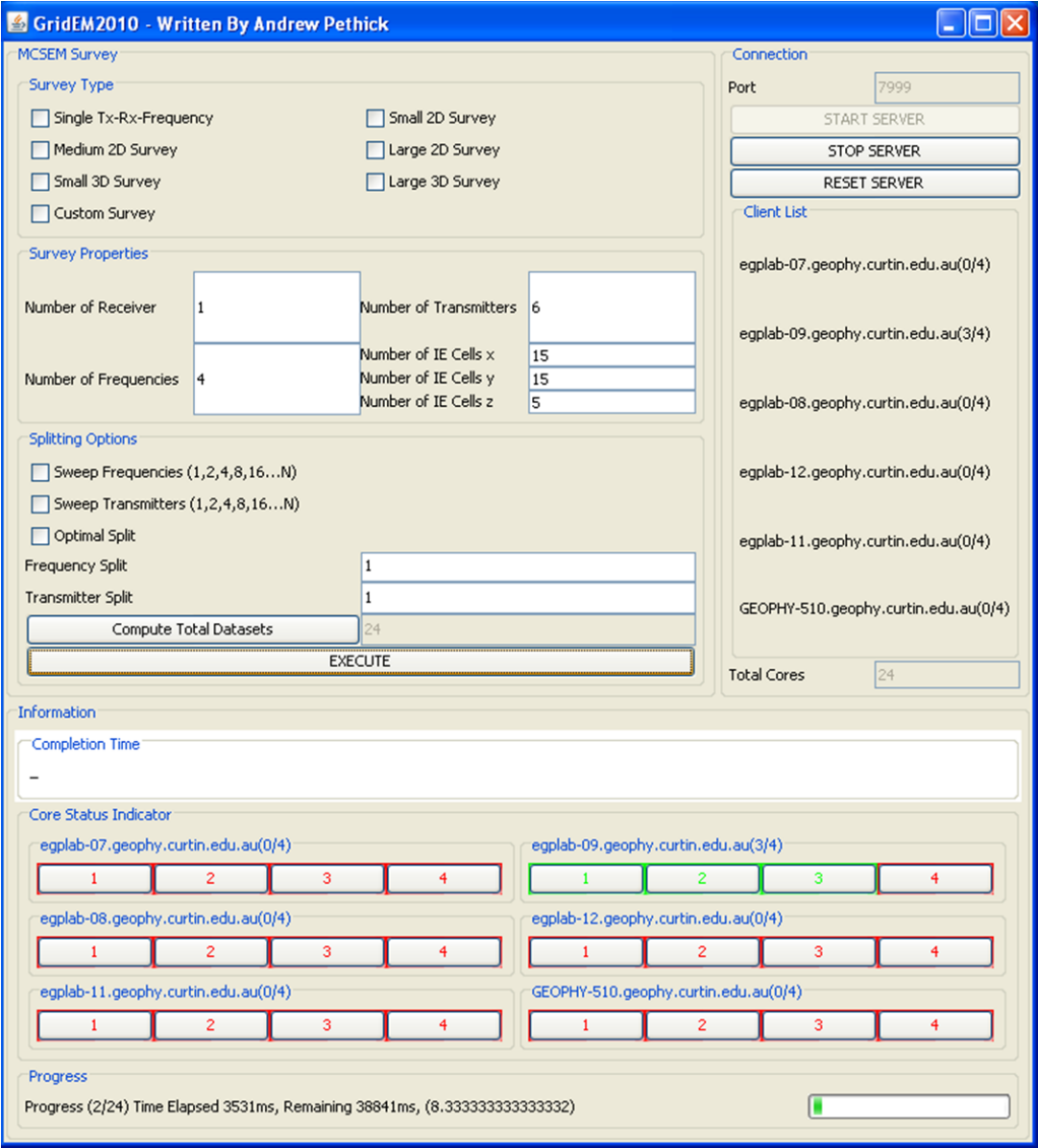
where,

$N_s$ — Number of Sources

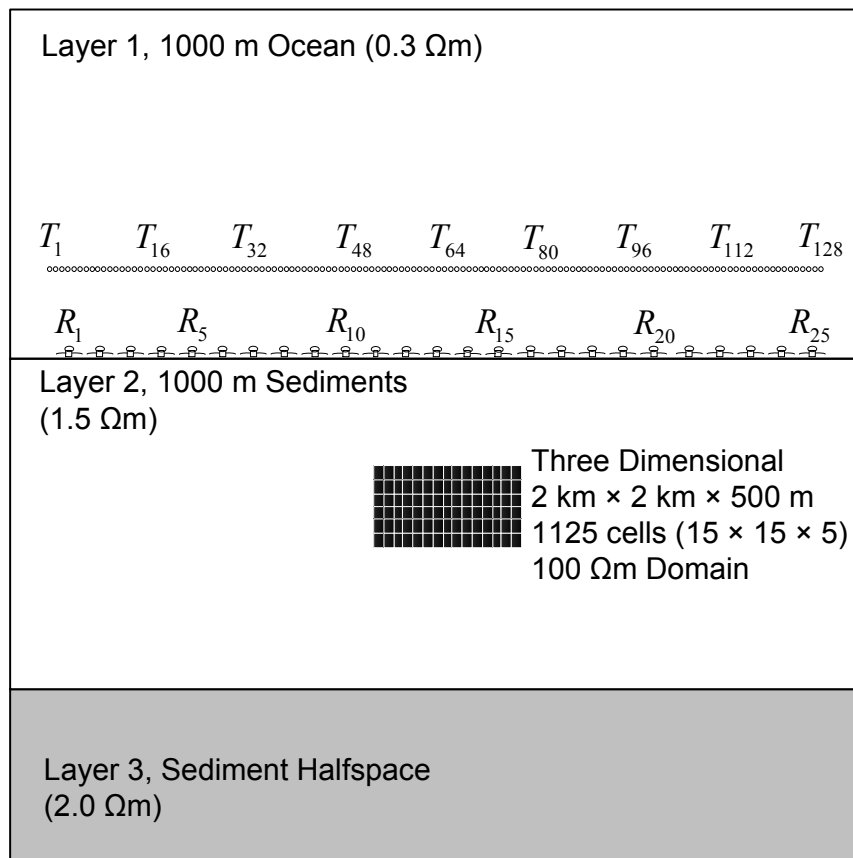
$N_f$ — Number of Frequencies



**Figure 4-5:** Sequence diagram showing the interactions between the server and client in the macro parallelisation process. The steps involved in the parallelisation process are: (1) During the connection process the server obtains the number of available cores from the client and an independent execution environment is created. (2) Once a command to model a survey is obtained from the user, the survey is split into a number of partial surveys based on frequency and transmitter location. The corresponding partial surveys are sent to each of the clients asynchronously (i.e., the clients start computation with the arrival of a new partial survey instance). (3) Once modelled, the partial results are then sent to the server. Once the server detects that all results are transferred, the results are compiled and given back to the user.



**Figure 4-6:** The developed server grid computing GUI. This grid computing interface is built upon a generic MCSEM data structure and has integrated a single-threaded implementation of AMIRA’s IE Marco executable. In this example a grid of 6 quad-core computers are connected to simulate the appearance of a single PC with 24 cores.



**Figure 4-7:** Simulated MCSEM survey layout and geo-electric structure. The Integral Equation (IE) macro parallelisation is demonstrated using a MCSEM survey consisting of 25 receivers, 128 transmitters and 8 transmission frequencies. This particular survey is performed over a 3-layered earth model that includes a 1125 cell 3D scattering body. A single-threaded implementation to compute this survey would require 12 hrs on an Intel Core 2 Quad processor using the Marco IE algorithm (Xiong, 1992)

The problem can be split into 4 threads, each with a complexity of 256 (equation 4.17) for a quad-core CPU. The survey can be ordered by frequency or transmitter locations as shown in Table 4.1. Two timing methods for calculating the efficiency of the macro parallelisation method are used. These are wall time and CPU time (Srivastava and Widom, ). Wall time is the total time taken from the start of execution to the termination of the last thread (Goux et al., 2001). CPU time is the total time each thread actively runs on its CPU core. The effectiveness of the macro parallelisation is defined by 'speedup' and 'efficiency'. Speedup and efficiency are defined in equations 4.18 and 4.19 respectively.

$$Speedup = t_{WS}/t_{WN} \quad (4.18)$$

$$Efficiency = Speedup_N/N \quad (4.19)$$

where,

$t_{WS}$  – Waltime on a single CPU

$t_{WN}$  – Waltime on a N CPU's

$N$  – N is the total number of CPU's utilised

Core	Splitting By Transmitter	Splitting By Frequency
1	$T_n=1..32, \omega_n=1..8, R_n=1..25$	$T_n=1..128, \omega_n=1..2, R_n=1..25$
2	$T_n=33..64, \omega_n=1..8, R_n=1..25$	$T_n=1..128, \omega_n=3..4, R_n=1..25$
3	$T_n=65..96, \omega_n=1..8, R_n=1..25$	$T_n=1..128, \omega_n=5..6, R_n=1..25$
4	$T_n=97..127, \omega_n=1..8, R_n=1..25$	$T_n=1..128, \omega_n=7..8, R_n=1..25$

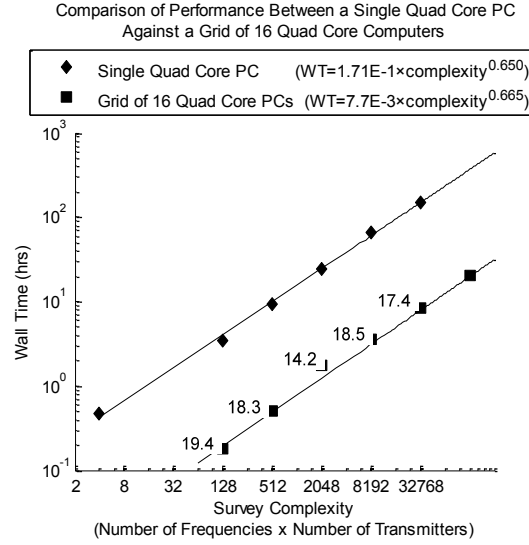
**Table 4.1:** Distribution of an independent set of survey parameters for 'macro' parallelisation on a quad-core CPU architecture. The two methods shown divide the survey by transmitter position or frequency.

	Splitting By Transmitter	Splitting By Frequency
Number of Cores	Wall Time/Speedup/Efficiency	
1	11.99 hrs/1.0/1.0	
2	6.31 hrs/1.90/0.95	6.30 hrs/1.90/0.95
4	3.24 hrs/3.70/0.92	3.20 hrs/3.75/0.93

**Table 4.2:** A comparison of wall time, speedup and efficiency for computing the 128 transmitter, 8 frequency survey on one, two and four cores.

#### 4.5.1 Frequency and Source Dependence

We complete a computational experiment to establish the importance of each parallelisation method (i.e., frequency splitting and source splitting) for optimal survey division. A computer with an Intel Core 2 Quad 2.6 GHz CPU and 4 GB of RAM was used to compute the following results. The forward modelling algorithm is AMIRA's IE 3D forward modelling software called Marco (Xiong, 1992). Forward computation of the MCSEM survey was completed in 11.99 hrs wall time with a single-threaded structure (i.e., no parallelisation). The computation time was



**Figure 4-8:** Results from the grid computing simulation comparing the performance between a single PC versus a grid architecture for varying survey complexities over the earth model shown in Figure 4-7. Each marker (i.e., diamond or square) represents an independent timed simulation test. The speedup achieved by using a grid computing architecture is shown on the corresponding data points. Since the difference between each power law gradient (e.g., 0.650 versus 0.665) is negligible, there is practically no loss of efficiency with increasing survey complexity. The parallel relationship of the complexity versus computation time shows that this parallelisation method can be scaled to any number of CPUs.

reduced by 1.9 times as the number of threads doubled. This was true for both frequency and source threaded experiments. This simply reflects the observation that source and frequency are computed independent of each other (see Table 4.2).

We completed a computational experiment to demonstrate the benefits of multithreading for the numerical simulation of MCSEM surveys using the IE method. Of particular interest is the scalability of the problem. Computational speed on a single quad-core 2.8 GHz PC is compared to a grid of 16 2.8 GHz, quad-core PCs (64 cores). A 16 times increase in performance was obtained when using the grid implementation for all survey complexities greater than 64 (see Figure 4-8). These power law curves are parallel, demonstrating the potential scalability of our MCSEM macro parallelisation method (see Appendix B or Figure 4-5). The efficiency is not lost despite having network I/O overheads (i.e., distribution/transmission and receiving of tasks). Parallelisation of the IE method for computing electromagnetic fields at the macro level falls into a category sometimes referred to as “embarrassingly parallel”.



### 4.5.2 Implications for Macro Integral Equation Parallelisation

There are some limitations that are encountered by this parallelisation method; these are algorithmic and network related. The independent execution environment prevents concurrency issues however the main computational setback is the network transfer bottleneck. This occurs when multiple executions finish within a short time and start to transfer their computed results to the servers. It is common for all instances to finish within seconds of each other due to the equal survey complexity. Typically, modelled datasets are not large (i.e., much less than 10 MB) but when hundreds of instances begin to transfer their data simultaneously, a large volume of data may be encountered by the server. Luckily for electromagnetic methods in most cases the volume of data is considered small for modern standards (hundreds of megabytes) which is not problematic for current dataset sizes. In the context of modelling the time required for file transmission is negligible compared to the several hours or days required for modelling.

There are a number of optimizations that may influence our macro parallelisation method's effectiveness. The first example we use a simple model consisting of only a single block. However many circumstances may require many irregularly positioned prisms with much larger numbers of cells. In the case of Marco (Xiong, 1992), it has two solvers, direct and iterative. For surveys with a single transmitter position, iterative methods are generally faster than the direct method. Optimisation methods that involve symmetry or algorithms that factorise the Green's Tensor for all excitations (such as in the direct solver) may result in time reductions on the same level as grid computing methods. Algorithms that exploit the Toeplitz block structure form reduce or negate some gains related to our of macro parallelisation, in particular when only part of the tensor Green's function is required to be recomputed. Fang et al. (2003) states that the computational efficiency of the Hursan and Zhdanov (2002) approach is  $O(Nx \times Ny \times Nz \times Nz \times \log_2 Nx \times \log_2 Ny)$  compared to Marco's  $O(Nx^2 \times Ny^2 \times Nz^2)$ . Despite these optimisation methods, most algorithms can still be used in conjunction with the type of grid parallelisation we present to improve efficiency when modelling a large number of geo-electric parameters.

Three dimensional forward modelling of EM fields is computationally expensive. Inversion is likely two (2) orders of magnitude more intensive due to large numbers of forward computations. Clearly inversion of large datasets is not practical on a single core for complex earth structures. As the number of cells increases, the task of computing the tensor Green's function places a serious constraint on the viability of inversion. Figure 4-9 illustrates the relationship between

wall time and the number of cells used to discretise a simple rectangular prism with dimensions  $1\text{km} \times 1\text{km} \times 200\text{m}$  using the full implementation of the Marco algorithm (Xiong, 1992). An inversion of a 2D survey consisting of 8 frequencies, 4,000 transmitters, 200 receivers, with 20 iterations, and an earth model consisting of 50,000 cells is considered small. Figure 4-10 provides a representation of one forward modelling realization out of a possible 640,000 images representing the electric and magnetic field distribution (i.e., streamlines) that may be required for inversion. Using this integral equation algorithm implemented in Marco, this survey requires approximately 1120 days of computational time (56 days per iteration) to be inverted on a 1,000 node cluster. The problem clearly needs to be optimised or simplified so the inversion can be completed in a practical time frame. The concept of a moving footprint (e.g., Cox et al., 2010) in combination with sparse matrix inversion (Yuster and Zwick, 2004) addresses this problem. However the advantage of clever application of grid computing remains as a significant technique for practical applications of 3D EM inversion. Most optimization methods can benefit from grid computing enabling even more rapid MCSEM inversion.

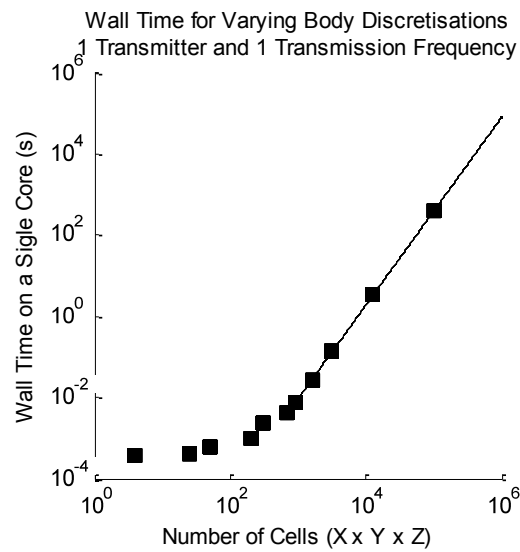
## 4.6 Grid Computing Airborne EM Inversion

An airborne survey was performed in Allanooka, in the Northern Perth Basin, Western Australia. Some 93,819 source positions were recovered from the survey. The Allanooka Airborne TEM dataset used was acquired over a large sedimentary basin with clear layering and so was highly suitable for 1D inversion. Inversion results have been compared to resistivities derived from induction wire-line logs completed in over 20 wells with surprisingly good correlation (Martin et al., 2012).

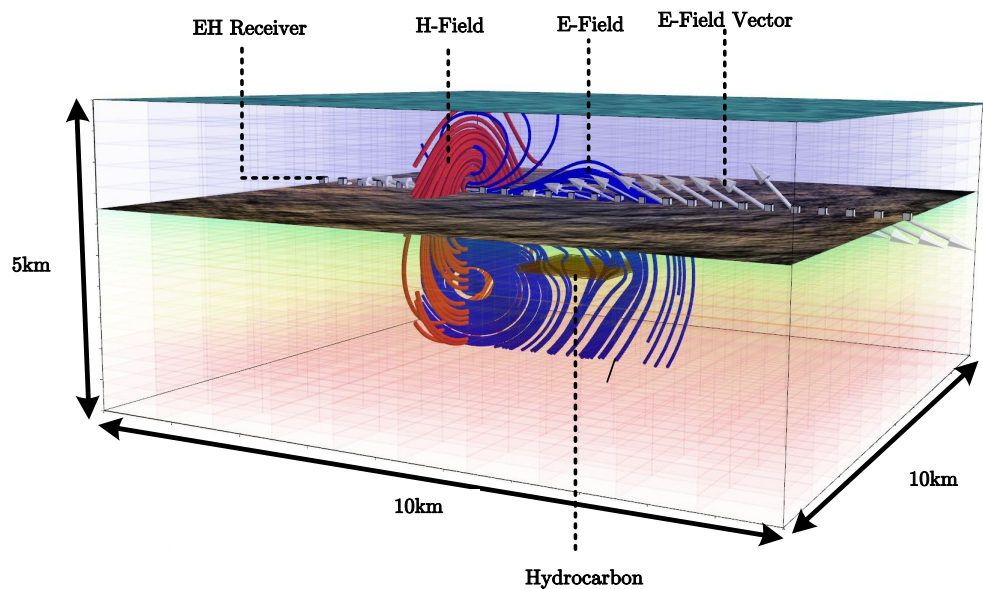
The inverse airborne EM problem can also be easily parallelised. The Airbeo AMIRA (2012) inversion algorithm has been integrated into our grid computing software. Parallelisation was performed over only source-receiver positions. The number of source positions is equal to the survey complexity.

### 4.6.1 Execution

An experiment was carried out to establish the efficiency and potential of our macro parallelisation method (see Appendix B or Figure 4-5). For the Allanooka Airborne TEM dataset, the memory and storage requirements were negligible. That is, the control file size



**Figure 4-9:** Timed forward modelling results showing the power law relationship between computation time and the number of IE cells. Each square marker is a single independent test of execution time for varying number of 3D IE cells while the line represents the power law relationship for computation time versus number of cells. The integral equation technique implemented in Marco, becomes computationally expensive as the number of cells increases according as seen by the line showing the power law relationship. For example, a 2D survey simulated over an anomalous 3D volume made up of 50,000 cells set in a 1D layered earth requires 3 days and 6 hrs to compute for a single frequency and source position. With computations of less than 1000 cells the wall time is dominated by computing the 1D response and general I/O calls. As a result the trend line was not continued through these results.



**Figure 4-10:** Schematic of electric and magnetic fields generated by a time harmonic 0.25 Hz electric bipole source displayed at  $t = 0.5$  s. The earth model consists of multiple 1D layered earth and 3D resistive prism (i.e., the hydrocarbon). The computations of the EM field required to generate the image above is computed on one thread. This Figure was created to provide perspective on scale of the electromagnetic field created by an MCSEM transmitter and the computational intensity needed to represent fields created during MCSEM surveys. This visualisation represents just one of the 65,000 images which were created during the parallelised forward modelling experiment. In excess of half a million images like this are computed during an inversion of data consisting of 8 frequencies, 4000 transmitter locations over 20 iterations. Using a macro parallelisation implementation of Marco this type of inversion of a 50,000 cell region would require over 3 years to complete. This leads us to suggest that approximate IE solutions, or heavy optimisation are required for large scale inversions.

was 2 kb, the sent data size was 17 MB and the total received data size was 34 MB. Modern network speeds enable this quantity of data to be sent and received in negligible time. For our numerical experiments we used 16 quad-core hyperthreaded Intel Core i7 computers. The core i7 has 4 cores but hyperthreading allows up to 8 threads to be executed at any given time. Hyperthreading on a 4 core CPU is 30% faster compared to a 4 core CPU, which does not have hyperthreading (Marr et al., 2002). We chose to compare a multi-threaded implementation on one CPU rather than a single-threaded version.

#### 4.6.2 Results and Discussion

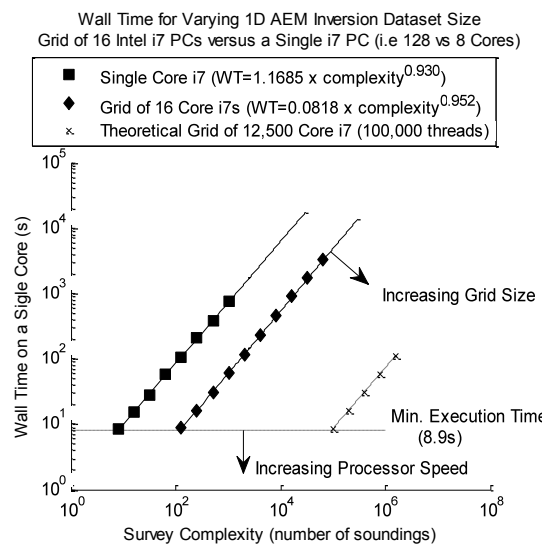
The results show an improvement of 14.2 times when computing is performed on a grid of 16 computers (Figure 4-11). 1D Inversion of airborne TEM data scales well.

Figure 4-11 highlights the simple power law relationship between survey complexity and wall time. Inversion for the complete survey (93,819 source positions) was computed in 65 hours on a single thread, 20 hours on 8 threads (e.g., one CPU) and 1.4 hours on 128 threads (e.g., a grid of 16 computers). Our results indicate inversion for the 93,819 source positions of the Allanooka airborne TEM survey could reasonable be computed in less than 20 seconds on a 12,500 grid of core i7 CPUs. The airborne TEM method is highly suitable for macro parallelisation.

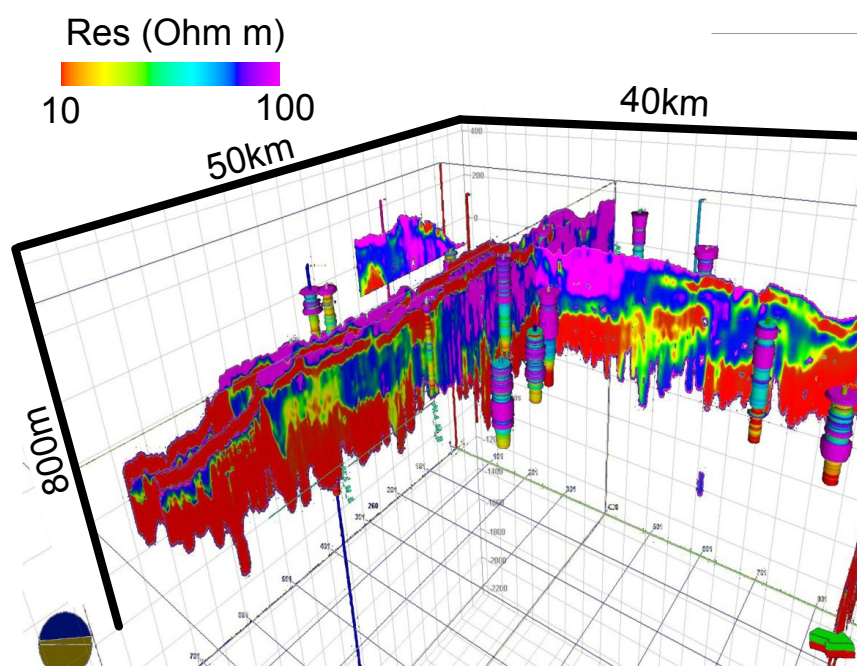
### 4.7 Conclusion

Many computational problems in geophysics are highly suitable for grid computing, and we believe this relatively new technology could be more widely used by exploration geophysicists. We provide description along with class diagrams and pseudo-code for rapid implementation of grid computing for CSEM problems. Two examples illustrate how several orders of magnitude reduction in computation time can be achieved by application of our macro parallelization. We set four requirements for our algorithm: (i) it must be simple to understand and implement, (ii) it should require no modification of source EM code, (iii) implementation should yield reduction in computation time by orders of magnitude and (iv) it should be scalable from a grid of 10 CPUs to clusters with hundreds of thousands of CPUs.

Our first example illustrated how macro parallelization can be implemented for the forward simulation of the magnetic and electric fields generated during a marine controlled source



**Figure 4-11:** Chart of wall time versus survey complexity for inversion of data generated by a large scale airborne EM dataset. We compare wall time for a single PC and several grid architectures up to 100,000 threads. The average “speed up” for a grid 16 computers compared with a single PC is 14.4 times. From the above image we could reasonably infer that for a grid of 12,500 2.8 GHz i7 computers a survey consisting of 100,000 source positions requires approximately 10 seconds which suggest that real time inversion of entire datasets is possible.



**Figure 4-12:** Example of 1D inversion images within a 3D volume. Conductivity distributions after 1D inversion were exceedingly well matched to resistivities derived from wireline logging. The complete inversion of the 93,819 source Allanooka survey was computed in 65 hours on a single thread (one i7 CPU core non-hyperthreaded), 20 hours on a CPU core (4 cores hyperthreaded) and 1.4 hours on a grid of 16, 2.8 GHz, i7 computers. There was a resulting performance increase of 14.3 times from a single CPU to a grid of 16 computers. After inversion the data is converted to SEG-Y format with real-world coordinates (i.e. GDA-94 Zone 51). Images can then be displayed in any seismic interpretation package. The above is displayed in Schlumberger's Petrel software.

electromagnetic survey over a three dimensional sub-ocean electrical conductivity distribution. Parallelisation of MCSEM integral equation code was achieved by distributing computational tasks on the basis of transmission frequency and/or source position. We use concepts of “complexity”, “wall time” and “speed up” to express results from our computation experiments and were able to verify that our macro parallelization can deliver orders of magnitude reduction in computations time with relatively little additional effort.

For the second example macro parallelization was applied to inversion of data generated by a large airborne TEM survey. The 1D airborne TEM inverse problem is demonstrated to be highly suitable for grid computing. An approximately 100-fold improvement in computation time is observed when applying our macro parallelisation algorithm on a small grid of 16 Intel i7 computers when compared with a single-threaded implementation. The computational experiments we have completed demonstrate for a basin scale application where 1D layered earth inversion suitable entire airborne TEM surveys can reasonably be inverted in a matter of seconds (i.e., in near real time).

The software we have developed can be implemented on any number of cores and on different architectures (e.g., a multi-core processor or a grid of computers). That is, our design is highly scalable and flexible.

For a broad class of EM applications in exploration geophysics, the additional computational time requirements associated with passing information to and from large grids of computers is negligible, provided suitable traffic management (i.e., data passing) strategies are followed. These types of computation problems can be referred to as “embarrassingly parallel” and are highly suitable for grid computing. We have described “macro” parallelization and underlying CSEM data structures that are able to massively reduce computations times for MCSEM forward modelling, airborne 1D TEM inversion and many other EM applications.



## 4.8 Macro Parallelisation Pseudo-Code

### Server Pseudo-Code

This section includes the most basic steps create a parallelisation server. The server has several roles,

- i Manage incoming client connections
- ii Manage outgoing client connections
- iii Monitor client progress
- iv Manage survey instance interactions such as survey splitting and joining

```

Class Server {
    ServerSocket socket; //The open server socket
    List<ClientThread> clients; //The list of clients
    //initialise server on the specified port ID

    StartServer(int port) {
        Socket = new ServerSocket(port)
        listen(); //Listen for incoming client connections
    }

    private void listen() {
        //Listen on its own thread
        Thread t = new Thread() {
            //Listen until Server is shutdown
            while(true) {
                Socket clientSocket = socket.accept();
                //Found new client, add client to client list
                clients.add(new ClientThread(clientSocket));
            }
        };
        t.start();
    }

    // Model the current survey instance, splitting by mode into N pieces
    public SurveyInstance model(SurveyInstance instance, int mode) {
        //determine total available cores by iterating over all clients
        int totalCores = 0;
        for(ClientThread t : clients) totalCores += t.availableCores;
        //Split survey instance using established available cores and user
        //Defined method
        List<SurveyInstance> instances = instance.split(mode, totalCores);
        int nInstances = instances.length(); //total partial surveys
        int instancesRemaining = nInstances; //instances to send
        int instancesCompleted = 0; //instances returned
        //Distribute instances
        for(ClientThread t : clients) {
            t.receivedInstances = new List(); //reinitialise received surveys
            //send survey's asynchronously to each client
            new Thread {
                for(int i = 0 ; i < t.availableCores && instancesRemaining > 0; i++) {
                    t.sendSurvey(instances.get(instancesRemaining));
                    instancesRemaining--;
                }
            }.start();
        }
        //wait for all partial instances to be completed
        while(instancesCompleted != nInstances) {
            Thread.sleep(10); //Check every 10ms
            //Determine number of instances completed
            instancesCompleted = 0;
        }
    }
}

```

```

        for(ClientThread t : clients)
            instancesCompleted += t.receivedInstances.length();
    }
    return SurveyInstance.join(instances);
}
}

```

## ClientThread Pseudo-Code

The 'ClientThread' is run server side. A 'ClientThread' is created for every incoming grid client connection. The code handles input and output from the client.

```

Class ClientThread {
    Socket socket;
    BufferedReader inputStream; //Reads incoming requests from client
    PrintWriter outputStream; //Sends commands to the client
    int availableCores = 0; //Maximum number of cores on Client PC
    List<SurveyInstance> receivedInstances; //List of completed partial surveys instances

    //Setup server side client connection
    public ClientThread(Socket socket) {
        this.socket = socket;
        inputStream = new BufferedReader(socket.getInputStream()); //initialise input stream
        outputStream = new PrintWriter(socket.getOutputStream()); //initialise output stream
        outputStream.print("CONNECTED") //Notify grid client of connection success
        getAvailableCores(); //Send request to grid client to obtain number of cores
        listeningForIncomingRequests(); //listen on input stream for client response
    }

    //Continually read input stream for client requests
    public void listeningForIncomingRequests() {
        Thread t = new Thread() {
            while((String input = in.readLine()) != null) {
                command(input); //Read and parse each incoming line
            }
        }
    }

    // do something with each incoming client request
    // We have structured each commands as a single String with a new line terminator
    // format : COMMAND(PROPERTY):VALUE
    // for example the file input command has the structure
    // FILE(FILENAME):N_LINES
    public void command(String input) {
        else if(input.contains("NCORES")) setNAvailableCores(input);
        else if(input.contains("FILE")) receiveFile(input);
        else if(input.contains("SURVEY")) receiveSurvey(input);
    }

    //Send request to get number of cores
    public void getAvailableCores() {
        outputStream.writeln("GETNCORES()");
    }

    //Save survey instance as a file and send to grid client
    public void sendSurvey(SurveyInstance instance) {
        sendFile(instance.saveAsFile());
    }

    //Send file to the grid client line by line via the output stream
    public void sendFile(File f) {
        /* send file line by line to client via outputStream*/
        for(String s : f.getLines())
            outputStream.writeln("FCOMPLETE(" + f.getName() + "):" + s)
    }

    //Receive the completed survey instance from the client via the input stream
    public void receiveSurvey(String line) {
        /* send file line by line to client via outputStream*/
        int lines = new Integer(line.splitAt(":")[1]); //get number of lines
        File f = new File(line);
        for(int i = 0 ; i < lines ; i++) {
            f.write(inputStream.readLine());
        }
        f.close();
    }
}

```

```

        //Re-create survey instance
        SurveyInstance i = SurveyInstance.read(f);
        receivedInstances.add(i);
    }
}

```

## Client Pseudo-Code

The 'Client' class contains the connection with the server. The client is structured similarly to the 'ClientThread', however the client controls the final execution of the survey instance.

```

Class Client {
    Socket socket;
    BufferedReader inputStream; //Input stream from Server
    PrintWriter outputStream; //Output stream to client
    GlobalAlgorithmExecutionHandler execution; //Handles multi-threading, execution and queuing

    //Connect to the server
    public Client(Int port, String address) {
        this.socket = new Socket(port, address);
        inputStream = new BufferedReader(socket.getInputStream()); //initialise input stream
        outputStream = new PrintWriter(socket.getOutputStream()); //initialise output stream
        listeningForIncomingRequests(); //continually read input stream for server requests
    }

    public void listeningForIncomingRequests() {
        //While server is active continually read input stream for new commands
        Thread t = new Thread() {
            while((String input = in.readLine()) != null) {
                command(input);
            }
        }
    }

    public void command(String input) {
        else if(input.contains("GETNCORES")) sendAvailableCores();
        else if(input.contains("FILE")) receiveFile(input);
    }

    // send the number of available cores of this client to the server
    public void sendAvailableCores() {
        outputStream.writeln("NCORES(" + System.getNCores() + ")")
    }

    // read and convert file to a partial survey instance.
    public void receiveFile(input) {
        SurveyInstance i = SurveyInstance.load(getFile(input));
        //Add survey instance to computation list
        runSurvey(i);
    }

    // execute the received survey instance
    public void runSurvey(SurveyInstance i) {
        // create a new algorithm execution instance
        AlgorithmExecution e = new AlgorithmExecution(i);
        // add execution instance to execution queue
        execution.add(e);
        //wait until execution is finished
        while(e.isExecuting()) Thread.sleep(10);
        //send completed survey instance, now with updated data and/or earth models
        sendFile(SurveyInstance.save(e.surveyInstances.get(0)));
    }
}

```



# Electromagnetic Streamlines

Using the software developed in Chapter 2 and 3 I integrate an interactive streamline generator and apply it to a number of problems. This streamline generator is used to investigate the electromagnetic field interactions in a complex geo-electrical earth. I present the first published case of visualising the airwave as a circulating vortex using streamlines. This chapter is composed of a journal article and two conference papers all written by myself and Dr. Brett Harris from Curtin University, department of Exploration Geophysics. This chapter is an amalgamation of articles. The first section is currently published in the Computers and Geoscience Journal. Following on from the first section the second section presents work presented at the 2013 EAGE London conference, it attempts to answers the question “What is the airwave?” with the assistance of streamline visualisation. The third section applies our real time interactive streamline electromagnetic visualisation method to investigate the influence of bathymetry on CSEM surveys. We use a 2.5D finite difference algorithm to model the response for several different geoelectrical scenarios and analyse the response with the help of streamlines. This paper follows on from the work of Li and Constable (2007). This section has been taken from a paper written by myself and Dr. Brett Harris from Curtin University, department of Exploration Geophysics. Portions of this paper are from the conference paper presented at the 2012 ASEG Brisbane, Australia conference.

## Contents

<b>5.1</b>	<b>Interactive MCSEM Streamlines</b>	<b>171</b>
5.1.1	Summary	171
5.1.2	Introduction	171
5.1.3	Streamline Generation	172
5.1.4	Software Development	173
5.1.5	Streamline Interpretation	176
<b>5.2</b>	<b>The Scale of the Electromagnetic Fields Generated by an MCSEM Survey</b>	<b>187</b>
5.2.1	Three-Dimensional Streamlines	189
5.2.2	Conclusion	194
<b>5.3</b>	<b>Poynting vector streamlines and the Airwave</b>	<b>195</b>
5.3.1	Summary	195
5.3.2	Introduction	195
5.3.3	Theory and Method	195
5.3.4	Results	196
5.3.5	Conclusions	199
5.3.6	Acknowledgements	199
<b>5.4</b>	<b>Streamlines and Bathymetry</b>	<b>200</b>
5.4.1	Summary	200
5.4.2	Introduction	200
5.4.3	Method and Results	201
5.4.4	Conclusions	206



## 5.1 Interactive Marine Controlled Source Electromagnetic Streamlines

### 5.1.1 Summary

Streamlines represent particle motion within a vector field as a single line structure and have been used in many areas of geophysics. We extend the concept of streamlines to interactive three dimensional representations of the coupled vector fields generated during marine controlled source electromagnetic surveys. These vector fields have measurable amplitudes throughout many hundreds of cubic kilometres. Electromagnetic streamline representation makes electromagnetic interactions within complex geo-electrical setting comprehensible. We develop an interface to rapidly compute and interactively visualise the electric and magnetic fields as streamlines for 3D marine controlled source electromagnetic surveys. Several examples highlighting how interactive use has value in marine controlled source electromagnetic survey design, interpretation and teaching are provided. The first videos of electric, magnetic and Poynting vector field streamlines are provided along with the first published example of the airwave represented as streamlines. We demonstrate that the electric field airwave is a circulating vortex moving down and out from the air-water interface towards the ocean floor. The use of interactive streamlines is not limited to marine controlled source electromagnetic methods. Streamlines provides a high level visualization tool for interpreting the electric and magnetic field behaviour generated by a wide range of electromagnetic survey configurations for complex 3D geo-electrical settings.

### 5.1.2 Introduction

The Marine Controlled Source Electromagnetic Method (MCSEM) is one tool used for offshore hydrocarbon exploration and development (Hesthammer et al., 2010). MCSEM utilizes an electrical bipole source to generate time varying coupled electric and magnetic fields. For a typical survey, ocean bottom receivers record the electric and magnetic fields generated by the EM transmitter. These electromagnetic fields may be represented by a number of methods. Typical representations include; profiles (Key, 2009a), two-dimensional grids (Zhdanov et al., 2010) and electromagnetic vectors (Pethick, 2008). Less common visualization techniques include, polarization ellipses (Key and Lockwood, 2010) and isosurfaces (Pethick, 2008). Streamlines represent the path of a particle through a vector field at a particular time Hansen and Johnson (2004). Streamlines are commonly applied in physical modeling of fluid flow (Zehner et al., 2010) and mantle flow (Billen et al., 2008). They have also been used in electromagnetic studies to express the electric field point charge (Bakshi and Bakshi, 2009), 3D coronal magnetic fields (Regnier et al., 2002) and electrical current flow (Sachse and Taccardi, 2004). We believe the application of streamlines in applied geophysics can be particularly valuable for understanding complex sub-sea electromagnetic field interactions such as the airwave. The purpose of this paper is not to present a new streamline visualisation method, but rather the application of streamline to the interpretation of MCSEM electromagnetic field behaviour. Full expression of the coupled electric and magnetic vector fields as interactive streamlines can facilitate new ideas about how to configure and deploy resources (i.e. transmitting and receiving antenna) for deep ocean MCSEM surveys.

### 5.1.3 Streamline Generation

2D streamline generation begins with simulating the electromagnetic field generated from a MCSEM survey throughout a 2D region. This includes populating a 2D grid with three component electromagnetic receivers then forward computing the EM fields at each receiver position. Secondly seed positions are populated through the 2D section. Lastly at each of the streamline seed positions second order vector interpolation is used to step the streamline through the electromagnetic vector fields. The streamline color represents the total vector amplitude and is computed at each interpolation step by bi-cubic interpolation of the vector field.

The EM fields generated during MCSEM survey propagate at exceedingly low frequencies (e.g. much less than 10Hz) and electromagnetic receivers are spread throughout large volumes (i.e. hundreds of cubic kilometres). The fields in the immediate vicinity of the transmitter vary rapidly over small distances. For practical applications, interpretation of this near field (i.e. within 10m of the transmitter) is not required. In this case we use a constant step length, since the path of the streamline in space is dictated by the direction of the field and not the amplitude of the vector field.

The first step of our method is to compute a 2D grid of the electromagnetic fields generated by the horizontal electric bipole transmitting antenna just above the sea floor. A structured receiver grid was used to speed up subsequent interpolation methods. Our example MCSEM surveys are completed in the frequency domain. These streamlines represent the EM fields at an instant in time so they can be utilized to visualize the EM field behaviour resulting from any transmitter waveform (e.g. a 50% or 100% duty cycle square waveform).

Electromagnetic fields are composed of coupled time varying electric and magnetic fields. Amplitude and phase is computed for each vector components of the electric and magnetic fields (i.e.  $E_x$ ,  $E_y$ ,  $E_z$ ,  $H_x$ ,  $H_y$  and  $H_z$ ) and these are used to describe the complete time harmonic oscillation via Equation 5.1. That is, Equation 5.1 describes the full behavior of each of the electric and magnetic vector field components for each location on the grid. The two resulting vector field grids are the electric and magnetic fields.

$$A(t) = A \sin(2\pi ft + \phi) \quad (5.1)$$

where,

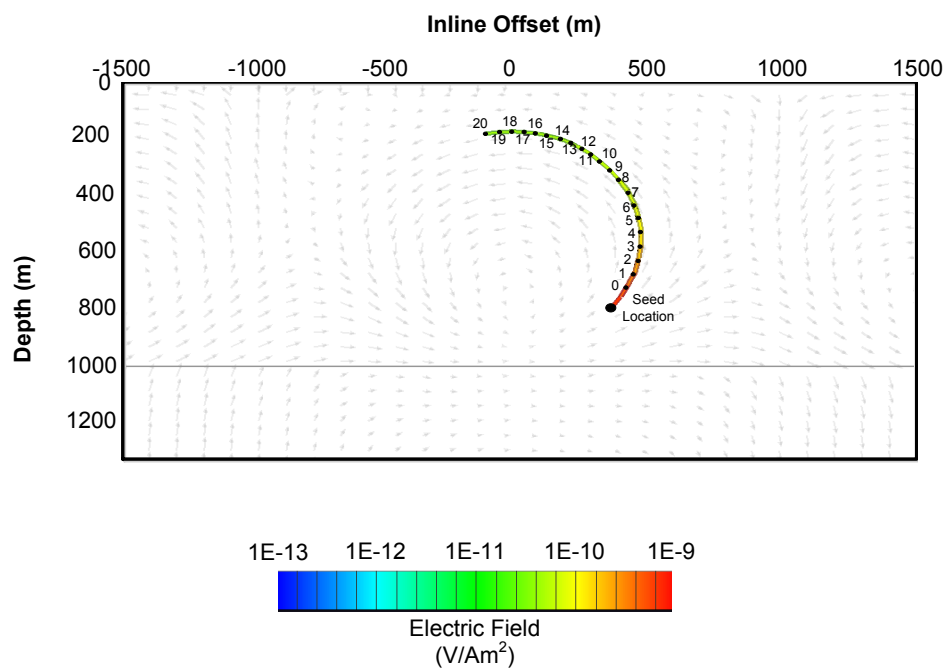
- $A(t)$ - Amplitude at time  $t$
- $A$ - Total Amplitude ( $A = \sqrt{Re^2 + Im^2}$ )
- $f$ - Frequency (Hz)
- $\phi$ - Phase ( $\phi = \text{atan2}[Im/Re]$ )

The second step requires seed positions to be populated throughout the data area. The seed positions can be placed in either (i) the grid, (ii) the ocean bottom or (iii) placed interactively. The streamline density is important. If the streamline density is low the EM field behaviour is not fully represented. Equally, a very high density of streamlines can obscure information and complicate interpretation. The most suitable streamline density is situation dependent and should be user controlled.

The third step requires the propagation and visualization of the streamlines from the seed positions. Electromagnetic fields are continuous in nature. The computed electromagnetic



fields however, are discrete. Streamlines require the field to be computed at any position within the grid. Euler integration (Tricoche et al., 2006) and the Runge-Kutta method (Hansen and Johnson, 2004) can be used to approximate the streamline path in a discretely sampled dataset in time and space. Exceedingly low frequencies are used for the MCSEM method (e.g. 0.01 to 10Hz). Under these circumstances it is highly reasonable to interpolate both the orientation and amplitude of the vector field between grid points. A small step size was chosen to avoid the possible errors associated with second order vector interpolation (i.e. one-tenth of the data spacing). Termination of the streamline occurs when either the maximum number of steps is reached or the streamline exits the data area. Figure 5-1 provides an illustration of how MCSEM streamlines are constructed. Here the streamlines were created from 200, propagation steps (10m per step) through an inline electric vector field at 0.1768s. The transmitting antenna was an electric bipole operating with a time harmonic frequency of 1.5Hz.

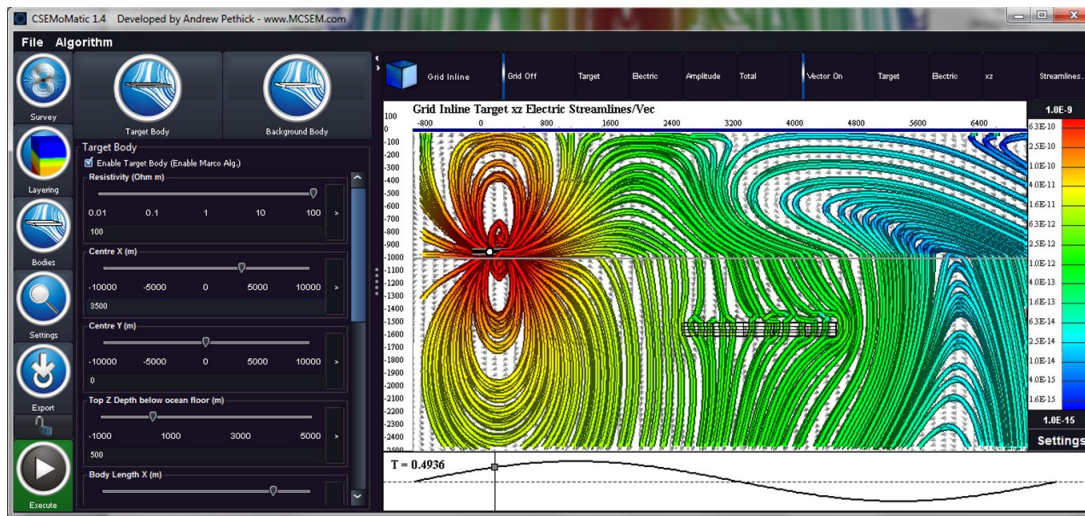


**Figure 5-1:** Propagation of a streamline through a vector field from a single seed location. This Figure shows the first 200 steps of a single inline electric field streamline through the associated vector field (arrows show direction of the field) at a time 0.1768s using a transmission frequency of 1.5Hz. The numbers show every tenth integration step. The streamlines were generated using a second order vector interpolation. The electromagnetic fields generated by MCSEM are at such low frequencies a constant step length could be used. In this Figure a step length of 10m was used.

#### 5.1.4 Software Development

We developed an interactive MCSEM software package including streamline modules written in the Java programming language. The software has been written to facilitate research and education in deep ocean electromagnetic methods. Multi-touch devices have allowed experimentation with computer human interaction to provide an interactive and user-friendly experience. A number of interface features were implemented. These included, touch and drag axis, color scales, time selector, large menu combo boxes and single touch streamline generation (see Figure 5-2). The development of the software has been overviewed by Pethick

and Harris (2012).



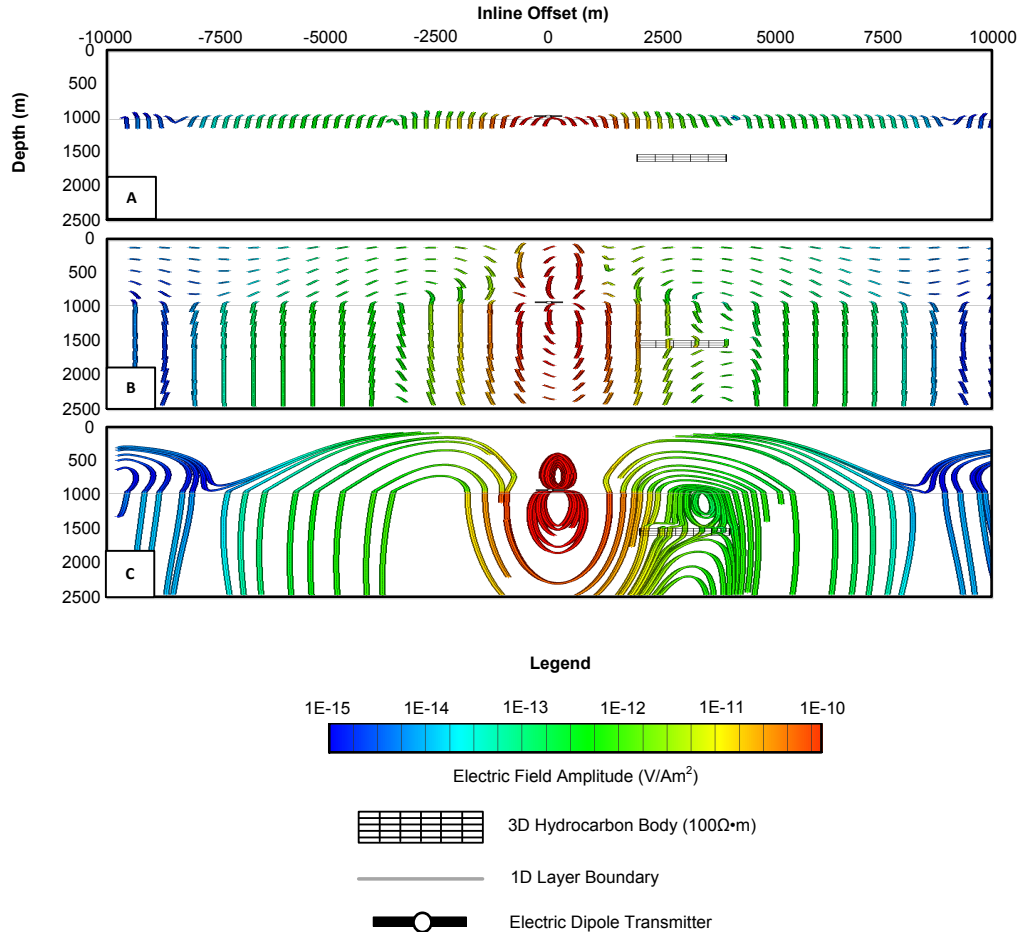
**Figure 5-2:** Graphic showing the software GUI developed for interactive real time streamline generation. This interface was designed for multi-touch devices running on Linux Ubuntu, Windows or MacOSX operating systems. Interactive touch and drag color scale plus axis and time selectors have been included. Other features that facilitate interactivity include single touch streamline generation and large option menu buttons.

Several MCSEM forward modeling algorithms have been integrated into the software and can be used with our streamline generating algorithm. These include Dipole1D, which is a 1D MCSEM forward modeling algorithm developed by Key (2009a) and Marco, which is a 3D integral equation forward modeler (Xiong, 1992). These were both chosen because they are open source, cross-platform and can quickly and accurately model electromagnetic fields that could be generated by a MCSEM survey.

Our approach to streamline generation is intended for representing synthetic data (i.e. forward modeled data), however if enough data is collected it should in principle be possible to represent field data as streamlines. For example, streamlines could be computed from records made from three component magnetic and electric field receivers distributed within the Ocean volume. Field data is typically sparse, but a structured grid of the recorded field can be obtained through Delaunay triangulation (Floater and Iske, 1996) to improve performance. Clearly, this would be limited by the spatial domain and sampling of receivers (i.e. the actual grid of receivers).

We have integrated the streamline algorithm our software package. The package includes creation and display options. Streamline options include (i) seed mode, (ii) maximum integration steps, (iii) step length, (vi) interpolation in both forward and reverse directions, (v) selection of the number of seed positions in the x and y directions and (vi) associating the color of the streamline with phase, amplitude at time or total amplitude. Seed mode defines the positions and consequently density of the streamlines. The seed position options include ocean bottom, grid and custom options (see Figure 5-3). An interactive streamline placement feature has been included in the software. Using the standard the standard Swing mouse button and motion listeners users can add additional single or multiple seed positions via single-click or click-and-drag mouse interactions respectively. This interactive feature allows

users to increase the density of streamlines around features of interest in real time and with minimal effort.

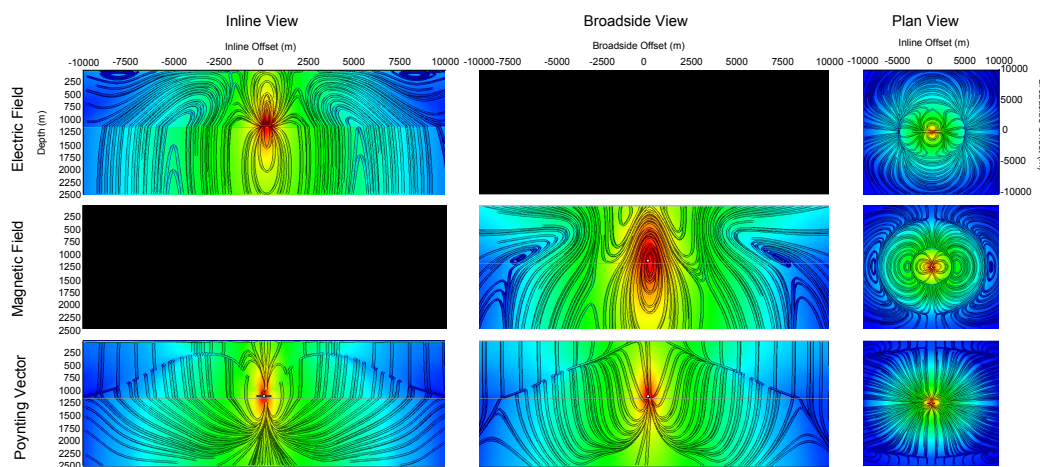


**Figure 5-3:** Example of different streamline seed modes observed at 0.2s for a transmitter frequency of 1.5Hz. The images are for the synthetic inline xz plane for: (A) an ocean bottom seed mode, (B) a grid seed mode, and (C) a custom seed placement. The custom seed placement allows both streamline position and density to be selected.

To produce real-time streamline generation a number of traditional speed-up techniques have been applied. Parallelising the streamline generation dramatically increases the performance of the algorithm. Each thread consisted of the propagation of the streamline from a single streamline seed location. The final fully defined streamline (i.e. positions and colours) are then added to the master streamline list. Double-buffering is a traditional graphical technique which utilises separate offscreen pre-rendering to improve performance (Roberts and Picard, 1998). The scene is pre-rendered on a Java 'Graphics' object (i.e. the buffer). Double buffering reduces the communication between the video card memory buffer and the primary memory buffer because each frame is rendered offscreen in the primary memory and only replaces the video memory buffer once the scene is fully constructed.

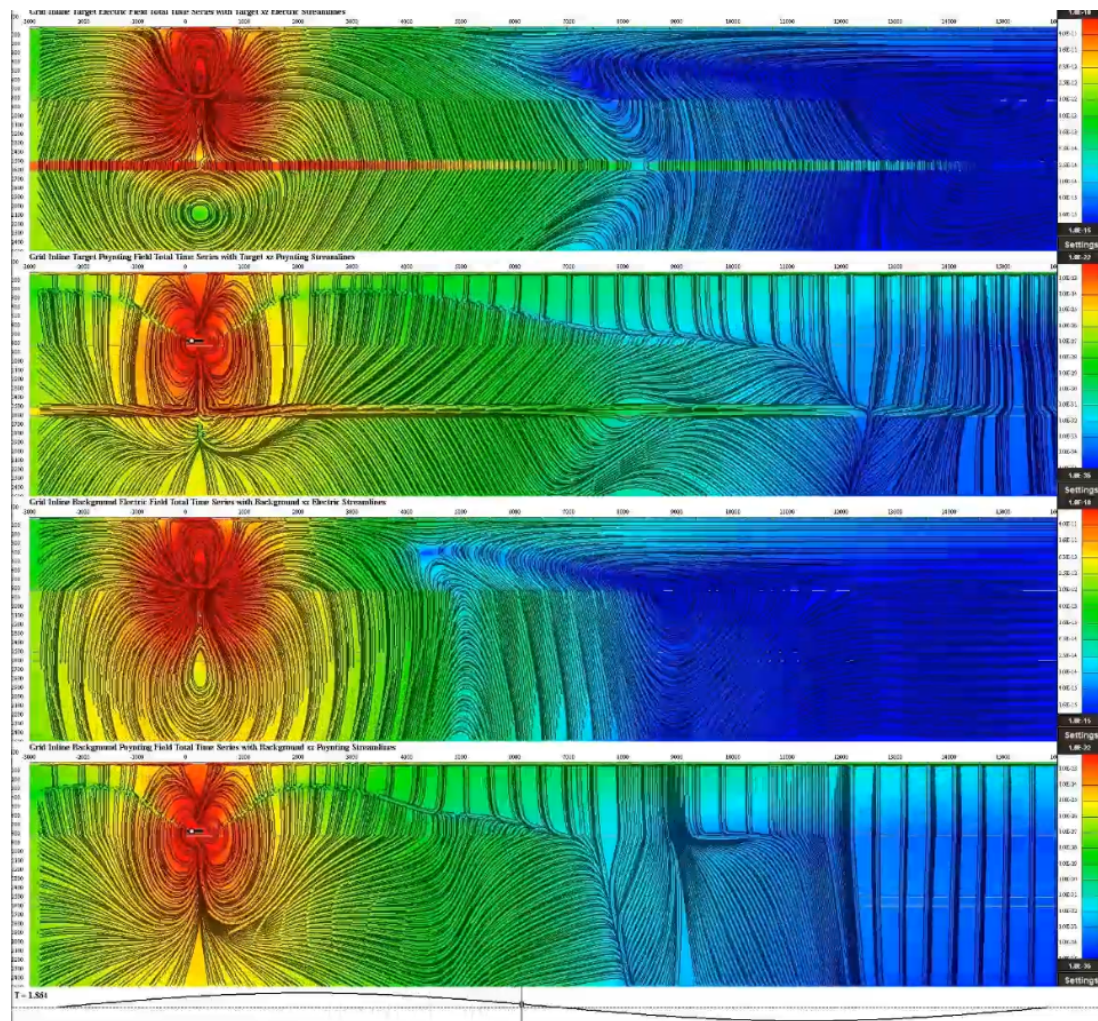
### 5.1.5 Streamline Interpretation

In electro-statics, the electric field exists in the region of space around a charged object (i.e. the source). Put simply, the electric field is the force on a free electron when placed in the region of space around a charged object. In the electromagnetics the magnetic field is inexorably coupled to the electric field and behaves in accordance to Maxwell's equations Maxwell (1881). The Poynting vector is considered to be the flow of energy flux (Weidelt, 2007) which in free space is oriented by the vector computed by the cross product of the electric and magnetic field vectors. The electric, magnetic and Poynting vector fields can all be represented by streamlines, but the interpretation must be put in perspective of its physical properties. Streamlines represents flow and flow paths, so for ease of interpretation the electric field can be considered to visualise the direction of the flow of charged particles, the magnetic field the direction of the force on moving charged particles and the Poynting vector the flow of energy flux. Figure 5-4 shows the electric, magnetic and Poynting vector fields generated during a MCSEM survey. The inline, broadside and ocean floor planes have been generated for streamline visualisation. The inline magnetic and broadside electric fields are blanked out because the fields are perpendicular to the plane. The three videos (Figures 5-5, 5-6, 5-7) show the transient response of the electric, magnetic and Poynting vector field streamlines over a complete waveform cycle (i.e. 0.25Hz or 4s) in the inline (XZ), broadside (YZ) and ocean floor (XY) planes respectively. Each video compares the electromagnetic field responses generated for two typical marine 1D layered geo-electrical earth models. The first model consists of a 1000m thick  $0.3\Omega \cdot m$  seawater layer overlying a  $1.5\Omega \cdot m$  half-space containing a  $100\Omega \cdot m$  hydrocarbon layer buried 500m below the sea-floor.



**Figure 5-4:** Streamline visualisation of electric, magnetic and Poynting vector fields in the inline, broadside and ocean bottom planes. The electric field streamlines can be thought to represent the flow of electrons, the magnetic field streamlines the force exerted on moving free electrons and the Poynting vector streamlines the flow of energy.

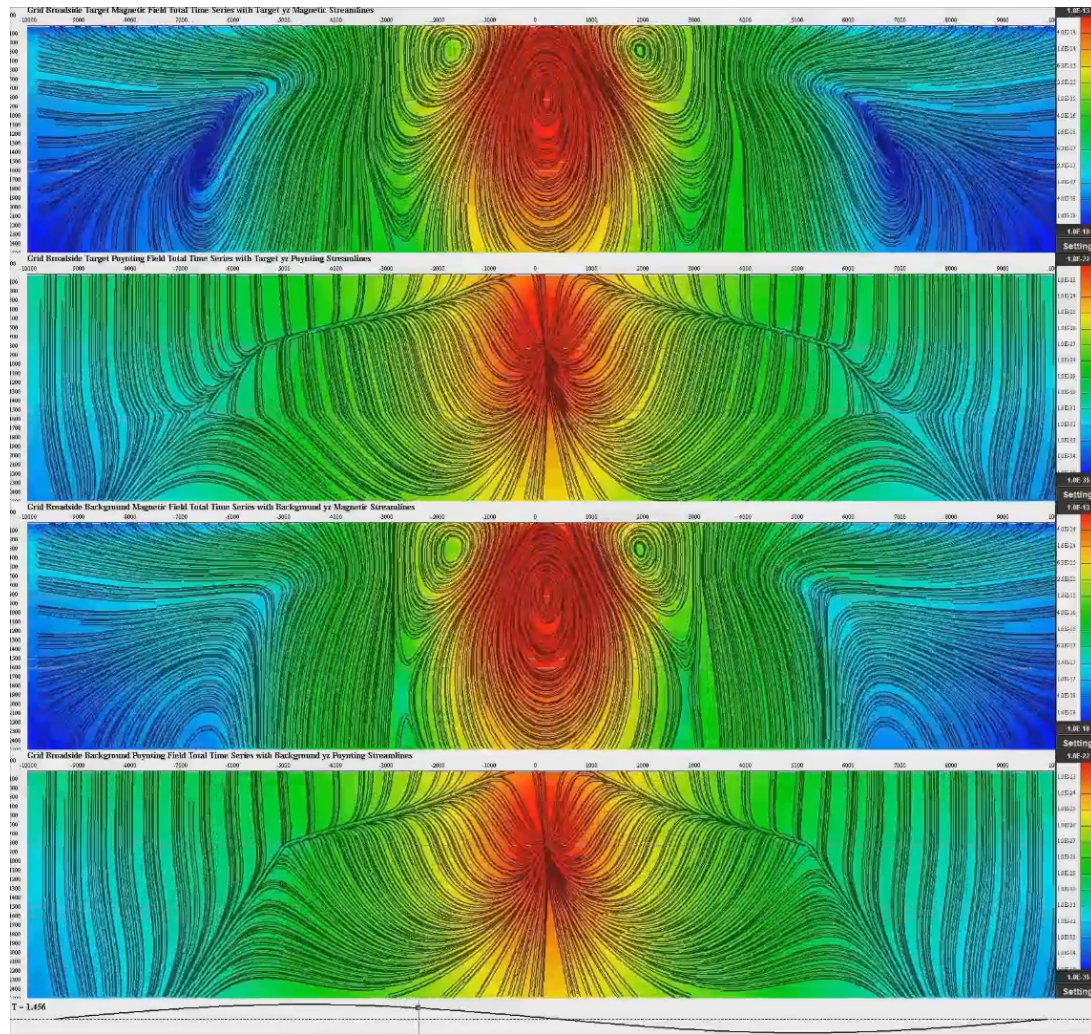




**Figure 5-5:** The full time series of the inline (XZ) electric and Poynting vector streamlines for a time harmonic transmission frequency of 0.25Hz for two earth models. From top to bottom i. E-field streamlines with HC, ii. S-field streamlines with HC, iii. E-field streamlines without HC and iv. S-field streamlines without HC.

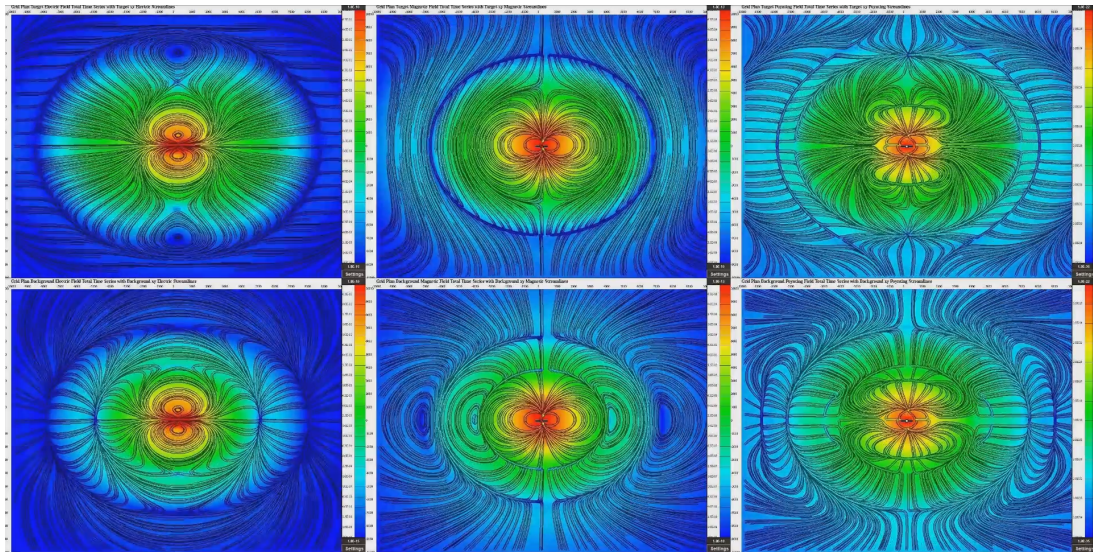
See [Videos/Inline.avi](#) for video source





**Figure 5-6:** The full time series of the broadside (XZ) electric and Poynting vector streamlines for a time harmonic transmission frequency of 0.25Hz for two earth models. From top to bottom i. E-field streamlines with HC, ii. S-field streamlines with HC, iii. E-field streamlines without HC and iv. S-field streamlines without HC.

See [Videos/Broadside.avi](#) for video source



**Figure 5-7:** The full time series of the plan (XZ) electric and Poynting vector streamlines for a time harmonic transmission frequency of 0.25Hz for two earth models. From top to bottom i. E-field streamlines with HC, ii. S-field streamlines with HC, iii. E-field streamlines without HC and iv. S-field streamlines without HC.

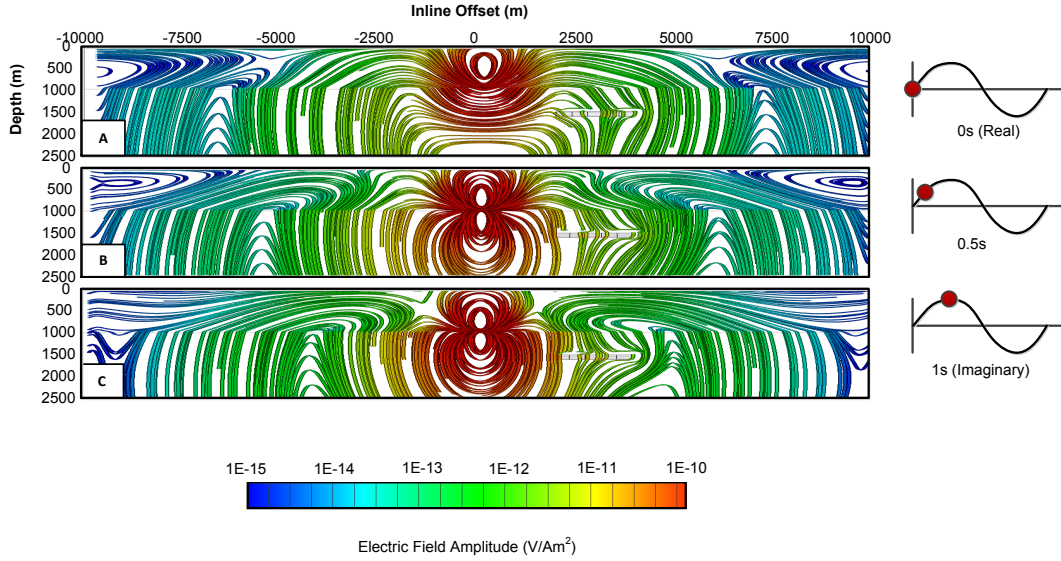
See [Videos/Plan.avi](#) for video source



Streamlines can be used to interrogate EM field behavior for any MCSEM configuration, given any geo-electrical setting. In the following examples we model data in the inline and broadside directions. The inline fields exist in a vertical plane through, or inline with the bipole transmitter, while the broadside field is measured perpendicular to the bipole transmitter orientation. Examples of electric and magnetic field streamlines are provided. The field components of the CSEM data are shown rather than the Poynting vector because these fields represent the real life measured quantities of current flow and force applied to electrical charges. We demonstrate the computation of streamlines through a synthetic 3D hydrocarbon reservoir (i.e. 3D resistive slab) embedded in a layered medium (i.e. air, ocean, and host rock). The ocean layer is 1000m thick with a resistivity of  $0.3 \Omega \cdot m$  and the lower half-space (i.e. host sediments) is given a resistivity of  $2.5 \Omega \cdot m$ . The reservoir is assigned a resistivity of  $100 \Omega \cdot m$  and has dimensions of  $2000m \times 2000m \times 100m$ . The reservoirs centre has an offset of 3 km from the transmitter and is 500m below the ocean floor (see Figure 5-8). Figure 5-8 shows consecutive time snap shots of the electrical field streamlines for three inline sections taking at 0, 0.5, and 1 seconds for a transmission frequency of 0.25Hz. The x and z components of the electric field within the inline section are expressed as equations 5.2 and 5.3 below.

$$E_x(t) = E_x \sin[(2\pi 0.75t + \phi)] \quad (5.2)$$

$$E_z(t) = E_z \sin[(2\pi 0.75t + \phi)] \quad (5.3)$$

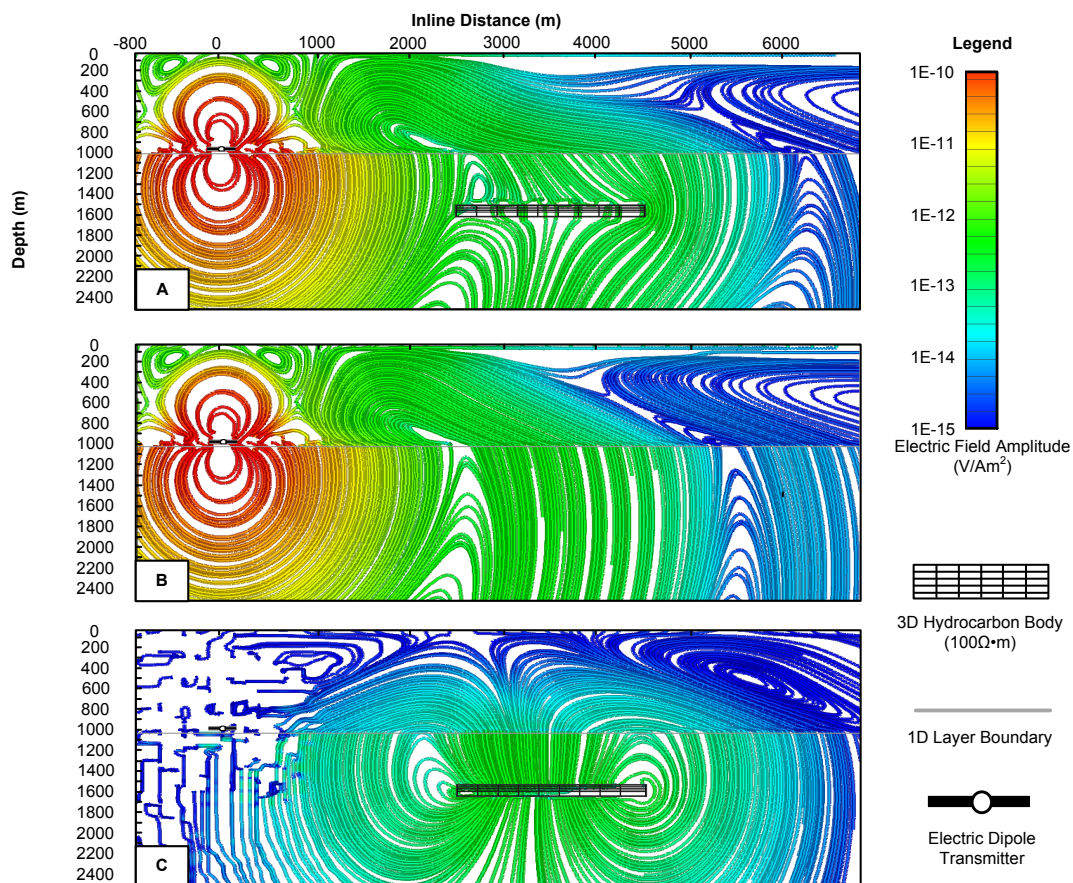


**Figure 5-8:** MCSEM streamlines over a hydrocarbon target at three instances in time. The three time shots of the inline electric field streamlines were captured for a 0.25Hz (4s period) transmitted waveform. The resulting electromagnetic field streamlines vary significantly when viewed at different times. The image shown at for zero seconds visualises the airwave reaching the sea floor at -9500m and 10000m offset. Phase fronts are also visible towards the transmitter out from -4000m and 10000m at 0.5s.



The largest changes in the streamline behaviour occur at 90 degree phase offsets from the primary field. Each time snapshot provides a new visual representation of the electric field distribution. Multiple times are required to fully appreciate the EM field behavior because phase fronts and airwaves can obscure information at each position for different times (See Figure 5-8). A phase front of an electromagnetic wave is the surface formed by all points having the same oscillatory phase (Zhdanov, 2009). These phase fronts appear as 'V' or 'U' shaped arches with the peak of the arch representing the point of zero oscillatory phase. Um and Alumbaugh (2007) state that background electromagnetic fields and the airwave are “nearly horizontal at the air-seawater boundary”. Figure 5-8 shows that the electric field become increasingly horizontal as it approaches the high resistivity contrast air-seawater boundary, backing up the findings of Um and Alumbaugh (2007).

Figure 5-9 provides a further illustration of the behavior of electric field streamlines proximal to a synthetic MCSEM target reservoir. The images show how the streamlines tend to “avoid” more electrically resistive areas; either bending around resistive bodies or “jumping” across the resistive area along the shortest possible path. In particular note how the streamlines travel perpendicular across the high resistivity reservoir (i.e. the resistive slab). Conversely the electric field streamlines tend to concentrated in the more conductive geo-electric features.



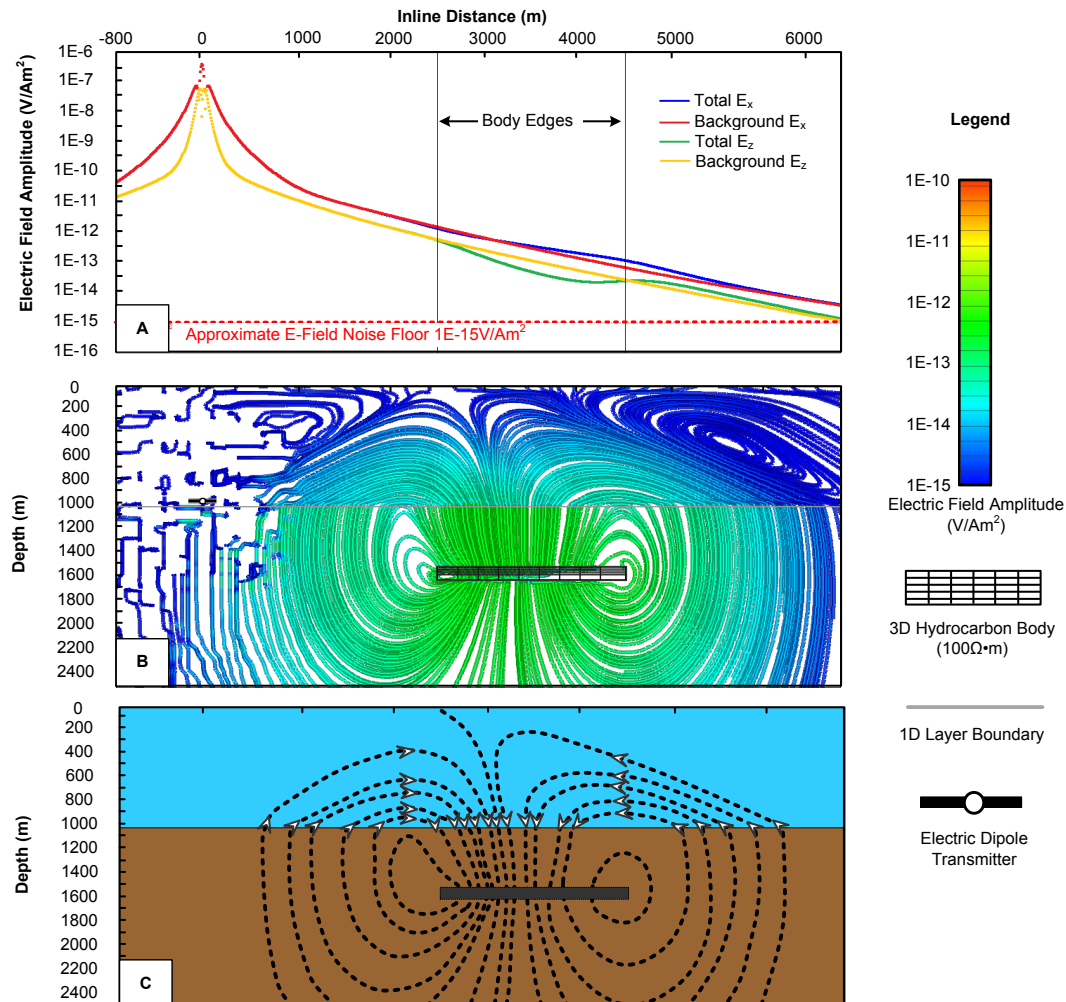
**Figure 5-9:** Streamline visualization of total (a), layering (b) and scattering (c) components of the electric field generated during a synthetic MCSEM survey. Inline (xz) electric field streamlines at 0.3s at a transmission frequency of 0.75Hz over of a layered earth (1000m water column of 0.30Ωm and 2.5 Ωm halfspace) with a 3D (2km x 2km x 100m) resistive body (i.e. 100 Ωm) with and offset of 3.5km from the transmitter at a depth of 500m below the ocean floor. The electric fields tend avoid resistive features; bending around the bodies resulting in the flux lines to emerge at further offsets on the ocean floor and only propagating through the body vertically. For this example the flux lines at the ocean bottom are clearly altered by the presence of the hydrocarbon body.

The rate of change of EM fields close to the transmitter becomes extreme and computation near to the transmitter tends to break down due to numerical instabilities. As noted earlier, locations very close to the transmitter are of little consequence in the practical application of MCSEM and in most circumstances can be neglected.

Streamlines provide an intuitive sense of the global circulation of EM fields and this can assist interpretation of typical MCSEM profiles. The total electric or magnetic fields can split into “layering” fields (i.e. the EM fields from the layering only) and “scattering” fields to assist in survey design or interpretation. Equation 5.4 shows the relationship between the layering and scattering components of the total electric field. Splitting total field into a layering and scattering component enables visual expression of the influence of the 3D reservoir body within the total EM response.

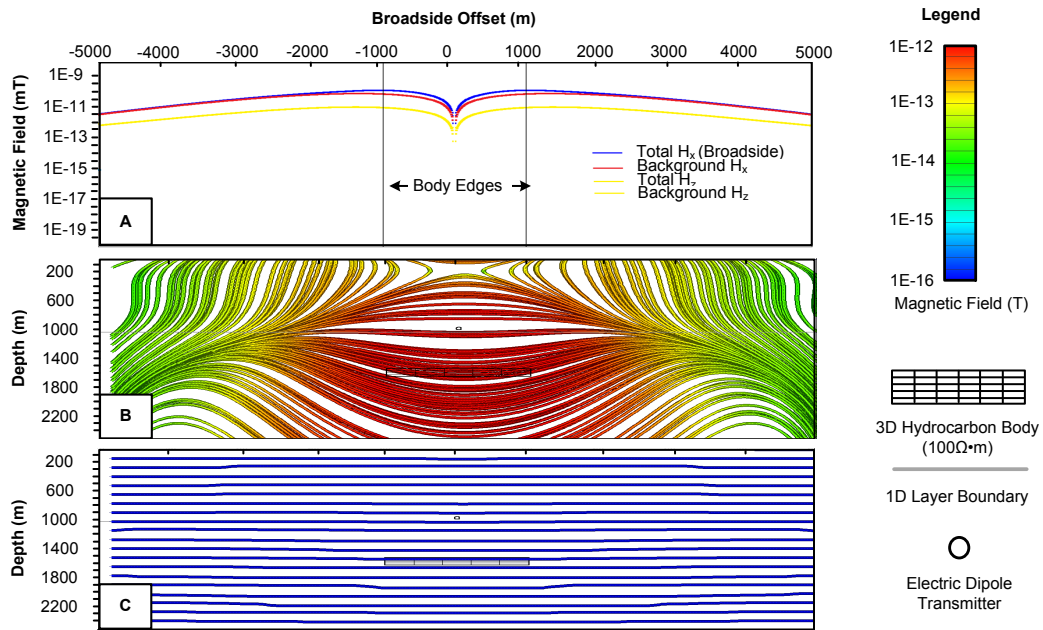
$$E_{total} = E_{layering} + E_{scattering} \quad (5.4)$$

To illustrate the scattering responses, models have been created with and without (i.e. layering only) the 3D hydrocarbon reservoir. Figure 5-10 includes the inline scattered electric field streamlines and a corresponding electromagnetic profile recorded on the ocean floor. The electric field streamlines can help explain the character of electric field profiles measured along the receiver line at the ocean floor. For example the increase in the horizontal electric ( $E_x$ ) and decrease in vertical electric ( $E_z$ ) field amplitudes seen the profiles can be attributed to the directionality of the streamline expression of the scattering component of E field.



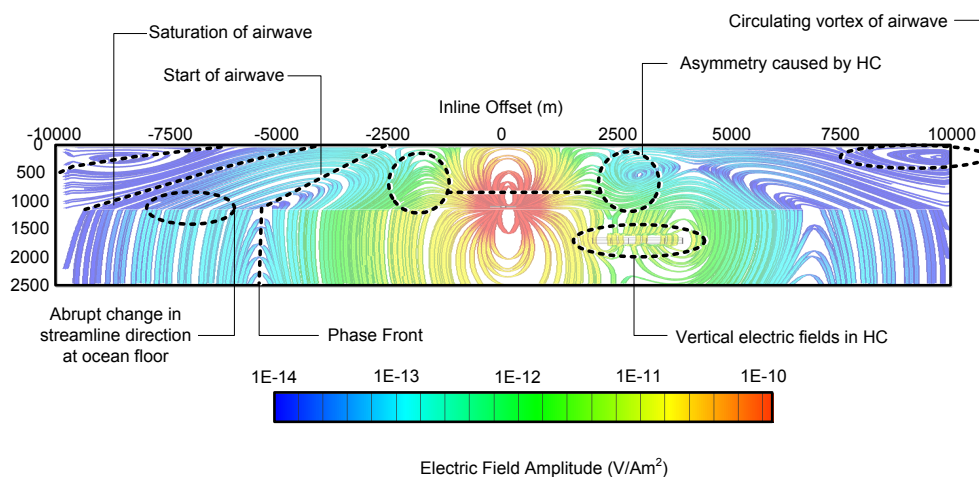
**Figure 5-10:** Interpretation of a streamline representation of the expected anomalous electrical fields associated with a hydrocarbon target at the seafloor. The set of images compares inline 1D electric field profiles with inline scattered electric field streamlines at 0.3s. The survey and geoelectric structure is the same as Figure 5-8. (A) illustrates the amplitude profile of the total and background layered response for the inline (x) and (z) components of the electric field. (B) shows the inline scattered electric field streamlines colored with total scattered amplitude. (C) shows an interpretation of the electric field. The streamline representation can be used to rapidly interpret profile information or as an aid to survey planning. The anomalous features in the profile such as the increase in E<sub>x</sub> and decrease in E<sub>z</sub> can easily be explained by the streamline orientation. Note we can observe numerical error (i.e. in the computation of E fields) as noisy streamlines at far offsets. Here the anomalous E-field amplitudes are extremely small and would not be measurable in a MCSEM survey.

In MCSEM it is commonly asserted that vertical magnetic field is insensitive to flat thin resistive structures (e.g. flat lying hydrocarbon reservoir). We can use streamlines to demonstrate why. Figure 5-11 visualises the total broadside magnetic field response, the scattered broadside magnetic hydrocarbon response and the associated magnetic field profile recorded on the ocean floor over the center of a target body (thin flat electrically resistive structure). The scattered magnetic field streamlines are horizontal and have exceedingly small amplitudes. Weidelt (2007) explains this effect as the “resistive-layer” TM-mode. The dominant horizontal energy flow within the resistive body is carried by  $H_y$  and the strong  $E_z$  component (Weidelt, 2007). The Figure illustrates and supports the findings of Weidelt (2007) and shows that the anomalous scattered magnetic field resulting from a 3D hydrocarbon body is dominantly horizontal.



**Figure 5-11:** Comparison of broadside 1D magnetic field profiles and broadside scattered magnetic field streamlines at 0.3s given a 0.75 Hz time harmonic transmitter waveform. The survey and geo-electric structure is the same as Figure 5-10. (a) shows broadside magnetic field amplitude profiles of the total and background layered response (i.e. 1D air, ocean, host layering) for the broadside (x) and vertical components (z). Figure (b) shows the total broadside electric field streamlines. Figure (c) shows broadside scattered magnetic field streamlines colored with total scattered amplitude (i.e. the scattering H field is total H field minus layering only H field). The scattering field has negligible influence on the total field amplitude and direction. The magnetic field streamlines reveal why the vertical magnetic field is insensitive to thin flat horizontal resistive geo-electric targets below the ocean.

Visualising the MCSEM fields using streamlines makes it possible to interrogate field interactions occurring in different spatial zones of a complex geo-electrical model. Figure 5-12 is an annotated version of Figure 5-8. We can identify a rotating vortex as being associated with the “airwave” phenomena. The airwave has been described by Um and Alumbaugh (2007) as “energy diffusing up and down through the seawater column and propagating along the air-seawater interface”. This airwave feature is due to the EM interactions at the interface between the highly resistive air layer, the ocean and the conductive earth. These interactions result in a sharp changes in the oscillatory phase direction caused by the upwardly and downwardly diffusing electric fields. This rapid change in oscillatory phase causes the electric field to rotate. The onset of this rotation can be identified as the location where the airwave becomes evident in the data, while the axis of rotation can be associated with location where the “airwave effect” tends to “saturates” the electric field data. The center of the airwave vortex is the geometric location where the upwardly and downwardly diffusing electromagnetic field’s negate each other and has no electric field amplitude. Other features such as phase fronts, asymmetry due to the influence of the hydrocarbon, sharp changes in direction at layer boundaries due to resistivity contrast and near hydrocarbon EM field behaviour are also identified in Figure 5-12.

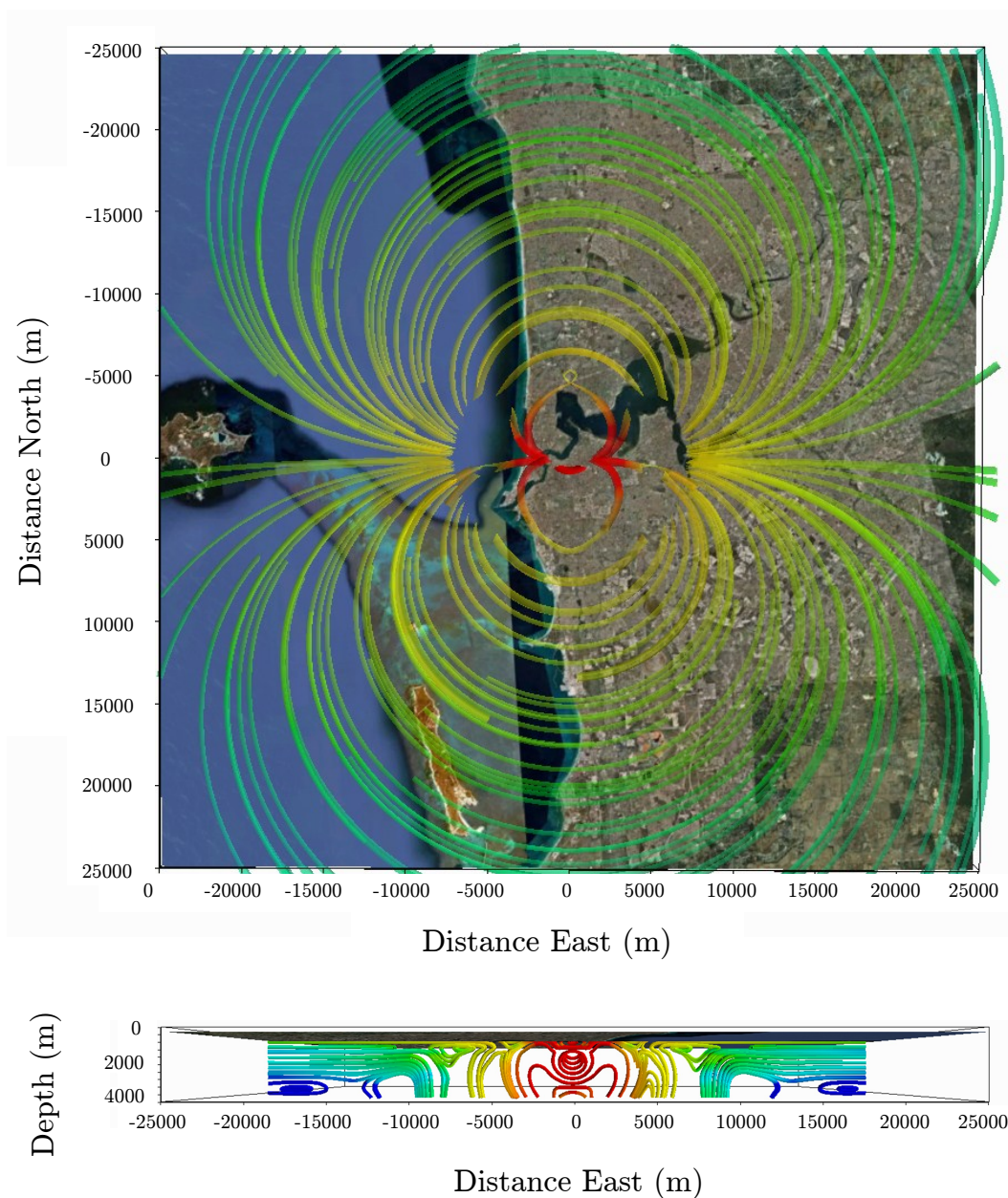


**Figure 5-12:** Interpretation of inline electric field streamlines. A number of features are identified in the streamline representation of the EM fields generated during a MCSEM survey. The airwave is represented as a circulating vortex associated with electromagnetic field interaction between earth, ocean and air. All vortexes are caused by rapid changes in vector direction (e.g. when upward vertical fields change to downward fields). Similarly the phase fronts are associated with the transition between positive to negative amplitude. These phase fronts are caused by the change in polarity of the transmitted waveform (i.e. phase fronts either moves away from or towards the transmitter). Changes in electrical resistivity can cause the electric-field to change direction abruptly. High electrical conductivity contrast at ocean floor (i.e. from 0.3 Ohm.m in the ocean to 1.5 Ohm.m in the host sediments) causes rapid change in streamline direction. Global asymmetry, about the bipole transmitter is also evident in the streamlines which highlights the influence of the hydrocarbon through a very large volume within the ocean column. The hydrocarbon is highly influential and it is clear the E fields try to “avoid” the resistive body or pass vertically through the target body.



## 5.2 The Scale of the Electromagnetic Fields Generated by an MCSEM Survey

It is easy to lose sight of the scale of the EM field generated during a MCSEM survey. The electromagnetic field generated by a MCSEM survey is large and is detectable in hundreds of cubic kilometers of earth and ocean. The scale of the electromagnetic field compared to other active source EM methods should not be understated. Streamlines allows the sheer scale of the electromagnetic field to be appreciated (Figure 5-13). Base frequencies as low as 0.05Hz are often recovered from MCSEM surveys. An earth consisting of a 1.5km ocean depth and halfspace resistivity of  $1.5\Omega \cdot m$ , covers a volume of  $50km \times 50km \times 4km$ . Figure 5-13 shows the generated electric field streamlines overlayed on the large sprawling metropolitan city of Perth, with a population of approximately 1.7 million people. The electric field is detectable within all areas this large volume of earth if conducted under a kilometer of seawater. The field is not just detectable on a local scale, but almost a regional scale. For example this electromagnetic field spans the complete east-west extent of the Perth Sedimentary Basin. The scale of the EM field can truly be appreciated through the use of streamlines.

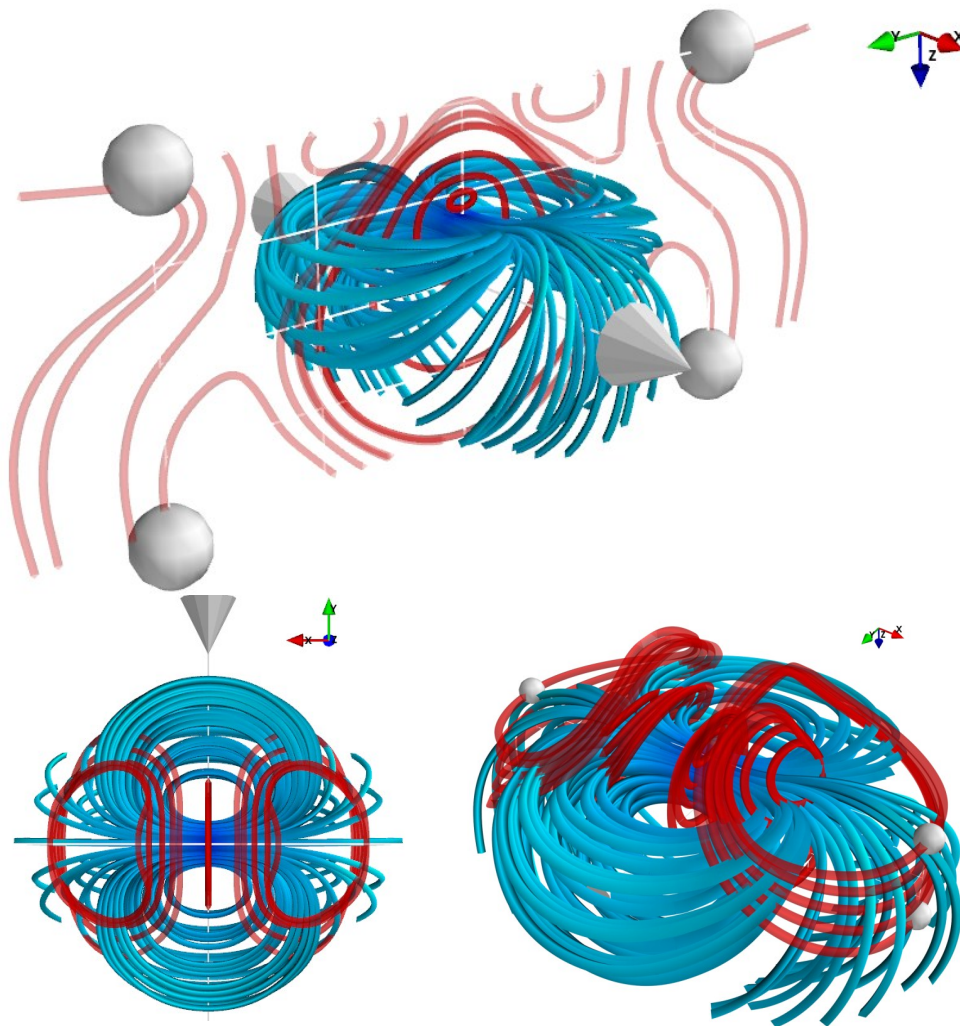


**Figure 5-13:** The detectable electric field streamlines generated by the lowest MCSEM frequency (0.1Hz), from a earth with an ocean depth of 1.5km and halfspace resistivity of 1.5Ohm m are overlayed above the city of Perth, Western Australia. The volume engulfed by the electromagnetic field is large ( $50km \times 50km \times 4km$ ) and would easily span the sprawling metropolitan city of 1.7 million people. Many MCSEM surveys will use a higher base frequency and as a result will reduce the volume of influence. They would in most cases halve the volume of influence. Appreciation of the scale of the EM fields generated during a MCSEM survey can be done using streamlines.



### 5.2.1 Three-Dimensional Streamlines

Full three dimensional representation of coupled electric and magnetic fields enhance the geophysicist's understanding of global electromagnetic-field behaviour within and around 3D geo-electrical structures. Figure 5-14 shows a range of perspectives of the electromagnetic fields circulating around the electrical bipole transmitter during a MCSEM survey. Since the source is an electric bipole, the electric fields can look something like the magnetic flux around a bar magnet. However the magnetic fields tend to express the more complex electromagnetic behaviour related of dynamic coupling of the magnetic and electric fields created during a MCSEM survey. While full 3D representations may contribute to understanding electric and magnetic fields (e.g. 3D bathymetry investigations), in general we have found that mapping streamlines at a 2D plane represents EM field behaviour in a more accessible, clear, intuitive and helpful way.

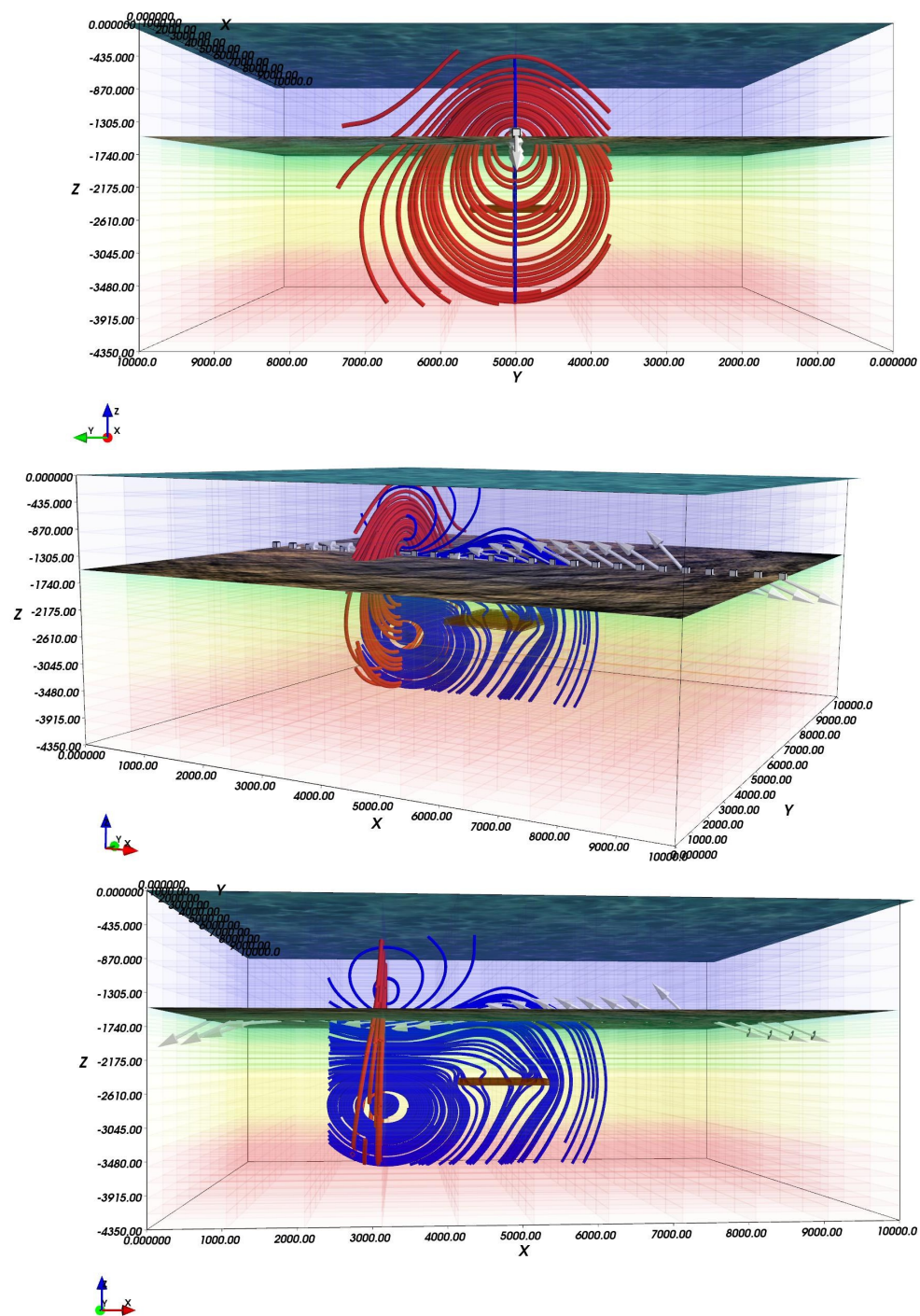


**Figure 5-14:** Three perspectives of the electric (blue) and magnetic (red) fields generated by a horizontal electrical dipole (HED) source. The electrical field displayed tends to look like the magnetic field seen around a bar magnet. However the magnetic field (red streamlines) reveals the dynamic coupling of circulating electric and magnetic fields in a 3D earth.

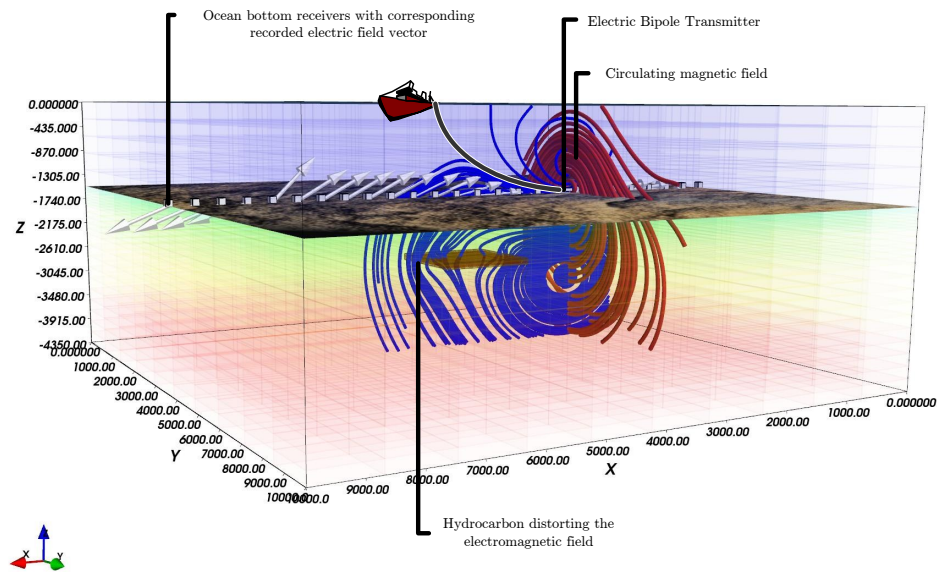
## **5.2. The Scale of the Electromagnetic Fields Generated by an MCSEM Survey**

---

Using streamlines show the true nature of the fields generated during a CSEM survey. Streamlines provides another perspective for the basics of the CSEM method. Figure 5-15 and 5-16 shows how the MCSEM method can be represented in three dimensions. The Figure demonstrates how the electric field interacts with the resistive hydrocarbon and circulating magnetic fields.



**Figure 5-15:** Example of 3D streamlines with seafloor 3D vectors in the front (top) oblique (middle) and inline view (bottom).



**Figure 5-16:** Labeled 3D streamlines in the oblique view.

### 5.2.2 Conclusion

We provide the first computer-generated streamline animation of propagation electric, magnetic and Poynting vector fields that occur during low frequency Deep Ocean Electromagnetic surveying. These make otherwise unintuitive EM field behaviors comprehensible throughout hundreds of cubic kilometers of ocean and earth. Streamline generating Java code and a well tested 3D integral equations algorithm are integrated into our interactive 2D marine controlled source electromagnetic modelling and interpretation software package. A key outcome from this research representation EM field behaviour during and MSCEM survey. We provide the first published example of the airwave represented as streamlines and demonstrate that the airwave is a circulating vortex moving down and out towards the ocean floor. More generally our methods and code can be used to visualize electromagnetic fields for a wide range of applications.

## 5.3 Poynting Vector Streamlines and the Marine Controlled Source Electromagnetic Method Airwave

### 5.3.1 Summary

We investigate the airwave using streamline visualisation of the Poynting vector. The airwave is a principal feature of marine controlled source electromagnetic method (MCSEM) surveys. The airwave has the potential to couple with or mask the hydrocarbon response. The airwave is in no doubt a complex interaction with all the geo-electrical elements; the highly resistive air, conductive seawater column and sub-ocean sediments and hydrocarbons all influence its signature. The number of published descriptions and seemingly contradictory explanations may have led to confusion over its physical reality. The airwave has been described mathematically, as an analogy to refraction seismic and as a downwardly diffusing wave. We attempt to determine what is the airwave? We employ streamline visualisation to investigate the electromagnetic airwave. We found that the airwave presents differently in each of the field components. Using electric and magnetic vector field streamlines, we show that the upwardly diffusing 'earth' wave vortex and downwardly diffusing airwave vortex results in a toroidal wavefront which rapidly varies in spatial oscillatory phase. We found that the airwave presents as a discontinuous front in the Poynting vector. This wavefront represents the region in space where the earth and air energy flow destructively interfere. We believe the airwave should be defined as a toroidal circularly rotating diffusing electric and magnetic field vortex which represents the area where the upwardly diffusing earth wave and downwardly diffusing air wave destructively interfere.

### 5.3.2 Introduction

The "airwave" is a key consideration for shallow marine controlled source electromagnetic surveying. The airwave has been described as a,

1. "downward-diffusing" wave (Weiss, 2007),
2. as the, "direct part of the primary field from the source to the sea surface" which reflects "back to the sea bottom" (Wang and Zhdanov, 2010),
3. "energy refracted at the air-water interface, travelling through the air at the speed of light and continuously transmitting energy downward into the water" (Hunziker et al., 2011) or
4. mathematically via up going and down going EM field decomposition (Amundsen et al., 2006).

So which is it; a downwardly diffusing wave, a reflection from the sea surface to sea bottom or is it refracted energy? We visualise the Poynting, electric and magnetic vector fields with streamlines to explicitly show and clarify the "airwaves" mode of propagation.

### 5.3.3 Theory and Method

In linear isotropic homogeneous media the Poynting vector ( $\vec{S}$ ) can be interpreted as "an energy current density or power flux" (Wang, 1986). It is the intensity of EM energy flow at a given point (Zhdanov, 2009) whose direction is the "same as" that of the instantaneous flow of

energy (Wangsness, 1986) or more explicitly the energy per second crossing a unit area whose normal is oriented in the direction  $\vec{E} \times \vec{H}$  (Zhdanov, 2009) (see equation 5.5). Equation 5.5 is applicable for both steady state and time varying fields (Wangsness, 1986). (Weidelt, 2007) used the time-averaged energy flow to interpret the typical electromagnetic flow of energy (see equation 5.6).

$$\vec{S} = \vec{E} \times \vec{H} \quad (5.5)$$

$$\vec{S}_a = \frac{1}{2\mu_0} \text{Re}(\vec{E} \times \vec{H}^*) \quad (5.6)$$

where,

$\vec{S}$  – Poynting vector ( $W \cdot m^{-2}$ )

$\vec{S}_a$  – time averaged Poynting vector ( $W \cdot m^{-2}$ )

$\vec{E}$  – electric field ( $V/Am^{-2}$ )

$\vec{H}$  – magnetic field ( $T$ )

$\vec{H}^*$  – complex conjugate of the magnetic field ( $T$ )

The integral of the component normal to the time averaged real Poynting vector has a physical meaning as energy per unit time in the enclosed volume dissipated by heat (Wangsness, 1986 and Weidelt, 2007). According to Weidelt (2007) the local interpretation of  $\vec{S}_a$  as “energy flow density at a point” may be problematic since non-divergent fields can be added to  $\vec{S}_a$ . Despite this, streamline visualisation of  $\vec{S}_a$  and  $\vec{S}$  provides a generalised idea of energy flow. Weidelt (2007) identified two relevant “guided waves”, the airwave and the resistive-layer mode using the time averaged real Poynting vector the contribution. I expand on the concept of “guided” waves expressed as time averaged real Poynting vectors to clarify the definition of the airwave.

The “air-wave” is commonly described in terms of “energy flow” (i.e. Weidelt, 2007) but field components rather than the Poynting vector is typically recorded and interpreted. The airwave investigation is performed by forward modelling the Poynting vector and field components using a horizontal electrical dipole (HED) source shown in a two dimensional grid of electric and magnetic receivers. The transmission frequency is set to 0.25Hz. We forward model the response over a four layer (i.e. seawater, overburden, hydrocarbon and half-space). Equation 5.5 was used to compute the Poynting vector field from the electric and magnetic components. Streamlines are computed at 0.5s. The complete survey is shown in Figure 5-17.

### 5.3.4 Results

The resulting synthetic electric and Poynting vector fields are represented by streamlines in Figure 5-18. For this model the approximate onset of the airwave is marked by a solid black line at an offset of 11000m from the transmitter. The airwave onset is seen as a flattening of the inline phase (Figure 5-18B), a sharp rise in the vertical phase (Figure 5-18B) and a drop in amplitude (Figure 5-18A). The profiles shown at the top of Figure 5-18 correlate with the 2D inline streamline representations (i.e. Figures 5-18C and 5-18D).

Figure 5-18C shows two circulating electric field vortices. The first vortex ( $x=7000m$  and  $z=0m$ ) is an “outwardly and up going” diffusing earth wave. The second vortex ( $x=15000m$  and  $z=600m$ ) is an “inwardly and down going” diffusing air wave. These “earth” and “air” wave vortices combine at the sea floor at 11000m creating the effects seen in the electric field profiles. The Poynting vector streamlines show energy flowing vertically upwards and downwards from the HED source. The energy flowing upwards from the HED preferentially



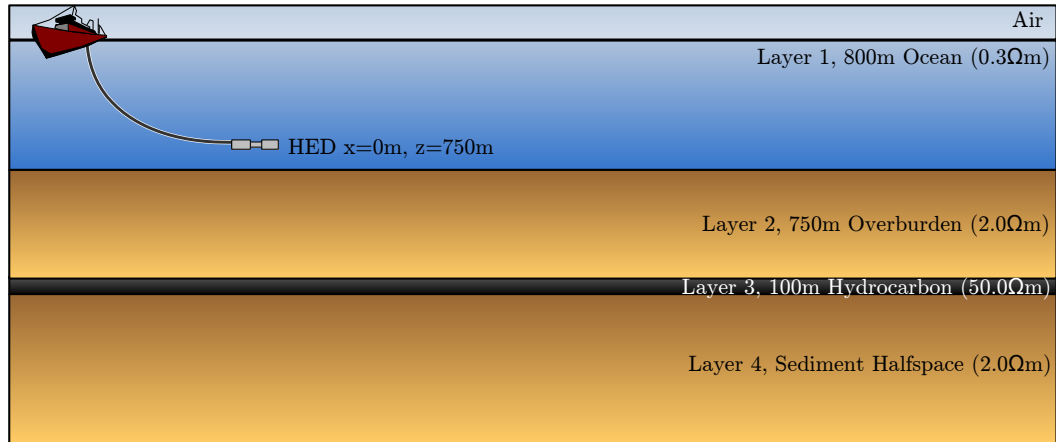


Figure 5-17: The geo-electrical model used to investigate the Poynting vector and the airwave.

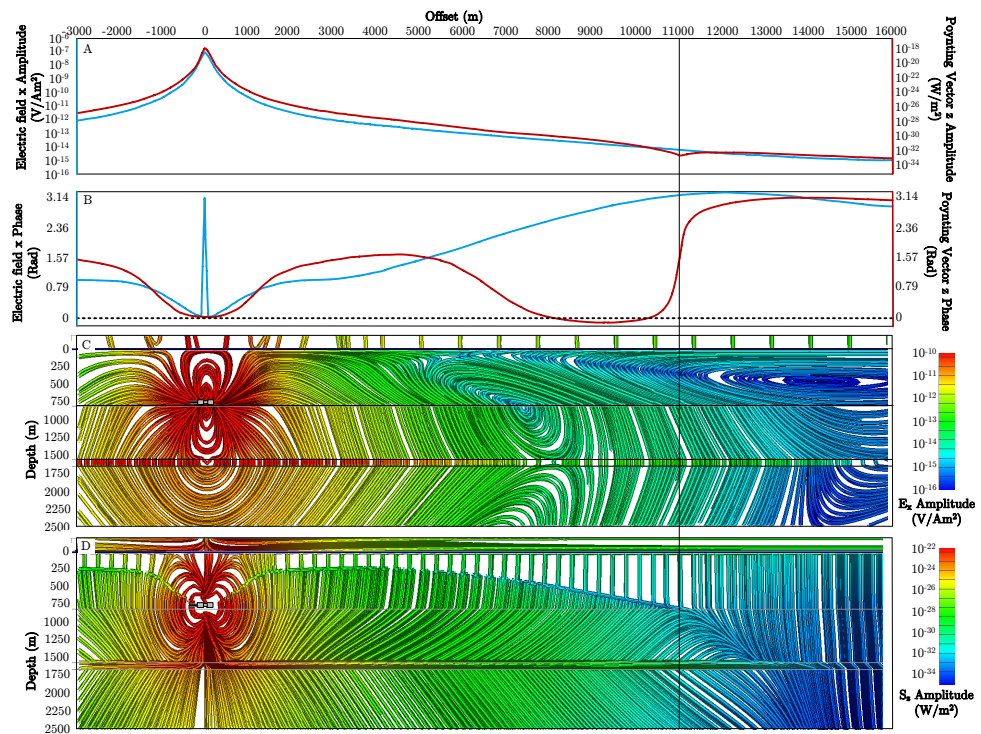
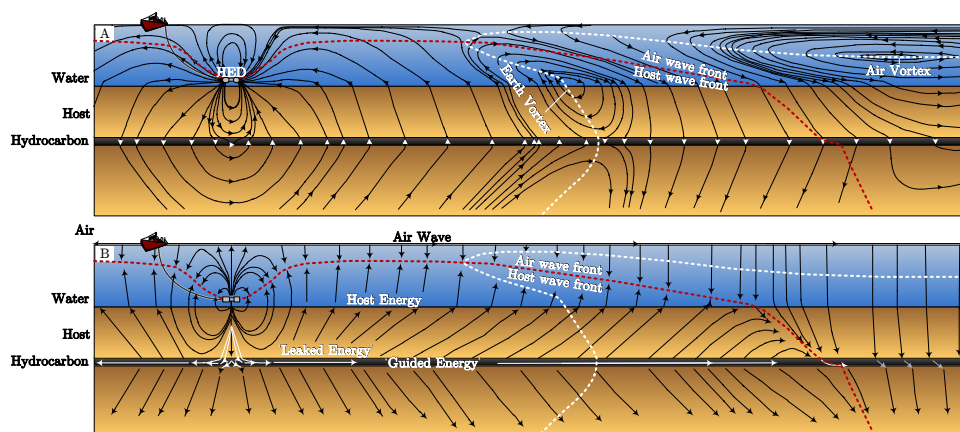


Figure 5-18: Time domain Poynting vector and electric field streamlines and profiles highlighting the airwave onset (11000m). The Figure shows the 1D inline profile response for (A) the electric field  $x$  amplitude and Poynting vector  $z$  amplitude (B) the electric field  $x$  phase and the Poynting vector  $z$  phase and 2D inline streamlines of the (C) inline electric field at 0.5s (D) inline Poynting vector at 0.5s.

flows horizontally along the resistive air-ocean boundary (i.e. “guided” (Weidelt, 2007) along the air-ocean boundary) and finally downwardly to the sea floor. The downwardly flowing energy dominates and is “guided” within the resistive hydrocarbon which emerges upwards towards the sea floor and into the water column. The up-going and down-going energy meet to form a boundary (i.e. the host wave front and air wave front). This boundary extends from the HED up into the water column, down to the ocean floor and into the earth (see Figure 5-18). The intersection of the front with the sea floor correlates with variations seen in the 1D profile amplitude and phase responses (see Figure 5-18A and 5-18B). From our results there is no indication of the presence of any “direct”, “refracted” or “reflected” energy. However extremely near offsets (i.e. less than 500m) a “direct” wave could be present. An interpretation of the electric and Poynting vector fields highlighting the airwave is shown in Figure 5-19.



**Figure 5-19:** The inline electric and Poynting vector interpretations of the airwave. The electric field streamlines show the airwave as the interaction between two vortices; the earth vortex and air vortex. The centre of the earth vortex corresponds with the  $E_x$  phase inflection point seen in Figure 5-18B. The air wave front (indicated by the dashed red line) represents the point where the contribution of “earth” and “air” energy flow is equal. There is no apparent direct, reflected or refracted energy, however it appears to have “guided” energy flow (Weidelt, 2007) within the hydrocarbon and along the air-ocean boundary.

### 5.3.5 Conclusions

The airwave is a complex interaction between all geo-electrical elements including; the highly resistive air, conductive seawater column and sub-ocean sediments which may include a hydrocarbon target. All components influence the flux of electromagnetic energy around the transmitter. The airwave is seen as a downwardly diffusing vortex in the field components. The airwave presents differently when identified with Poynting vector field streamlines. Energy appears to flow vertically upwards from the transmitter, is “guided” along the air-ocean interface and then down towards the ocean floor. The energy flowing upwards from the earth interacts with this downwardly flowing energy to form an airwave front. This front represents the point where the contribution of earth and air energy flow is equal. Streamline representations of the field component and the Poynting vector field highlights the nature of the airwave in a direct way that description alone cannot match.

### 5.3.6 Acknowledgements

We would like to acknowledge the Australian Government and Fugro Electro Magnetic for the research scholarship they have provided.

## 5.4 Bathymetry, Electromagnetic Streamlines and the Marine Controlled Source Electromagnetic Method

### 5.4.1 Summary

Sea floor topography influences the propagation of the low frequency electromagnetic fields generated during a marine controlled source electromagnetic survey. Small changes in water column thickness affect the electromagnetic field strength and direction. The propagation of electromagnetic fields in complex 3D geo-electrical settings is not easily understood through mathematical equations, simple rules of thumb or field measurements. Streamline visualization can reveal the full character of electromagnetic field propagation. We use a 2.5D finite difference algorithm to simulate the electromagnetic fields for geo-electrical models with strong bathymetry. We then provide and compare the full EM streamline representation for models with and without a hydrocarbon targets. Locations where the hydrocarbon response is masked by strong electric fields associated with varying ocean bottom topography are readily identified with our interactive streamline representation. Other phenomena such as the airwave are quickly identified in the electric field streamlines as circulating vortices, coming down and out from the ocean surface with a shape that again is strongly influenced by the seafloor variation. The relationship between the ocean bottom shape and the distribution and amplitude of circulating electric and magnetic fields would certainly lead to misleading artifacts if 1D inversion were applied. Our streamline visualization method can aid interpretation and improve survey design through as it clearly represents the global distribution of electromagnetic fields where MCSEM is applied in the presence of strong bathymetry.

### 5.4.2 Introduction

The marine controlled source electromagnetic method (MCSEM) is a geophysical technique applied for hydrocarbon exploration in ocean settings. The success of a MCSEM survey depends on factors including; water depth, bathymetry, water currents, survey parameters and the geo-electrical setting (e.g., Phillips, 2007 and Hesthammer et al., 2010). Our work focuses on identifying and representing the impact of bathymetry on MCSEM application. Li and Constable (2007); Chen and Alumbaugh (2011); Han et al. (2010) and Davydycheva and Rykhliniski (2011) have all described the airwave impact on MCSEM data and even discussed mitigation of problematic bathymetric effects. Li and Constable (2007) demonstrated that bathymetry is a major effect because of the large conductivity contrast between the sea water and the sea floor. We have elected to investigate the electromagnetic fields created by a MCSEM transmitter in the presence of bathymetry with aid of streamlines. In particular we investigate the complex relationship between bathymetry and the airwave.

Electromagnetic fields are three dimensional continuous vector fields. Vector fields are analysed by computing the EM fields with a time harmonic sinusoidal transmitted waveform. These fields can be characterized by direction, amplitude and phase at each receiver location. The electromagnetic fields generated during MCSEM surveys are typically represented by profiles, 2D grids, glyphs and iso-surfaces (Pethick, 2008). Streamlines represents the path of a particle through a vector field at a particular time (Hansen and Johnson, 2004) and can be used to visualise the electric and magnetic fields generated during a MCSEM survey. The use of electromagnetic streamlines potentially captures the character of these very large scale circulating coupled vector fields where traditional methods cannot offer. Profiles, iso-surfaces and grids have their place, but are limited in their ability to show one or two properties (i.e. amplitude, phase or direction). Streamlines represent the flow of the electromagnetic fields in

a continuous and natural way.

We investigate the influence of ocean bottom topography with a MCSEM configuration and geo-electrical model similar to that presented in the research of Li and Constable (2007). Li and Constable (2007) found that all electric and magnetic field components are influenced by bathymetry, but to very different degrees. They also found that the bathymetric effect is dependent on water depth, transmission-frequency, sediment resistivity and transmitter-receiver geometry. Li and Constable (2007) found that the vertical electrical field measured on the ocean floor is unaffected by airwaves, however large variations can occur in relatively shallow water.

### 5.4.3 Method and Results

While a number open source 1D and 3D algorithms exist, they are not ideally suited to modelling MCSEM data over complex ocean floor geometries. We have elected to use a proprietary 2.5D finite difference algorithm developed by Fugro Electro Magnetic to simulate the electromagnetic fields (Scholl and Sinkevich, 2012). The 2.5D irregular finite difference code is controlled under the open source modelling and visualization platform, CSEMoMatic (Pethick and Harris, 2012). A further proprietary plug-in (i.e. to CSEMoMatic) was developed to construct and modify irregular finite difference grids.

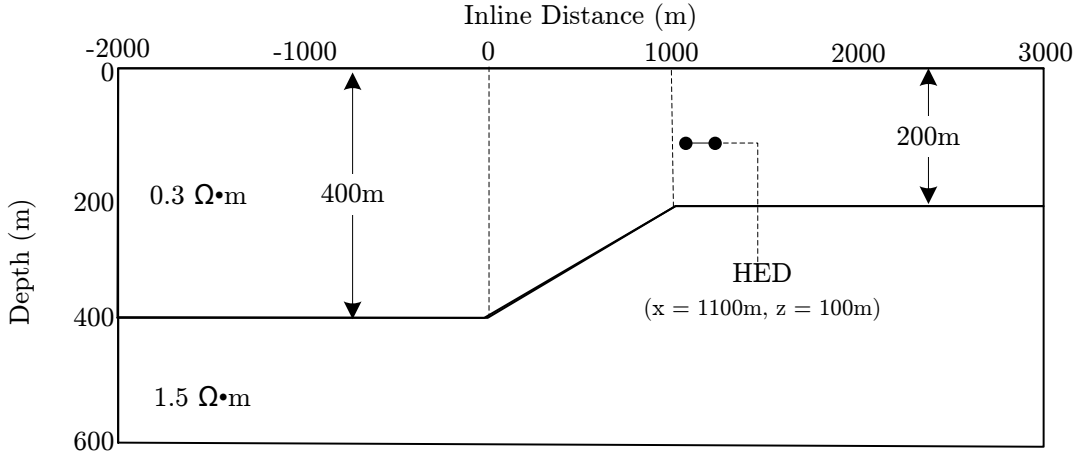
A real time streamline generation module was developed to compute and visualise the electromagnetic field. Once the full wave form on a 2D plane or in a 3D volume was computed, streamline visualisation were performed to reveal the flow of electromagnetic energy in time and space.

Our first example highlights the relationship between bathymetry and the airwave. In particular we consider the influence of bathymetry on the airwave onset for each of the electric field components;  $E_x$  and  $E_z$ . Figure 5-20 shows the electrical conductivity distribution. Our geo-electrical model (Figure 5-20) was chosen to be the same as the model found in Li and Constable (2007) for its simplicity and as a comparison to published work. It was constructed to examine the MCSEM response across a uniformly dipping slope at the ocean floor. Hydrocarbon was not included to facilitate the focus of this analysis on the influence of bathymetry only.

The survey configuration consisted of a horizontal electrical bipole transmitting antenna positioned 100 m above the ocean floor operating with a 0.5 Hz time harmonic waveform. The inline and vertical electric fields were computed on a vertical in-line plane on a  $90 \times 90$  receiver grid (e.g., 8100 receivers). The streamlines were generated using a 20m step length and with a limit of 100 steps.

Figures 5-21a, b and c shows the streamline representation of the electric field streamlines projected onto a vertical inline plane for,

- a the total electric field generated by the electrical antenna
- b the electromagnetic field generated by layering only
- c the streamline representation of the vector subtraction of the total and layering electric field



**Figure 5-20:** The schematic of the basic bathymetric uniform dip ocean floor model as found in Li and Constable (2007). Their model was used to investigate the influence of bathymetry on the evolution of the “air-wave” using streamlines.

vectors (i.e,  $c = a - b$ ).

Figure 2a reveals strong asymmetry associated with the bathymetry in the electric field streamlines on both sides of the transmitter bipole. As expected the electric field streamlines become concentrated within the water column as the ocean thickness decreases. This concentration is the result of the electric field being constrained within the conductive water column (i.e.  $0.3 \Omega \cdot m$ ) by the bounding resistive sub-ocean sediment (i.e.  $1.5 \Omega \cdot m$ ) and the air ( $1 \times 10^8 \Omega \cdot m$ ). Larger electric field amplitudes and higher streamline density are encountered on the upper slope due to this confining behaviour.

Phase fronts are visible by the dotted white line. Zhdanov (2009) defines phase fronts as “a surface formed from all points at which the phase has the same value” (i.e. contours of constant phase offset from the transmitter waveform). The phase front velocity of a spherical electromagnetic wave in a whole-space from a dipole source can be represented in terms of resistivity and transmission period (see equation 5.9). Starting with the skin depth equation,

$$\delta = \sqrt{\frac{2}{\mu_0 \omega \sigma}} \quad (5.7)$$

substituting the wavelength  $\lambda$  for  $2\pi\delta$ , as seen in the fundamental solutions to the wholespace EM wave equation,

$$v = \lambda f = 2\pi\delta \quad (5.8)$$

inserting 5.7 into 5.9,

$$v = \lambda f = 2\pi \sqrt{\frac{2}{\mu_0 \omega \sigma}} f = \sqrt{\frac{2 \times (2\pi)^2 f^2}{4\pi \times 10^{-7} \times 2\pi f \times \sigma}} = \sqrt{10^7 \frac{\rho}{T}} \quad (5.9)$$

where,

$v$  – phase front velocity ( $ms^{-1}$ )

$$\rho - \text{resistivity } (\Omega \cdot m)$$

$$T = \frac{1}{f} - \text{period } (s)$$

The two phase fronts shown in Figure 5-21a are located at -800m and 1200m offset from the transmitter. The increased phase front offset to the right of the transmitter results from the “faster” diffusion of the electromagnetic field within the resistive shelf (see equation 1).

Figure 5-21b is the anomalous electric field produced from the bathymetric slab (i.e. the sediments above the 400m ocean floor). Upper slope MCSEM receivers would record a larger horizontal electric field signal component when compared to a similar position on the platform below the lower slope (Figure 5-21b). The comparative lower platform receivers would also record a much larger vertical electric field component.

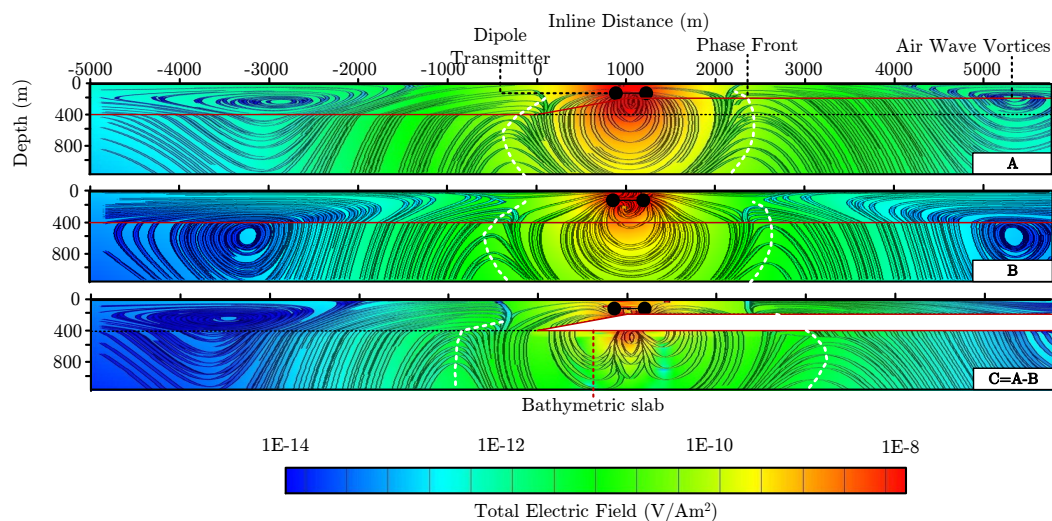
The airwave potentially masks the hydrocarbon response leading to significant challenges in the application of shallow MCSEM interpretation. Several approaches have been published to minimise the influence of the airwave, including applying frequency differencing (Nguyen and Roth, 2010), airwave decomposition (Amundsen et al., 2006) and employing acquisition and interpretation strategies (Andreis and MacGregor, 2008). The airwave has been described as a complex and highly influential feature of shallow MCSEM methods. Thirud (2002), Fischer (2005), Pound (2007), Carstens (2009), (Wang and Zhdanov, 2010) and many others have described the airwave mathematically, as an analogy to seismic or as a diffusing shell. Our streamline representation of the EM vector field highlights the changes in amplitude, shape and direction of the evolving airwave caused by ocean floor bathymetry.

Our streamline representation indicates that the interaction of the EM response at the air ocean interface with the electric fields from the ocean sediment interface results in spiralling vortices. Figure 5-21a visualises the airwaves with closed spiral vortex geometries. This is seen in the total electric field streamlines at the coordinates  $x=-3000$  m and  $y=200$  m. The centres of these spirals have no detectable amplitude. These vortices spiral downwards from the air-water interface. The airwave generated from the anomalous ‘bathymetry field’ occurs at farther offsets to the HED than the total response. The fields generated from the resultant anomalous ‘bathymetric source’ contributes to the total response. More importantly the interaction between the airwave and the geo-electrical model in the shallow water column is very different from the one visualised in the deeper water. The air-wave vortex has a smaller lateral offset in shallow water.

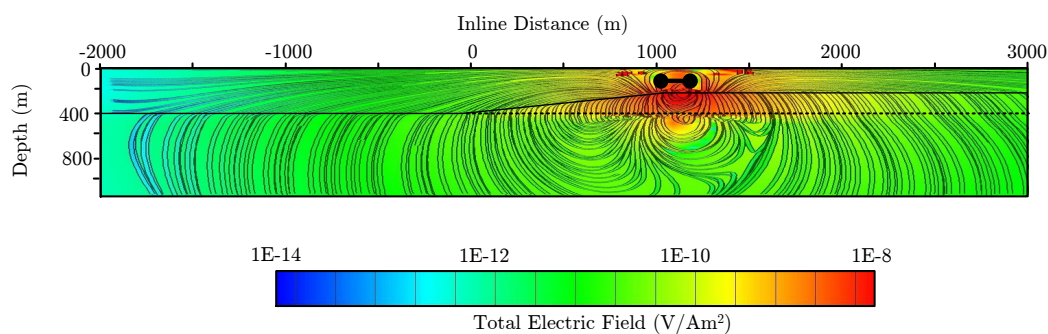
In Figure 5-22 we have zoomed in to a 5 km in-line section through the earth to highlight streamlines close to the transmitter. Figure 5-22 shows the electric field related to the anomalous wedge and slab to the right of the image. A time has been selected to reduce the visual impact of the phase fronts near the slope seen in Figure 5-21. A strong vertical electric field response can be observed inside the bathymetric slab. The electric fields emerges the sea floor with a larger horizontal component than along the top of the dipping slope than at the base of the slope.

A second model was created to investigate the electromagnetic interactions between the airwave, bathymetry and a hydrocarbon. The geo-electrical framework is shown in Figure 5-23. The model consists of a 5km,  $100 \Omega \cdot m$  hydrocarbon reservoir buried 800m below the sea floor. This is similar to the 2D resistive reservoir model with the ocean floor topography as presented in Li and Constable (2007). The difference is that our hydrocarbon body lies parallel to the bathymetry. We investigate the relative influence of various large components of the geo-electrical framework by calculating the differences between electromagnetic vector





**Figure 5-21:** Streamline representations of electromagnetic field propagation over the dipping ocean floor model. These streamlines were created from the 0.5 Hz time harmonic transmission frequency at a time of 0.5s. (A) The total electric field as streamlines. (B) The electromagnetic fields resulting from layering only as shown by the solid line at 400m depth. (C) The streamline representation of the vector field resulting from subtraction of the total electric fields and the electric field resulting from layering only (i.e.  $C=A-B$ ). The white dashed line represents a phase front location. The airwave is also seen by the spiralling vortices. The shape and offset of the airwave is influenced by the ocean floor topography.



**Figure 5-22:** A close-up of the anomalous electric field amplitude and total electric field streamlines at 0s. The streamlines indicate that the wedge marked in red results in a strong internal vertical anomalous electric field and a much greater change in direction at the ocean floor. Simplistically the effect of the wedge is like that of a long vertical electric field sheet source sitting above the ocean floor.



fields computed with and without target geo-electrical components of the total vector field (i.e. the total vector field is the result of computations using the layering, bathymetry and hydrocarbon). In reality the entire geo-electrical model is inexorably “coupled” and can be separated into the “apparent” influence of each component of the geo-electrical framework. In Figure 5-24 we show the individual influence of the hydrocarbon and bathymetry by computing,

- a total electric field
- b a 1D layering electric field response in the absence of any hydrocarbon or bathymetry
- c hydrocarbon electric field response with no bathymetry
- d anomalous bathymetric electric fields (no hydrocarbon without bathymetry).

Vector computations were then performed on these four models to obtain the isolated bathymetric effect and hydrocarbon response (See Table 5.1). We then compute the normalised response on the vector norm  $\|\vec{E}\|$  by equation 5.10.

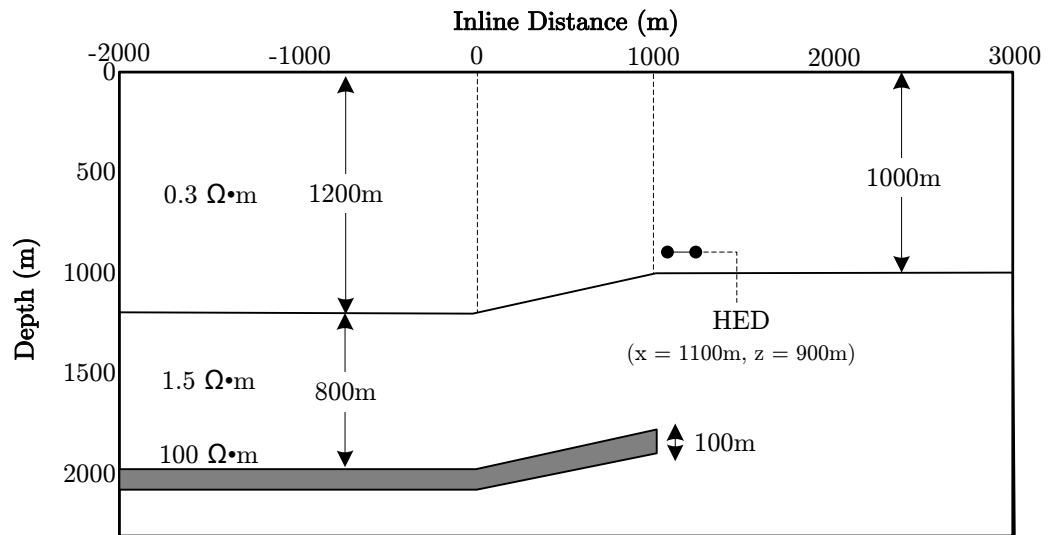
$$\vec{E}_{Norm} = \frac{\|\vec{E}_{Target}\| - \|\vec{E}_{Background}\|}{\|\vec{E}_{Background}\|} \quad (5.10)$$

where,

$\vec{E}_{Target}$ — target electric field vector ( $V/Am^2$ )


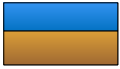

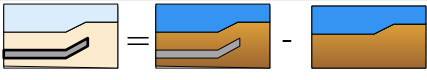

$\vec{E}_{Background}$ — background electric field vector ( $V/Am^2$ )

$\vec{E}_{Norm}$ — normalised electric field (%)



**Figure 5-23:** Schematic of the sloped bathymetric model with a hydrocarbon body. This model has been used to demonstrate the interaction of the electric field with the bathymetry and hydrocarbon.

Figure 5-24 shows the total and anomalous electric field streamlines generated by the transmitting antenna. As seen previously, the electric field becomes concentrated in conductive

Vector Field	Computation	Pictorial Representation
Bathymetry and HC	$\vec{E}_T$	
Layered	$\vec{E}_L$	
Bathymetry no HC	$\vec{E}_{Bath}$	
Hydrocarbon Only	$\vec{E}_{HC} = \vec{E}_T - \vec{E}_L$	
Bathymetry Only	$\vec{E}_B = \vec{E}_T - \vec{E}_{Bath}$	

**Table 5.1:** A table showing how the electric vector fields are computed to obtain the individual influence of the hydrocarbon and bathymetry.

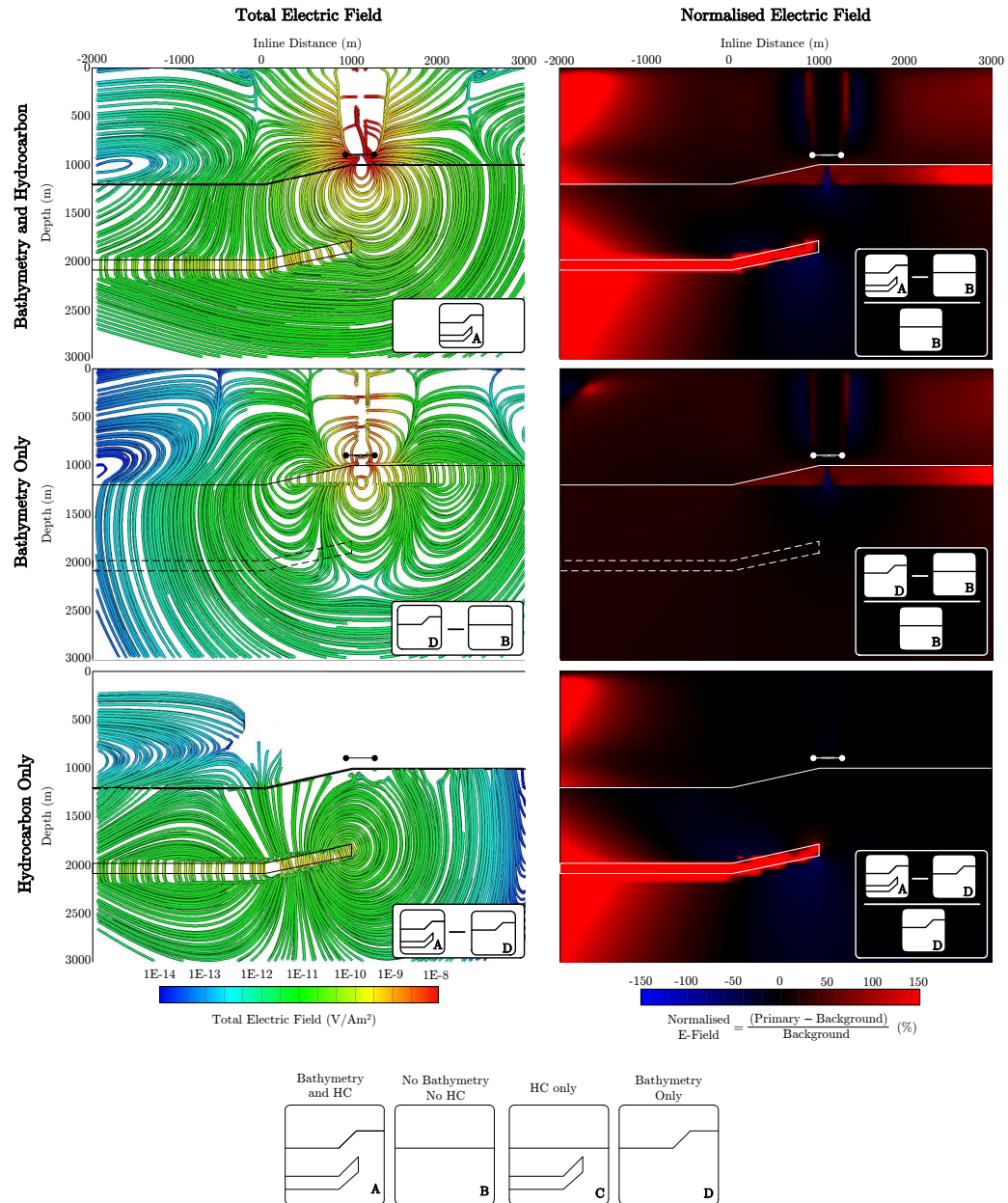
regions while tending to 'avoid' the electrically resistive regions (i.e. hydrocarbon). The electric field streamlines are exceedingly close to perpendicular when located in the resistive hydrocarbon. The normalised amplitude (Equation 5.10) resulting from the presence of the hydrocarbon is much larger than the bathymetry but its effect is localised in a smaller volume of earth. The bathymetry contains lower normalised amplitudes, but its effect is more widespread, influencing a much larger volume of earth.

A strong negative vertical electric field component exists at the end of the hydrocarbon ( $x = 1000$  m and  $y = 2000$  m). Given this, it may be wise to place vertical electric field receivers in a shallow (e.g. 800 m) slotted or uncased borehole at 0m. Our streamline representations alert the MCSEM survey designer to areas with the potential for poor or ambiguous resolution. They also provide a direction on an unconventional survey design that may improve sensitivity to target structures.

#### 5.4.4 Conclusions

The influence of ocean bathymetry on the propagation of electromagnetic fields generated by MCSEM surveys transmitters near the ocean floor can make the interpretation for hydrocarbon exploration in both shallow and deep water environments challenging. Ocean floor topography potentially masks or complicates a hydrocarbon response. Streamlines represent the electromagnetic field in an intuitive and natural way. Streamlines can be used to identify commonly discussed features such as phase fronts and the "airwave". The electric field airwave is seen as a closed loop vortex moving down and out from the air ocean interface on either side of the transmitter bipole. The bathymetry creates asymmetry in the movement and shape of the electric field airwave vortices. The geometry, path and offset of the evolving vortices can be associated with variations in water column thickness. The location of the phase fronts must also be impacted as the electric field travels preferentially in the conductive water column.

Streamlines can provide a representation of the relative influence of each component of a geo-electrical framework, such as hydrocarbon and bathymetry on the total fields as measured by the receivers. A clear benefit of various streamline representations of electromagnetic field propagation is that they provide a pointer to possible advantages from unconventional survey



**Figure 5-24:** The inline electric field streamlines (left) and normalised electric field (right) showing the contribution of each of the major components of the geo-electrical framework including, (i) total (top), (ii) bathymetry (middle) and (iii) hydrocarbon (bottom). See table 1 for an explicit description of how each image was derived. Note that streamlines were created from the 0.5Hz time harmonic transmission frequency at a time of 0.5s. The geo-electric models used in each case are seen at the extreme bottom of the Figure.

geometries which may not have been considered. For example some geo-electrical settings may benefit considerably by having receivers located higher in the water column or within drill holes located in the shallow subsurface. This could be of particular importance for 4D MCSEM surveys. Our streamline visualization of the electromagnetic fields generated during MCSEM surveys with ocean floor topography can aid interpretation and improve survey design by highlighting potential problems and opportunities which may have been unidentified.

## Acknowledgments

We would like to thank Fugro Electromagnetic for making their proprietary 2.5D finite difference EM modelling algorithm available for this study. We are also grateful to the Australian federal government, Curtin University and from Fugro Electro Magnetic Pty Ltd for the scholarship support which has enabled Andrew to complete his PhD research program.

# Conclusion



# Conclusion

---

## 6.1 Summary

Electromagnetism presents a methods for revealing the subsurface. The broad and diverse applications of electromagnetic methods include hydrothermal characterisation, sequestered CO<sub>2</sub> monitoring, water resource management, mineral and hydrocarbon exploration. The key to unlocking the information content contained within a modern electromagnetic data set is software tools available. I have engineered a framework within which multi-dimensional computation and visualisation of electromagnetic fields can occur. It is open source so can be built upon by other researchers. The software framework I created has been used to reveal the nature of electromagnetic propagation in the earth with a clarity that has not previously existed.

I have shown how an all purpose electromagnetic framework can be created to assist solving electromagnetic data models. The steps to design, develop and test a modern electromagnetic framework covering data structure, algorithms, three-dimensional visualisation and interactive graphical user interface from the ground up were presented in Part I of the thesis. The framework integrates computer science concepts ranging from parallel computing, networking, computer human interaction to three-dimensional visualisation into a software package tailored to marine controlled source electromagnetic computation. The electromagnetic framework is comprised of more than 100,000 lines of new Java code which integrates several third party libraries to provide low level graphical, network and execution cross-platform functionality. An object-oriented design has been crucial in the development of the EM data model. The data model is easily modifiable, extendable and maintainable and can be utilised in any electromagnetic modelling package. The data model was proven efficient in storing, retrieving and representing electromagnetic data from both real world and synthetic environments. Computational engines and algorithms can be integrated into the framework with minimal effort enabling rapid interactive forward modelling, inversion and visualisation of electromagnetic data.

Applied parallel computing and streamline visualisation are covered in Part II of the thesis. These topics investigated and tested novel ideas to solve issues found in modern controlled source electromagnetism. Electromagnetic modelling and inversion of three-dimensional datasets may require days or even weeks to be performed on single-thread personal computers. A distributed massively parallelised 'macro' electromagnetic forward modelling and inversion method was devised to significantly reduce computational time. The 'macro' parallelisation method was shown to facilitate the reduction in computational time of several orders of magnitude with relatively little additional effort and without modification of the internal electromagnetic algorithm. The method provides the possibility to invert large airborne surveys in seconds.

Real-time 2D and 3D streamlines are highly useful for understanding electromagnetic problems. I have used streamlines to represent coupled vector fields generated during modern

marine controlled source electromagnetic surveying for hydrocarbon exploration. Streamlines facilitate the interpretation of circulating electric and magnetic fields and promote improved understanding of EM propagation in complex geo-electrical settings. The air wave is a controversial and significant component of marine controlled source electromagnetic surveys. The airwave has been described as a reflected, refracted, direct or diffusing wave and has been thought of as noise, useable signal or both noise and signal, which has lead to confusion over its physical reality. Real-time interactive streamlines were used to more accurately represent the electric, magnetic and Poynting vector fields. The first images of the evolving air wave are provided. The energy propagation (i.e., the Poynting vector) of the air wave exhibits refractive qualities; the energy propagates upwards from the transmitter, along the air-water boundary and down to the ocean floor. It was found there is no significant direct or reflected wave at mid-offsets. The electric and magnetic air wave is identified as a downwardly diffusing rotating vortex caused by the interaction between the upwardly diffusing earth wave and downwardly diffusing wave from the air-water interface. This shape, onset and path of the evolving vortices are highly influenced by the ocean floor shape.

This thesis represents one of the first electromagnetic publications fusing concepts from the fields of electromagnetic geophysics and computer science. I have successfully developed a modelling and inversion framework to solve a diverse range of electromagnetic problems spanning computational speed, understanding the nature of electromagnetic fields generated during a controlled source electromagnetic program and ascertaining the detectability of sequestered carbon dioxide. The developed software is a living scientific work and has been made freely available to encourage research for the advancement of electromagnetic methods.



# Appendix



# The Project Website

---

## Contents

---

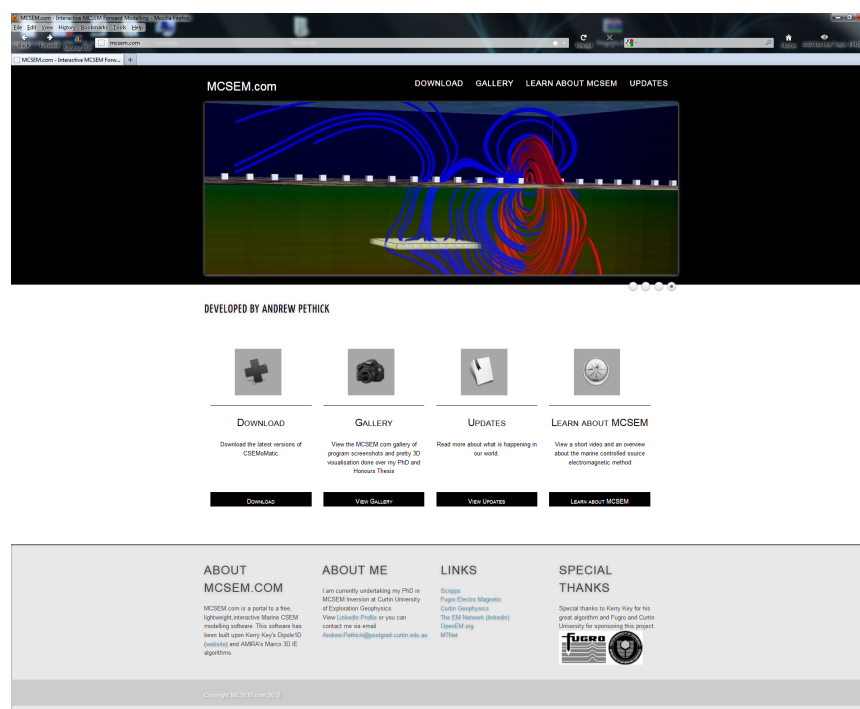
<a href="#">A.1 Overview</a> . . . . .	216
--	-----

---

## A.1 Overview

MCSEM.com is a portal to my work undertaken over the duration of my PhD candidacy. It provides access to free information and software. The website is based on the Wordpress content management system. Wordpress is a freely available popular content management system for developing websites, mainly blogs (See Figure A-1). Using Wordpress as my base CMS the content was generated using a publically themes. Using the simple interface it was easy to add and modify functionality by writing a third party PHP scripts and CSS style sheets.

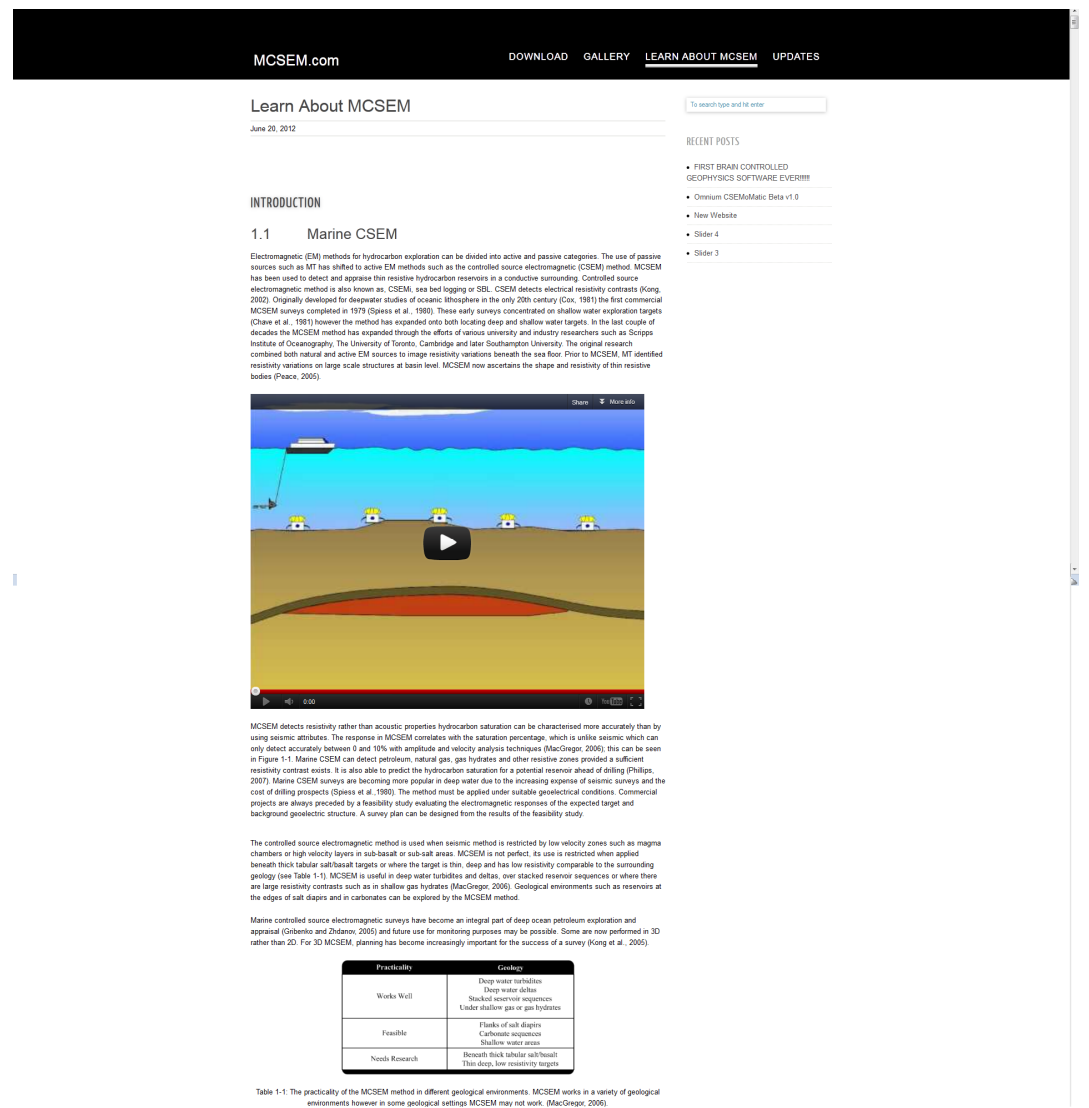
The has a dual purpose. Firstly to promote the MCSEM method and secondly distribute



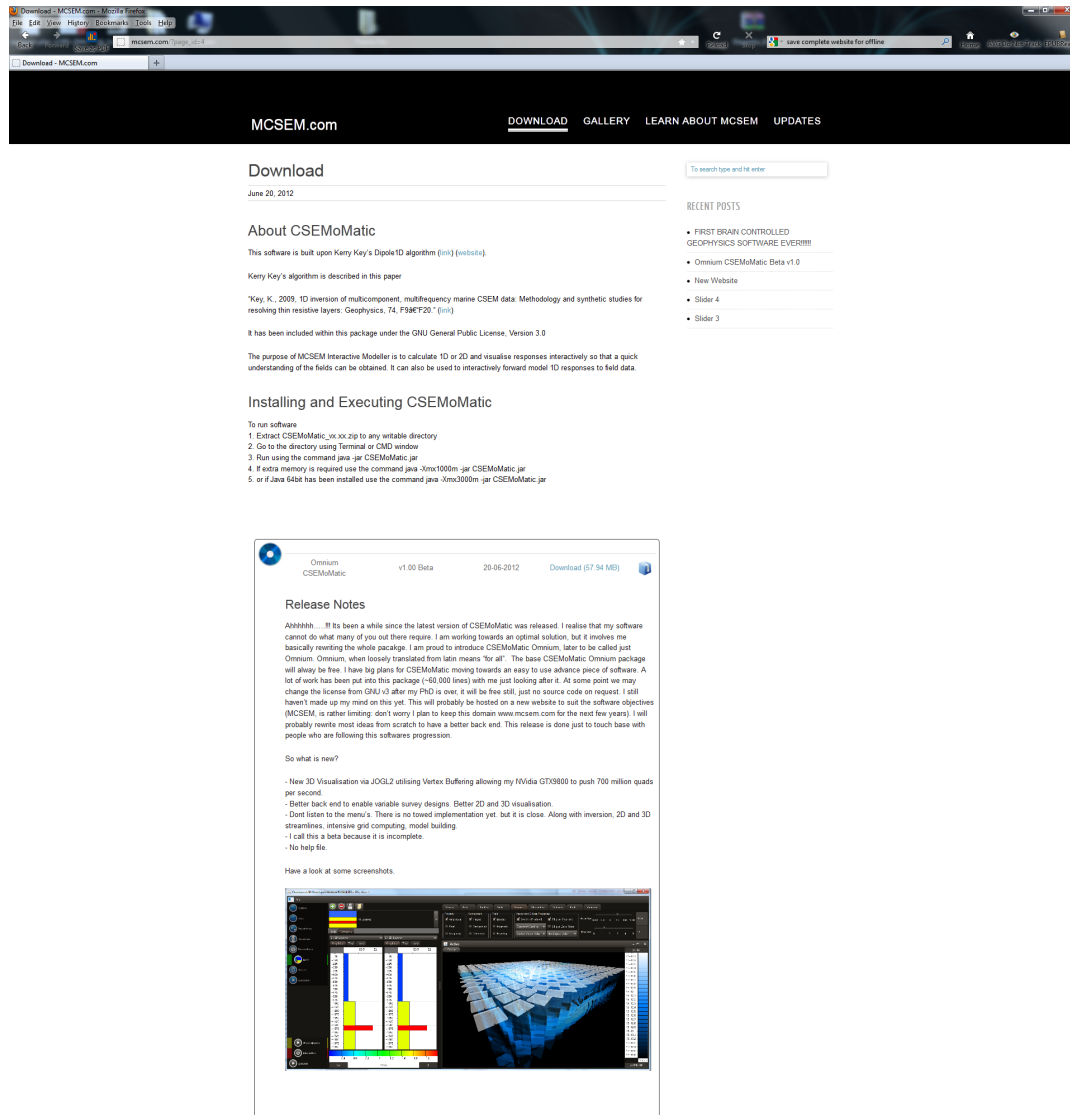
**Figure A-1:** The front webpage of [www.MCSEM.com](http://www.MCSEM.com). The website was created using the Wordpress content management service. The content was generated using a publically available theme and by writing number of PHP and CSS style sheets. The website a method to promote the MCSEM method, distribute my software and as a way to educate through the learning portal.

my software. To promote the MCSEM method the learning portal was created (See Figure A-2). The portal overviewed the basics of electromagnetism and the marine CSEM method. My software was made available to everyone. The two methods for free distribution are in binary form with a direct download from the MCSEM.com server or as source from a SVN service located externally to the website (See Figure A-3). All versions have been made public.

The website has been a success with in excess of 3000 unique visitors from over 300 institutions spanning worldwide as many as 80 countries.



**Figure A-2:** A screenshot of MCSEM.com learning portal. The learning portal explains the basics of the MCSEM method.



**Figure A-3:** A screenshot of the download page of MCSEM.com. All software is freely distributed, either in binary form with a direct download or as source from a CVS service located externally to the website.

# Conditioning of the 3D Marine Controlled Source Inversion

---

## Contents

---

B.1	Summary . . . . .	220
B.2	Introduction . . . . .	220
B.3	Method and Results . . . . .	221
B.4	Conclusion . . . . .	225

---

## B.1 Summary

Three dimensional inversion of Marine Controlled Source Electromagnetic data (MCSEM) data is complex. Achieving an acceptable outcome in a reasonable time frame requires considerable manual input to the problem. We proposed a methodology for preconditioning the inversion for integral equation approximated forward modeller. Both pre-conditioning of the inversion process and feed-back during the inversion process are used to streamline the overall 3D MCSEM inversion process. We demonstrate the influence each of the components ( $E_x$ ,  $E_y$ ,  $E_z$ ,  $H_x$ ,  $H_y$  and  $H_z$ ) have on inversion. We demonstrate how preconditioning and iterative analysis of MCSEM data can lead to a more satisfactory result for 3D inversion.

## B.2 Introduction

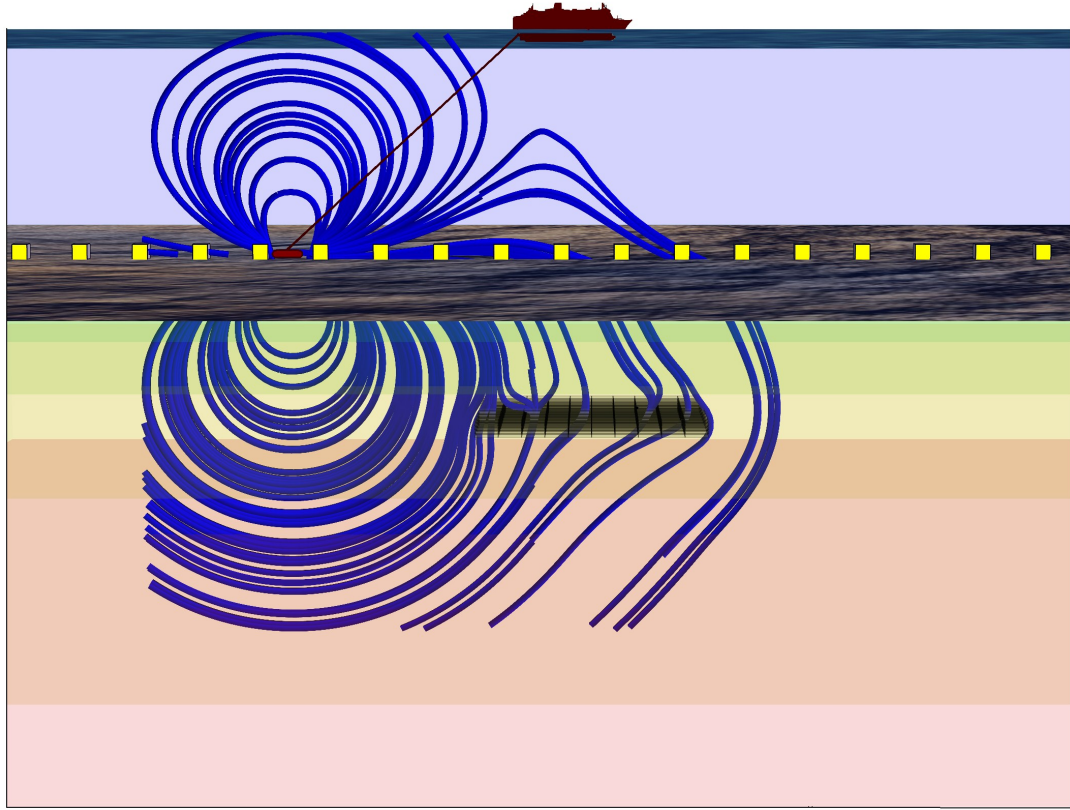
The MCSEM method uses electromagnetic fields to detect resistivity variation below the ocean floor. The method is performed by transmitting an electromagnetic field via a towed electric bipole transmitter and using ocean bottom receivers to measure the resulting electromagnetic field.(Figure B-1). Any resistive entity (i.e. hydrocarbon, salt body or air) set within a more conductive background (i.e. ocean, host rock etc) will tend to produce higher amplitude measurements and reduced phase difference at the receivers on the ocean floor. MCSEM data can be modelled by a variety of numerical methods such as the integral equation (rigorous or approximated), finite difference or finite element methods. The correct choice of numerical simulation method for inversion is often critical for achieving sensible results. A number of characteristics of the geo-electrical system and numerical technique need to be considered. These include and are not limited to; computational speed, phase and amplitude accuracy, model discretisation and model representation (e.g. bathymetry, anisotropy etc). Sensible inversion requires both good data and a well preconditioned geo-electric model for stable convergence.

The inversion is also influenced by the choice of forward algorithm and code implementation. MCSEM requires a high level of computational accuracy for both amplitude and phase. Computational efficiency is also necessary, even for relatively simple 3D geoelectric models. The full or complete integral equation (IE) method is considered the most robust for data accuracy, but is computationally slow and limits the range of geoelectric models that can be represented. Approximations of the full IE method such as the Born approximation (Masashi et al., 2008) and Quasi Analytical method (Gribenko and Zhdanov, 2006) are considerably faster but can suffer from phase instability. Finite difference (FD) and finite element (FE) forward modelling methods tend to be less computationally expensive for complex models than the full IE method. FD and FE methods also offer the most flexibility in model definition. A number of publications have investigated MCSEM inversion. Numerical optimisation features such as source receiver CMP inversion have also been used successfully for field data (Mittet, 2007). Gribenko and Zhdanov (2006), Zhdanov et al. ( ) and Wang et al. (2008) have demonstrated the success of integral equation methods in inverting both synthetic and field data to an isotropic 3D sub ocean geo-electric model with flat ocean floor. Many of these articles emphasise proof of concept ideas rather than demonstrating inversion methodology.

We provide a methodology for generated and tested inversion on synthetic data by using the Quasi-Analytical inversion developed by the Centre of Exploration Targeting (CEMI). The inversion framework used includes discretisation, weighting, preconditioning and constraining the geoelectric model. We provide the synthetic example as a precursor to the next stage



of our research which consists of applying a range of inversion techniques (i.e. IE and FD methods) to a number of real MCSEM data sets.



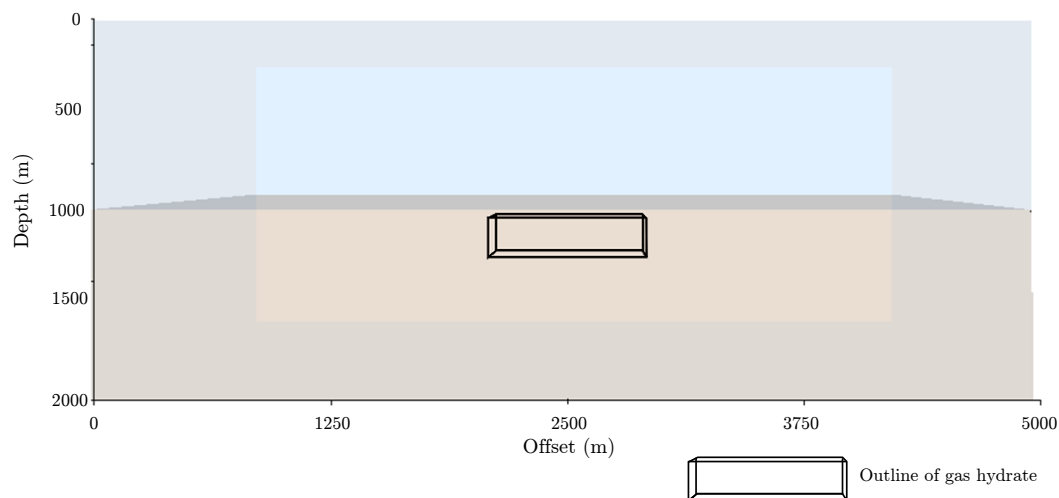
**Figure B-1:** Schematic of the inline electric field streamlines from a electric bipole transmitter (0.25Hz) interacting with 1D layering and highly resistive hydrocarbon body at a single point in time. The transmitted EM fields interact with hydrocarbon by reducing amplitude loss and phase differences at the ocean bottom receivers.

## B.3 Method and Results

A simple model (see Figure B-2) consisting of a shallow resistive gas hydrate was created to investigate the preconditioning procedure. The effect of varying acquisition parameters on results obtained from a 3D approximated IE inversion was investigated using this model. A simulated survey was performed over the  $1 \times 1\text{km}$  gas hydrate with a single transmitter position and  $500 \times 500\text{m}$  grid of ocean bottom receivers (Figure B-5).

A number of factors need to be considered when performing MCSEM inversion. Steps required prior to inversion include; area discretisation, data selection and weighting (i.e. offset, component, frequency and quality), and selection of reasonable geoelectric model constraints.

IE methods are based on calculating a response of 3D scattering bodies set in a 1D layered

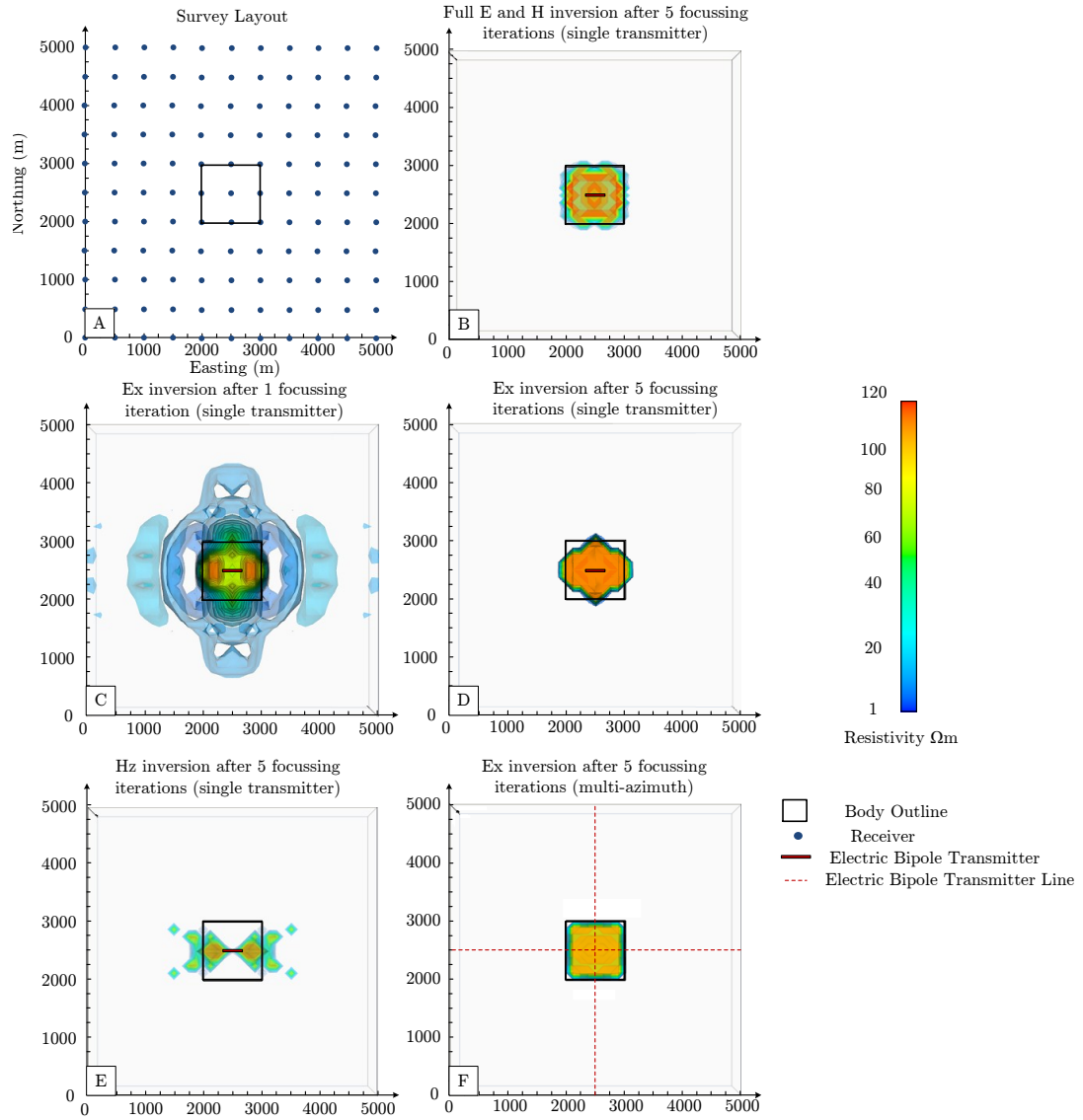


**Figure B-2:** The target model consists of a  $1\text{km} \times 1\text{km} \times 100\text{m}$ ,  $100\Omega \cdot \text{m}$  gas hydrate at a target depth of 100m below the ocean floor in a  $1.5 \Omega \cdot \text{m}$

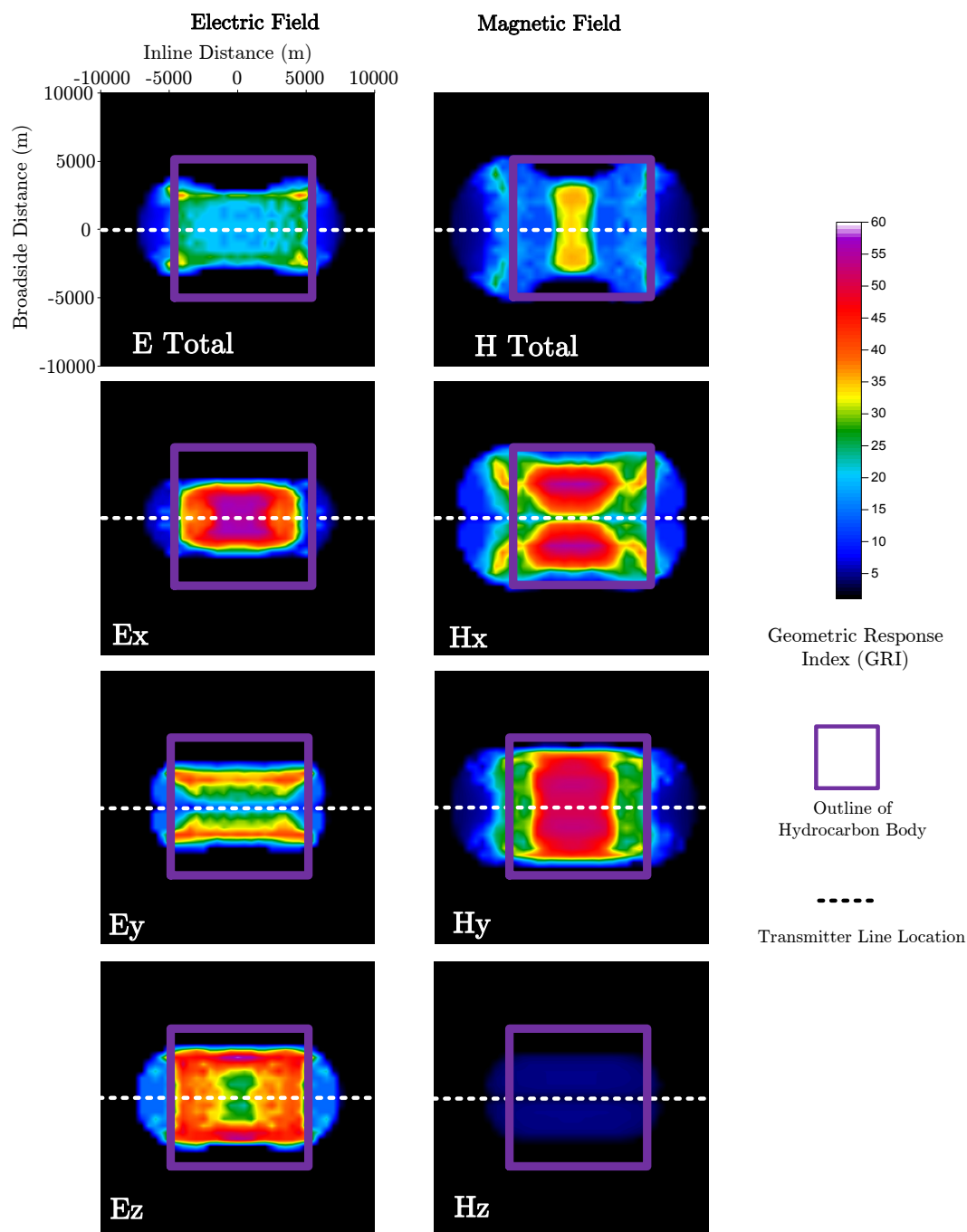
medium. For this purpose it is important to perform a 1D inversion to obtain the background layering response without the effect of anomalous responses. This can be performed by inverting with survey geometries or components that are insensitive to thin resistive bodies. For example the geometric response indicator (GRI) can show the sensitivity of the target for a given survey geometry (see Figure B-4). Simple source-receiver mid-point configurations located vertically over target bodies tend to be more sensitive to anomalous responses. The target clearly needs to be discretised sufficiently. The optimal level of discretisation is dependent on target depth, bathymetry and survey complexity.

The method and level of discretisation for electromagnetic methods remains a matter of contention. It is easy to either over or under discretise a region and there must always be a trade off between computational efficiency and resolution. More adaptive methods where the level of discretisation is tied to the rate of convergence within the inversion processing could be considered. Two examples of discretisation methods are by dividing the area with equally spaced rectangular prisms or by using quadtree or octree methods as described by Haber and Heldmann (2007). Either way, discretisation must provide sufficient resolution to represent a reasonable level of geo-electric complexity, considering the spatial distribution of sources and receivers and transmitter frequency range. For example, the area near the sources and receivers are highly sensitive to conductivity variation and must be sufficiently discretised if geo-electrical complexity exists at or immediately below the ocean floor. Since the MCSEM method is diffusive, deeper geo-electric features are physically less resolvable than shallower ones and can be discretised to represent this reduction consequential resolution.

An inversion was performed on the data produced from a single east-west oriented transmitter running over the centre of the body. The inversion discretisation consisted of  $41 \times 41 \times 21$  cells, each with a size of  $25 \times 25 \times 10\text{m}$ . The volume necessary for the inversion must be much larger than the anticipated target size (i.e. the gas hydrate body in this case). Inversions using components of the total electric and total magnetic fields in various combinations were performed. The inversions of each individual component is supported by the geometric sensitivity (GRI) shown in Figure B-4. An Ex only field was performed and analysed after 1



**Figure B-3:** Survey layout and the inversion results using the various EM components. (A) Survey layout over a shallow gas hydrate consisting of a single transmitter position and a grid of 11x11 receivers. This survey layout is to test the sensitivity of various electromagnetic components (Ex, Ey, Ez, Hx, Hy and Hz) on inversion. (B) Inversion using all components for a single transmitter after 5 focussing iteration. (C) Inversion results of Ex only data only for a single transmitter after 1 focussing iteration overlayed by the outline of the gas hydrate and transmitter location. The diffuse nature of electromagnetic fields is shown in the initial smooth model after the first iteration. (D) Inversion using Ex data only for a single transmitter after 5 focussing iteration. The Ex inversion is sensitive to the lateral edges inline with the transmitter location. It is also visible that broadside outline of the body is not sufficiently defined. (E) Inversion using Hz data only for a single transmitter after 5 focussing iteration. The vertical magnetic field is insensitive to thin resistive bodies and the inversion will never converge on a sensible result. (F) Ex only multi azimuth inversion results.



**Figure B-4:** Geometric response indicator of the various electromagnetic components for a transmitter line over a rectangular resistive body. Geometric response indicator (GRI) is a modelled attribute that describes the amount of EM energy expected to reach the seabed from the subsurface (Lindhom, Ridyard, and Wicklund 2007). The higher the indicator, the larger the impact it has on inversion. Higher responses are red and lower responses are blue.

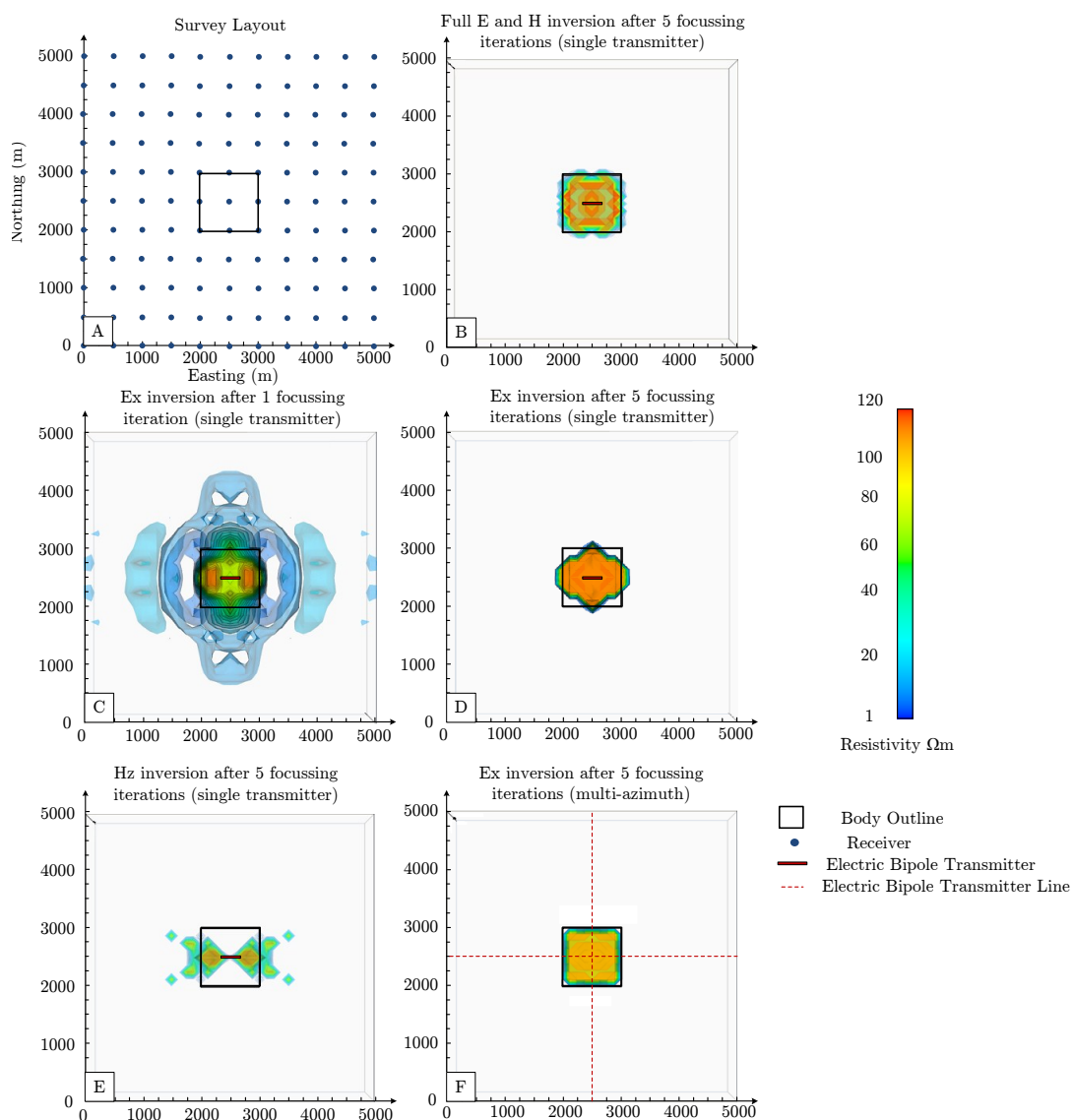
and 5 inversions (see Figure B-5). After 1 iteration a east-west resistive feature is apparent. After 5 focussing iterations the inversion was able to establish the inline edges of the resistive body. Conversely, it is well established that vertical magnetic fields are insensitive to thin resistors. This was made clear by the attempt to invert using Hz data (see Figure B-5). Both the Ex and Hy inversions correspond to the sensitivity analysis of the geometric response index (Figure B-4). The body was better characterised spatially using more orientations (e.g. a multi-azimuth survey) than if more components were included in the inversion (Figure B-5).

Constraining and preconditioning the geoelectric model is paramount. The resistivity thickness product also has an impact upon the received amplitude rather than resistivity alone. Phase behaves differently to amplitude. It appears to characterise the resistivity more effectively. However in many cases phase data collected in the field is highly inaccurate and if possible should be weighted separately from the amplitude data.

Various methods can be applied to obtain the basic input geometry or the resistivity of the target for field data. Resistivity information can be interpreted from well log resistivity (i.e. some modern induction tools can measure the full electrical conductivity tensor) and the target's geometry can be established using seismic or midpoint normalisation techniques. Resulting attempts to invert to the data without geoelectric constraints diverged and sufficient iterations were unsuccessfully completed. The models seen in Figure B-5 have been preconditioned to invert within  $1$  to  $120\Omega \cdot m$ .

## B.4 Conclusion

We have presented an inversion analysis methodology that has included the consideration of discretisation, weighting, preconditioning and the constraint of the geo-electric model. This method was successful at inverting synthetic data to a shallow synthetic rectangular gas hydrate. We have shown that the “geoemetric response indicator” (GRI) is linked to the sensitivity and convergence of the inversion process and provides insight into optimal design of inversion work flows. Our future work will move from synthetic case studies as presented here to analysis of inversion work flows for several MCSEM field data sets using both IE and FD forward modelling engines.



**Figure B-5:** Survey layout and the inversion results using the various EM components. (A) Survey layout over a shallow gas hydrate consisting of a single transmitter position and a grid of 11x11 receivers. This survey layout is to test the sensitivity of various electromagnetic components (Ex, Ey, Ez, Hx, Hy and Hz) on inversion. (B) Inversion using all components for a single transmitter after 5 focussing iteration. (C) Inversion results of Ex only data only for a single transmitter after 1 focussing iteration overlaid by the outline of the gas hydrate and transmitter location. The diffuse nature of electromagnetic fields is shown in the initial smooth model after the first iteration. (D) Inversion using Ex data only for a single transmitter after 5 focussing iteration. The Ex inversion is sensitive to the lateral edges inline with the transmitter location. It is also visible that broadside outline of the body is not sufficiently defined. (E) Inversion using Hz data only for a single transmitter after 5 focussing iteration. The vertical magnetic field is insensitive to thin resistive bodies and the inversion will never converge on a sensible result. (F) Ex only multi azimuth inversion results.

# Comparison of a vertical electric and a vertical magnetic source for cross well CSEM monitoring of CO<sub>2</sub> injection

---

## Contents

---

<b>C.1</b>	<b>Summary</b>	<b>228</b>
<b>C.2</b>	<b>Introduction</b>	<b>228</b>
<b>C.3</b>	<b>Method</b>	<b>229</b>
<b>C.4</b>	<b>Example</b>	<b>230</b>
<b>C.5</b>	<b>Conclusion</b>	<b>234</b>

---

## C.1 Summary

Controlled source electromagnetic transmitters create highly geometric coupled electric and magnetic vector fields that propagate in a way that is dependent on both the orientation of the transmitter and electrical conductivity distribution. There may be a good case for using cross well controlled source electromagnetic methods for monitoring injection of CO<sub>2</sub> into deep saline or brackish sandstone reservoirs. The expected range of geo-electrical frameworks that can be used to represent CO<sub>2</sub> injection into a saline or brackish sandstone water saturated reservoir is reasonably constrained. That is injection of CO<sub>2</sub> would likely create an expanding zone of elevated electrical resistivity that would move out from the injector well into the reservoir. The reservoir would typically be confined above and possibly below by conductive clay or shale dominated sediments. Given this type geo-electrical framework we consider the relative merits of a time harmonic vertical electric and vertical magnetic source for monitoring CO<sub>2</sub> injection. We compare numerically generated electric and magnetic fields created in a heterogeneous horizontally layered injection zone with and without injection of CO<sub>2</sub>. Examples are first provided for a layered earth and then for an expanding 3D volume within permeable layers. We provide images indicating that the vertical electric dipole source is sensitive to CO<sub>2</sub> injection into thin resistive sandstone layers in a conductive background. We explore why the more common vertical magnetic dipole source is comparatively insensitive to an increase in resistivity in thin sandstone layers. In summary the vertical magnetic dipole source is a common and practical in-hole source, however in principle the vertical electrical dipole source is likely to be more suitable for monitoring CO<sub>2</sub> injection. Certainly the use of a vertical electric dipole source would need to be facilitated within the monitoring well design. Ideally the monitoring interval should be open hole or at least the casing should be slotted, non-metallic and have considerable open area to the formation.

## C.2 Introduction

Electromagnetic techniques like MT (i.e. the magnetotelluric method) and LOWTEM (i.e. the Long Offset Transient Electromagnetic method) have been identified as possible technologies for monitoring large scale carbon dioxide (CO<sub>2</sub>) injection during sequestration. However for monitoring CO<sub>2</sub> injection into deep saline reservoirs both methods suffer from a significant problem. That problem is transmitter and receiver distance from the injection zone. This problem was highlighted by Suryopranoto (2009) who shows many examples of the rapidly diminishing “detectability” of electrically resistive gas filled layers with increasing depth for both LOWTEM and MT. Suryopranoto’s basic conclusion was that given typical surface noise levels and the ever present reality of electrical equivalence, depths greater than 1000 m would be highly challenging for any surface based electromagnetic (EM) method.

The potential of surface EM measurements for monitoring CO<sub>2</sub> injection could be significantly improved if inversion were constrained with resistivity distributions derived from cross-well, surface to hole or wire-line induction logging integrated with a geological framework developed from seismic reflection. That is, aside from independent monitoring of CO<sub>2</sub> injection, in-hole EM methods could act as an important constraint on inversion of surface EM measurements. This is because in-hole methods should robustly express the relationship between CO<sub>2</sub> injected and local conductivity changes in the injection zone. Considerable work remains before surface methods can claim a space in CO<sub>2</sub> monitoring, however if any success is to be achieved it is likely that time lapse in-hole measurements with EM methods will need to play a role.



Unlike time lapse surface EM techniques, time lapse induction logging has proved valuable for monitoring both CO<sub>2</sub> gas injection (Xue et al., 2006) and in monitoring injection of low solute concentration water for aquifer recharge projects (Malajczuk, 2010). Further multifrequency tri-axial induction logging tools are now available (Wang et al., 2006) and present the possibility of recovering full tensor conductivity by transmitting and receiving electromagnetic fields via small coils with multiple orientations (i.e. a 3C magnetic dipole transmitter and receiver system).

Background or pre-injection electrical conductivity distribution for CO<sub>2</sub> injection into a saline or brackish reservoir will likely be dominated by solute concentration distribution combined with clay/shale type and distribution. Solute concentration typically increases with depth, however the opposite can be true if basin hydrodynamic is such that lower solute concentration water is driven below clay/shale dominated sediments. However in general deep reservoirs are often highly saline and of little value as water supply. Changes in formation electrical resistivity that may be associated with injecting CO<sub>2</sub> into a saline reservoir are examined by Xue et al. (2006) and Kim et al. (2010). Laboratory tests of CO<sub>2</sub> injection into brine filled permeable sands tend to show greater change in resistivity than do results from time lapse induction logging. This difference is likely a result of clay content and the common use of vertical magnetic dipole (VMD) source and receiver EM logging systems (i.e. the typical induction logging tool). Such systems tend to be more “sensitive” to conductive layers. One clear weakness of using the VMD source for detecting resistivity layers is that it can only senses horizontal resistance to current flow if logging is completed a vertical hole penetrating horizontal layering. Field examples of the application of a vertical electric dipole (VED) source and receiver systems are far from common and often not ideally suitable for detailed cross well monitoring of CO<sub>2</sub> injection. Several studies consider the possibility of deploying a VED source in steel casing (e.g. Wang et al. (2006)). Many other model studies do exist (e.g. Kong et al., 2009 and Spies and Habashy, 1995).

### C.3 Method

One reasonable question to ask is, how are relative “sensitivities” for the various source configurations assessed. We choose to make a direct comparison of the EM fields computed for a VED and VMD source for geoelectrical models representing resistivity distribution before and after injection of CO<sub>2</sub>. We also compare a normalized amplitude. This is the ratio of vector field amplitudes before and after injection as a percent. Injection of CO<sub>2</sub> is geo-electrically represented by an increase in electrical resistivity in thin high permeability layers. That is, electrical resistivity increases in the layers where CO<sub>2</sub> has displaced some fraction of the saline or brackish water. The formulation for computing the electric and magnetic fields generated by a time harmonic dipole electromagnetic source is well known (e.g. Wait, 1970). We use open source software to compute the electromagnetic fields about different time harmonic dipole sources. These software include the general purpose 3D integral equation code Marco (Xiong, 1992) and the layered earth code Dipole1D developed by Key (2009a). These algorithms are coordinated by the java based EM data management and visualization software developed by Pethick and Harris (2012) (i.e. [www.MCSEM.com](http://www.MCSEM.com)).

A vertical magnetic dipole source within a horizontal layered earth will generate electrical fields circulating in the plane of the layering. That is, the electric fields generated by a VMD source have no vertical component. Conversely a VED source will generate magnetic fields that circulate in the plane of the layering. That is, for a VED source the generated magnetic fields will have no vertical component. Intuitively we should suspect that the VMD will be

relatively insensitive to an increase in resistivity for resistive layers as would be expected for CO<sub>2</sub> injection into thin high permeability sandstone layers within a more clay/shale dominated background. Our aim is to examine and illustrate the basic difference between a VMD and VED source. We do this by showing streamlines and or vector fields before and after injection for the VED and VMD source. We also provide sections showing the ratio of field amplitudes before and after injection as a percent. An example is provided below.

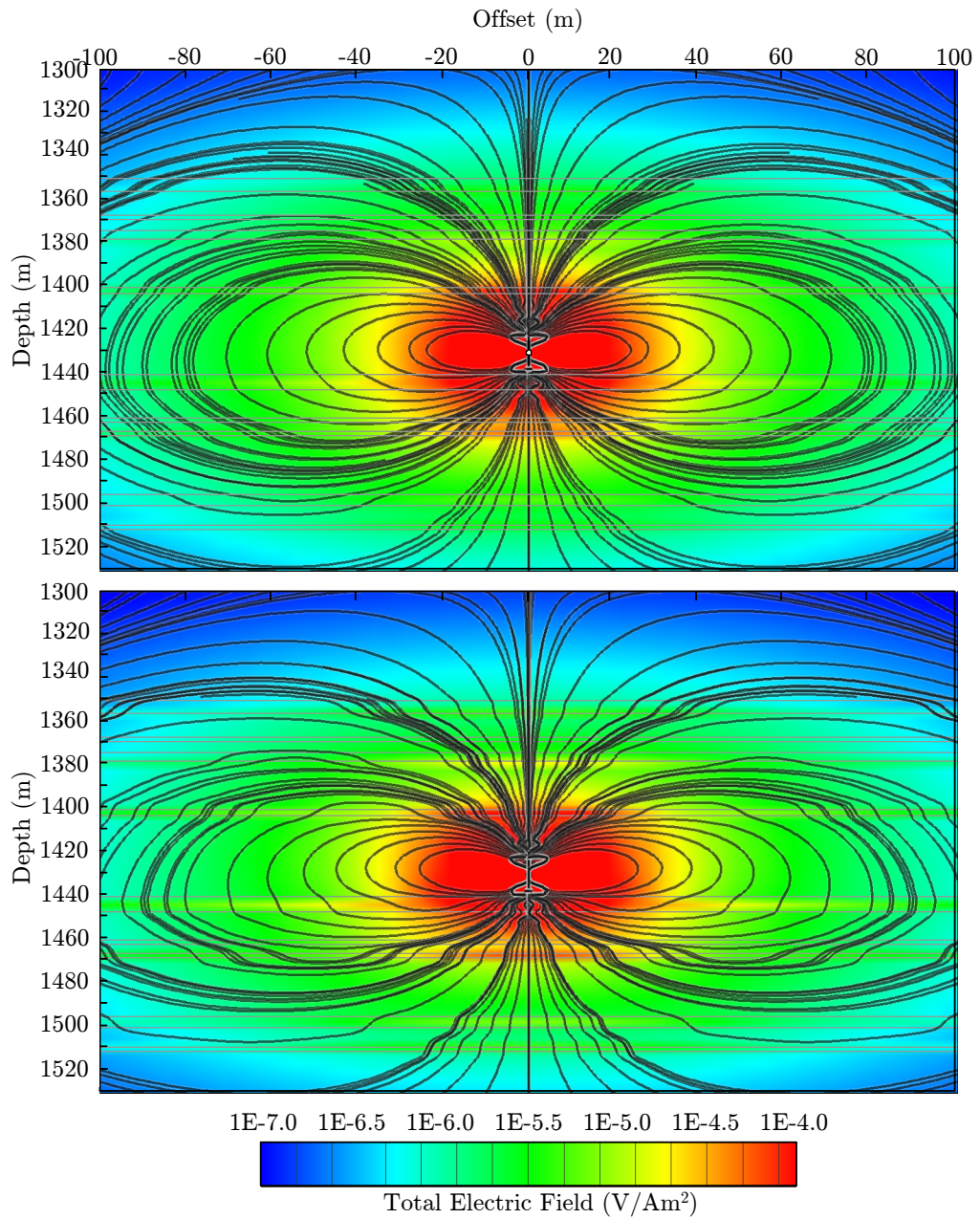
## C.4 Example

To illustrate difference between the VED and VMD source we chose a geo-electrical model broadly based on the distribution permeable sands in the lower approximately 200 m of the Paaratte Formation in the OTWAY basin, Victoria Australia (i.e., see Bunch, 2010). The Paaratte is a brackish reservoir and resistivity distribution can be observed from wire-line logs completed in drill hole CRC2 (Bunch, 2010). Drill hole CRC2 was completed as part of the Australian government funded CO<sub>2</sub>CRC research project. The example provided here compares electric field generated by a VED (see Figure C-1) and the magnetic fields generated by the VMD (see Figure C-2). The lower part of the Paaratte at CRC2 appears to be a heterogeneous mix of high permeability sandstone layers (e.g. plus 4000 mD) and generally lower permeability background sediments (e.g. silty, cemented and or shale dominated sediments).

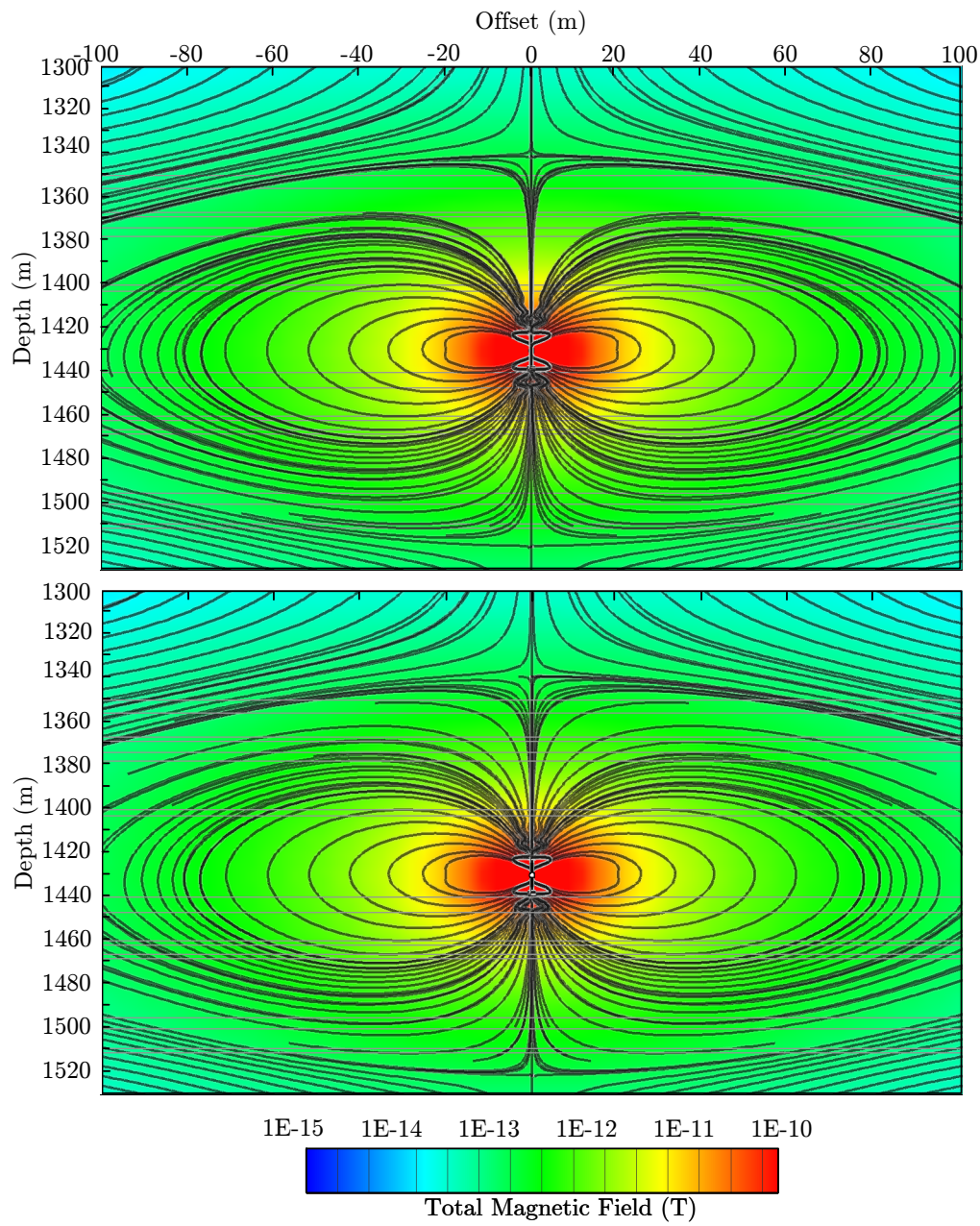
We have constructed a highly simplified resistivity distribution based on nine thin high permeability layers. We group all low permeability sediments as “background” and assign a resistivity of  $10 \Omega \cdot m$ . Higher permeability sandstone dominated layers are regarded as the “injection” intervals and are assigned a resistivity of  $20 \Omega \cdot m$  before injection. We assign the post injection resistivity (i.e. maximum CO<sub>2</sub> saturation) in the thin high permeability layers of  $40 \Omega \cdot m$ . Clearly formation complexity and the reality of CO<sub>2</sub> injection is far more complicated, with CO<sub>2</sub> expected to migrate and partly fill all connected porous layers. Also any change in resistivity related to CO<sub>2</sub> injection is highly dependent on post injection connectivity of residual saline or brackish water. Again the example provided is mainly intended to highlight the difference between a VED and VMD source for monitoring CO<sub>2</sub> injection into resistive thin sandstone layers. We compared EM fields generated at many frequencies and from many perspectives, however for this example a frequency of 1000 Hz is selected. We chose a relatively high frequency as monitoring should be expected to recover the detailed nature on injection. We have also considered a full range of transmitter positions however to illustrate the general principle in this example we show one position towards the middle of the injection zone (see the dipole position in Figures C-1, C-2 and C-3).

The strong impact of increasing the thin layer resistivity from 20 to  $40 \Omega \cdot m$  is clear from Figure C-1 (see the change in amplitude and direction of the electric field in bottom image). It is also evident from the stream lines that the direction of the vertical component of the electric field is significantly changed after injection. This is important because measurement with a VED receiving antenna in a vertical open hole or through perforated non-metallic casing is a far more reasonable proposition than the measurement of the other components. Ultimately cross well inversion constrained by well logs would be used to aid in recovering changes in formation resistivity related to CO<sub>2</sub> injection.

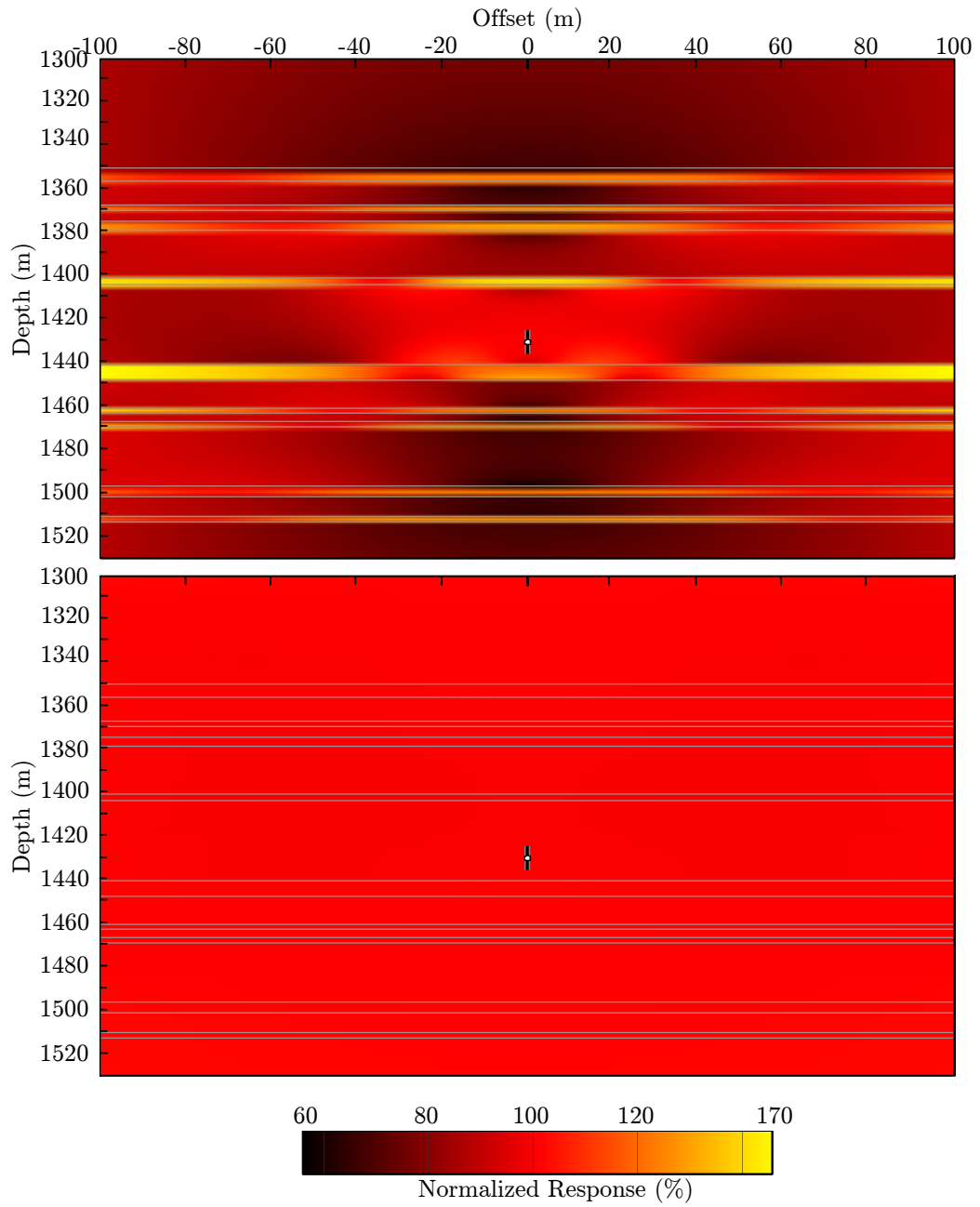
Figure C-2 serves to highlight how poorly the magnetic fields generated by a VMD source would express an increase in resistivity of thin sandstone layers. There is only small percent difference between the images above (i.e. less than a few percent). While an increase of 20 to  $40 \Omega \cdot m$  for the thin layers sees the electric field amplitudes resulting from a VED



**Figure C-1:** Vertical sections showing computed electric field stream lines around a VED source before (top image) and after (bottom image) injection of CO<sub>2</sub> into thin high resistive permeability layers. Injection of CO<sub>2</sub> is represented by an increase in thin layer resistivity from  $20 \Omega \cdot m$  before injection to  $40 \Omega \cdot m$  after injection. Background resistivity remains at  $10 \Omega \cdot m$ . The thin layers are marked in grey. The key point from the above is that an increase in electrical resistivity in the thin layers is expressed as a significant change in amplitude and direction of the electric field.



**Figure C-2:** Vertical sections showing computed magnetic field stream lines from a VMD source before and after injection into thin high permeability layers. Injection is represented by an increase in layer resistivity from 20 Ohm.m before injection to 40  $\Omega \cdot m$  after injection within a 10  $\Omega \cdot m$  background. Thin layers are marked in grey. The key point from the above is that the thin layers have negligible impacts on amplitude and direction of the magnetic field when resistivity is increased from 20 (top image) to 40  $\Omega \cdot m$  (bottom image).



**Figure C-3:** Top image shows the ratio of computed total electric field amplitude around a VED source before and after CO<sub>2</sub> injection and the bottom image shows the ratio of computed total magnetic field amplitude around a VMD source before and after CO<sub>2</sub> injection. The ratio is provided as a percent. CO<sub>2</sub> injection is represented by an increase in layer resistivity from 20 to 40  $\Omega \cdot m$  in the thin layers and background resistivity is 10  $\Omega \cdot m$ . Both images are shown with the same colours scale to highlight the significant difference in normalized responses in the thin layers.



increase in placed by more than 50% the magnetic fields resulting from a VMD source remain almost unaltered. We choose to make comparisons with magnetic fields generated by VMD source as this arrangement represents a commonly available cross well EM configuration.

Figure C-3 is provided to highlight the significant difference between a VED source and a VMD source. The percent difference in electric field around a VEM source before and after injection is mostly large and positive in all the layers (i.e. often more than 50%). That is time lapse changes for the VED are clear. We choose to provide an example with very thin layers for good reason. For monitoring CO<sub>2</sub> injection the objective should be to monitor in detail how the CO<sub>2</sub> passes from the injection well (e.g. screened or perforated interval) into the formation. Initially the injectant is expected to move out much faster in the high permeability layers than in the lower permeability layers. For the Paaratte the highest permeability layers are in places less than two meters thick. It is the rapid initial movement of CO<sub>2</sub> into high permeability layers and subsequent filling of connected porous layers that need to be monitored. We provide clear examples of why in principle measuring electric field around a VED should be preferred over measuring the magnetic field around a VMD. Although highly problematic it is still conceivable that horizontal electric fields could be measured around a VMD source. However the problem remains that EM response is dominated by current flowing in the more conductive layers for a VMD source. That is for a vertical hole penetrating thin horizontal layering the VMD source generates current that must travel in the plane of the layering and at best electric fields can only express horizontal resistance to current flow.

## C.5 Conclusion

Our work is intended to highlight the reasons why, in principle, a vertical electrical dipole source should be more suited to monitoring CO<sub>2</sub> injection into deep thin brine saturated sandstone layers when compared with a vertical magnetic dipole source. Our direct comparison of magnetic fields generated by a VMD and the electric fields generated by a VED source in a layered medium with and without CO<sub>2</sub> injection gives good insight into the relative merits of these two EM transmitter types. However given that only VMD cross well EM systems are in common use a full and practical comparison is problematic. That is, there are practicalities related to tool and casing design that in the short term may outweigh the theoretical benefit of one source over the other. For example the electrodes for a VED source or receiver should ideally be in direct communication with the formation. The ideal monitoring well design for a VED source and receiver system would be open hole (i.e. no casing) over the full injection interval. This is unlikely to be acceptable, so alternatively a monitoring well could be designed such that the injection interval were cased with slotted or perforated non-metallic materials.

In the long term a multi-frequency, multi-separation, multiorientation cross well EM system using electric and magnetic field transmitters should be able to provide full time lapse tensor conductivity for any conductivity distribution. For the present, steps to prototype and build new VED based EM systems for monitoring injection of CO<sub>2</sub> into deep permeable sandstone reservoirs are proceeding.

## Acknowledgements

We acknowledge the funding provided by the Australian government through the CRC Program to support CO<sub>2</sub>CRC research.

# Open Source Interactive Electromagnetic Modelling

---

## Contents

---

D.1 Summary . . . . .	236
D.2 Introduction . . . . .	236
D.3 Method and Results . . . . .	236
D.4 Interactive Data Investigation . . . . .	238
D.5 Conclusions . . . . .	240

---

## D.1 Summary

The marine controlled source electromagnetic method has developed during the last decade for direct hydrocarbon indication. Marine controlled source electromagnetic software is still in its infancy with only a small number of open source algorithms and even fewer integrated software environments. We have developed an open source software package to encourage the development and use of the marine controlled source electromagnetic method in both industry and educational institutions. The software was written in Java and was made to perform interactive real-time synthetic modeling for varying earth models or survey parameters.

## D.2 Introduction

The marine controlled source electromagnetic method (MCSEM) has been developed during the last decade to detect the presence of hydrocarbon. Development of marine controlled source electromagnetic software is still at its infancy in comparison to seismic. As a result, software is mainly available through commercial or research consortiums. This includes organisations such as EMGS, Interaction AS, Blueback Reservoir, Scripps Institution of Oceanography, CEMI and UBC. Buying software from these institutions may not be viable or inviting for many organisations, particularly if they are reluctant to venture into MCSEM. An open source paradigm removes financial constraints and encourages experimenting with this field. Seismic products ranging from Seismic Unix (Stockwell, 1997), (de Groot and Bril, ) , CPSeis<sup>TM</sup> (CPSeis, 2012) and numerous Fortran and C++ geophysical libraries have been successful in the open source market. For MCSEM modeling there are several algorithms that utilize open source licensing. These include Dipole1D written by Kerry Key (Key, 2009a) and Marco (Xiong, 1992), as part of the AMIRA software package (AMIRA, 2012).

Our open source CSEMoMatic (Pethick, 2012a) software package was developed for the benefit of prospective and in contribution to existing MCSEM communities including both commercial and educational institutions. CSEMoMatic facilitates rapid forward modeling and visualization of marine controlled source electromagnetic data through the integration of open source algorithms Dipole1D and Marco.

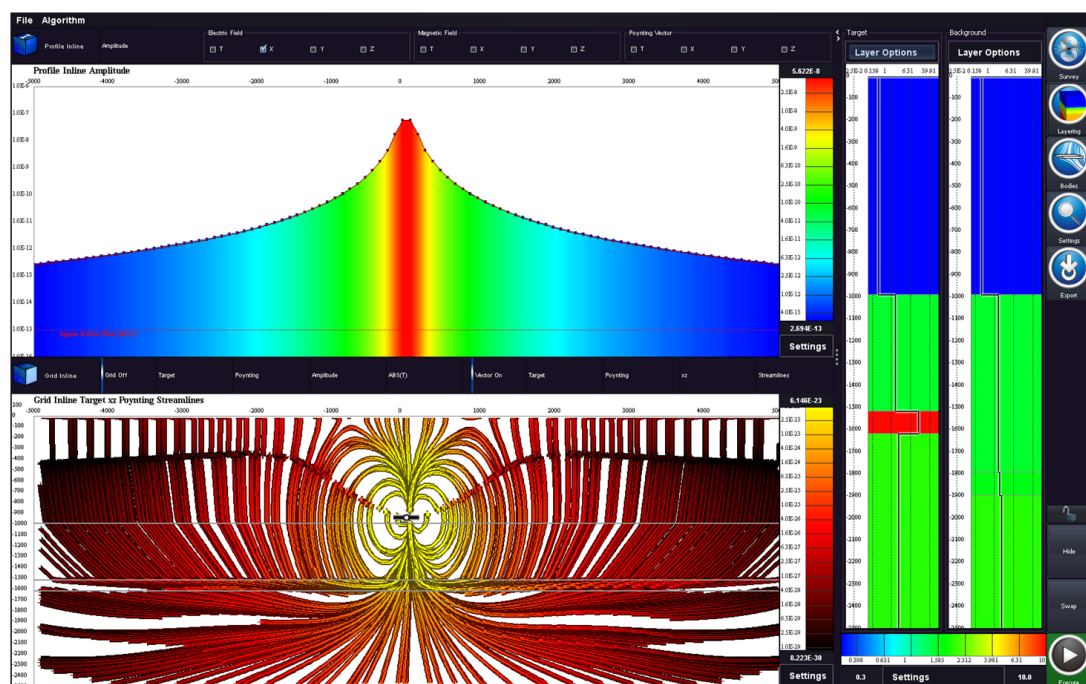
## D.3 Method and Results

CSEMoMatic is licensed under the GNU v3.0 agreement (GNU, 2007). The GNU GPL license allows the free modification and distribution of source code.

We developed the software as an interactive 3D forward modeling package using Java 1.6 SDK with Eclipse Ganymede IDE. Java was used because of its portability and object oriented design. Our software was designed to work under Debian Linux, Mac OSX and Windows operating systems. One of the objectives was to develop the software to be algorithm independent, but a number of algorithms had to be integrated. This was achieved by using a generic data structure, by writing methods to import and export data and by providing command line execution tags. As of now, the Dipole1D (Key, 2009a) algorithm and AMIRA's 3D Integral Equation Marco (Xiong, 1992) algorithm have been integrated into CSEMoMatic. An in program screenshot is seen in Figure D-1.

We have employed every effort to make our software interactive, efficient and intuitive. The 14 Principles of Polite Applications (Cooper, 1999), 8 Golden Rules of Human Computer Interaction (Shneiderman and Ben, 1998) and 10 Usability Heuristics (Nielsen, 1994) were





**Figure D-1:** A in program screenshot of CSEMoMatic. The top panel shows the target inline Ex field profile. The bottom shows the target pointing vector streamlines. The right panel contains the settings for the software including survey, geoelectric, visualization and export parameters. The earth layers, transmitter, colour scales and grids are multi-touch interactive.

applied to make the software as interactive and user friendly as possible. CSEMoMatic was designed primarily to be used without a keyboard and can be easily transferred onto a modern touch screen tablet on either Windows or Linux operating systems.

The primary goal of our software is to perform interactive real time forward modeling. All user interactions can be performed by using a mouse. The effect of parameters can be investigated by a mouse drag. The software encapsulates input file creation, importing and sorting export files and visualising data. This reduces user input and improves modeling speed. Rapid forward modeling improves the ability of users to understand how selected parameters influence data. One of the primary uses of our software is to perform feasibility studies. Target detectability can be established for various survey parameters by comparing the electromagnetic responses generated by target and background geoelectric models. Using Dipole 1D and Marco algorithms each synthetic electromagnetic response must be independently computed for each geoelectric model. Using this concept, the execution of target and background models can be multithreaded. Since each model is independent, there is a 50 percent improvement in execution time over batch execution.

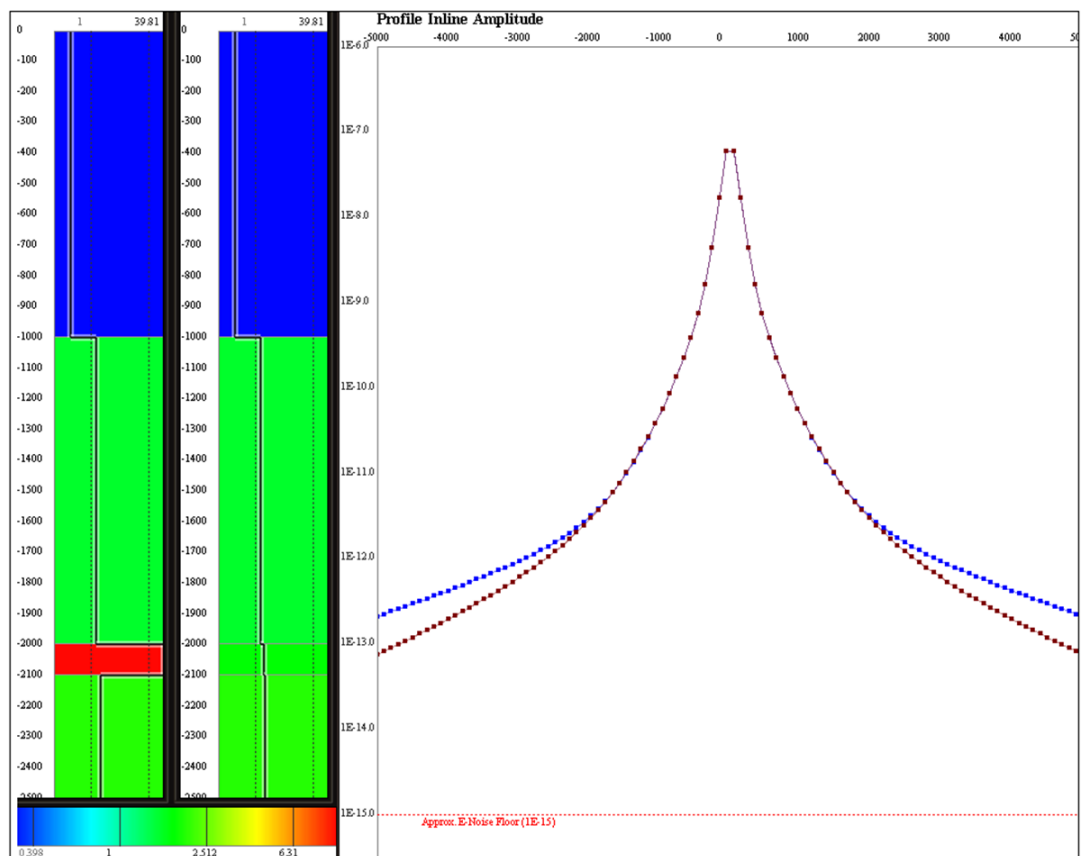
Importing, sorting and displaying of a single transmitter and transmission frequency for 100 receivers over a 1D layered earth requires 0.16 seconds using Dipole1D on an Intel Core 2 Quad 2.4GHz for each execution. The execution of the algorithm is the time limiting factor. It constitutes 99.8% of the total time between the interaction and visualization. Figure D-2 shows an interactive geoelectric model and the corresponding 1D target and background responses. In addition to this, a  $20 \times 20$  2D grid is updated every 0.5s.

Real time 3D modeling is restrictive due to limited modeling speeds of Marco3D and CPU speeds. For example, a survey with a 200 cell ( $8 \times 5 \times 5$ ) 3D prism requires 3.3 seconds and 7.9 seconds for the same survey profile and grid respectively.

## D.4 Interactive Data Investigation

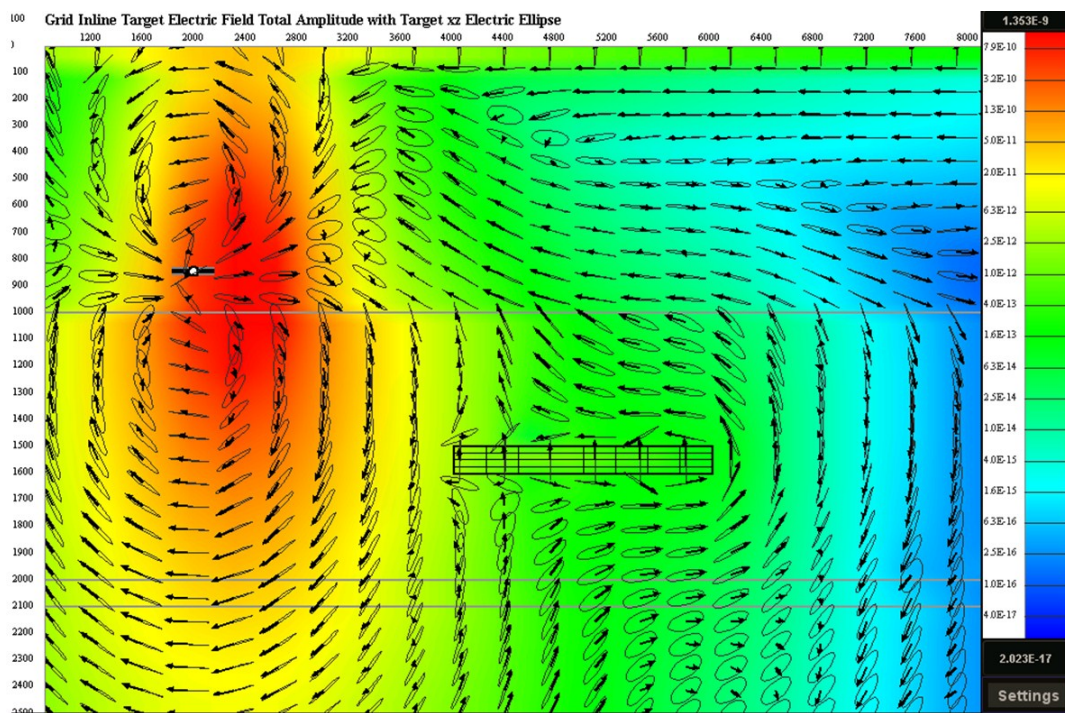
The interaction of an electromagnetic field with a 3D resistive body is complex. Attempting to understand the behavior of the field by using profiles is both unproductive and exhausting. The interaction of field paths with their geoelectric environments can be clearly explained by using other representations. A number of features have been created to assist in the understanding of the electromagnetic fields generated from an MCSEM survey. The ability to visualize any component independently is required (i.e. inline, broadside and vertical components of the electric, magnetic and Poynting vector fields) to perform a thorough investigation. The electromagnetic field is typically analyzed by comparing amplitude, normalized amplitude, phase and phase difference and real and imaginary components. Our software allows the visualization and interpretation of these common properties. Interpreting these representations may be complex. A number of atypical representations are used to demystify complexities in the electromagnetic field. These include amplitude time series, polarization ellipses, time varying vectors and 2D streamlines.

For example, polarization ellipses represent the full range of time domain vector orientations as a single static structure. They illustrate the polarization of the electric, magnetic or Poynting vector fields on any 2D plane (i.e. Inline, broadside or plan). Figure D-3 shows a typical total electric field amplitude inline grid from a horizontal electric dipole for a 1D layered earth with a resistive three-dimensional body. The Figure also overlays the inline (x-z) electric field polarization ellipses with the initial field vectors at zero time. Perturbations in fields due to the presence of the resistive body can be seen; wrapping around the resistive prism resulting



**Figure D-2:** CSEMoMatic profile modeling. A single electric bipole transmitter and 100 multi-component electromagnetic receivers are positioned over two 1D geoelectric models (left) in turn, and these are forward modeled and visualized (right) within 0.16s on a Intel Core 2 Quad 2.4GHz (approximately six updates per second).

in a varied field on the ocean floor.

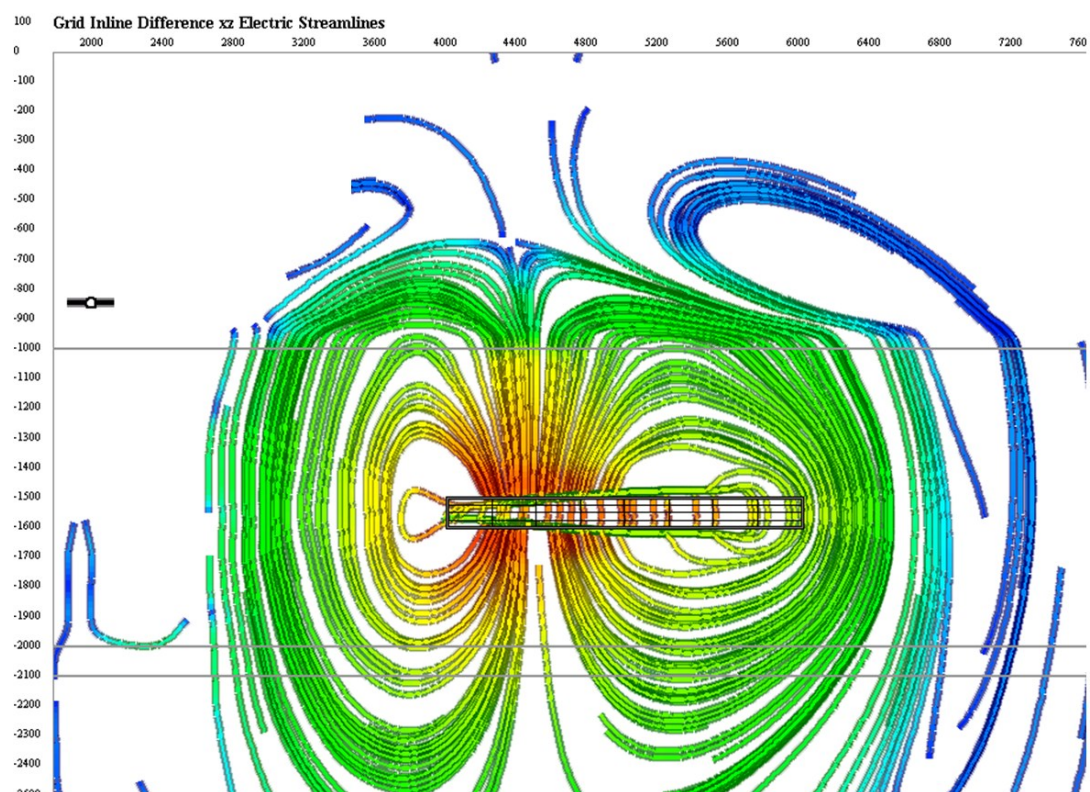


**Figure D-3:** Inline total electric field electric field amplitude grid and inline electric field polarization ellipses resulting from 1Hz horizontal electric dipole transmitter.

It may be necessary to investigate the influence of a single geoelectric feature. This is performed by calculating the difference in the electromagnetic fields between two geoelectric models. The background response (layered response) in this example is subtracted from the total field response (layered and 3D prism response). Streamlines can be used to show the flux lines from electromagnetic sources. We have used second order interpolation to quickly approximate the streamline path in our implementation. Figure D-4 shows scattered streamlines at the maximum transmitted amplitude. The physical mechanism behind the variation in profiled data can be explained by using this representation. The streamlines can be interactively placed in any area of interest. Streamlines are added by painting seed positions in the synthetic data.

## D.5 Conclusions

Marine controlled source electromagnetic software is still in its infancy. An open source marine controlled source electromagnetic modeling package has been created. This software will facilitate research and further development to introduce its use for organizations reluctant to enter the MCSEM market. Our software CSEMoMatic allows the free modification and distribution of its source code. It was written in Java for use in multiple operating systems. The software has a generic data structure tailored towards MCSEM, allowing the integration of any suitable algorithm; proprietary or open source. CSEMoMatic was created to be interactive. 1D modeling can be performed interactively in real time, allowing users to rapidly investigate the effect of varying the survey and geoelectric parameters. 3D modeling and 2D visualization can also be performed. Static profile representations of data were found to be inadequate due



**Figure D-4:** Scattered (target minus background response) streamlines resulting from a 3D prism in a 1D Layered earth. The colors represent amplitude. Using this representation, complex variations in profiled data can be easily explained.

to the complex nature of electromagnetic fields. The software visualizes fields in the form of polarization ellipses, vectors and streamlines to overcome this. Overall our open source software was successful in the application of real time forward model and gives the users to represent and understand electromagnetic data with greater ease.



# Computing, Brains and Geophysics?

---

This chapter has stemmed from my personal interest into brain computer interfaces. I use the NeuroSky Mindwave, an electroencephalographic device and interface the device with my software, CSEMoMatic. I used it to control different parameters and in turn interactively model the electromagnetic CSEM response. To my knowledge, this is the first brain controlled geophysical software package. Despite being rudimentary, I investigate the application of brain controlled interfaces (BCI) in geophysicist training. BCI has the potential for widespread future application within the next 10 to 20 years rather than being limited to CSEM or geophysics.

I have written this article with my PhD supervisor Dr. Brett Harris and medical practitioner Dr. Karen Cathy Lam (MBBS) as an expanded abstract and as a full journal article for the ASEG 2013 geophysical conference, Melbourne.

## Contents

<b>E.1 Overview</b>	<b>244</b>
<b>E.2 Introduction</b>	<b>244</b>
<b>E.3 Methodology</b>	<b>246</b>
<b>E.4 Results</b>	<b>247</b>
<b>E.5 Discussion</b>	<b>250</b>
<b>E.6 Conclusion</b>	<b>250</b>

---

## E.1 Overview

Brain computer interface (BCI) systems emerging as a breakthrough technology of the 21st century. As is the case with other developing technologies, proof of concept must be demonstrated before advanced methods are pursued. This article presents the first published case study of a brain controlled geophysical software package. We show how brain computer interface systems can facilitate accelerated learning in the geoscience community. Our results show that processed brainwaves from the NeuroSky MindWave electroencephalography (EEG) device can be used to control various geophysical survey parameters with an acceptable degree of accuracy and to model the corresponding data in real-time.

## E.2 Introduction

Brain computer interface (BCI) systems establish a connection between the brain and the computer. Progress in the area of computational neuroscience has exploded over the last 30 years. Accelerated development has been observed in the area of brain computer interface systems providing improved communication, recording and control capabilities (Ekandem et al., 2012). There is an increasing use and demand for BCI systems including applications such as lie detectors that use functional magnetic resonance imaging (fMRI), video games controlled using electroencephalography devices (Ekandem et al., 2012). The increase in use and development of BCI can be attributed to improved signal processing, electrical components and growing awareness of its capabilities. BCI works by measuring, processing and translating the electrical signals of the brain into a computer response. No geophysical software controlled by BCI technology exists to our knowledge. The acquisition device we have used for our experiment is the NeuroSky MindWave (Neurosky, 2012).

The NeuroSky MindWave is one of the first commercially portable electroencephalography (EEG) devices (Neurosky, 2012). It functions as a lightweight and wireless basic EEG device. An EEG measures the electrical activity recorded at the level of the scalp by electrical potentials generated from the firing of neurons during various levels of mental activity (Hall and Guyton, 2011). It is commonly quoted that the human brain contains 100 billion neurons and ten times more glial cells, but the absolute number of neurons remains unknown (Azevedo et al., 2009) but it is expected that the number remains in the billions. These neurons generate electrical signals which are propagated throughout the brain. This can be likened to a complex system of electrical wires. In order to generate recordable electrical potentials at the level of the scalp, an action potential (i.e. a voltage) must be generated.

An action potential is a chemically induced process resulting in a rapid change in the cells membrane potential. This rapid change produces a voltage. The action potential allows the transmission nerve signals along nerve fibre membranes. A complex series of chemical changes must occur within a nerve fibre in order to generate an action potential, explained at length in Hall and Guyton (2011). This process begins with the normal resting membrane potential of approximately -90mV. An influx of positively charged sodium ions into the cell via open sodium channels pushes the resting potential into the required voltage threshold (approximately -55mV) to produce an action potential. The action potential is terminated by both the inactivation of the initial sodium channels opening and then the opening of potassium channels, allowing positively charged ions to escape out of the cell returning the nerve fibre membrane to its original state (Hall and Guyton, 2011).



Many action potentials occur throughout the human brain, which generate a potential difference, measured in voltage. An EEG device consists of several electrodes placed on the scalp that measures the potential difference between these electrodes (Schalk et al., 2004). The EEG records transient potentials generated from synchronous firing of individual neurons, the sum of which is sufficient to be recorded from the scalp (Hall and Guyton, 2011 and Nunez and Srinivasan, 2006). These transient potential differences are transformed into frequency bands via the fast Fourier transform (NeuroSky, 2009).

Neurons acting together at a specific moment in time to perform a specific function or task, oscillate at particular frequencies (Demanuele et al., 2012) which have been grouped into frequency bands. The universally accepted EEG bands include theta ( $\theta$  4-8Hz), alpha ( $\alpha$  8-13Hz), beta ( $\beta$  13-30Hz) gamma ( $\gamma$  30-49Hz) and delta ( $\delta$  0.1-3Hz) (Miller, 2007; Demanuele et al., 2012; NeuroSky, 2009; Hall and Guyton, 2011). Alpha, beta and gamma waves are found in the normal waking EEG (i.e. alert state), whereas theta and delta activities are rarely found in wakefulness (theory of normal waking EEG article).

Alpha waves indicate relaxed consciousness (NeuroSky, 2009) or being awake but at rest (Hall and Guyton, 2011). It has also been traditionally thought of as an “idling rhythm” (Miller, 2007). Beta waves represent a level of increased alertness (NeuroSky, 2009) and manifests when a person has their attention focused on specific mental activities (Hall and Guyton, 2011). The degree of alertness is differentiated by the amplitude level in sub-frequency bands within the greater beta frequency band. The higher the beta frequency spectra the greater the agitation, while the lower frequency spectra indicates wakefulness and alertness without agitation (NeuroSky, 2009). The gamma band is of the highest frequency and is thought to represent motor functions and higher level mental activity (NeuroSky, 2009). The theta band is thought to encapsulate creativity and imagination (NeuroSky, 2009) and more commonly found in children but can be found in adults in moments of emotional stress and in those with degenerative disorders of the brain (Hall and Guyton, 2011). Delta is associated with deep, slow wave sleep (Hall and Guyton, 2011) and unconsciousness (NeuroSky, 2009). Other research suggests that lower frequency oscillations of delta, theta and alpha waves are useful for integration across far flung cortical regions (Knyazev, 2011). Higher oscillations of gamma and beta are thought to handle localised computations, which do not require the same level of integration between various cortical areas (Knyazev, 2011). We focus on the ‘attention’ and ‘meditation’ components of the brain wave. We utilise the Neurosky derived values of alpha and beta waves.

The Neurosky Mindwave records a 12 bit voltage at 512Hz with the measurements recorded as raw voltage. These signals are processed by the proprietary NeuroSky Mindwave drivers and processing algorithm, ‘eSense’, into values labelled as ‘attention’ and ‘meditation’, the neuroscience defined frequency bands are also computed (NeuroSky, 2009). An ‘eSense’ blink detector is also included in the NeuroSky package (NeuroSky, 2009) but has not been utilised in our study. These ‘eSense’ readings are recovered at 1Hz intervals and attention and meditation values are derived from the alpha 1 and 2 (attention) and beta 1 and 2 (relaxation) waves respectively. Attention is related to focus whilst meditation is related to relaxation.

BCI systems have been used throughout the world at an ever increasing rate and we are only truly beginning to see its full potential. BCI systems have traditionally been used in medical settings, for example in assisting patients with severe motor disabilities (Dornhege et al., 2007), in assisting wheelchair navigation (Leeb et al., 2007) and even controlling a virtual keyboard through spontaneous EEG Activity (Obermaier et al., 2001). BCI systems have

also been implemented in the field of geophysics. The experiments involve the application of understanding geophysical data interpretation (e.g. Sivarajah et al., 2012). The continued development of this technology suggests a possible future where BCI systems would be able to control computer interfaces at unprecedented levels. Intel Corp. research scientist Dean Pomerleau suggests that users may be able to surf the web and open documents by the year 2020 (Gaudin, 2009).

Our goal is to perform the first proof of concept experiment to show that brain controlled geophysical software is possible. Using the developed BCI software we believe that BCI technology can assist in the training of geophysicists through associating a particular geophysical data state with a thought pattern (i.e. classical conditioning). Participants are in direct control of the survey parameter and associate the change of on-screen data with their level of focus, as measured by the BCI system. This learning method is similar to Pavlovian associated style (Baeyens et al., 1995) where the amount of mental effort required is remembered to achieve a particular stimulus (i.e. the visualised data). We propose that brain controlled geophysical software packages can provide an accelerated learning environment.

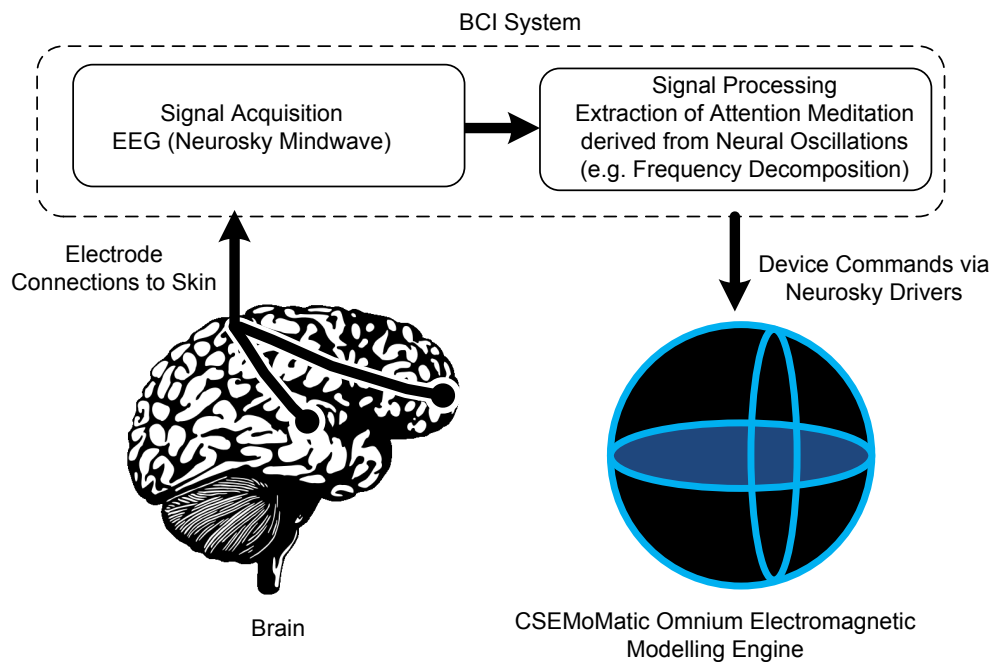
### E.3 Methodology

Achieving a brain controlled software is possible by creating a BCI system which enables communication between the brain and the software. The recording apparatus used is the NeuroSky MindWave EEG device. The Neurosky device is a non-invasive head piece which consists of a dry electrode placed on the forehead skin above the prefrontal cortex of the brain and a dry bipole electrode clip that attaches to the right earlobe. Standard EEG systems have reference points, many located either at the earlobe or on the mastoid process (NeuroSky, 2009). In the case of the Neurosky, the signals are collected from the forehead site are compared with the reference point (i.e. the earlobe). These points are chosen as reference points as they are unaffected by cerebral activity (NeuroSky, 2009). The Neurosky Mindwave EEG then measures the difference in the activity between what is known as the 'active site' (i.e. forehead) and the reference point (i.e. earlobe). As a result, it mainly captures activity at the prefrontal cortex. Beta waves are recorded primarily from the frontal region of the brain during activation and alpha waves are also recorded from here, although these tend to occur more intensely at the occipital region (Hall and Guyton, 2011).

We are using the ThinkGear Communications Driver (TGCD) written in C/C++ programming language. These drivers are connected to Java through JNI (JNI, 2012). These drivers reads serial device output and parse the incoming data stream. A training program was also created using The ThinkGear drivers. The training program allows users to control an on screen virtual ball. The ball's position was dictated by the amount of user concentration (i.e. the NeuroSky derived attention value). The training program allows users to practice controlling their 'thoughts'. These drivers were integrated into our CSEMoMatic EM forward modelling engine. CSEMoMatic (Pethick and Harris, 2012) is an interactive 3D electromagnetic forward modelling engine built for marine controlled source electromagnetic investigations. The interactive modelling engine ran the Dipole 1D MCSEM modelling algorithm (Key, 2009a), providing real time feedback to the user. The CSEMoMatic engine computes and visualises data from 1D CSEM surveys in real time. Updates to survey and geo-electrical parameters invokes the recalculation and visualisation of MCSEM data. We linked selected parameters directly to the processed NeuroSky attention stream. As the neurosky input value varies, the on screen data continuously updates. The 1Hz limitation in attention calculation (i.e. updates

to the attention stream occurs every one second). To overcome the slow and potentially 'jarring' updates the attention stream is sub-sampled to 10Hz (i.e. 0.1s). The stream is linearly interpolated between each recording to produce smoother forward modelling updates. Our BCI CSEMoMatic build was then executed on an ASUS EP121 tablet. To reduce this experiment's complexity we used the touchscreen, removing the need for keyboard input. Our experimental setup is described below in Figure E-1. This configuration is found in most BCI setups (e.g. Schalk et al. (2004), Xu et al. (2004) and Guger et al. (1999)).

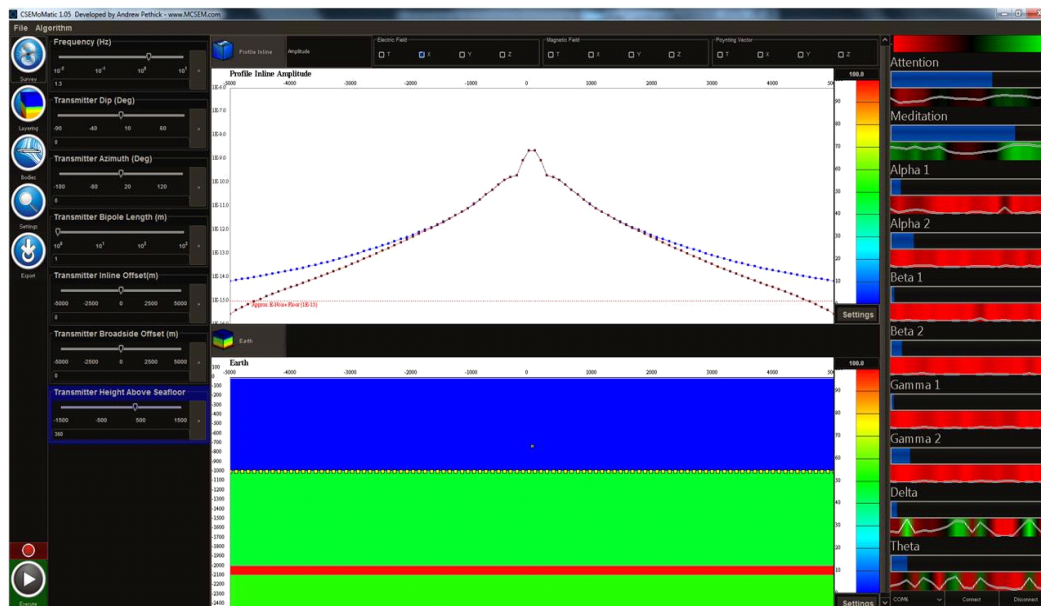
We tested the our BCI geophysical modelling program with eight subjects, each having varying levels of geophysical knowledge. Each person was given a training exercise for about 20 minutes to control the virtual ball using the training program (Figure E-3). The ball was raised and lowered in direct relationship to the user's concentration. Once the user was able to sufficiently control the ball they were asked to control the CSEMoMatic software. A screenshot of the CSEMoMatic engine running with the NeuroSky drivers can be seen in Figure E-2. The interface has three components, the parameters, data viewer and Neural and eSense recorder. Figure E-2 has two visualised panes, the survey layout showing electromagnetic receiver locations, earth model and the electrical bipole transmitter position and orientation. The experiment tests the influence of the vertical transmitter position on the data.



**Figure E-1:** The brain controlled interface system (Derived from Schalk et al., 2004)

## E.4 Results

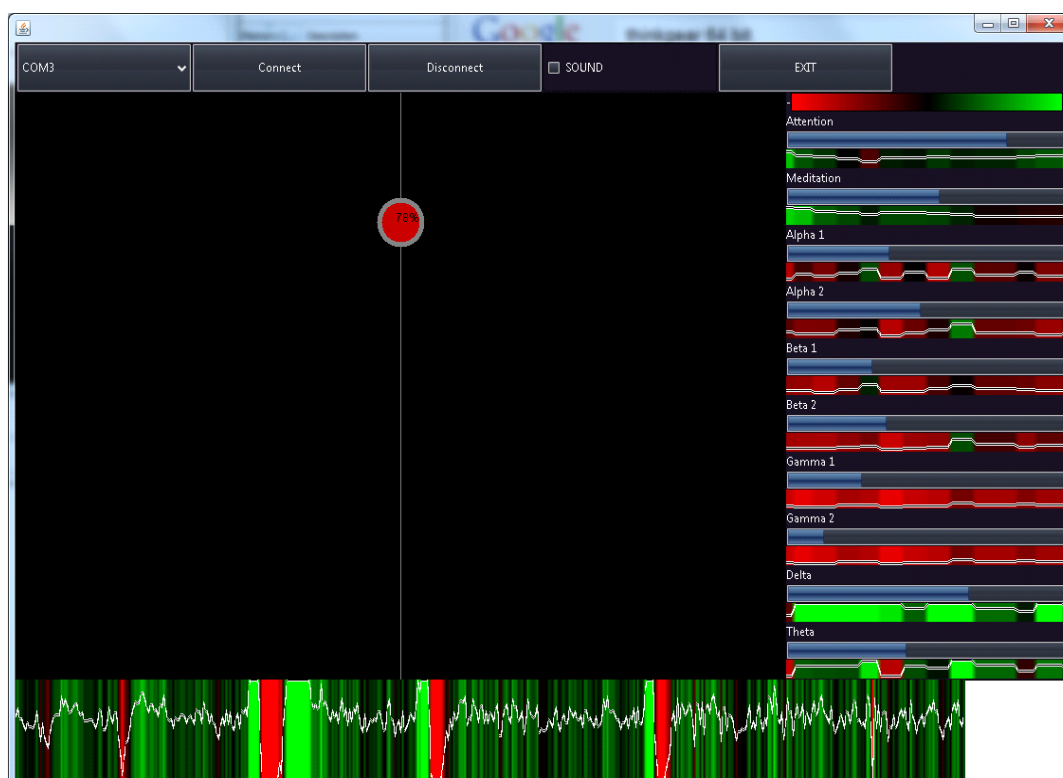
The experiments were carried out on the real time interactive BCI MCSEM modelling program utilising the Neurosky Mindwave EEG device. All users successfully raised and lowered the



**Figure E-2:** Screenshot of the BCI connected CSEMoMatic forward modelling engine. The BCI System parameters can be seen on the right of the screenshot. The main component is the attention bar. This attention level is connected to the transmitter height above sea floor survey parameter highlighted in blue on the left side of the screenshot. The data is interactively modelled and the resulting dataset is visualised (center-top) along with the corresponding survey geometry (center-bottom).

virtual ball within the training program. We found that the optimal approach to control the position of the ball was to imagine the ball rising to increase its height and lowering it by relaxing and de-focusing. For our experiment we used transmitter height above sea floor as our parameter. It was chosen to best replicate the training exercise. For BCI controlled CSEM modelling all users were able to control the vertical position of the transmitter location with varying degrees of accuracy in all eight cases. The positioning of the transmitter was highly granular, with it being located within  $\pm 5$  to 30% of the desired vertical location. The transmitter position ranged from -1500m to 1500m height above sea floor, which correlated with an error of between 150 to 750m.

The participants observed the effect of transmitter height on the modelled CSEM data for 5 to 10 minutes. They were then asked to describe the influence of the changing transmitter height on the 1D MCSEM data. All participants were expected to describe the flattening of the profile and reduction of peak amplitude with increased distance from the seafloor. All participants could describe this effect accurately. However, most found it difficult to fully control the ball's position and interpret data concurrently. This effect had been described by various participants as a "vicious cycle", "highly dynamic" and "overwhelming". Users could not easily examine data associated with a low transmitter positions (i.e. low attention level) because attention increased the moment they begin to examine the data. This effect was cyclical. The users were also asked to perform the same experiments with frequency and transmitter inline offset. The results were similar but not as successful due to the dissimilarity to the ball training exercise.



**Figure E-3:** A Screenshot of the Neuro Training Program. This training program taught each participant how to control a virtual ball with concentration. The balls position is related to concentration level. The higher the attention, the higher the position of the ball.

## E.5 Discussion

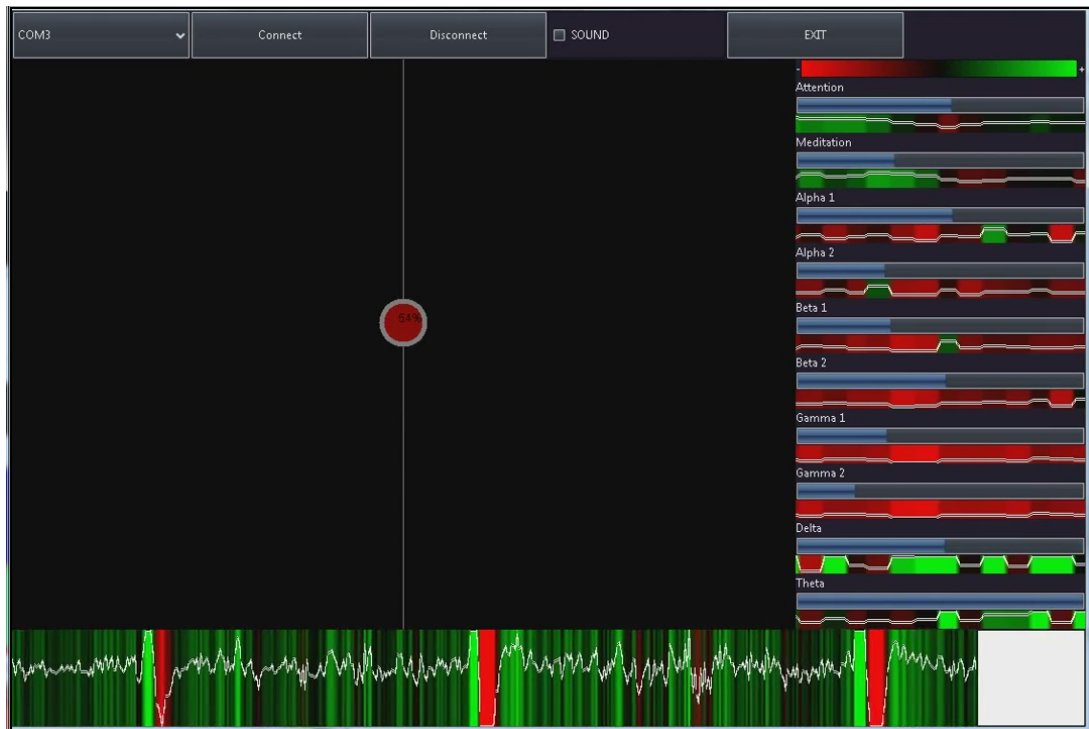
This study was designed to prove that BCI systems can be successfully applied to geophysical modelling and learning. Despite the successful implementation, we found there were more pitfalls than benefits in using BCI systems for operant conditioning. Firstly participants required 10 minutes or more to learn how to operate the device before using the system. At the start of training many users felt that the virtual ball was in fact "controlling itself", but could control it with varying degrees of success after several more minutes. The training period varied widely due to different testing environments, participant rest levels and characteristics individual to the participant. A freshly rested participant in quiet room with no distractions produced the best results.

The experiment was only designed as a proof of concept and was made simple to match the EEG apparatus limitations. Typically subjects found the learning experience too dynamic since modelling results changed with varying attention levels. Data changes occurred when users interrogated the data, resulting in a further changes in attention levels and in turn transmitter location. This compounding effect was not considered to be an effective learning experience despite the all participants describing the effect of changing parameters on the data.

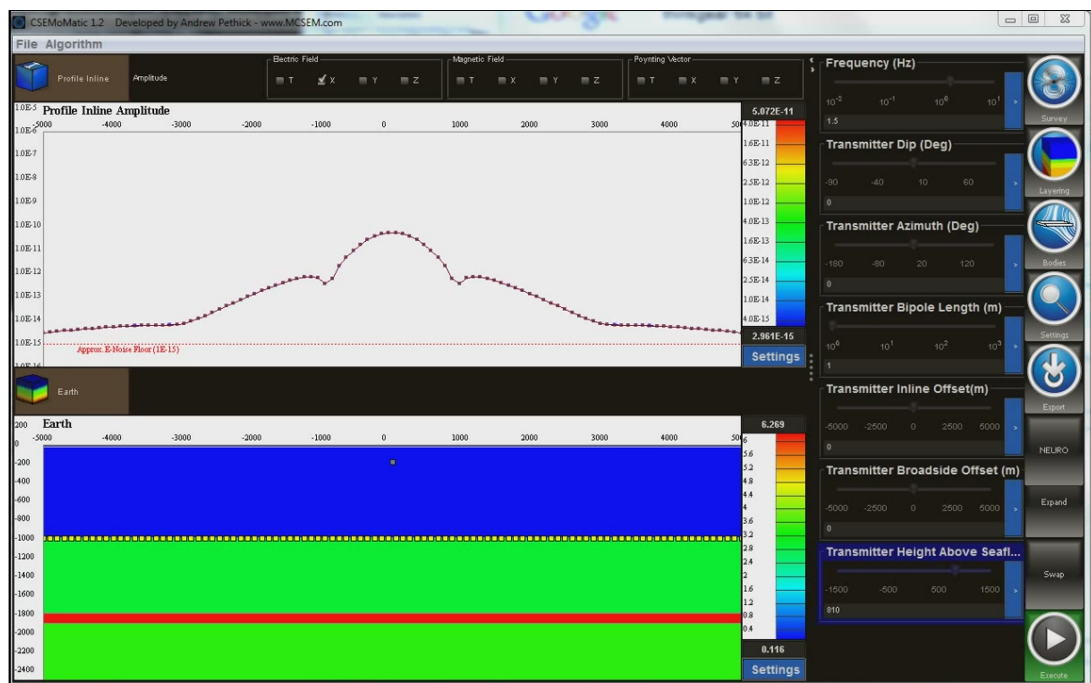
Overall the BCI program could be controlled by using only brain signal, but with varying success. That being said, using traditional user input such as the keyboard and mouse would still be considerably superior to BCI systems.

## E.6 Conclusion

The results show that it is possible to control geophysical software using a BCI system. The training phase was considered to be most crucial for achieving this. The level of control over the BCI software depended on both individual and environmental conditions. All participants were successful in describing the effect of parameter variation on marine controlled source electromagnetic data. However, the level of success was limited due to what was described by participants as strong cyclical and compounding thought levels. Despite this setback the experiment did show some level of connection between thought level and the effect on parameter variation. The emerging field of BCI systems has many hurdles to clear before reaching functionality but we hope this pioneering proof of concept experiment demonstrates the feasibility of future brain computing applications in geophysics.



**Figure E-4:** Neuro Training Software.  
See [Videos/BCITraining.mp4](#) for video source



**Figure E-5:** Neuro CSEM Modelling Software.  
See [Videos/BCISoftware.mp4](#) for video source





# Copyright Release Information

---

CSIRO PUBLISHING

***Licence to Publish***

Exploration Geophysics

Manuscript No. ASEG2010ab198Title of the paper (the 'Work') Conditioning of the 3D Marine Controlled Source InversionCorresponding Author Andrew Pethick

By submitting this paper, the Author (Authors if a multi-authored paper) has the right or has obtained authorisation to enter into this Licence and agrees to its submission by signing below.

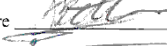
The Author warrants that the Work:

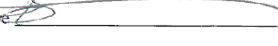
- Has not been published before
- Is not presently being considered for publication elsewhere
- Does not violate any intellectual property right of any person or entity
- Does not contain any subject matter that contravenes any laws (including defamatory material and misleading and deceptive material) and
- Meets ethical standards applicable to the research discipline.

**Terms of the Licence to Publish**

1. In consideration for publication of the Work, the Author grants to the Australian Society of Exploration Geophysicists, through **CSIRO PUBLISHING** (the 'Publisher') an exclusive worldwide licence to:
  - o Reproduce, publish and communicate the Work, or any part of the Work, to the public in any and all media, whether existing before or after the date of this Licence, for commercial, educational and all other purposes for the full remaining term of the copyright subsisting in the Work in each applicable jurisdiction
  - o Approve fair and reasonable permission requests from third parties to reuse material contained in the Work for the purpose of study, research or subsidiary publication.
2. In addition to the Author's moral rights in respect of the Work, the Author retains the right to:
  - o Use copies of the work for non-commercial purposes within his/her institution subject to the usual copyright/licencing agency arrangements
  - o Use the work for further research and presentations at meetings and conferences
  - o Use the illustrations (line art, photographs, figures, plates) and research data in his/her own future works
  - o Share print or digital copies of his/her work with colleagues for personal use or study
  - o Include the work in part or in full in a thesis provided it is not published for commercial gain
  - o Place his/her pre-publication version of the work on a pre-print server
  - o Place his/her pre-publication version of the work on a personal website or institutional repository on condition that there is a link to the definitive version on the **CSIRO PUBLISHING** website.
3. The Author agrees to:
  - o Include a link and/or reference to the Work as published by the Publisher on all digital copies used within his/her institution
  - o Not reproduce or authorise others to reproduce adaptations of the Work that are substantially identical to the Work for any commercial publication
  - o Not permit digital copies of the Work as published by the Publisher to be systematically networked to external users
  - o Not use the Work in any way that implies that the Publisher, the Australian Society of Exploration Geophysicists, the Journal or the Editors endorse any product or procedure described in the Work.
4. When exercising any of the rights assigned or granted, each party is required to give sufficient acknowledgement of the contribution made by the other party to the published material including a citation to the Journal.
5. If the paper is rejected, all rights under this licence revert to the Author.

All authors are requested to sign this form. If not signed by all authors, the corresponding author acknowledges that he/she is signing on behalf of all the authors and with their authorisation. Faxed signatures and multiple forms are acceptable provided the corresponding author collates all the material and submits it in one batch.

(1) Author signature  Print name Andrew Pethick Date \_\_\_\_\_

(2) Author signature  Print name Brett Harris Date \_\_\_\_\_

(3) Author signature \_\_\_\_\_ Print name \_\_\_\_\_ Date \_\_\_\_\_

(4) Author signature \_\_\_\_\_ Print name \_\_\_\_\_ Date \_\_\_\_\_

(5) Author signature \_\_\_\_\_ Print name \_\_\_\_\_ Date \_\_\_\_\_

(6) Author signature \_\_\_\_\_ Print name \_\_\_\_\_ Date \_\_\_\_\_

Authorisation (if required) \_\_\_\_\_ Print name \_\_\_\_\_ Date \_\_\_\_\_

Completed forms should be sent to:

**CSIRO PUBLISHING (Journals)**, PO Box 1139, Collingwood, Vic. 3066, Australia.  
 Fax: +61 3 9662 7611 Email: publishing.journals@csiro.au

CSIRO PUBLISHING

***Licence to Publish***

Exploration Geophysics

Manuscript No. ASEG2012ab241Title of the paper (the 'Work') Open Source Marine Controlled Source Electromagnetic  
Interactive ModellingCorresponding Author Andrew Pethick

By submitting this paper, the Author (Authors if a multi-authored paper) has the right or has obtained authorisation to enter into this Licence and agrees to its submission by signing below.


The Author warrants that the Work:

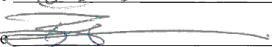
- Has not been published before
- Is not presently being considered for publication elsewhere
- Does not violate any intellectual property right of any person or entity
- Does not contain any subject matter that contravenes any laws (including defamatory material and misleading and deceptive material) and
- Meets ethical standards applicable to the research discipline.

**Terms of the Licence to Publish**

1. In consideration for publication of the Work, the Author grants to the Australian Society of Exploration Geophysicists, through **CSIRO PUBLISHING** (the 'Publisher') an exclusive worldwide licence to:
  - o Reproduce, publish and communicate the Work, or any part of the Work, to the public in any and all media, whether existing before or after the date of this Licence, for commercial, educational and all other purposes for the full remaining term of the copyright subsisting in the Work in each applicable jurisdiction
  - o Approve fair and reasonable permission requests from third parties to reuse material contained in the Work for the purpose of study, research or subsidiary publication.
2. In addition to the Author's moral rights in respect of the Work, the Author retains the right to:
  - o Use copies of the work for non-commercial purposes within his/her institution subject to the usual copyright licencing agency arrangements
  - o Use the work for further research and presentations at meetings and conferences
  - o Use the illustrations (line art, photographs, figures, plates) and research data in his/her own future works
  - o Share print or digital copies of his/her work with colleagues for personal use or study
  - o Include the work in part or in full in a thesis provided it is not published for commercial gain
  - o Place his/her pre-publication version of the work on a pre-print server
  - o Place his/her pre-publication version of the work on a personal website or institutional repository on condition that there is a link to the definitive version on the **CSIRO PUBLISHING** website.
3. The Author agrees to:
  - o Include a link and/or reference to the Work as published by the Publisher on all digital copies used within his/her institution
  - o Not reproduce or authorise others to reproduce adaptations of the Work that are substantially identical to the Work for any commercial publication
  - o Not permit digital copies of the Work as published by the Publisher to be systematically networked to external users
  - o Not use the Work in any way that implies that the Publisher, the Australian Society of Exploration Geophysicists, the Journal or the Editors endorse any product or procedure described in the Work.
4. When exercising any of the rights assigned or granted, each party is required to give sufficient acknowledgement of the contribution made by the other party to the published material including a citation to the Journal.
5. If the paper is rejected, all rights under this licence revert to the Author.

All authors are requested to sign this form. If not signed by all authors, the corresponding author acknowledges that he/she is signing on behalf of all the authors and with their authorisation. Faxed signatures and multiple forms are acceptable provided the corresponding author collates all the material and submits it in one batch.

(1) Author signature  Print name Andrew Pethick Date 27/02/13

(2) Author signature  Print name Brett Harris Date 27/02/13

(3) Author signature \_\_\_\_\_ Print name \_\_\_\_\_ Date \_\_\_\_\_

(4) Author signature \_\_\_\_\_ Print name \_\_\_\_\_ Date \_\_\_\_\_

(5) Author signature \_\_\_\_\_ Print name \_\_\_\_\_ Date \_\_\_\_\_

(6) Author signature \_\_\_\_\_ Print name \_\_\_\_\_ Date \_\_\_\_\_

Authorisation (if required) \_\_\_\_\_ Print name \_\_\_\_\_ Date \_\_\_\_\_

Completed forms should be sent to:

**CSIRO PUBLISHING** (Journals), PO Box 1139, Collingwood, Vic. 3066, Australia.  
Fax: +61 3 9662 7611 Email: publishing.journals@csiro.au

CSIRO PUBLISHING

*Licence to Publish*

Exploration Geophysics

Manuscript No. ASEG2013ab347Title of the paper (the 'Work') Computing, Brains and Geophysics?

Corresponding Author \_\_\_\_\_

By submitting this paper, the Author (Authors if a multi-authored paper) has the right or has obtained authorisation to enter into this Licence and agrees to its submission by signing below.


The Author warrants that the Work:


- Has not been published before
- Is not presently being considered for publication elsewhere
- Does not violate any intellectual property right of any person or entity
- Does not contain any subject matter that contravenes any laws (including defamatory material and misleading and deceptive material) and
- Meets ethical standards applicable to the research discipline.


**Terms of the Licence to Publish**

1. In consideration for publication of the Work, the Author grants to the Australian Society of Exploration Geophysicists, through **CSIRO PUBLISHING** (the 'Publisher') an exclusive worldwide licence to:
  - o Reproduce, publish and communicate the Work, or any part of the Work, to the public in any and all media, whether existing before or after the date of this Licence, for commercial, educational and all other purposes for the full remaining term of the copyright subsisting in the Work in each applicable jurisdiction
  - o Approve fair and reasonable permission requests from third parties to reuse material contained in the Work for the purpose of study, research or subsidiary publication.
2. In addition to the Author's moral rights in respect of the Work, the Author retains the right to:
  - o Use copies of the work for non-commercial purposes within his/her institution subject to the usual copyright licencing agency arrangements
  - o Use the work for further research and presentations at meetings and conferences
  - o Use the illustrations (line art, photographs, figures, plates) and research data in his/her own future works
  - o Share print or digital copies of his/her work with colleagues for personal use or study
  - o Include the work in part or in full in a thesis provided it is not published for commercial gain
  - o Place his/her pre-publication version of the work on a pre-print server
  - o Place his/her pre-publication version of the work on a personal website or institutional repository on condition that there is a link to the definitive version on the **CSIRO PUBLISHING** website.
3. The Author agrees to:
  - o Include a link and/or reference to the Work as published by the Publisher on all digital copies used within his/her institution
  - o Not reproduce or authorise others to reproduce adaptations of the Work that are substantially identical to the Work for any commercial publication
  - o Not permit digital copies of the Work as published by the Publisher to be systematically networked to external users
  - o Not use the Work in any way that implies that the Publisher, the Australian Society of Exploration Geophysicists, the Journal or the Editors endorse any product or procedure described in the Work.
4. When exercising any of the rights assigned or granted, each party is required to give sufficient acknowledgement of the contribution made by the other party to the published material including a citation to the Journal.
5. If the paper is rejected, all rights under this licence revert to the Author.

All authors are requested to sign this form. If not signed by all authors, the corresponding author acknowledges that he/she is signing on behalf of all the authors and with their authorisation. Faxed signatures and multiple forms are acceptable provided the corresponding author collates all the material and submits it in one batch.

(1) Author signature  Print name Andrew Pethick Date 27/02/13

(2) Author signature  Print name Brett Harris Date 27/02/13

(3) Author signature  Print name Karen Lam Date 27/02/13

(4) Author signature \_\_\_\_\_ Print name \_\_\_\_\_ Date \_\_\_\_\_

(5) Author signature \_\_\_\_\_ Print name \_\_\_\_\_ Date \_\_\_\_\_

(6) Author signature \_\_\_\_\_ Print name \_\_\_\_\_ Date \_\_\_\_\_

Authorisation (if required) \_\_\_\_\_ Print name \_\_\_\_\_ Date \_\_\_\_\_

Completed forms should be sent to:

**CSIRO PUBLISHING** (Journals), PO Box 1139, Collingwood, Vic. 3066, Australia.  
 Fax: +61 3 9662 7611 Email: [publishing.journals@csiro.au](mailto:publishing.journals@csiro.au)

CSIRO PUBLISHING

***Licence to Publish*****Exploration Geophysics**Manuscript No. ASEG2013ab347Title of the paper (the 'Work') Computing, Brains and  
Geophysics?

Corresponding Author \_\_\_\_\_

By submitting this paper, the Author (Authors if a multi-authored paper) has the right or has obtained authorisation to enter into this Licence and agrees to its submission by signing below.

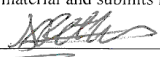
The Author warrants that the Work:


- Has not been published before
- Is not presently being considered for publication elsewhere
- Does not violate any intellectual property right of any person or entity
- Does not contain any subject matter that contravenes any laws (including defamatory material and misleading and deceptive material) and
- Meets ethical standards applicable to the research discipline.

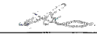
**Terms of the Licence to Publish**

1. In consideration for publication of the Work, the Author grants to the Australian Society of Exploration Geophysicists, through **CSIRO PUBLISHING** (the 'Publisher') an exclusive worldwide licence to:
  - o Reproduce, publish and communicate the Work, or any part of the Work, to the public in any and all media, whether existing before or after the date of this Licence, for commercial, educational and all other purposes for the full remaining term of the copyright subsisting in the Work in each applicable jurisdiction
  - o Approve fair and reasonable permission requests from third parties to reuse material contained in the Work for the purpose of study, research or subsidiary publication.
2. In addition to the Author's moral rights in respect of the Work, the Author retains the right to:
  - o Use copies of the work for non-commercial purposes within his/her institution subject to the usual copyright licencing agency arrangements
  - o Use the work for further research and presentations at meetings and conferences
  - o Use the illustrations (line art, photographs, figures, plates) and research data in his/her own future works
  - o Share print or digital copies of his/her work with colleagues for personal use or study
  - o Include the work in part or in full in a thesis provided it is not published for commercial gain
  - o Place his/her pre-publication version of the work on a pre-print server
  - o Place his/her pre-publication version of the work on a personal website or institutional repository on condition that there is a link to the definitive version on the **CSIRO PUBLISHING** website.
3. The Author agrees to:
  - o Include a link and/or reference to the Work as published by the Publisher on all digital copies used within his/her institution
  - o Not reproduce or authorise others to reproduce adaptations of the Work that are substantially identical to the Work for any commercial publication
  - o Not permit digital copies of the Work as published by the Publisher to be systematically networked to external users
  - o Not use the Work in any way that implies that the Publisher, the Australian Society of Exploration Geophysicists, the Journal or the Editors endorse any product or procedure described in the Work.
4. When exercising any of the rights assigned or granted, each party is required to give sufficient acknowledgement of the contribution made by the other party to the published material including a citation to the Journal.
5. If the paper is rejected, all rights under this licence revert to the Author.

All authors are requested to sign this form. If not signed by all authors, the corresponding author acknowledges that he/she is signing on behalf of all the authors and with their authorisation. Faxed signatures and multiple forms are acceptable provided the corresponding author collates all the material and submits it in one batch.

(1) Author signature  Print name Andrew Pethick Date 27/02/13

(2) Author signature  Print name Brett Harris Date 27/02/13

(3) Author signature  Print name Karen Lam Date 27/02/13

(4) Author signature \_\_\_\_\_ Print name \_\_\_\_\_ Date \_\_\_\_\_

(5) Author signature \_\_\_\_\_ Print name \_\_\_\_\_ Date \_\_\_\_\_

(6) Author signature \_\_\_\_\_ Print name \_\_\_\_\_ Date \_\_\_\_\_

Authorisation (if required) \_\_\_\_\_ Print name \_\_\_\_\_ Date \_\_\_\_\_

Completed forms should be sent to:

**CSIRO PUBLISHING** (Journals), PO Box 1139, Collingwood, Vic. 3066, Australia.  
Fax: +61 3 9662 7611 Email: publishing.journals@csiro.au

**Ted Bakamjian** <Tbakamjian@seg.org>

Mar 18 (1 day ago) ☆



to Andrew, Permissions, b.harris ▾

Dear Andrew,

You have SEG's permission to include both papers in your thesis. I am not aware at this moment of the status of the Geophysics submission. Please have your thesis reflect it's status accurately. Please also acknowledge SEG copyright in any materials you reproduce in your thesis.

Thank you for publishing with SEG, and best of luck with your thesis.

Sincerely,

Ted

---

Ted Bakamjian  
Director, Publications  
Society of Exploration Geophysicists  
P. O. Box 702740, Tulsa, OK 74170-2740 USA  
Shipping: 8801 S. Yale Ave., Suite 500, Tulsa, OK 74137  
Phone: (918) 497-5506; Fax: (918) 497-5557  
E-mail: [tbakamjian@seg.org](mailto:tbakamjian@seg.org); Web: <http://www.seg.org/>

**Fraukje Heida** <fha@eage.org>

6:52 PM (19 hours ago) ☆



to me ▾

Dear Andrew,

We have received the form in good order. Thank you for your response.  
Yes you can indeed include the abstract in your own thesis. Not a problem at all.

Kind regards,

Kia

---

Ms. Fraukje (Kia) Heida  
Conference Coordinator

**EAGE** Conferences bv  
PO Box 59  
3990 DB Houten  
The Netherlands

Ph: [+31 88 995 5055](tel:+31889955055)  
Fax: [+31 30 834 3524](tel:+31308343524)  
Email: [fha@eage.org](mailto:fha@eage.org)

Visit us at:  
[www.eage.org](http://www.eage.org)

# References

- Al Dallal, J. and L. C. Briand (2010). An object-oriented high-level design-based class cohesion metric. *Information and Software Technology* 52(12), 1346–1361. (Cited on page 42.)
- AMIRA (2012). p223 - em modelling software. <http://www.amirainternational.com/WEB/site.asp?section=news&page=projectpages/p223>. (Cited on pages 7, 158 and 236.)
- Amundsen, L., L. Laseth, R. Mittet, S. Ellingsrud, and B. Ursin (2006). Decomposition of electromagnetic fields into upgoing and downgoing components. *Geophysics* 71(5), G211–G223. (Cited on pages 23, 195 and 203.)
- Anderson, D., J. Cobb, E. Korpela, M. Lebofsky, and D. Werthimer (2002). Seti@ home: an experiment in public-resource computing. *Communications of the ACM* 45(11), 56–61. (Cited on page 143.)
- Andreis, D. and L. MacGregor (2008). Controlled-source electromagnetic sounding in shallow water: Principles and applications. *Geophysics* 73(1), F21–F32. (Cited on page 203.)
- Apache (2012a). Apache commons exec. <http://commons.apache.org/exec/>. (Cited on pages 89 and 125.)
- Apache (2012b). Apache commons math. <http://commons.apache.org/math/>. (Cited on page 127.)
- Archie, G. (1942). The electrical resistivity log as an aid in determining some reservoir characteristics. *Transactions of the AIME* 146(1), 8. (Cited on page 30.)
- Azevedo, F. A. C., L. R. B. Carvalho, L. T. Grinberg, J. M. Farfel, R. E. L. Ferretti, R. E. P. Leite, W. J. Filho, R. Lent, and S. Herculano-Houzel (2009). Equal numbers of neuronal and nonneuronal cells make the human brain an isometrically scaled-up primate brain. *The Journal of Comparative Neurology* 513(5), 532–541. (Cited on page 244.)
- Baeyens, F., P. Eelen, and G. Crombez (1995). Pavlovian associations are forever: On classical conditioning and extinction. *Journal of Psychophysiology*. (Cited on page 246.)
- Bakshi, U. and A. Bakshi (2009). *Electromagnetic Wave Theory*. Technical Publications. (Cited on page 171.)
- Barequet, G., B. Chazelle, L. J. Guibas, J. S. B. Mitchell, and A. Tal (1996). Bboxtree: A hierarchical representation for surfaces in 3d. *Computer Graphics Forum* 15(3), 387–396. (Cited on page 110.)
- Bien (2012). The enterprise side of javafx. (Cited on page 127.)
- Bilkadi, Z. (1984). *Bitumen: a history*. Aramco. (Cited on page 2.)
- Billen, M. I., O. Kreylos, B. Hamann, M. A. Jadamec, L. H. Kellogg, O. Staadt, and D. Y. Sumner (2008). A geoscience perspective on immersive 3d gridded data visualization. *Computers and Geosciences* 34(9), 1056–1072. (Cited on page 171.)
- Bridge (2012). Bridge electromagnetics. [www.blueback-reservoir.com/bridge](http://www.blueback-reservoir.com/bridge). (Cited on page 7.)
- Bunch, M. (2010). Site characterization at the co2crc otway basin. *Presentation at the China Australia Geological Storage Workshop II*. (Cited on page 230.)

- Buonora, M., A. Zerilli, T. Labruzzo, and L. Rodrigues (2009). Detecting hydrocarbon reservoirs from marine csem in the santos basin, brazil. *Search and Discovery* 40402. (Cited on page 142.)
- Cali, A., D. Calvanese, G. De Giacomo, and M. Lenzerini (2002). *A Formal Framework for Reasoning on UML Class Diagrams Foundations of Intelligent Systems*, Volume 2366 of *Lecture Notes in Computer Science*, pp. 423–427. Springer Berlin / Heidelberg. (Cited on pages 42, 43 and 44.)
- Carstens, H. (2009). Technology: Changing exploration - using non-seismic technology. *GEO ExPRO* 6(1). (Cited on pages 10 and 203.)
- Ceaparu, I., J. Lazar, K. Bessiere, J. Robinson, and B. Shneiderman (2004). Determining causes and severity of end-user frustration. *International Journal of Human-Computer Interaction* 17(3), 333–356. (Cited on page 123.)
- Chave, A. D. (2009). On the electromagnetic fields produced by marine frequency domain controlled sources. *Geophysical Journal International* 179(3), 1429–1457. (Cited on page 68.)
- Chen, J. and D. L. Alumbaugh (2011). Three methods for mitigating airwaves in shallow water marine controlled-source electromagnetic data. *Geophysics* 76(2), F89–F99. (Cited on page 200.)
- Commer, M., G. Newman, J. Carazzone, T. Dickens, K. Green, L. Wahrmond, D. Willen, and J. Shiu (2008). Massively parallel electrical-conductivity imaging of hydrocarbons using the ibm blue gene/l supercomputer. *IBM Journal of Research and Development* 52(1.2), 93–103. (Cited on page 139.)
- Constable, S. (2010). Ten years of marine csem for hydrocarbon exploration. *Geophysics* 75(5), 75A67–75A81. (Cited on pages 4, 10 and 23.)
- Constable, S. (2013). Review paper: Instrumentation for marine magnetotelluric and controlled source electromagnetic sounding. *Geophysical Prospecting* 61, 505–532. (Cited on page 13.)
- Constable, S. and C. S. Cox (1996). Marine controlled-source electromagnetic sounding 2. the pegasus experiment. *J. Geophys. Res.* 101(B3), 5519–5530. (Cited on page 13.)
- Constable, S. and C. J. Weiss (2006). Mapping thin resistors and hydrocarbons with marine em methods: Insights from 1d modeling. *Geophysics* 71(2), G43–G51. (Cited on pages 15 and 28.)
- Constable, S. C., A. S. Orange, G. M. Hoversten, and H. F. Morrison (1998). Marine magnetotellurics for petroleum exploration; part i, a sea-floor equipment system. *Geophysics* 63(3), 816–825. (Cited on pages 12, 13 and 18.)
- Cooper, A. (1999). 14 principles of polite apps. *Visual Basic Programmer's Journal* June, 5. (Cited on pages 78, 86, 87, 92, 123 and 236.)
- Coraggio, F., P. Bernardelli, and G. Gabbriellini (2012). *Structural reconstruction using potential field data in hydrocarbon exploration*, pp. 1–6. (Cited on pages 2 and 5.)
- Cox, C. S. (1981). On the electrical conductivity of the oceanic lithosphere. *Physics of the Earth and Planetary Interiors* 25(3), 196–201. (Cited on page 4.)
- Cox, L., G. Wilson, and M. Zhdanov (2011). 3d inversion of airborne electromagnetic data using a moving footprint. *Exploration Geophysics* 41(4), 250–259. (Cited on page 143.)
- Cox, L. and M. Zhdanov (2007). Large scale 3d inversion of hem data using a moving footprint. In *2007 SEG Annual Meeting*. (Cited on page 143.)



- Cox, L. H., G. A. Wilson, and M. S. Zhdanov (2010). 3d inversion of airborne electromagnetic data using a moving footprint. *Exploration Geophysics* 41(4), 250–259. (Cited on page 158.)
- Cox, L. H. and M. S. Zhdanov (2006). Rapid and rigorous 3d inversion of airborne electromagnetic data. *SEG Technical Program Expanded Abstracts* 25(1), 795–799. (Cited on page 143.)
- CPSeis (2012). Cpseis. <http://cpseis.org/>. (Cited on page 236.)
- Davydycheva, S. and N. Rykhliniski (2011). Focused-source electromagnetic survey versus standard csem: 3d modeling in complex geometries. *Geophysics* 76(1), F27–F41. (Cited on page 200.)
- de Groot, P. and B. Bril. The open source model in geosciences and opendtect in particular. In *2005 SEG Annual Meeting*. (Cited on page 236.)
- Demanuele, C., S. J. Broyd, E. J. Sonuga-Barke, and C. James (2012). Neuronal oscillations in the eeg under varying cognitive load: A comparative study between slow waves and faster oscillations. *Clin Neurophysiol* 14(12), 00578–0. Using Smart Source Parsing Sep pii: S1388-2457( doi: 10.1016/j.clinph.2012.07.021. (Cited on page 245.)
- Dobrich, A. (2010). *Developing a Real-Time Look up Table of the Airwave Effect for the Marine Controlled Source Electromagnetic Method*. B. sc. (Cited on pages 32 and 130.)
- Dornhege, G., J. Millán, T. Hinterberger, D. McFarland, and K. Müller (2007). *Toward brain-computer interfacing*, Volume 74. MIT press Cambridge, MA. (Cited on page 245.)
- Eidesmo, T. and S. Ellingsrud (2002). How electromagnetic sounding technique could be coming to hydrocarbon e and p. *First Break* 20(3), 11. (Cited on pages 8 and 28.)
- Eidesmo, T., S. Ellingsrud, L. M. MacGregor, S. Constable, M. C. Sinha, S. Johansen, F. N. Kong, and H. Westerdah (2002). Sea bed logging (sbl), a new method for remote and direct identification of hydrocarbon filled layers in deepwater areas. *First Break* 20(3), 8. (Cited on pages 26, 28 and 29.)
- Ekdandem, J. I., T. A. Davis, I. Alvarez, M. T. James, and J. E. Gilbert (2012). Evaluating the ergonomics of bci devices for research and experimentation. *Ergonomics* 55(5), 592–8. Ekdandem, Joshua I Davis, Timothy A Alvarez, Ignacio James, Melva T Gilbert, Juan E Randomized Controlled Trial England *Ergonomics*. 2012 May;55(5):592-8. doi: 10.1080/00140139.2012.662527. Epub 2012 Apr 16. (Cited on page 244.)
- Ellingsrud, S., T. Eidesmo, S. Johansen, M. Sinha, L. MacGregor, and S. Constable (2002). Remote sensing of hydrocarbon layers by seabed logging (sbl): results from a cruise offshore angola. *Leading Edge* 21(10), 972–982. (Cited on pages 4 and 28.)
- EMGS (2012). Modelling. <http://www.emgs.com/content/598/Modelling>. (Cited on page 143.)
- Encom (2012). Software - emvision. <http://web2.encom.com.au/pages/swev.htm>. (Cited on page 7.)
- Endo, M. and M. Zhdanov (2009). Multiple domain integral equation method for 3d electromagnetic modeling in complex geoelectrical structures. (Cited on page 143.)
- Enthought (2010). Csem. <http://www.enthought.com/consulting/csem.php>. (Cited on page 7.)
- Ewan and R. Biddle (2000). Simulating multiple inheritance in java. *Journal of Systems and Software* 55(1), 87–100. (Cited on page 46.)

- Fang, S., G.-z. Gao, and C. Torres-Verd  n (2003). Efficient 3-d electromagnetic modeling in the presence of anisotropic conductive media using integral equations. *ASEG Extended Abstracts 2003*(1), 1–8. (Cited on page 157.)
- Farquharson, C. G., K. Duckworth, and D. W. Oldenburg (2006). Comparison of integral equation and physical scale modeling of the electromagnetic responses of models with large conductivity contrasts. *Geophysics* 71(4), G169–G177. (Cited on page 142.)
- Fischer, P. (2005). New em technology offerings are growing quickly. *World Oil* 226(6), 9. (Cited on pages 10 and 203.)
- Fleming, A. P. (1967). *The "Pioneer" Kerosene Works at American Creek (Mount Kembla) NSW, 1865-1878:(with a brief reference to the succeeding companies)*. Illawarra Historical Society. (Cited on page 2.)
- Floater, M. S. and A. Iske (1996). Multistep scattered data interpolation using compactly supported radial basis functions. *Journal of Computational and Applied Mathematics* 73(1–2), 65–78. (Cited on page 174.)
- Flosadattir, A. and S. Constable (1996). Marine controlled-source electromagnetic sounding 1. modeling and experimental design. *J. Geophys. Res.* 101(B3), 5507–5517. (Cited on page 17.)
- Garbee, B., J. Fern  ndez-Sanguino, H. Koptein, N. Lohner, W. Lowe, B. Mitchell, I. Murdock, M. Schulze, and C. Small (2010). A brief history of debian chapter 2 - leadership. (Cited on page 85.)
- Gaudin, S. (2009). Intel: Chips in brains will control computers by 2020. [http://www.computerworld.com/s/article/9141180/Intel\\_Chips\\_in\\_brains\\_will\\_control\\_computers\\_by\\_2020](http://www.computerworld.com/s/article/9141180/Intel_Chips_in_brains_will_control_computers_by_2020). (Cited on page 246.)
- GNU (2007). Gnu general public license. (Cited on pages 84 and 236.)
- Goux, J., S. Kulkarni, J. Linder  th, and M. Yoder (2001). Master-worker: an enabling framework for applications on the computational grid. *Cluster Computing* 4(1), 63–70. (Cited on page 154.)
- Gribenko, A. and M. Zhdanov (2006). Rigorous 3-d inversion of marine csem data based on the integral equation method. *SEG Technical Program Expanded Abstracts* 25(1), 815–819. (Cited on page 220.)
- Gribenko, A. and M. Zhdanov (2007). Rigorous 3d inversion of marine csem data based on the integral equation method. *Geophysics* 72(2), WA73–WA84. (Cited on pages 6 and 140.)
- Guger, C., A. Schlogl, D. Walterspacher, and G. Pfurtscheller (1999). Design of an eeg-based brain-computer interface (bci) from standard components running in real-time under windows-entwurf eines eeg-basierten brain-computer interfaces (bci) mit standardkomponenten, das unter windows in echtzeit arbeitet. *Biomedizinische Technik/Biomedical Engineering* 44(1-2), 12–16. (Cited on page 247.)
- Gumhold, S. and W. Straber (1998). Real time compression of triangle mesh connectivity. In *Proceedings of the 25th annual conference on Computer graphics and interactive techniques*, pp. 133–140. ACM. (Cited on page 111.)
- Haber, E. and S. Heldmann (2007). An octree multigrid method for quasi-static maxwell’s equations with highly discontinuous coefficients. *Journal of Computational Physics* 223(2), 783–796. (Cited on page 222.)
- Hale, D. (2006). The java and c++ platforms for scientific computing. *Project Review CWP-548*. (Cited on pages 97 and 98.)

- Hall, C. A. and J. W. Day (2009). Revisiting the limits to growth after peak oil in the 1970s a rising world population and the finite resources available to support it were hot topics. interest faded—but it's time to take another look. *American Scientist* 97(3), 230–237. (Cited on page 2.)
- Hall, J. E. and A. C. Guyton (2011). *Guyton and Hall textbook of medical physiology*. Philadelphia, Pa.: Saunders/Elsevier. (Cited on pages 244, 245 and 246.)
- Han, N., M. Nam, and H. Kim (2010). An analysis on 3d marine csem responses based on a finite difference method. *AGU Fall Meeting Abstracts*. (Cited on page 200.)
- Hansen, C. and C. Johnson (2004). *Visualization Handbook*. Elsevier Science. (Cited on pages 110, 171, 173 and 200.)
- Harris, B. (2001). *Transient Electromagnetic Methods and their Application to the Delineation and Assessment of Groundwater Resource in the Eastern Goldfields*. Ph. d. (Cited on pages 76 and 142.)
- Harris, B. and A. Pethick (2008). Marine controlled source electromagnetic methods for hydrocarbon exploration. *Preview* 137, 4. (Cited on pages 8 and 32.)
- Hesthammer, J., A. Stefatos, M. Boulaenko, A. Vereshagin, P. Gelting, T. Wedberg, and G. Maxwell (2010). Csem technology as a value driver for hydrocarbon exploration. *Marine and Petroleum Geology* 27(9), 1872–1884. (Cited on pages 11, 171 and 200.)
- Hocevar, S. (2004). Wtfpl - do what the fuck you want to public license. <http://sam.zoy.org/wtfpl/>. (Cited on page 85.)
- Hogan, P. (2011). Nasa world wind: infrastructure for spatial data. (Cited on pages 97 and 98.)
- Hohmann, G. W. (1987). *Numerical Modeling for Electromagnetic Methods of Geophysics*. Electromagnetic Methods in Applied Geophysics. Society of Exploration Geophysicists. (Cited on page 141.)
- Hoversten, G. M., F. Cassassuce, E. Gasperikova, G. A. Newman, J. Chen, Y. Rubin, Z. Hou, and D. Vasco (2006). Direct reservoir parameter estimation using joint inversion of marine seismic ava and csem data. *Geophysics* 71(3), C1–C13. (Cited on pages 15 and 22.)
- Hughes, M. (1998). 3d graphic java: Render fractal landscapes. <http://www.javaworld.com/jw-08-1998/jw-08-step.html>. (Cited on page 117.)
- Hunziker, J., E. Slob, and W. Mulder (2011). Effects of the airwave in time-domain marine controlled-source electromagnetics. *Geophysics* 76(4), F251–F261. (Cited on page 195.)
- Hursan, G. and M. S. Zhdanov (2002). Contraction integral equation method in three-dimensional electromagnetic modeling. *Radio Sci.* 37(6), 1089. (Cited on pages 89, 140 and 157.)
- Interaction (2012). Interaction. [www.2interaction.com](http://www.2interaction.com). (Cited on page 7.)
- Jain, M., S. N. Mohanty, and S. V. Yalamanchili (2008). *Gravity, magnetic and seismic data integration for structural configuration and its hydrocarbon evaluation in the San Juan-Tumaco Basins, offshore Colombia*, pp. 774–778. (Rao). (Cited on pages 2 and 5.)
- Jakobus, U. (1997). Parallel computing based on integral equations. *Parallel Computing*, 9. (Cited on page 142.)
- Java (2012). Package java.net. <http://docs.oracle.com/javase/6/docs/api/java/net/package-summary.html>. (Cited on page 89.)

- JavaDB (2012). Java db. <http://www.oracle.com/technetwork/java/javadb/overview/index.html>. (Cited on pages 78 and 127.)
- JavaFX (2012). Javafx 2 documentation. <http://docs.oracle.com/javafx/>. (Cited on page 127.)
- JNI (2012). Java native interface. <http://docs.oracle.com/javase/7/docs/technotes/guides/jni/index.html>. (Cited on pages 97 and 246.)
- JOGAMP (2012). Javadoc javax.media.opengl.fixedfunc interface glightingfunc. (Cited on page 110.)
- JOGL (2012a). Jogl. <http://jogamp.org/jogl/www/>. (Cited on pages 85, 89, 97 and 111.)
- JOGL (2012b). Jogl deployment. <http://jogamp.org/jogl/doc/deployment/JOGL-DEPLOYMENT.html>. (Cited on page 127.)
- Johansen, S.E.; Amundsen, H. R. T. E. S. E. T. B. A. (2005). Subsurface hydrocarbons detected by electromagnetic sounding. *First Break* 23, 6. (Cited on page 28.)
- Key, K. (2003). *Application of Broadband Marine Magnetotelluric Exploration to a 3D salt Structure and a Fast-Spreading Ridge*. Ph. d. (Cited on pages 13 and 18.)
- Key, K. (2009a). 1d inversion of multicomponent, multifrequency marine csem data: Methodology and synthetic studies for resolving thin resistive layers. *Geophysics* 74(2), F9–F20. (Cited on pages 58, 79, 89, 171, 174, 229, 236 and 246.)
- Key, K. (2009b). Scripps undersea electromagnetic source instrument. <http://marineemlab.ucsd.edu/instruments/suesi.html>. (Cited on page 21.)
- Key, K. and A. Lockwood (2010). Determining the orientation of marine csem receivers using orthogonal procrustes rotation analysis. *Geophysics* 75(3), F63–F70. (Cited on page 171.)
- Key, K. and J. Oval (2011). A parallel goal-oriented adaptive finite element method for 2.5-d electromagnetic modelling. *Geophysical Journal International* 186(1), 137–154. (Cited on page 139.)
- Kim, J., Z. Xue, and T. matsuoaka (2010). Experimental study on co2 monitroing and saturation with combined p-wave velocity and resistivity. *International Oil and Gas Conference and Exhibition in China*. (Cited on page 229.)
- Knyazev, G. (2011). Eeg delta oscillations as a correlate of basic homeostatic and motivational processes. *Neuroscience and Biobehavioral Reviews*. (Cited on page 245.)
- Kong, F., F. Roth, P. Olsen, and S. Stalheim (2009). Casing effects in the sea-to-borehole electromagnetic method. *Geophysics* 74(5), F77–F87. (Cited on page 229.)
- Kong, E.N.; Westerdahl, H. E. S. E. T. J. S. (2002). Seabed logging: A possible direct hydrocarbon indicator for deepsea prospects using em energy. *Oil and Gas journal* 100, 6. (Cited on pages 4 and 23.)
- Kulkarni, P. (2005). Lower tertiary play: Is it gulf of mexico’s final frontier? (Cited on page 2.)
- Leeb, R., D. Friedman, G. Müller-Putz, R. Scherer, M. Slater, and G. Pfurtscheller (2007). Self-paced (asynchronous) bci control of a wheelchair in virtual environments: a case study with a tetraplegic. *Computational intelligence and neuroscience* 2007. (Cited on page 245.)

- Leff, A. and J. T. Rayfield (2001). Web-application development using the model/view/controller design pattern. In *Enterprise Distributed Object Computing Conference, 2001. EDOC '01. Proceedings. Fifth IEEE International*, pp. 118–127. (Cited on page 119.)
- Li, Y. and S. Constable (2007). 2d marine controlled-source electromagnetic modeling: Part 2 - the effect of bathymetry. *Geophysics* 72(2), WA63–WA71. (Cited on pages 169, 200, 201, 202 and 203.)
- Li, Y. and K. Key (2007). 2d marine controlled-source electromagnetic modeling: Part 1 – an adaptive finite-element algorithm. *Geophysics* 72(2), WA51–WA62. (Cited on page 103.)
- Liang, L., A. Abubakar, and T. M. Habashy (2012). *Joint inversion of time-lapse crosswell electromagnetic, seismic, and production data for reservoir monitoring and characterization*, pp. 1–7. SEG Technical Program Expanded Abstracts. Society of Exploration Geophysicists. doi:10.1190/segam2012-0261.1. (Cited on page 6.)
- Lindholm, T., F. Yellin, G. Bracha, and A. Buckley (2012). The java virtual machine specification: Java se 7 edition. <http://docs.oracle.com/javase/specs/jvms/se7/html/index.html>. (Cited on page 88.)
- Lindholm, B., D. Ridyard, and T. Wicklund (2007). Electromagnetic prospect scanning-seabed logging moves from risk reduction to value creation. In *International Oil Conference and Exhibition in Mexico*. (Cited on page 224.)
- Maa0, F. A. and A. K. Nguyen (2010). Enhanced subsurface response for marine csem surveying. *Geophysics* 75(3), A7–A10. (Cited on page 23.)
- MacGregor, L. M. (2006). Ohm short course. (Cited on pages 5, 6, 8, 13, 23, 28, 30 and 31.)
- MacGregor, L. M., S. Constable, and M. C. Sinha (1998). The ramessees experiment iii. controlled-source electromagnetic sounding of the reykjanes ridge at 57°45'n. *Geophysical Journal International* 135(3), 773–789. (Cited on pages 15 and 32.)
- Malajczuk, S. (2010). Time lapse thermal and induction logging in the near well environment, perth basin, wa. *Curtin University Report Report No. GPH 15/10*. (Cited on page 229.)
- Marr, D., F. Binns, D. Hill, G. Hinton, D. Koufaty, A. Miller, and M. Upton (2002). Hyper-threading technology architecture and microarchitecture. *Intel Technology Journal* 6(1). (Cited on page 161.)
- Marsh, A., A. Furniss, and G. Kidd (2000). 3d seismic visualization using multiple volume data sets. (Cited on page 96.)
- Martin, R., B. Harris, and D. Schafer (2012). Airborne tem for the recovery of basin scale solute distribution; perth basin, western australia. (Cited on page 158.)
- Martz, P. (1997). Generating random fractal terrain. *Game Programmer*. (Cited on page 117.)
- Masashi, E., C. Martin, and S. Z. Michael (2008). A multigrid integral equation method for large-scale models with inhomogeneous backgrounds. *Journal of Geophysics and Engineering* 5(4), 438. (Cited on page 220.)
- Mattsson, J., L. Lund, and J. Lima (2010). A towed em system for hydrocarbon exploration tested on a gas discovery in the north sea. (Cited on page 40.)
- Maxwell, J. C. (1881). *A treatise on electricity and magnetism*, Volume 1. Clarendon Press. (Cited on pages 67 and 176.)

- Menasce, D. and E. Casalicchio (2004). Qos in grid computing. *Internet Computing, IEEE* 8(4), 85–87. (Cited on page 143.)
- Miller, R. (2007). Theory of the normal waking eeg: From single neurones to waveforms in the alpha, beta and gamma frequency ranges. *International Journal of Psychophysiology* 64(1), 18–23. (Cited on page 245.)
- Mittet, R.; Maulana, H. B. K. W. T. A. (2007). Cmp inversion and post-inversion modelling for marine csem data. *EGM International Workshop April 15 – 18, 2007, Innovation in EM, Grav and Mag Methods: a new Perspective for Exploration April 15 - 18, 2007*. (Cited on page 220.)
- Mittet, R.; L  seth, L. E. S. (2004). Inversion of sbl data acquired in shallow waters. (Cited on page 28.)
- Murphy, G. C., M. Kersten, and L. Findlater (2006). How are java software developers using the eclipse ide? *Software, IEEE* 23(4), 76–83. (Cited on page 85.)
- Myer, D., S. Constable, and K. Key (2011). Broad-band waveforms and robust processing for marine csem surveys. *Geophysical Journal International* 184(2), 689–698. (Cited on page 13.)
- Myer, D., S. Constable, K. Key, M. E. Glinsky, and G. Liu (2012). Marine csem of the scarborough gas field, part 1: Experimental design and data uncertainty. *Geophysics* 77, 281. (Cited on page 30.)
- MySQL (2012). Mysql. <http://www.mysql.com/>. (Cited on page 78.)
- Nabighian, M. (1988). *Electromagnetic Methods in Applied Geophysics*. Society of Exploration Geophysicists. (Cited on pages 50, 68 and 142.)
- NeuroSky (2009). Brain wave signal (eeg) of neurosky, inc. (Cited on pages 245 and 246.)
- Neurosky (2012). Neurosky mindwave. <http://neurosky.com/Products/MindWave.aspx>. (Cited on pages 128 and 244.)
- Newman, G. and D. Alumbaugh (1997). Three-dimensional massively parallel electromagnetic inversion—i. theory. *Geophysical journal international* 128(2), 345–354. (Cited on page 139.)
- Newman, G. A. and G. W. Hohmann (1988). Transient electromagnetic responses of high-contrast prisms in a layered earth. *Geophysics* 53(5), 691–706. (Cited on page 142.)
- Nguyen, A. K. and F. Roth (2010, April 11–14, 2010). Application of the frequency differenced field to 3d inversion of shallow water csem data. (Cited on page 203.)
- Nielsen, J. (1994). *Heuristic Evaluation*. Usability inspection methods. New York: John Wiley and Sons, Inc. (Cited on pages 86, 87, 90, 91, 92 and 236.)
- Noel, B., A. W. Glenn, V. G. Alexander, and S. Z. Michael (2010). *3D inversion of time-lapse CSEM data for reservoir surveillance*, pp. 716–720. SEG Technical Program Expanded Abstracts. Society of Exploration Geophysicists. doi:10.1190/1.3513883. (Cited on page 6.)
- Noel, B., A. W. Glenn, V. G. Alexander, S. Z. Michael, and M. Ed (2011). *3D inversion of time-lapse CSEM data based on dynamic reservoir simulations of the Harding field, North Sea*, pp. 666–670. SEG Technical Program Expanded Abstracts. Society of Exploration Geophysicists. doi:10.1190/1.3628166. (Cited on page 6.)
- Nunez, P. L. and R. Srinivasan (2006). *Electric Fields of the Brain: The Neurophysics of EEG*. New York: Oxford University Press. (Cited on page 245.)
- OHM (2008). Ohm surveys. [www.ohmsurveys.com](http://www.ohmsurveys.com). (Cited on page 16.)



- Orange, A., K. Key, and S. Constable (2009). The feasibility of reservoir monitoring using time-lapse marine csem. *Geophysics* 74(2), F21–F29. (Cited on page 26.)
- Paten, T. (2010). *Electrical Anisotropy and Bathymetry in Marine Controlled Source Electromagnetic Exploration; Northern Carnarvon Basin, Australia*. B. sc. (Cited on pages 32 and 130.)
- Paterson, J. and S. Edlich (2006). *The Definitive Guide to db4o*. Apress. (Cited on page 127.)
- Peace, D. (2005, 2 May). How to plan for a successful c.s.e.m. survey. (Cited on pages 4 and 26.)
- Peitgen, H., H. JÃ¼rgens, and D. Saupe (2004). *Chaos and Fractals: New Frontiers of Science*. Springer. (Cited on page 117.)
- Pethick, A. (2008). *Planning and 4D Visualisation of the Marine Controlled Source Electromagnetic Method*. Ph. D. thesis. (Cited on pages 8, 10, 13, 26, 32, 33, 74, 103, 171 and 200.)
- Pethick, A. (2012a). Mcsem - open source electromagnetic software. <http://www.MCSEM.com>. (Cited on pages 128 and 236.)
- Pethick, A. (2012b). Mcsem.com - svn access. <http://mcsem.com/?p=351>. (Cited on pages 85 and 144.)
- Pethick, A. and B. Harris (2012). Open source interactive electromagnetic modelling. *ASEG Extended Abstracts 2012*(1), 1–4. (Cited on pages 86, 130, 174, 201, 229 and 246.)
- Phillips (2007). *Feasibility of the Marine Controlled Source Electromagnetic Method for Hydrocarbon Exploration*. B.sc. (Cited on pages 5, 15, 32 and 200.)
- Pilone, D. and N. Pitman (2005). *UML 2.0 in a Nutshell*. O'Reilly Media, Incorporated. (Cited on page 144.)
- Pound, G. (2007). Multi-transient em technology at pgs. *Tech Link* 7(4), 8. (Cited on pages 10, 13 and 203.)
- Quasar (2012). Quasar geo. [www.quasargeo.com](http://www.quasargeo.com). (Cited on pages 17 and 20.)
- Quin, L. (2012). Extensible markup language. <http://www.w3.org/XML/>. (Cited on page 88.)
- Raiche, A. P. (1974). An integral equation approach to three-dimensional modelling. *Geophysical Journal of the Royal Astronomical Society* 36(2), 363–376. (Cited on pages 140, 141 and 142.)
- Regnier, S., T. Amari, and E. Kersale (2002). 3d coronal magnetic field from vector magnetograms: non-constant- $\alpha$  force-free configuration of the active region noaa 8151. *A and A* 392(3), 1119–1127. (Cited on page 171.)
- Roberts, E. and A. Picard (1998). Designing a java graphics library for cs 1. In *ACM SIGCSE Bulletin*, Volume 30, pp. 213–218. ACM. (Cited on page 175.)
- Sachse, F. B. and B. Taccardi (2004). Visualization of electrical current flow with a new streamline technique: application in mono- and bidomain simulations of cardiac tissue. In *Engineering in Medicine and Biology Society, 2004. IEMBS '04. 26th Annual International Conference of the IEEE*, Volume 1, pp. 1846–1849. (Cited on page 171.)
- Sasaki, Y. and M. A. Meju (2009). Useful characteristics of shallow and deep marine csem responses inferred from 3d finite-difference modeling. *Geophysics* 74(5), F67–F76. (Cited on page 26.)

- Schalk, G., D. McFarland, T. Hinterberger, N. Birbaumer, and J. Wolpaw (2004). Bci2000: a general-purpose brain-computer interface (bci) system. *Biomedical Engineering, IEEE Transactions on* 51(6), 1034–1043. (Cited on pages 245 and 247.)
- Scholl, C. and R. N. Edwards (2007). Marine downhole to seafloor dipole-dipole electromagnetic methods and the resolution of resistive targets. *Geophysics* 72(2), WA39–WA49. (Cited on page 40.)
- Scholl, C. and V. Sinkevich (2012). Modeling mcsem data with a finite difference approach and an unstructured model grid in the presence of bathymetry. (Cited on pages 90 and 201.)
- SciLab (2012). Scilab. (Cited on pages 97 and 98.)
- Serway, R., J. John W. Jewett, and V. Peroomian (2010). *Physics for Scientists and Engineers, Volume 2: With Modern Physics*. Brooks/Cole. (Cited on page 67.)
- Shankland, S. (2009). Sun renews phone ambitions with javafx mobile. (Cited on page 127.)
- Sheriff, R. (2002). *Encyclopedic Dictionary of Applied Geophysics*. Society of Exploration Geophysicists. (Cited on page 10.)
- Shneiderman, B. and S. Ben (1998). *Designing the user interface*. Pearson Education India. (Cited on pages 86, 87, 92 and 236.)
- Simons, D. J. and D. T. Levin (1997). Change blindness. *Trends in Cognitive Sciences* 1(7), 261–267. (Cited on page 119.)
- Sivarajah, Y., E. Holden, R. Togneri, M. Dentith, and J. Shragge (2012). Analysing variability in geophysical data interpretation by monitoring eye gaze movement. *ASEG Extended Abstracts 2012*(1), 1–4. (Cited on page 246.)
- Slob, E. and P. van den Berg (2005, October 4). A new integral equation method for solving transient diffusive electromagnetic scattering problems. (Cited on page 142.)
- Smith, B. (2011). *Object-Oriented Programming Advanced ActionScript 3.0: Design Patterns*, pp. 1–25. Apress. (Cited on page 42.)
- Spies, B. and T. Habashy (1995). Sensitivity analysis of crosswell electromagnetics. *Geophysics* 60(3), 834–845. (Cited on page 229.)
- Srivastava, U. and J. Widom. Flexible time management in data stream systems. pp. 263–274. ACM. (Cited on page 154.)
- Stockwell, J. (1997). Free software in education; a case study of cwp/su; seismic un\* x. *The Leading Edge* 16(7), 1045–1049. (Cited on page 236.)
- Suryopranoto, B. (2009). Feasibility study on using electromagnetic methods for detection and monitoring of deep carbonate reservoirs, the bunga field, indonesia:. *Curtin University Report No. GPM 13/09*. (Cited on page 228.)
- Swanepoel, R. (2011). *Cross-Well Electromagnetic Methods for Monitoring CO2 Injection into Brine Reservoirs*. B. sc. (Cited on page 130.)
- Swing (2012). What is swing? (Cited on pages 89 and 96.)
- Tarricone, L. and A. Esposito (2004). *Grid Computing For Electromagnetics*. Artech House. (Cited on page 143.)
- TechnoImaging (2012). Technoimaging. <http://www.technoimaging.com/CSEM.html>. (Cited on page 143.)



- Thirud, P. (2002). Waves of information. *Scandinavian Oil and Gas Magazine* 3(4), 2. (Cited on pages 10 and 203.)
- Tompkins, M., R. Weaver, and L. M. MacGregor (2004). Sensitivity to hydrocarbon targets using marine active source em sounding: Diffusive em imaging methods. In *66th EAGE Conference*. (Cited on page 28.)
- Tricoche, X., C. Garth, and G. Scheuermann (2006). *Fast and Robust Extraction of Separation Line Features*, Chapter 15, pp. 249–263. Mathematics and Visualization. Springer Berlin Heidelberg. (Cited on page 173.)
- Tucker, A. (2004). *Computer Science: Handbook*. Chapman and Hall. (Cited on page 117.)
- Um, E. S. and D. L. Alumbaugh (March-April 2007). On the physics of the marine controlled-source electromagnetic method. *Geophysics* 72(2), WA13–WA26. (Cited on pages 181 and 186.)
- Upson, C. and M. Keeler (1988). V-buffer: visible volume rendering. In *ACM SIGGRAPH Computer Graphics*, Volume 22, pp. 59–64. ACM. (Cited on page 111.)
- Veit, M. and S. Herrmann (2003). Model-view-controller and object teams: A perfect match of paradigms. In *Proceedings of the 2nd international conference on Aspect-oriented software development*, pp. 140–149. ACM. (Cited on page 119.)
- Wait, J. (1970). Electromagnetic waves in stratified media. Institute of Electrical and Electronic Engineers. (Cited on page 229.)
- Wang, H., T. Barber, C. Morriss, R. Rosthal, K. Chen, J. Smits, G. Minerbo, M. Frey, D. Homan, and S. Davydycheva (2006). Triaxial induction logging: Theory, modeling, inversion and interpretation. In *International Oil and Gas Conference and Exhibition in China*. (Cited on page 229.)
- Wang, S. and M. S. Zhdanov (2010). Removal of the airwave effect on MCSEM data by separation of the main part of the anomalous field, pp. 732–736. SEG Technical Program Expanded Abstracts. Society of Exploration Geophysicists. doi:10.1190/1.3513887. (Cited on pages 195 and 203.)
- Wang, Y., W. Luo, Z. He, W. Sun, and Z. Wang (2008). Born approximation inversion for the marine csem data set. In *2008 SEG Annual Meeting*. (Cited on page 220.)
- Wangsness, R. (1986). Electromagnetic fields. *Electromagnetic Fields, 2nd Edition*, by Roald K. Wangsness, pp. 608. ISBN 0-471-81186-6. Wiley-VCH, July 1986. 1. (Cited on pages 195 and 196.)
- Wannamaker, P., G. Hohmann, and U. S. D. o. E. D. o. G. Energy (1982). *Electromagnetic Modeling of Three-dimensional Bodies in Layered Earths Using Integral Equations*. Earth Science Laboratory, University of Utah Research Institute. (Cited on pages 139 and 140.)
- Watt, A. and M. Watt (1991). Advanced animation and rendering techniques. Addison-Wesley. (Cited on page 111.)
- Weidelt, P. (2007). Guided waves in marine csem. *Geophysical Journal International* 171(1), 153–176. (Cited on pages 26, 28, 32, 68, 176, 185, 196 and 198.)
- Weiss, C. J. (2007). The fallacy of the “shallow-water problem” in marine csem exploration. *Geophysics* 72(6), A93–A97. (Cited on page 195.)
- Werthimer, D., J. Cobb, M. Lebofsky, D. Anderson, and E. Korpela (2001). Seti@home - massively distributed computing for seti. *Computing in Science and Engg.* 3(1), 78–83. (Cited on page 143.)

- WesternGeco (2008). Westerngeco. <http://www.westerngeco.com/content/services/electromagnetic/wgem.asp?> (Cited on pages 16, 17, 21 and 22.)
- Wirianto, M., W. A. Mulder, and E. C. Slob (2011). Exploiting the airwave for time-lapse reservoir monitoring with csem on land. *Geophysics* 76(3), A15–A19. (Cited on pages 23 and 28.)
- Wu, T. (2003). *An Introduction to Object-Oriented Programming with Java*. McGraw-Hill, Inc. (Cited on page 42.)
- Xiong, Z. (1992). Electromagnetic modeling of 3d structures by the method of system iteration using integral equations. *Geophysics* 57(12), 1556–1561. (Cited on pages 89, 123, 140, 154, 155, 157, 158, 174, 229 and 236.)
- Xiong, Z. and A. C. Tripp (1995). Electromagnetic scattering of large structures in layered earths using integral equations. *Radio Sci.* 30(4), 921–929. (Cited on page 140.)
- Xu, N., X. Gao, B. Hong, X. Miao, S. Gao, and F. Yang (2004). Bci competition 2003-data set iib: enhancing p300 wave detection using ica-based subspace projections for bci applications. *Biomedical Engineering, IEEE Transactions on* 51(6), 1067–1072. (Cited on page 247.)
- Xue, Z., D. Tanase, and J. Watanabe (2006). Estimation of co2 saturation from time-lapse co2 well logging in an onshore aquifer, nagaoka, japan. *Exploration Geophysics* 37(1), 19–29. (Cited on page 229.)
- Yang, H., Y. Zhang, B. Wen, S. Yu, X. Qi, D. Ma, and Z. Xu (2011). *Exploring shallow biogenic gas with high-precision gravity data*, pp. 892–896. (Cited on pages 2 and 5.)
- Youn, C., T. Kaiser, D. Seber, and C. Santini (2008). Web-based simulating system for modeling earthquake seismic wavefields on the grid. *Computers and Geosciences* 34(12), 1936–1946. (Cited on page 143.)
- Yuster, R. and U. Zwick (2004). Fast sparse matrix multiplication. (Cited on page 158.)
- Zehner, B., N. Watanabe, and O. Kolditz (2010). Visualization of gridded scalar data with uncertainty in geosciences. *Computers and; Geosciences* 36(10), 1268–1275. (Cited on page 171.)
- Zhdanov, M. (2009). *Geophysical Electromagnetic Theory and Methods*. Elsevier. (Cited on pages 10, 181, 195, 196 and 202.)
- Zhdanov, M., A. Gribenko, and M. Cuma. Regularized focusing inversion of marine csem data using minimum vertical support stabilizer. In *2007 SEG Annual Meeting*. (Cited on page 220.)
- Zhdanov, M., u. M., A. Gribenko, G. Wilson, and N. Black (2010). 3d inversion of marine csem data: A feasibility study from the shtokman gas field in the barents sea. (Cited on pages 143 and 171.)
- Zhdanov, M. S. and L. H. Cox (2008). Advanced computational methods for rapid and rigorous 3d inversion of airborne electromagnetic data. *Communications in Computational Physics* 3(1), 19. (Cited on page 123.)
- Zhdanov, M. S., V. I. Dmitriev, S. Fang, and G. Hursan (2000). Quasi-analytical approximations and series in electromagnetic modeling. *Geophysics* 65(6), 1746–1757. (Cited on pages 90 and 143.)
- Ziolkowski, A. (2008). First shallow-water multi-transient em survey. (Cited on page 40.)

---

Ziolkowski, A. and D. Wright (2010). *Signal-to-Noise Ratio of CSEM data in Shallow Water*, pp. 685–689. (Cited on page [23](#).)

*Every reasonable effort has been made to acknowledge the owners of copyright material. I would be pleased to hear from any copyright owner who has been omitted or incorrectly acknowledged.*



